USDOE PROGRESS REPORT COO-3496-75

STUDIES OF HEAVY ION REACTIONS AND TRANSURANIC NUCLEI

JOHN R. HUIZENGA
PRINCIPAL INVESTIGATOR

AUGUST 1, 1979 - JULY 31, 1980

DISCLAIMER

STUDIES OF HEAVY ION REACTIONS AND TRANSURANIC NUCLEI

Progress Report For

Period August 1, 1979 - July 31, 1980

John R. Huizenga

PRINCIPAL INVESTIGATOR

Departments of Chemistry and Physics
University of Rochester
Rochester, New York 14627

July 1980

Prepared For

THE UNITED STATES DEPARTMENT OF ENERGY
UNDER CONTRACT NO. EY-76-S-02-3496.A005

TABLE OF CONTENTS

PAGE

I. ABSTRACT

The bombarding energy dependence of the $^{209}Bi + ^{136}Xe$ reaction has been studied. Comparison of the experimental results at bombarding energies of 940 and 1130 MeV has confirmed our earlier finding that the energy-loss parameter is the most suitable quantity to describe the time evolution of the reaction. The bombarding energy dependence of the relationship between energy loss and the width of the charge distribution suggests that the Pauli blocking of occupied single particle levels is an important effect, leading to a smaller dispersion of the fragment Z distribution for a given energy loss than expected from classical theory. In order to study in more detail the effect of Pauli blocking on nucleon exchange and dissipation mechanisms operating in heavy-ion reactions, all such available data for damped nuclear reactions has been systematically analyzed. The observed correlations between the energy loss and the variances of the fragment A and Z distributions are understood on the basis of a nucleon-exchange-induced dissipation mechanism, if account is taken of the Pauli exclusion principle. This interpretation of the data suggests that nucleon exchange is the dominant mechanism for the dissipation of kinetic energy.

In order to study isobaric charge distributions $\sigma_Z^2(A)$ and isotopic mass distributions $\sigma_A^2(Z)$ as a function of various parameters, the fragment yields for specific Z and A have been measured for projectile-like fragments produced in the reaction of 8.3 MeV/u ^{56}Fe ions with targets of ^{56}Fe,

^{165}Ho, ^{209}Bi and ^{238}U. Analyses of the variances reveal that a saturation value of $\sigma_Z^2(A) \approx 0.8$ is reached within the first 30-50 MeV of energy loss and a saturation value of $\sigma_A^2(Z) \approx 3.0\text{-}4.0$ is reached after about 60-80 MeV of energy loss. These data are compared with various N/Z equilibration models. These studies have led also to the discovery of a number of new neutron-rich isotopes of Sc, Ti, V, Cr, Mn and Fe.

Time distributions of fragments from delayed fission after muon capture have been measured for muonic ^{235}U, ^{238}U, ^{237}Np, ^{239}Pu and ^{242}Pu. Comparison of these data with previously measured lifetimes using muon decay electrons, neutrons and γ-rays emitted after muon decay indicates that the observed systematic discrepancies are due to atomic muon capture by fission fragments after prompt fission induced by radiationless muonic transitions.

II. INTRODUCTION

The research activity of the group supported under United States Department of Energy Contract EY-76-S-02-3496.A005 is focussed on two outside-user programs. The principal program is a study of heavy-ion reaction mechanisms at the SuperHILAC accelerator of the Lawrence Berkeley Laboratory. The other program is concerned with a study of muon-induced reactions on heavy targets at the Los Alamos Meson Physics Facility - LAMPF.

In Section III, preprints of five articles and manuscripts of four recent conference papers are included. These articles describe some of the current experimental and theoretical results of our research group. A more complete listing of the Publications and Activities of the group is given in Section IV. Scientific Personnel are listed in Section V.

The principal investigator has devoted 40% of his time during the academic year and 100% of his time during the summer to this contract and expects to continue at these rates during the remainder of the current term. Research Associates, J.R. Birkelund, W.U. Schröder and W.W. Wilcke have devoted 100% of their time to this contract and will continue at this level for the remainder of the term. Research Associate H.J. Wollersheim joined the group on Nov. 1, 1979 and has devoted all of his time to this contract and will continue to do so. Graduate students, A.D. Hoover and L.E. Tubbs have devoted 100% of their time to this contract and will continue at this level for the remainder of the contract period. Graduate student, R.A. Atcher received his Ph.D. degree during this

period and is now a postdoctoral fellow in nuclear medicine at Harvard. Graduate student J.P. Kosky joined our research group in June.

To the best of our knowledge we have complied with the contract requirements. It is a pleasure to acknowledge the direct support of our research programs by the United States Department of Energy. In addition, we are grateful to the National Science Foundation for providing indirect support through the use of the facilities at the Nuclear Structure Research Laboratory.

III. RESEARCH PROGRAM

A. Actinide Muonic Atom Lifetimes Deduced from Muon-Induced Fission

ACTINIDE MUONIC ATOM LIFETIMES DEDUCED FROM MUON-INDUCED FISSION

W.W. Wilcke, M.W. Johnson, W.U. Schröder, D. Hilscher
J.R. Birkelund and J.R. Huizenga

Departments of Physics and Chemistry
and
Nuclear Structure Research Laboratory
University of Rochester
Rochester, New York 14627

and

J.C. Browne and D.G. Perry

Los Alamos Scientific Laboratory
Los Alamos, New Mexico 87544

ABSTRACT:

Time distributions of fragments from delayed fission after muon capture have been measured for muonic ^{235}U, ^{238}U, ^{237}Np, ^{239}Pu and ^{242}Pu. Comparison of these data with previously measured lifetimes using muon decay electrons, neutrons and γ-rays emitted after muon capture indicates that the observed systematic discrepancies are due to atomic muon capture by fission fragments after prompt fission induced by radiationless muonic transition. The deduced capture rates are compared with theoretical models, and very good agreement is found with a giant-resonance excitation model.

[RADIOACTIVITY Muonic atoms ^{235}U, ^{238}U, ^{237}Np, ^{239}Pu and ^{242}Pu. Measured fission fragment time distributions, deduced total muon-capture rates and isotopic effect, present data compared to lifetimes based on all other decay channels.]

I. INTRODUCTION

The interaction of negative muons with actinide nuclei has been studied by numerous experiments[1-12] in recent years. These heavy muonic atoms are of particular interest because theories on muon capture rates, which have been applied successfully for lighter nuclei, can be tested more stringently with very neutron-rich, heavy nuclei.

Experiments designed to determine the capture rate usually measure the time difference between the arrival of a muon in the target and the appearance of any reaction product associated with the capture of the muon by the nucleus. Since muon-capture excites a heavy nucleus on the average to approximately 15 MeV, various reaction products including neutrons, fission fragments and γ-rays can be observed. In addition, it is possible to infer the muon-capture rate from the time distribution of electrons emitted in the leptonic decay of muons in the 1s state of a muonic atom. It was generally assumed that all these methods yield the same lifetimes for a particular muonic atom, but it soon became obvious that lifetimes measured by detecting fission fragments emitted after muon capture were consistently slightly shorter than lifetimes determined with any other method. Hadermann[13] pointed out the likely cause of this discrepancy: It is well known that 'prompt fission' may occur during the atomic cascade of a muon to its ground state due to a radiationless transfer of the muonic transition energy to the nucleus. In the course of such a prompt fission process, the muon may become bound in

an atomic orbital of one of the fission fragments and may later be captured by the fragment or undergo leptonic decay. In a singles experiment as described above, electrons, neutrons and γ-rays resulting from muonic fission fragments cannot be distinguished from those stemming from muon-capture by the actinide nuclei. Hence, the time distributions of electrons, neutrons and γ-rays consist of a superposition of two exponential components. The characteristic lifetimes are 70-80 nsec for muonic actinides and about 130 nsec[14,15] for heavy muonic fission fragments. The capture of muons by the light fission fragment does occur only with low probability[14,15]. However, the statistics of most experiments is not sufficient to allow a distinction of the various components of the measured time distributions such that least-square fits assuming a simple exponential decay law for these distributions will yield lifetimes that are too long.

In contrast, because muon capture by a fission fragment cannot induce fission of this fragment, time distributions of delayed fission fragments produced by muon-capture are not disturbed by prompt fission events. There are, however, two secondary effects that lead to insignificant contamination of these time distributions: The radiationless atomic transition of a muon can cause the emission of one neutron from the target nucleus before subsequent fission of the daughter nucleus occurs after muon capture. This process has a probability similar to prompt fission, but since the lifetime difference between two neighboring isotopes is only about 1.5 nsec for actinide nuclei (as estimated

from a study[11] of $^{235,238}U$ and $^{239,242}Pu$), the effect of this admixture on the lifetimes deduced is more than one order of magnitude smaller than the effect of prompt fission on measurements of electrons, neutrons and γ-rays described above, and is well within the statistical uncertainties of all experiments performed so far. The second mechanism that may affect the time distribution of fission fragments is the possible excitation of shape-isomeric nuclear states during the muonic cascade, as suggested by Bloom[16]. A quantitative discussion[11] shows, however, that the influence of this effect on the measured lifetime is very small.

Muon capture by fission fragments as proposed by Hadermann[13] and delayed fission after prompt neutron emission, however, have been observed directly in coincidence experiments, where the emission of fission fragments in coicidence with decay electrons[14] and neutrons[15] was measured. In addition, a measurement[11] with very good statistics confirmed the presence of a long-lifetime component in the singles time spectrum of neutrons emitted from muonic ^{239}Pu. Therefore, it is concluded that measurements employing the experimentally rather unambiguous fission technique are required to provide meaningful data on muon capture rates for actinides that can be compared to theoretical models of muon capture. Coincidence experiments would be even better, but their statistical accuracy is inherently lower than that of singles measurements. Since the effects of prompt neutron emission and isomeric-state excitation on fission time distributions are negligible, the present study of singles fission

measurements was initiated with the aim of obtaining data of high statistical accuracy.

II. EXPERIMENTAL PROCEDURE

The experiments were performed using the stopped-muon channel of the Los Alamos Meson Physics Facility (LAMPF). Muons from the channel passed through a three-element plastic scintillator telescope and were stopped in a fission chamber containing nine Ti foils, on which the actinide targets (^{235,238}U, ^{237}Np and ^{239,242}Pu) were deposited as 0.5 mg/cm^2 thick oxide layers. Since inspection of previous experiments[1-12] indicated that systematical errors are frequently more important than statistical ones, care was taken to minimize the latter by measuring three isotopes simultaneously. As shown in Fig. 1, three foils carrying one particular isotope formed an ionization chamber, and three such chambers constituted the whole fission chamber. All timing signals were processed in the same time-to-pulse-height converter and the same ADC, using routing signals to distinguish the ionization chamber that had fired. Time calibrations were performed frequently with several independent methods. In addition, only two isotopes were replaced at a time, so that the third isotope remaining in the chamber served as an additional cross check for the consistency of the results for different runs. A typical time spectrum is shown in Fig. 2. The data were analyzed with a least-squares code

and a fitting function representing an exponential distribution on a constant background. A trial fit assuming two exponentials failed to find a second lifetime component in the spectra, as was to be expected.

III. EXPERIMENTAL RESULTS AND DISCUSSION

The experimental results are compiled in Table I along with all previously published data on muonic actinide lifetimes τ_i . The indices e, n, γ and f refer to electron-, neutron-, γ-ray- and fission fragment measurements, respectively. The weighted averages $\bar{\tau} \pm \sigma$ have been calculated[17,22] by weighting the data τ_i according to the published error $\tau_i \pm \sigma_i$ using the following equations:

$$\bar{\tau} = \frac{\Sigma(\tau_i/\sigma_i^2)}{\Sigma(1/\sigma_i^2)} \tag{1}$$

$$\sigma_A = \left(\frac{\Sigma(\tau_i - \bar{\tau})^2/\sigma_i^2}{(n-1)\Sigma(1/\sigma_i^2)}\right)^{1/2} \tag{2}$$

$$\sigma_B = (\Sigma(1/\sigma_i^2))^{-1/2} \tag{3}$$

$$\sigma = \max(\sigma_A, \sigma_B) \tag{4}$$

Eq. (2) for the error σ_A of the weighted mean can yield unphysical values for very small samples. Therefore, σ_B was introduced which sets a lower limit for σ based on the published errors. Inspection of Table I shows that for all isotopes the averaged lifetime $\bar{\tau}_f$ is shorter than either τ_n, $\bar{\tau}_\gamma$ or $\bar{\tau}_e$.

Although there is no question about the occurrence of muon capture by fission fragments, it has not been shown that this mechanism is the only one responsible for the differences between measured lifetimes. A systematical study of all muonic actinides may be helpful to shed light on this question, since a monotonic increase of the (positive) difference $\tau_n - \bar{\tau}_f$ is expected with increasing probability for prompt fission, if muon capture by fission fragments were the dominant contribution to these differences. It is possible to define a characteristic parameter allowing a systematic classification of muonic actinides. Such a suitable parameter is represented by the product of the probability of a radiationless muonic transition and the fissility of the target nucleus. As has been shown by Zaretski and Novikov[18], the ratio of radiationless to radiative transition probabilities is given approximately by

$$\frac{\Gamma_{r\ell}}{\Gamma_r} \approx Z\alpha \qquad (5)$$

where $\alpha = e^2/\hbar c$ is the fine-structure constant. The probability of fission after a radiationless transition depends in a complicated way on the detailed shape of the double-humped fission barrier, which is augmented in the presence of the muon. It is

assumed, however, that the general trend of the fissility be still given by the liquid-drop expression for the fissility[13] $\chi \sim Z^2/A$. Combining χ with Eq. 5, one obtains a suitable scale $p(Z,A)$ for discussing the lifetimes:

$$p = \chi \cdot \frac{\Gamma_{r\ell}}{\Gamma_{r\ell}+\Gamma_r} = \frac{\alpha Z^3}{50.13\ A(1+Z\alpha)} \qquad (6)$$

In the upper part of Fig. 3 the difference $\tau_n - \bar{\tau}_f$ of lifetimes is plotted versus p. Except for ^{232}Th, the difference $\tau_n - \bar{\tau}_f$ is seen to increase with increasing values of p as expected, if muon capture by fission fragments were the dominant cause of the lifetime differences. It is known[8], however, that the prompt fission probability of muonic ^{242}Pu is very large, even larger than that for ^{239}Pu. Hence, the high value of $\tau_n - \bar{\tau}_f$ for ^{242}Pu is understandable, but the result for ^{232}Th is puzzling. It is known[6] that ^{232}Th has a very low probability ($5 \cdot 10^{-4}$) for prompt fission, which is consistent with its low p-value. Therefore, muon capture after prompt fission cannot explain the large difference of the lifetimes. It should be pointed out, however, that the weighted average of τ_f for ^{232}Th is dominated by one measurement[12]. More data are needed to firmly establish the abnormal behavior for ^{232}Th shown in Fig. 3a.

As has been discussed in the introduction, both electron and neutron measurements are influenced by the occurrence of prompt fission, whence the difference of lifetimes $\bar{\tau}_e - \tau_n$ should be small. This difference may be non-zero, however, since the

two methods are of different sensitivity to the admixture of events resulting from muon-capture by a fission fragment: The multiplicity M_n of neutrons emitted after muon capture in a β-stable nucleus of mass A is approximately given[20] by

$$M_n \approx 0.3\ A^{1/3} \qquad (7)$$

In addition, the muon capture rate decreases rapidly with decreasing atomic mass, whereas the muon decay rate remains essentially constant. Thus the ratio of electron-to-neutron multiplicity is about twice as high for heavy muonic fission fragments as compared to muonic actinides. Therefore, the difference $\bar{\tau}_e - \tau_n$ should increase slightly with p, consistent with experimental results shown in the lower part of Fig. 3. With the possible exception of ^{232}Th, the systematic comparison of the data indicates that muon capture by fission fragments is the dominant contribution to the differences in lifetime. Therefore, $\bar{\tau}_f$ represents the best approximation to the true lifetime of a muonic actinide.

The experimental results may be compared to existing theories for muon capture rates λ, that are related to the measured lifetimes $\bar{\tau}_f$ by

$$\frac{1}{\bar{\tau}_f} = \lambda^{exp} + R\lambda_o \qquad (8)$$

Here λ_o is the free-muon decay rate, and R (≈ 0.85) accounts for the reduction of the decay rate due to effects of atomic binding[28]. Two theoretical approaches have been applied to the study of muon capture rates in the actinide region. The well-known

Goulard-Primakoff formalism[21] has been proven useful in predicting muon capture rates over a wide range[22] of isotopes and provides a closed-form equation for the total muon capture rate λ^{GP}:

$$\lambda^{GP} = k \cdot Z_{eff}^{4}(1 - \frac{\epsilon_\mu}{m_\mu})^2(1 - \frac{m_\mu \epsilon_\mu}{m_N}) \times [1 - 0.03\frac{A}{2Z} + 0.25\,\frac{A - 2Z}{2Z} - 3.24\,(\frac{A - Z}{2A} + \frac{|A - 2Z|}{8Z - A})] \quad (9)$$

The notation is that of Ref. 11. A comparison of the Goulard-Primakoff predictions to the experimentally observed capture rates is given in Table II. The predicted rates are systematically smaller than the measured ones. The Goulard-Primakoff capture rates are proportional to the value of Z_{eff}^{4}, which has to be calculated independently, but a comparison of several isotopes of the same element, which nearly eliminates the dependence on Z_{eff}^{4}, indicates that this theory consistently overrates the sensitivity of the capture rate to the neutron excess. In the alternate model[23] of Kozłowski and Zgliński the capture mechanism proceeds solely via the excitation of giant-resonance states. The transition amplitude M_ν is given by the overlap integral of Pustovalov's muon wave function[24] and the neutrino wave function within the nuclear volume with an isovector transition operator and nuclear wave functions taken from the hydrodynamical model[25]. Multipolarities L from monopole to octupole are taken into account, and the total muon capture rate λ^{KZ} is the sum of the rates for each multipolarity:

$$\lambda^{KZ} = \frac{m_\mu^2}{2\pi} G_\mu^2 \sum_{L=0}^{3} |(M_V)_L|^2 \qquad (10)$$

This model has been applied[26] to the nuclei under investigation (Table II), and the agreement between theory and experiment is excellent. It has been shown[27] that for light nuclei (e.g. ^{16}O) the giant resonances are very effective doorway states for muon capture. In heavy nuclei, however, numerous non-collective states at 15-20 MeV excitation energy are expected to exist, which also fulfill the spin and isospin selection rules of the operators describing muon capture. Therefore, it is rather surprising that a model which incorporates only giant-resonance states describes the capture rates so well. It appears important to check other consequences of the proposed capture mechanisms by experiment. Measurements of the neutron multiplicity and energy spectra after muon capture in actinides currently under way will yield information on the excitation energy spectrum and can be compared to this model.

This work was supported by the U.S. Department of Energy. We would like to thank the technical staff of the Los Alamos Meson Physics Facility and especially L.E. Agnew and B.R. Rector for their hospitality and assistance, and J.G. Povelites for preparing the targets.

References

1. J.C. Sens, Phys. Rev. 113, 679 (1959).
2. O. Hashimoto, S. Nagamiya, K. Nagamine, and T. Yamazaki, Phys. Lett. 62B, 233 (1976).
3. M.W. Johnson, W.U. Schröder, J.R. Huizenga, W.K. Hensley, D.G. Perry, and J.C. Browne, Phys. Rev. C15, 2169 (1977).
4. B. Budick, S.C. Cheng, E.R. Macagno, A.M. Rushton, and C.S. Wu, Phys. Rev. Lett. 24, 604 (1970).
5. J.A. Diaz, S.N. Kaplan, and P.V. Pyle, Nucl. Phys. 40, 54 (1963).
6. D. Chultem, V. Cojocaru, Dz. Ganzorig, Kim Si Chwan, T. Krogulski, V.C. Kuznetsov, H.G. Ortlepp, S.M. Polikanov, B.M. Sabirov, V. Schmidt, and W. Wagner, Nucl. Phys. A247, 452 (1975).
7. V. Cojocaru, L. Marinescu, M. Petrascu, G. Vioculescu, A. Ignatenko, and M. Omelianenko, Phys. Lett. 20, 53 (1966).
8. B.M. Aleksandrov, G.V. Buklanov, W.D. Fromm, Dz. Ganzorig, A.S. Krivokhatski, T. Krogulski, S.M. Polikanov, and B.M. Sabirov, Phys. Lett. 57B, 238 (1975).
9. W.D. Fromm, H.G. Ortlepp, S.M. Polikanov, U. Schmidt, G.N. Zorin, R. Arlt, and G. Musiol, Nucl. Phys. A278, 387 (1977).
10. S.N. Kaplan, J.A. Monard, and S. Nagamiya, Phys. Lett. 64B, 217 (1976).
11. W.W. Wilcke, M.W. Johnson, W.U. Schröder, J.R. Huizenga, and D.G. Perry, Phys. Rev. C18, 1452 (1978).

12. Dz. Ganzorig, P.G. Hansen, T. Johansson, B. Jonson, J. Konijn, T. Krogulski, V.D. Kuznetsov, S.M. Polikanov, G. Tibell, and L. Westgaard, Phys. Lett. 78B, 41 (1978).

13. J. Hadermann, Phys. Lett. 67B, 35 (1977).

14. Dz. Ganzorig, P.G. Hansen, T. Johansson, B. Jonson, J. Konijn, T. Krogulski, V.D. Kuznetsov, S.M. Polikanov, G. Tibell, and L. Westgaard, Phys. Lett. 77B, 257 (1978).

15. W.U. Schröder, W.W. Wilcke, M.W. Johnson, D. Hilscher, J.R. Huizenga, J.C. Browne, and D.G. Perry, Phys. Rev. Lett. 43, 672 (1978).

16. S.D. Bloom, Phys. Lett. 48B, 470 (1974).

17. P.R. Bevington, Data Reduction and Error Analysis for the Physical Sciences, (McGraw-Hill, New York, 1969), Ch. 5.

18. D.F. Zaretsky and V.M. Novikov, Nucl. Phys. 28, 177 (1961).

19. R. Vandenbosch and J.R. Huizenga, Nuclear Fission, (Academic Press, New York 1973), Ch. 2.

20. P. Singer, Springer Tracts in Modern Physics, 71, 39 (1974).

21. B. Goulard and H. Primakoff, Phys. Rev. C10, 2034 (1974).

22. M. Eckhause, R.T. Siegel, R.T. Welsh, and T.A. Fillippas, Nucl. Phys. 81, 525 (1966). The Primakoff fit performed in this study corresponds to a theory preceding ref. 21 as described in H. Primakoff, Rev. Mod. Phys. 31, 802 (1959).

23. T. Kozłowski and A. Zgliński, Nucl. Phys. A305, 368 (1978).

24. G.E. Pustovalov, ZhETF (Sov. Phys.) 36, 1806 (1959).

25. A. Bohr and B.R. Mottelson, Nuclear Structure, Vol. 2 (Benjamin, New York, 1975).

26. A. Zgliński and T. Kozłowski, private communication.

27. J.D. Walecka "Semi-Leptonic Weak Interactions in Nuclei" in Muon Physics V.W. Hughes and C.S. Wu, editors, 1973

28. R.W. Huff, Ann. Phys. 16, 288 (1961).

TABLE I. Experimental lifetimes in nsec of muonic actinides deduced from measurements of decay electrons (τ_e), neutrons (τ_n), capture γ-rays (τ_γ) and fission fragments (τ_f). As discussed in the text, the electron, neutron and γ-ray lifetime measurements yield values systematically too high, because these three measurements are sensitive to contributions from muon capture by fission fragments after prompt fission. The lifetimes τ_f deduced from a detection of delayed fission fragments, however, are not affected by this effect. The weighted average $\bar{\tau}_f$ of the fission lifetimes is therefore believed to represent the best values for the true muonic actinide lifetimes.

TABLE I.

Isotope	τ_e	$\bar{\tau}_e$	τ_n	τ_γ	τ_f	$\bar{\tau}_f$
^{232}Th	80.4 ± 2.0[2] 79.2 ± 2.0[3]	79.8 ± 1.4	80.1 ± 0.6[11]	-	74.2 ± 5.6[5] 87.0 ± 4.0[6] 77.3 ± 0.3[12]	77.4 ± 0.5
^{233}U	-	-	-	-	61.7 ± 3.8[4]	61.7 ± 3.8
^{235}U	78 ± 4[2] 75.4 ± 1.9[3]	75.9 ± 1.7	75.0 ± 0.7[11]	-	65.3 ± 2.8[4] 66.5 ± 4.2[5] 75.6 ± 2.3[6] 72.9 ± 0.9[a]	72.6 ± 1.5
^{238}U	88 ± 4[1] 81.5 ± 2.0[2] 73.5 ± 2.0[3]	78.7 ± 3.5	78.3 ± 1.0[11]	78.6 ± 1.5[9] 79.1 ± 0.5[10] $\bar{\tau}_\gamma$: 79.0 ± 0.5	74.1 ± 2.8[4] 75.6 ± 2.9[5] 76.0 ± 1.0[6] 77.1 ± 0.2[12] 77.9 ± 0.5[a]	77.2 ± 0.2
^{237}Np	-	-	73.5 ± 1.4[11]	-	72 ± 2[8] 71.3 ± 0.9[a]	71.4 ± 0.8
^{239}Pu	77.5 ± 2.0[2] 73.4 ± 2.8[3]	76.1 ± 1.9	74.5 ± 0.5[11]	-	74 ± 14[7] 70 ± 3[8] 70.1 ± 0.7[a]	70.1 ± 0.7
^{242}Pu	-	-	81.1 ± 0.7[11]	-	79 ± 5[8] 75.4 ± 0.9[a]	75.5 ± 0.9

[a] Present study

TABLE II. Comparison of experimentally determined muon capture rates λ^{exp} with the predictions of the Goulard-Primakoff (λ^{GP}) and Kozłowski-Zgliński (λ^{KZ}) theories. Units are 10^5 sec^{-1}.

Isotope	λ^{exp}	λ^{GP}	λ^{KZ}
^{232}Th	125 ± 1	110	124
^{233}U	158 ± 9	131	-
^{235}U	134 ± 1	122	134
^{238}U	125 ± 1	108	122
^{237}Np	137 ± 1	123	138
^{239}Pu	139 ± 2	129	139
^{242}Pu	129 ± 2	116	128

FIGURE AND TABLE CAPTIONS

Fig. 1. Schematic drawing of the fission ionization chamber. The insert shows the arrangement of the target foils used to avoid cross-talk between different sets of foils: The foil on the left is part of the adjacent electrically decoupled chamber which uses the same gas volume.

Fig. 2. The experimental fission-fragment time distribution for muonic ^{239}Pu. The peak in the region near t = 0 corresponds to prompt fission events caused by radiationless muonic transitions. The horizontal dashed line represents a fit to the background to negative and large positive times. The curve drawn through the data points represents the sum of the exponential and the background distributions.

Fig. 3. The upper part shows the difference $\tau_n - \tau_f$ of the lifetimes measured by detecting neutrons and fission fragments, respectively, after muon capture, plotted versus the product p of liquid-drop fissility and probability for radiationless transitions. Large values of this quantity, which is an approximate measure for the prompt fission probability, are correlated with large lifetime differences.

The lower part shows the lifetime difference $\bar{\tau}_e - \tau_n$ between results of experiments detecting electrons and neutrons, respectively. Since $\bar{\tau}_e$ is more sensitive to contributions from muonic fission fragments than τ_n, this difference is also weakly correlated with p.

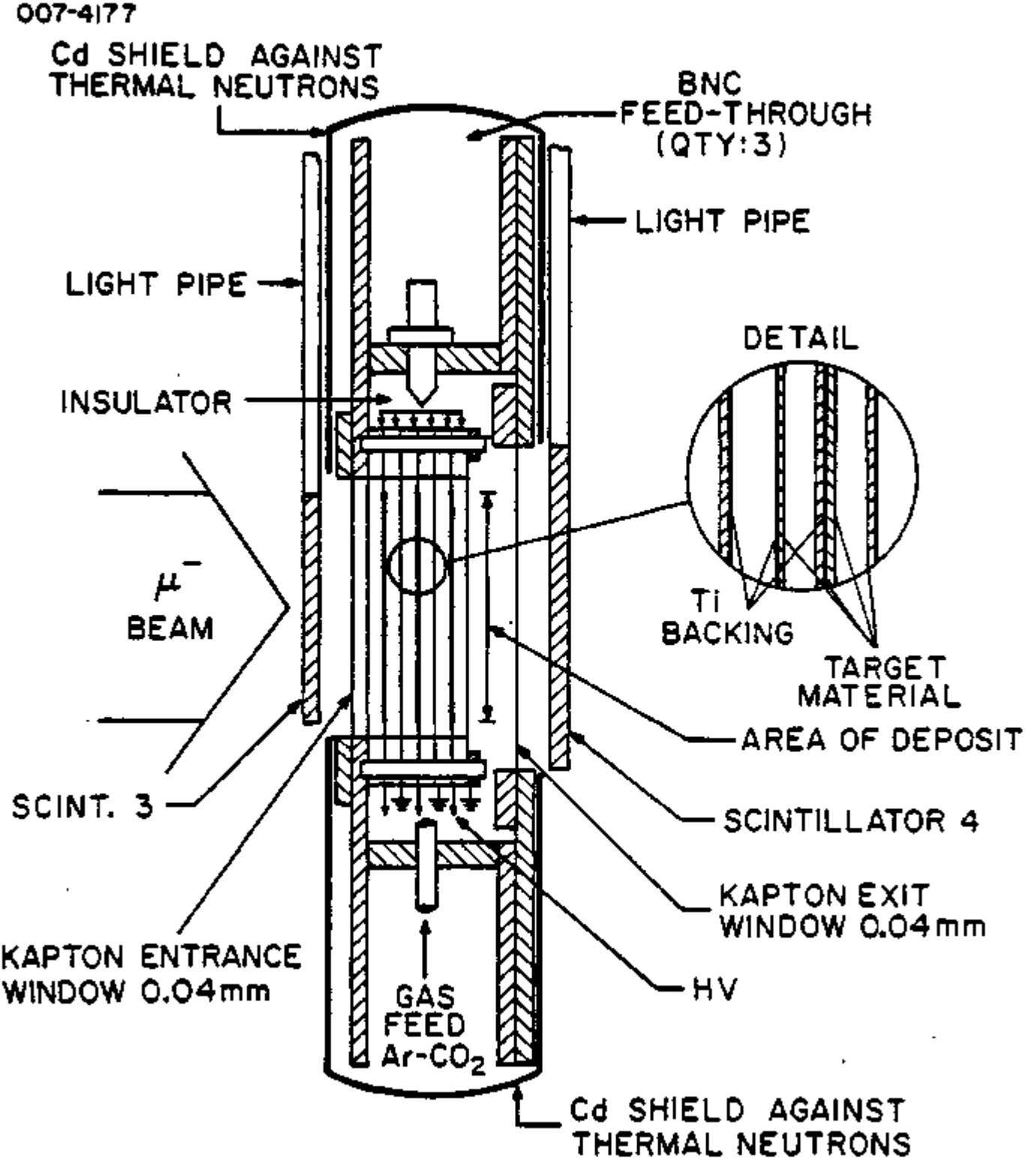

SIDE-VIEW

Fig. 1

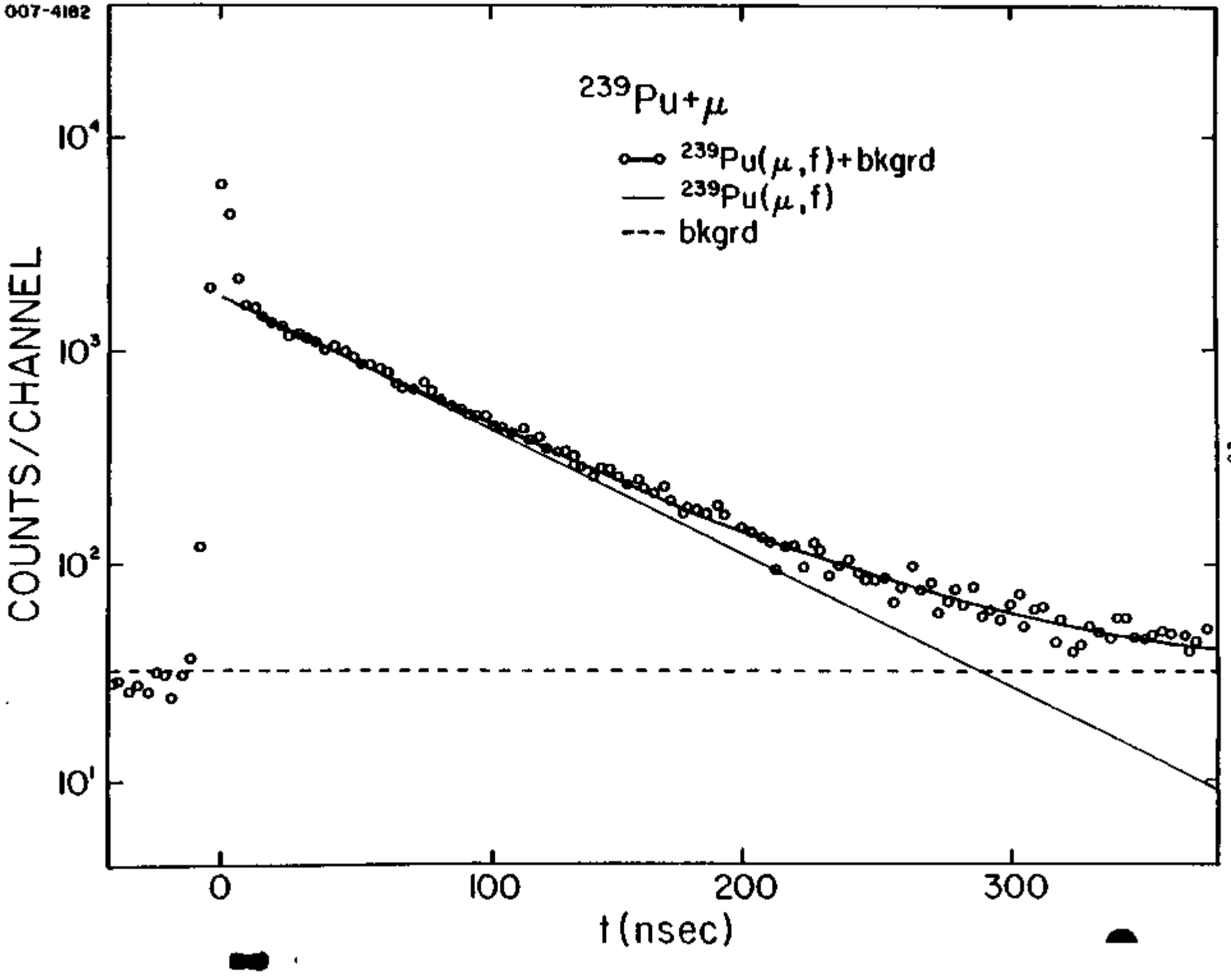
007-4182
$^{239}Pu+\mu$
$^{239}Pu(\mu,f)$+bkgrd
$^{239}Pu(\mu,f)$
bkgrd
COUNTS/CHANNEL
10^4
10^3
10^2
10^1
0
100
200
300
t(nsec)

Fig. 2

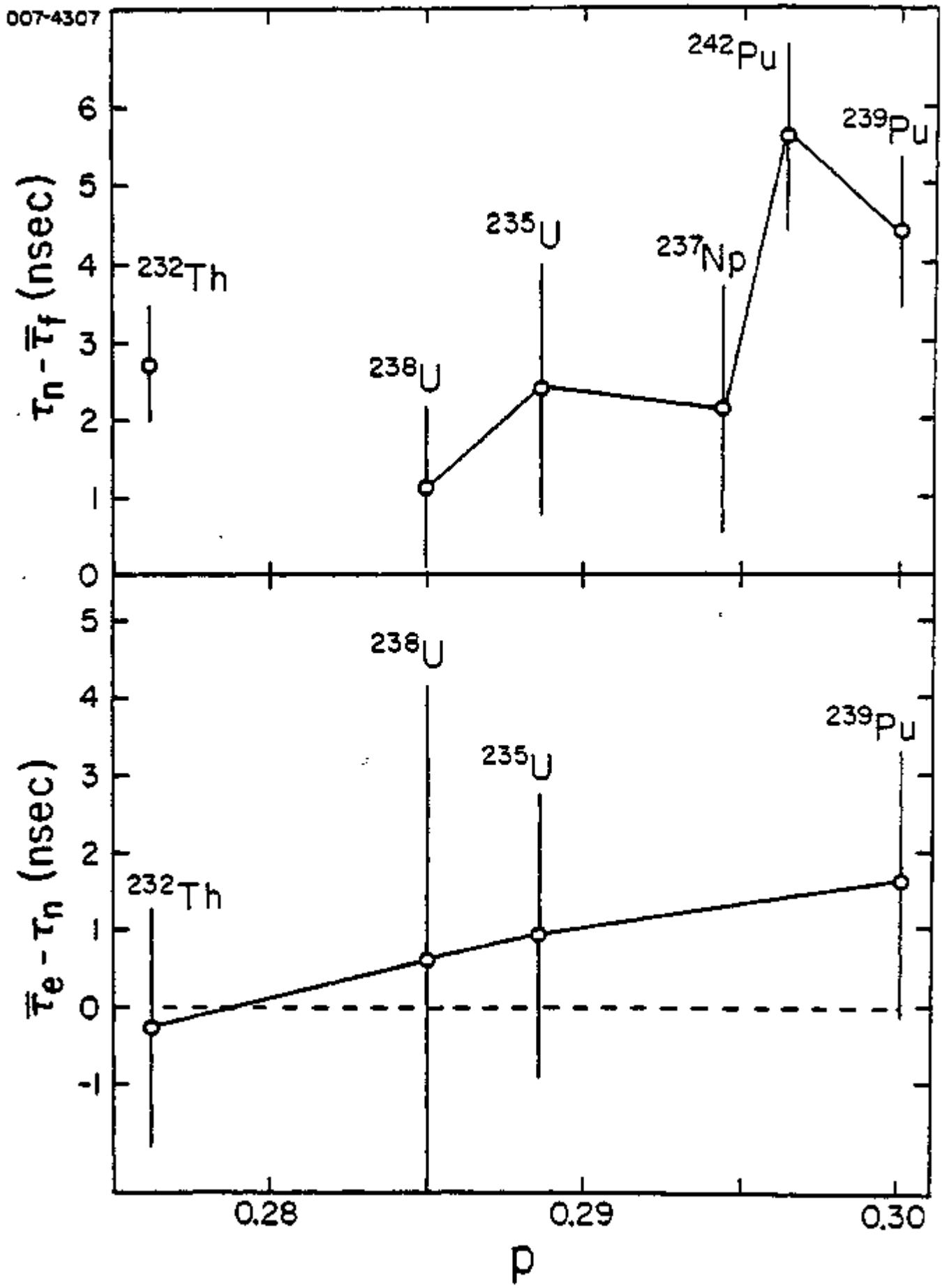
007-4307
$\bar{\tau}_n - \bar{\tau}_f$ (nsec)
$\bar{\tau}_e - \tau_n$ (nsec)
^{232}Th
^{238}U
^{235}U
^{237}Np
^{242}Pu
^{239}Pu
0.28
0.29
0.30
p

Fig. 3

B. Manifestation of the Quantum-Statistical Nature of Exchange and Dissipation Mechanisms Operating in Damped Nuclear Reactions

ifestation of the Quantum-Statistical Nature of Exchange and Dissipation Mechanisms rating in Damped Nuclear Reactions*

. U. Schröder, J. R. Birkelund, J. R. Huizenga and W. W. Wilcke

Departments of Chemistry and Physics and Nuclear Structure Research Laboratory
University of Rochester, Rochester, New York 14627, USA

and

J. Randrup

Nuclear Science Division, Lawrence Berkeley Laboratory
Berkeley, California 94720, USA

ABSTRACT

Systematic properties of dissipation and nucleon exchange mechanisms associated with damped nuclear reactions are obtained from available data. It is shown that correlations between energy loss and variances of the fragment A and Z distributions, which are not understood in a classical approach, find a natural explanation in terms of a nucleon exchange mechanism in which the Pauli exclusion principle plays a crucial role. A good overall description of experimental data is achieved with dynamical calculations taking account of the formation of a neck between the reaction partners.

1. Introduction

Despite the considerable progress made during recent years in understanding the damped-nuclear reaction mechanism, several of its most characteristic features have so far escaped a consistent theoretical description[1]. Of particular interest are the correlations between energy dissipation and nucleon exchange observed for many systems[2]. This experimental evidence is in accord with the assumption of successive exchange of nucleons proceeding simultaneously with dissipation of relative kinetic energy in many small steps.

Experimental studies of light particles[3] emitted in damped nuclear reactions indicate that thermalization of the fragments occurs during the reaction time, for the relatively low bombarding energies under consideration. Nuclear temperatures reached in these reactions, of the order τ=2-3 MeV, are small compared to the Fermi energy ($\varepsilon_F \approx 37$ MeV). In this regime, characterized by a nucleon mean free path comparable to the dimensions of the system, one expects that approaches involving the nuclear mean field may lead to adequate models of the nuclei and nuclear interactions. In the following, classical[1,2,4] and quantal[5] models of energy dissipation mediated by nucleon exchange are discussed that are based on such one-body assumptions.

2. Classical model of energy dissipation and nucleon exchange

In a phenomenological approach described recently[4] use was made of the microscopic time scale provided by the exchange mechanism to derive a dissipation rate

$$-dE/dN_{ex} \approx (m/\mu)\alpha\, E \qquad (1)$$

*Work supported by the U.S. Department of Energy

with respect to the number N_{ex} of nucleons exchanged. Here, $E=E_{cm}-V_{Coul}-E_{Loss}$ is the available relative kinetic energy above the Coulomb barrier V_{Coul}, m is the nucleon mass and μ is the reduced mass of the dinuclear system. The coefficient α conveys information on the character of the dissipation mechanism. It would be unity if all dissipation were due to the recoil induced by the exchange of classical particles which are initially either at rest or move with their Fermi velocity. The presence of additional dissipation mechanisms would yield increased values of α.

Under the assumption that α remains approximately constant during a given collision trajectory, Eq. (1) may be integrated yielding

$$E_{Loss} \approx (E_{cm}-V_{Coul})[1-\exp(-(m/\mu)\alpha N_{ex})] \qquad (2)$$

Whereas the energy E_{Loss} dissipated in the reaction may be approximataly related to the measured reaction Q-value, there is no unambiguous way to infer N_{ex} from experimental observables, although various relations between N_{ex} and the variances σ_A^2 and σ_Z^2 of the fragment A and Z distributions have been suggested[1,6]. Without restricting the generality of the conclusions to be drawn below, in the following it is assumed that $N_{ex}=\sigma_A^2$. If only σ_Z^2 is known, σ_A^2 is estimated from the relation $\sigma_A^2=(A/Z)^2\sigma_Z^2$, where A and Z apply to the dinuclear system.

Fig. 1 shows the resulting fits of Eq. (2) to the experimental[4,7] correlations $\sigma_Z^2(E_{Loss})$ for the reaction $^{209}Bi+^{136}Xe$ at 1130 and 940 MeV. As can be seen, an adequate representation of the data is provided by Eq. (2), with a constant value of α up to energy losses close to the initially available energies $E_0=E_{cm}-V_{Coul}$ indicated by arrows. However, it is observed that α decreases from 3.2 to 1.4 as the bombarding energy is increased from 940 to 1130 MeV. A similar behavior is borne out by all other reactions studied[1,4,7,12], as demonstrated in Fig. 2 exhibiting the dependence of α on the approach energy per nucleon $(m/2)U^2=(m/\mu)E_0$. The solid curve drawn through the data points emphasizes the average trend which is already rather well defined by the three

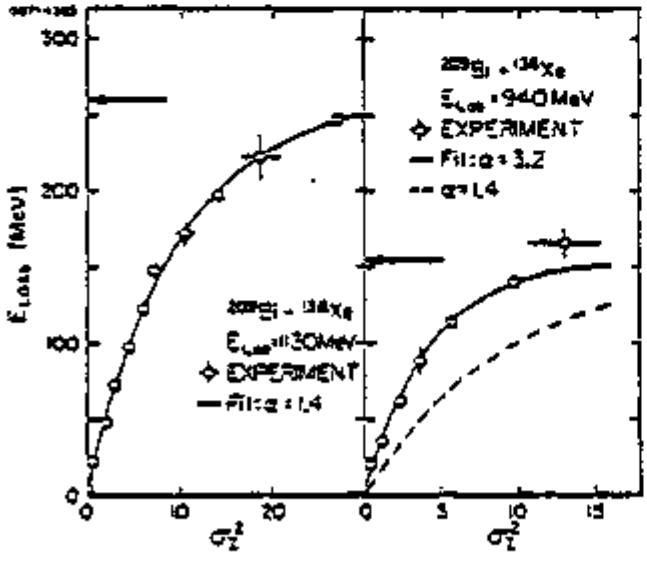

Fig. 1

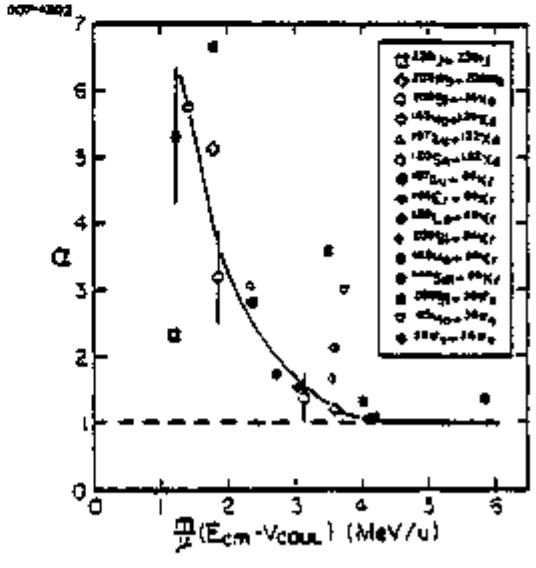

Fig. 2

nts[8] for the reaction $^{144}Sm+^{84}Kr$. Significant deviations from the average are observed for the relatively asymmetric systems[9] associated with the ^{56}Fe projectile, as well as for the $^{238}U+^{238}U$ reaction[10]. Neither a dependence of α on the bombarding energy nor on the system is expected from the above classical model which is based on kinematic considerations. Attributing this feature to the existence of additional dissipation mechanisms[2,4] or nuclear structure effects[13] resulted in a mere parameterization of data, lacking a profound theoretical basis.

3. Quantum-statistical approach

Although the insufficiency of the classical model presents a challenge to the validity of the basic dissipation mechanism, its failure to account for the data may result from the unjustified assumption of classicality of the processes involved. A quantum-statistical model[5,14] proposed recently describing energy dissipation associated with the exchange of nucleons between two almost degenerate Fermi-Dirac gases in slow relative motion offers a more meaningful test of the underlying reaction mechanism.

In this model, the mass drift coefficient v_A and the dissipation rate $-\dot{E}$ are given by

$$v_A = dA/dt = F_A N'(\varepsilon_F)$$

$$-\dot{E} = dE_{Loss}/dt = \langle\omega^2\rangle_F N'(\varepsilon_F) \qquad (3)$$

where, ε_F and F_A are the mean and the difference of the two Fermi levels, respectively. The form factor N' represents the differential current of nucleons between the two gases. The quantity $\omega = F_A - \vec{U}\cdot\vec{p}$ is the amount of intrinsic excitation produced by the exchange of a nucleon with the intrinsic momentum $\vec{p}$, and the brackets denote an average over the orbitals in the Fermi surface, the only ones participating. Whereas effects of the Pauli exclusion principle cancel in the calculation of the one-body quantities in Eq. (3), the mass dispersion σ_A^2 depends explicitly on such Pauli correlations. In the model, its rate of change is determined by

$$D_A = \frac{1}{2}\, d\sigma_A^2/dt = \tau^* N'(\varepsilon_F) \qquad (4)$$

Here, $\tau^* = \langle(1/2)\omega \coth(\omega/2\tau)\rangle_F$ is measure of the energy interval around the Fermi level contributing to exchange processes, and τ is the ordinary nuclear temperature. This effective temperature τ^* depends on both the available and already dissipated relative kinetic energy and, hence, introduces a bombarding-energy dependence of the exchange processes, due to the action of the Pauli principle. Fig. 3 shows values of τ^* for the reaction $^{209}Bi+^{136}Xe$ at two bombarding energies calculated as a function of energy loss with the dynamical model described below. As seen from Fig. 3, τ^* can initially be rather large but approaches the nuclear temperature τ for high energy losses with a rate depending on the bombarding energy. One interesting consequence of this behavior is the relatively small drift predicted by the Einstein relation $v_A = D_A F_A/\tau^*$, as compared to the classical relation $v_A = D_A F_A/\tau$.

Of interest to the classical model referred to earlier is the quantity $\alpha = -(\mu/m)\, d(\ln E)/d\sigma_A^2$, related to the slope of the experimental correlations $\bar{\varepsilon}_{Loss}(\sigma_A^2)$ exhibiting the previously unexplained bombarding-energy dependence.

For systems with $F_A \approx 0$, i.e. a negligible driving force, and peripheral collisions, Eqs. (3) and (4) predict a dependence

$$\alpha \approx T_F/(2\tau^*) \qquad (5)$$

where T_F is the Fermi kinetic energy. This relation predicts an approximate universal bombarding-energy dependence of α for systems with $F_A \approx 0$. Values of α increasing strongly with decreasing bombarding energy are expected, a behavior observed experimentally (see Fig. 2). Different systems at similar bombarding energies per nucleon above the barrier exhibit different values of α to the extent that the corresponding values of F_A differ.

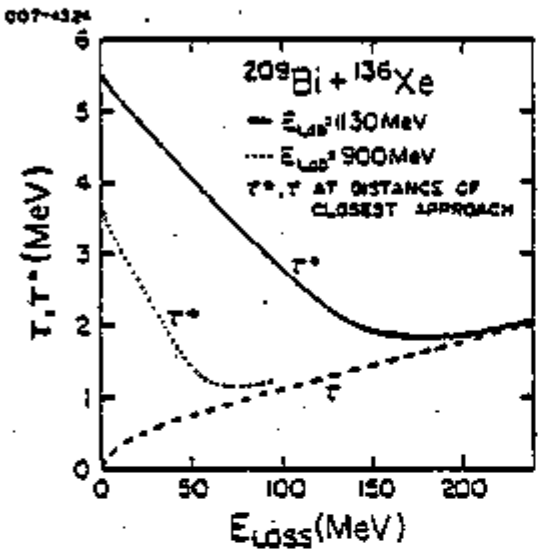

Fig. 3

The bombarding-energy dependence of the relation between nucleon exchange and energy dissipation as reflected by Eq. (5) is entirely due to the Fermion nature of the exchanged nucleons. The classical expressions derived earlier are regained in the limit where the Pauli principle is relaxed, yielding $\alpha \equiv 1$.

4. Dynamical calculations

Since the rough estimate represented by Eq. (5) relies on a number of idealizations, a more refined approach is taken in this work by performing dynamical calculations of collision trajectories in a coordinate space including the fragment-mass and -charge asymmetries. The dinuclear complex is parameterized by two spherical nuclei joined by a cylindrical neck. Conservative forces are calculated from droplet-model masses, the Coulomb repulsion and the surface and proximity energies of the neck region. Energy dissipation is provided by the nucleon exchange mechanism (cf. Eq. (3)), together with the damping due to the neck motion approximated by a wall-type dissipation formula. Inertial forces are calculated for two sharp rigid spheres. Energy loss and the accumulated variances σ_A^2 and σ_Z^2 are obtained from integrating along the trajectory the dissipation function and the diffusion coefficients, respectively, as given by the model. The corresponding form factors employed were those calculated by Randrup[5] but modified to allow for the formation of a neck. Consistent with the droplet model, account was taken of a neutron skin of the nuclear matter distribution. This results in theoretical ratios σ_A^2/σ_Z^2 that may exceed the values $(A/Z)^2$ for low bombarding energies or small energy losses. The various aspects of the model are discussed in detail elsewhere[5,14,15].

Typical results of the calculations (full curves) are compared to experiment in Figs. 4 and 5 for the reactions $^{209}Bi+^{136}Xe$ [Ref. 7], $^{209}Bi+^{56}Fe$ [Ref. 9] and $^{165}Ho+^{56}Fe$ [Ref. 12], that are associated with α-values far in excess of the classical limit. A good reproduction of the data is achieved for $^{209}Bi+^{136}Xe$ at 940 MeV. For systems such as $^{209}Bi+^{56}Fe$ and $^{165}Ho+^{56}Fe$ depicted in Figs. 4 and 5, where the static driving force

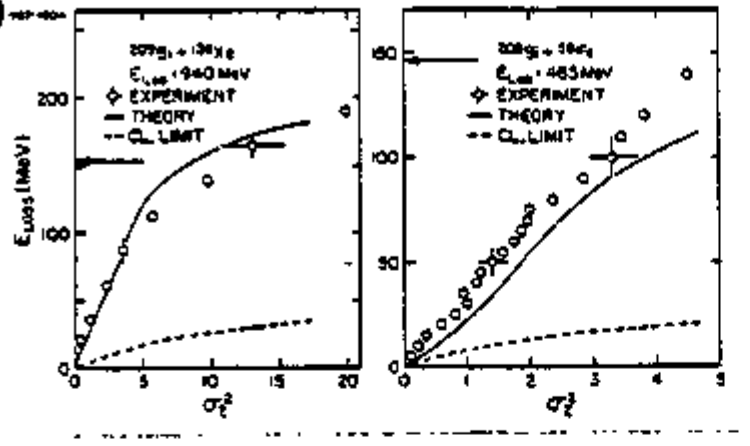

Fig. 4

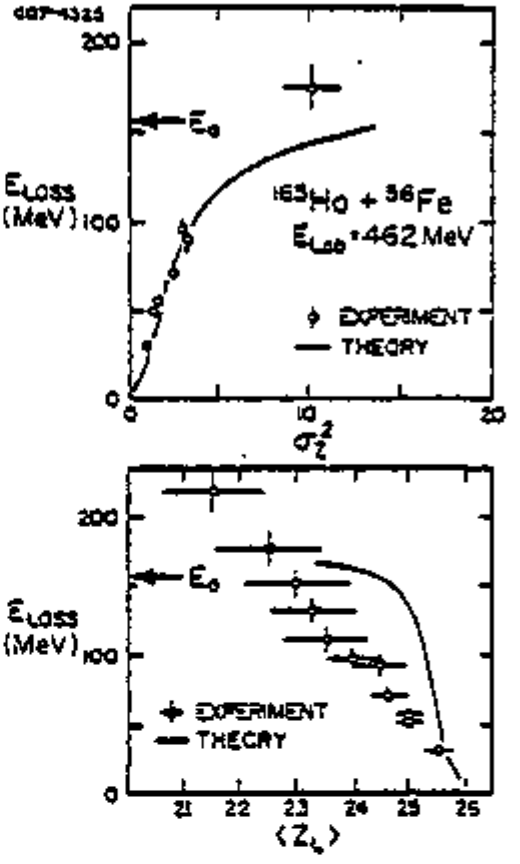

Fig. 5

is no longer negligible, satisfactory agreement with experiment is also obtained with respect to the correlations $\sigma_Z^2(E_{Loss})$ and $\sigma_A^2(E_{Loss})$. As is illustrated by the dashed curves in Fig. 4. representing the dynamical calculations in the classical limit, the Pauli principle is essential to the good agreement between data and the quantal model. For relatively high energy losses (E_{Loss} > 100-150 MeV), predictions of the quantal model deviate somewhat from the data, as is expected from the simplifications made in the model. Only for the reaction $^{238}U+^{238}U$, for which dominating sequential fission of both reaction partners prevents direct measurement of primary Z or A distributions[10], the model results in a poor description of the data.

5. Conclusions

In summary, it has been shown that the previously unexplained bombarding-energy dependence of the correlations between measured energy loss and fragment mass dispersion can be understood in terms of a nucleon exchange mechanism in which the Pauli exclusion principle plays a crucial role. The agreement between data and predictions of a dynamical model based on this approach further emphasizes the dominance of the one-body transport mechanisms operating in damped nuclear reactions, without the necessity to assume further processes of energy dissipation.

1. W.U. Schröder and J.R. Huizenga, Ann. Rev. Nucl. Sci. 27, 465 (1977).
2. W.U. Schröder et al., Report AED-CONF. 1978-007-022.
3. D. Hilscher et al., Phys. Rev. C20, 576 (1979).
   W.U. Schröder et al., Phys. Lett. 71B, 283 (1977); Phys. Rep. 45, 301 (1978).
5. J. Randrup, Nucl. Phys. A307, 319 (1978); ibid. A327, 490 (1979).
6. F. Beck et al., Z. Physik A289, 113 (1978).
7. W.W. Wilcke at al., to be published.
8. A.C. Mignerey et al., to be published.
9. H. Breuer at al., Phys. Rev. Lett. 43, 191 (1979).
10. K.D. Hildenbrand et al., Phys. Rev. Lett. 39, 1065 (1977).
11. H. Sann et al., Report CONF-770602; R. Vandenbosch et al., Phys. Rev. C17, 1672 (1978).
12. A.D. Hoover et al., to be published.
13. M. Dakowski et al., to be published.
14. J. Randrup et al., to be published.
15. W.J. Swiatecki, Report LBL-8950 (1979).

C. Bombarding Energy Dependence of Nucleon Exchange and Energy Dissipation in the Strongly Damped Reaction $^{209}Bi + ^{136}Xe$

Bombarding Energy Dependence of Nucleon Exchange and Energy Dissipation in the Strongly Damped Reaction $^{209}Bi + ^{136}Xe$*

W.W. Wilcke, W.U. Schröder, J.R. Huizenga and J.R. Birkelund
Departments of Chemistry and Physics
Nuclear Structure Research Laboratory
University of Rochester
Rochester, New York 14627

J. Randrup
Nuclear Science Division
Lawrence Berkeley Laboratory
Berkeley, California 94720

I. Introduction

Although considerable progress has been achieved in the understanding of strongly damped reactions at energies several MeV/u above the Coulomb barrier, some important experimental results are not yet clearly understood.

Among these is the degree of correlation between the nucleon exchange and the large energy losses observed. In a model[1] proposed by Swiatecki nucleons upon crossing a window between the colliding nuclei deposit their relative momentum within the recipient nucleus and thus convert kinetic energy of relative motion into intrinsic excitation energy. Although such a mechanism is consistent with experimental data, it has not yet been proven that energy loss induced by nucleon exchange is so dominant a mode of dissipation as to exclude other mechanisms such as the excitation of isoscalar giant resonances. Investigation of the bombarding-energy dependence of reaction phenomena is expected to yield essential information bearing on this question. In the following, experimental evidence is discussed, suggesting nucleon exchange as described by a one-body model to be the major component of the dissipation mechanism.

II. Experimental results

In an experiment[2] similar to the one described by Schröder et al.[3] the system $^{209}Bi + ^{136}Xe$ has been studied by measuring the triple-differential cross section $d^3\sigma/d\Omega dZdE$ at a bombarding energy of E_L=940 MeV. An overview of the data is shown in Fig. 1. The qualitative results are similar to the study[3] of this system at E_L = 1130 MeV, yielding Gaussian Z-distributions with variances σ_Z^2 strongly increasing with energy loss. In Fig. 2, the variances σ_Z^2 are plotted as a function of the energy loss for both bombarding energies. In the framework of one-body nucleon exchange models there is a simple relation between the variance σ_A^2 of the mass distribution and the energy loss, since both are produced by the same nucleon flux. In the classical limit and for peripheral collisions this relation can be written as

$$\ln (T_o/T) = \frac{m}{\mu} \sigma_A^2 \qquad (1)$$

where $T_o = E_{cm} - V_c$ and $T = T_o - E_{Loss}$ are the kinetic energies in the entrance and exit channels, respectively, μ denotes the reduced mass and m the nucleon mass. If a unique proportionality between σ_A^2 and σ_Z^2 exists throughout a reaction, a classical model of nucleon exchange predicts a linear relationship also between

*Work supported by the U.S. Department of Energy.

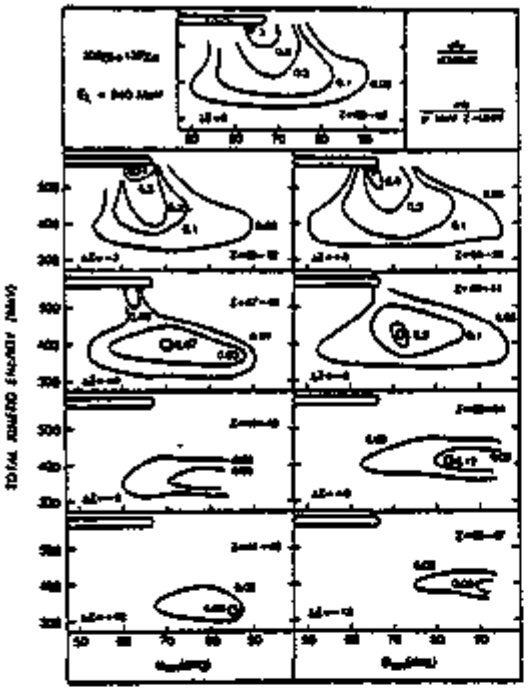

Figure 1

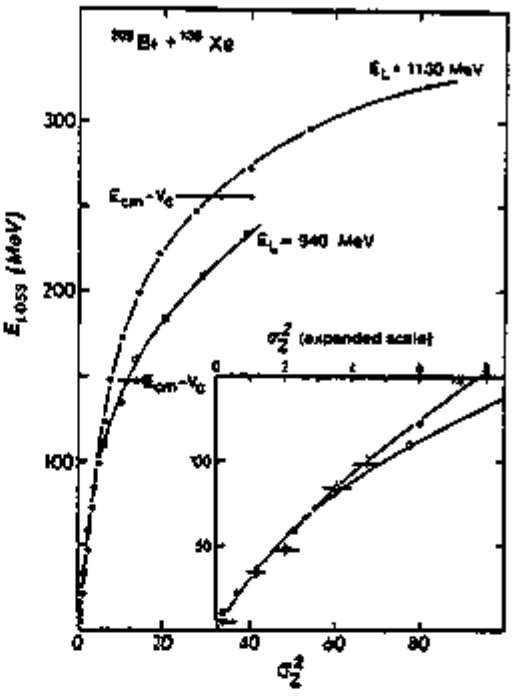

Figure 2

the quantities σ_Z^2 and $\ln(T_0/T)$, with a slope given by $\frac{m}{\mu}\left(\frac{A}{Z}\right)^2$, if the relation $\sigma_A^2 = (A/Z)^2\sigma_Z^2$ is assumed to hold. In Fig. 3 is shown that the data indeed follow straight lines, but quite in contrast to the prediction of Eq. 1, the slopes are strongly dependent on the bombarding energy.

It has been pointed out by Randrup[4] that it is important to incorporate the effect of the Pauli principle into models of nucleon exchange. Since the exclusion principle decreases the nucleon flux, the associated variances are reduced too. On the other hand, it can be shown, that the energy loss rate is not affected, since only nucleons with high relative momentum can participate in the nucleon exchange, which just compensates for the reduced flux. Therefore, the value $\ln(T_0/T)$ for a given σ_A^2 has to be increased by a factor $\alpha \approx j_{class}/j_{q.m.} \geq 1$ with respect to the one given by Eq. 1, in order to account for the Pauli principle. Three quantities determine the magnitude of α: the thermodynamic temperature of the colliding nuclei, the relative position of the Fermi-surfaces for non-identical nuclei and - most importantly - the relative momentun of the nuclei, which displaces the Fermi spheres with respect to each other. A straightforward geometrical calculation of the overlap volume of two intersecting Fermi spheres of equal radius T_F yields a universal energy dependence

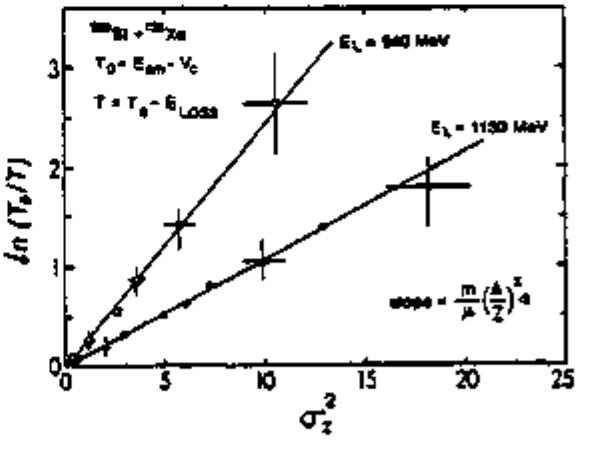

Figure 3

for α:

$$\alpha \approx \frac{2}{3}\left(\mu\, T_F/m(E_{cm} - V_c)\right)^{1/2}, \qquad (2)$$

approximately valid for peripheral collisions of cold nuclei. Consistent with experiment, α increases strongly with decreasing bombarding energy. These results are not restricted to the Xe + Bi system. In Fig. 4 experimental α-values for numerous systems are shown, where the broken line is calculated using Eq. 2. Although this simple model reproduces the qualitative trend of the data, there are still strong systematic deviations of the data from a universal curve. They are mainly associated with reactions induced by ^{56}Fe projectiles.

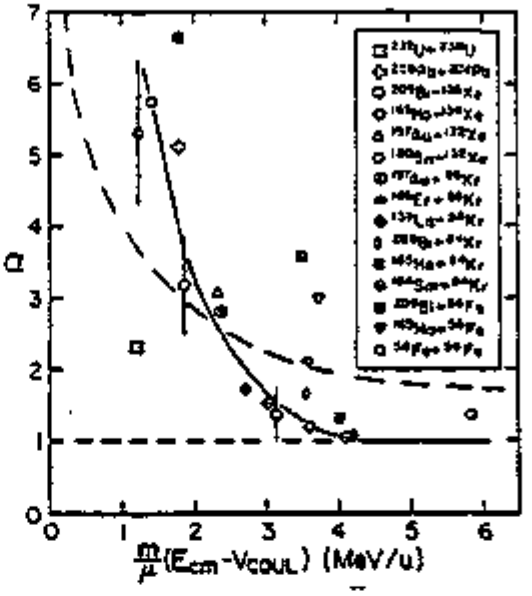

Figure 4

III. Trajectory calculations

The discussion so far has been restricted to peripheral reactions. For more penetrating collisions it is not possible to treat α as a constant during the interaction time. More detailed trajectory calculations have to be performed to allow a meaningful comparison with the data over a wide range of impact parameters. In Fig. 5 results of a partial-wave decomposition of experimental data are compared to a trajectory calculation using a model[5] with four degrees of freedom: the position vector (r,θ) connecting the centers of spherical nuclei and their respective angles of rotation. It should be pointed out, that theoretical values of none of the quantities depicted in Fig. 5 are affected by inclusion of the Pauli principle. Thus the effect of various potentials or a different set of degrees of freedom can be studied decoupled from the effect of the exclusion principle.

As can be inferred from Fig. 5, the calculation is unable to reproduce the large energy losses observed. This is not unexpected, since no deformation degrees of freedom are included, which puts an upper limit on the kinetic energy that can be dissipated. Therefore, an extended model,[6,7] where the two spherical nuclei are joined by a cylindrical neck has been adopted. Its radius and the mass and charge numbers of the projectile-like fragment are treated as three additional degrees of freedom. The proximity formalism and the liquid-drop

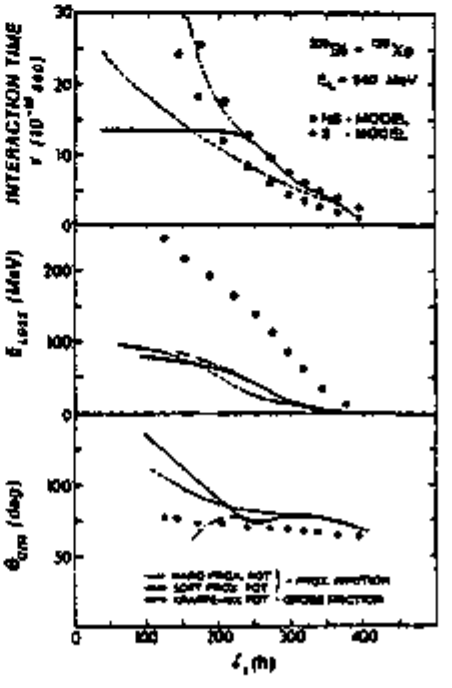

Figure 5

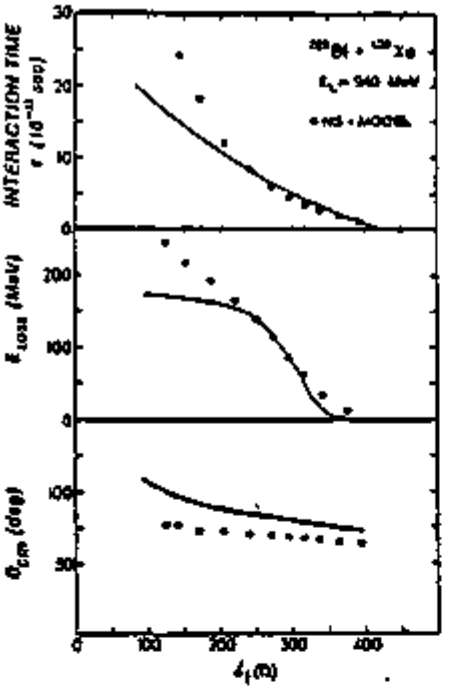

Figure 6

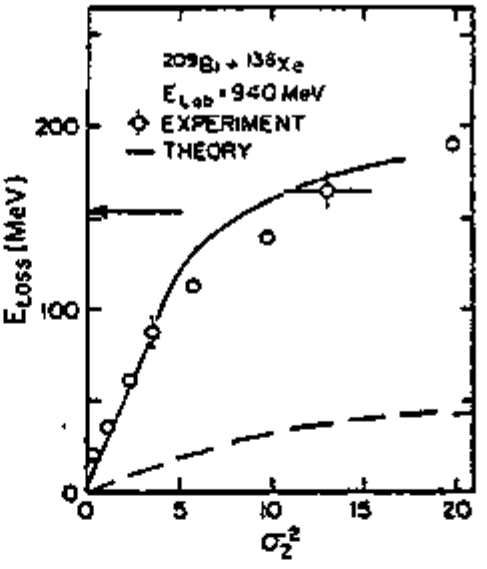

Figure 7

potential energy surface has been used to define the conservative and dissipative forces. In Fig. 6 the results of a calculation (without any adjusted parameters) are shown. Consistent with experiment, the calculated energy loss has strongly increased. The charge variances σ_Z^2 calculated by integrating the time-dependent proton flux for each trajectory are shown in Fig. 7 as a function of energy loss. It can be seen, that the inclusion of the Pauli principle (solid line) leads to good agreement with the data, whereas a classical treatment fails.

In conclusion, it appears, that the previously unexplained bombarding energy dependence between energy loss and fragment charge dispersion can be understood on the basis of a nucleon exchange model, provided the Pauli exclusion principle is taken into account. No necessity is seen to invoke further energy dissipation mechanisms to explain the present data, although such processes cannot be ruled out on basis of this comparison.

---

1. J. Błocki et al., Ann. Phys. 113, 330 (1977).
2. W.W. Wilcke et al., Phys. Rev. C (in press).
3. W.U. Schröder et al., Phys. Rep. 45, 301 (1978).
4. J. Randrup, Nucl. Phys. A307, 319 (1978); ibid. A327, 490 (1979).
5. J.R. Birkelund et al., Phys. Rev. Lett. 40, 1123 (1978).
6. W.J. Swiatecki, Report LBL-8950 (1979).
7. W.U. Schröder et al., Phys. Rev. Lett. 44, 308 (1980).

D. Light-Particle Emission as a Probe of Dissipation and Deexcitation Mechanisms in Heavy-Ion Reactions

LIGHT-PARTICLE EMISSION AS A PROBE OF DISSIPATION AND DEEXCITATION MECHANISMS IN HEAVY-ION REACTIONS†

W. U. SCHRÖDER
Departments of Chemistry and Physics and
Nuclear Structure Research Laboratory
University of Rochester, Rochester, New York 14627

The relevance of studies of light-particle emission associated with damped nuclear reactions for investigating properties of the reaction mechanism, in particular of the energy dissipation mechanism, is discussed. Processes of instantaneous particle emission are reviewed, relating to heavy-ion reactions. Methods are outlined concerning information on the conditions of the intermediate nuclear system at scission revealed in the processes of statistical particle evaporation from the reaction fragments. They are employed in studies of neutron emission in the damped reactions ^{165}Ho+^{56}Fe and ^{165}Ho+^{136}Xe yielding evidence for a rapid thermalization and a relaxation of the mass-to-charge asymmetry of the system. Progress is reported for attempts to achieve a unified description of energy dissipation, nucleon exchange and particle emission in damped nuclear reactions.

I. INTRODUCTION

Extensive experimental and theoretical investigations of damped nuclear reactions at bombarding energies a few MeV/u above the interaction barrier have lead to a much

†Work reported was done in collaboration with J.R. Birkelund, D. Hilscher (HMI, Berlin), A.D. Hoover, J.R. Huizenga, and W.W. Wilcke (Univ. of Rochester); K.L. Wolf (Argonne Nat'l Lab); H.F. Breuer, A.C. Mignerey and V.E. Viola, Jr. (Univ. of Maryland); J. Randrup (LBL, Berkeley).

improved knowledge of the phenomenology of these reactions, which exhibit characteristics of both, fast ($\tau_{INT} \approx 10^{-22}$–$10^{-21}$sec) peripheral collisions and statistical processes[1]. The average values of various macroscopic variables can be adequately described in terms of classical dynamics involving conservative and dissipative forces or of classical transport phenomena. However, there are indications[2-4] that these forces may be dynamical quantities themselves, originating from the response of intrinsic degrees of freedom to changing collective coordinates. Furthermore, certain statistical reaction features may be inconsistent[5,6] with theoretical descriptions not retaining essential quantal properties of the mechanisms involved.

In principle, rather complex investigations are required to assess the microscopic origin of the reaction mechanism, covering many aspects of a damped reaction. Consideration of isolated reaction channels may not only provide limited information but may lead to inadequate conclusions. It is hoped, however, that studies of the most frequent processes induced by damped reactions such as emission of light particles are sensitive to important components of the reaction mechanism. In particular, probabilities, energy and angular distributions of various associated particle species and the mechanisms that lead to their emission are expected to depend on the properties of the dissipation processes playing a crucial role in determining the condition of the interacting nuclei and the nature of their interaction. Depending on the way collective energy of relative motion is transferred to microscopic nucleonic degrees of freedom, the subsequent deexcitation of the system is expected also to follow different patterns.

In the following, several particle-emission mechanisms are discussed that are of potential relevance to damped reactions. Methods outlined are applied in experimental studies of neutron emission in $^{165}Ho+^{56}Fe$ and $^{165}Ho+^{136}Xe$ reactions representing typical examples of damped nuclear interactions. Conclusions to be drawn from such experiments are in support of a damped-reaction mechanism relating intimately energy dissipation and nucleon exchange. Recent progress in understanding damped nuclear collisions is discussed in terms of a quantum-statistical model based on this mechanism.

II. INSTANTANEOUS PARTICLE EMISSION IN DAMPED REACTIONS

The most primary information on the damped-reaction

mechanism may, obviously, be gained from particles emitted while the nuclear interaction is still in progress. Such instantaneous particle emission can, conceivably, occur at any stage of the reaction, before or after local equilibrium is achieved with respect to various degrees of freedom. Different mechanisms may be distinguished with respect to species, angular and energy distributions of the emitted particles, as well as according to their dependence on the projectile-target system, the bombarding energy and the initial angular momentum.

A. Fermi Jets

During the approach phase of the reaction, characterized by a high relative velocity, a small window may have already opened between projectile and target nuclei allowing nucleons with intrinsic momentum $\vec{p}$ and kinetic energy ε to be exchanged (Fig. 1). In the rest frame of the acceptor nucleus,

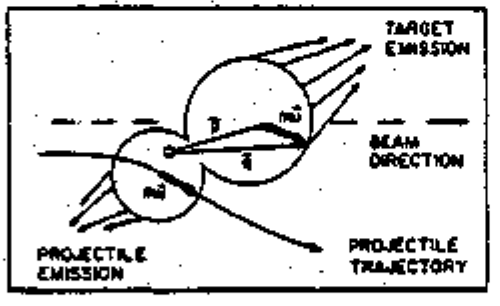

FIGURE 1, Fermi jets

the momentum of the nucleon will be augmented to $\vec{q} = \vec{p} + m\vec{u}$, where $\vec{u}$ is the relative nuclear velocity and m the nucleon mass. Depending on the relative directions of $\vec{p}$ and $\vec{u}$, the nucleon energy

(1) $E = \varepsilon + \vec{p}\cdot\vec{u} - V$

may be sufficiently high to overcome the potential barrier $V = V_N + V_C$ comprised of nuclear and Coulomb parts. With a

certain probability, such particles may be directly ejected from the nucleus. They have been termed "promptly emitted particles" by Bondorf et al[7] and "Fermi jets" by Swiatecki[4] and Robel[8]. Emission mechanisms similar in spirit have also been proposed by Gross and Wilczyński[9].

Kinematical conditions on the bombarding energy E_{Lab} and angular momentum ℓ allowing Fermi-jet emission may be summarized by[8]

$$(2)\quad E_{Lab} \geq \frac{A_P+A_T}{A_T}\left\{V_{Coul}(\bar{R}) + \mu(\sqrt{\bar{V}} - \sqrt{\epsilon})^2\right\}$$

$$\ell \leq \bar{R}\left\{2\mu[E_{cm} - V_{Coul}(\bar{R}) - \mu(\sqrt{\bar{V}} - \sqrt{\epsilon})^2]\right\}^{\frac{1}{2}}$$

where A_P and A_T are projectile and target mass numbers, respectively, μ the reduced mass and V_{Coul} the Coulomb interaction potential evaluated at a typical separation $\bar{R}$. For the reaction ^{165}Ho+^{56}Fe to be discussed below, Fermi-jet emission is energetically possible for $E_{Lab} = 470$ MeV and $\ell \leq 116$.

Neutrons are expected to be the most important Fermi-jet particles, charged-particle emission being drastically reduced due to the Coulomb barrier. Complex particles (e.g. d, α,..) are not considered in this single-particle model. Their emission probability, however, may be estimated, e.g. by using a coalescence model[10]. Due to the term $\vec{p}\cdot\vec{u}$ in Eq. 1 which determines the s.p. energy, the intensity, mean energy and width of the particle energy spectrum increase with relative velocity $u_o = \{2(E_{c.m.} - V_{Coul})/\mu\}^{\frac{1}{2}}$, the width reflecting the nucleon momentum distribution. Fermi-jet particles may be highly energetic in the c.m. system with the highest energies corresponding to forward directions. The angular distributions depend on the details of the dynamical trajectory. In general, a maximum intensity may be expected at angles between the directions of the beam (highest relative velocity) and of the momentum transfer (largest window area), and in the opposite direction.

Complications arise due to two-body interactions beyond the approximations of the single-particle model, increasing in importance with increasing particle energy and nuclear temperature. These processes inhibit primary Fermi-jet emission but induce emission of secondary particles. They can be treated within current pre-equilibrium cascade models (cf. Fig. 2a), e.g. those of Griffin and Blann[11]. Alternately,

as suggested earlier[12] for similar emission processes induced by muons, the trajectory S of (Fig. 2b) of a nucleon inside

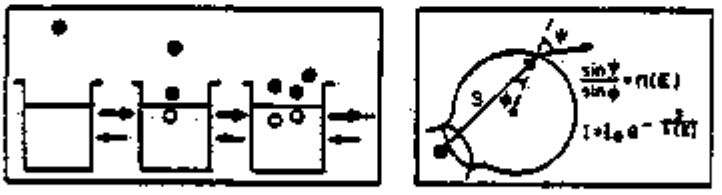

FIGURE 2a, Preequilibrium cascade (above left)
FIGURE 2b, Nuclear refraction (above right)

the nucleus may be considered, along which the nucleon is absorbed due to the optical potential with a rate corresponding to the mean free path $\lambda(E)$. With this rate, secondary particles may be excited in two-body collisions obeying the Pauli principle. At the nuclear surface, nucleons are deflected as given by the real refractive index $n(E)$. With a dynamcial calculation implementing an optical model approach such as described above, Bondorf et al[7] reproduced qualitative features of high-energy neutron spectra observed[13] in the $^{158}Gd+^{12}C$ reaction at E_{Lab} = 152 MeV.

B. Breakup Particle Emission

When rapid deceleration of the relative motion occurs during the approach phase of the reaction, the strongly time-dependent forces may induce breakup of the projectile, a process well studied for light-ion reactions[14]. A light breakup particle with mass m_α and charge Z_α may initially proceed approximately along the original trajectory characterized by the projectile velocity at breakup, somewhat reduced according to the separation energy S_α. The projectile remainder may or may not react further with the target nucleus. Early experiments by Britt and Quinton[15] involving 10.5 MeV/u ^{12}C, ^{14}N and ^{16}O projectiles and heavy targets yielded large cross sections ($\sigma_\alpha \approx 0.3\sigma_R$) mainly of high-

energy α particles focussed in forward directions. These

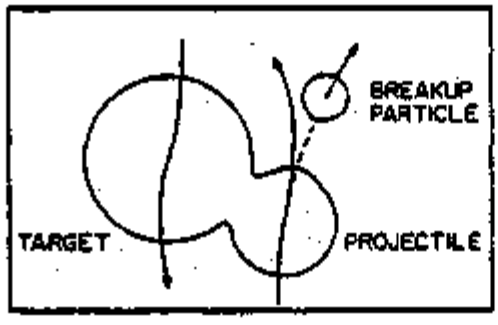

FIGURE 3, Projectile breakup

processes, also cermed "massive transfer" or "incomplete fusion", have attracted renewed attention as demonstrated by recent experiments[16-19] and theoretical attempts[20] to describe breakup of lighter heavy ions in a DWBA approach.

Generally, the energy spectra of light breakup particles are bell-shaped (Fig. 4, Ref. 15) with mean energies $\langle E^{\alpha}_{Lab} \rangle$

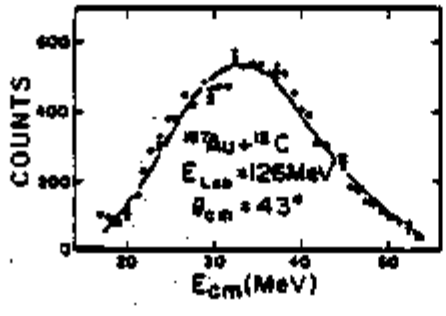

FIGURE 4, Breakup-α particle spectrum

decreasing with increasing emission angle from a maximum given by

$$(3)\quad \langle E^{\alpha}_{Lab}\rangle \leq \frac{m_\alpha}{A_p}\left[1+\left(\frac{A_p}{A_p+A_T}\right)^2\right]E_{Lab} + \frac{e^2}{\bar{R}}\left[Z_\alpha(Z_p+Z_T-Z_\alpha) - \frac{m_\alpha}{\mu}Z_pZ_T\right] - S_\alpha$$

where $\bar{R}$ is the breakup radius. The width reflects the momentum distribution of the particle inside the nucleus. Particle angular distributions are observed to be strongly peaked at angles between the projectile-like fragment reaction angle and the beam direction, which may, however, depend on the particular reaction. Recent observations[21] are consistent with local emission of breakup particles from the side of the projectile facing the target nucleus.

Breakup processes are usually observed to reflect strongly the individuality of the projectile, in particular its cluster structure. Hence, allowance has to be made for structure effects in drawing conclusions on the gross properties of the reaction mechanism.

C. Preequilibrium Emission from Hot Zones

If the energy dissipation mechanisms were sufficiently fast, a transient storage of a high amount of excitation energy in a complicated nuclear state may occur that may classically be described in terms of a localized "hot spot"[22]. Such a state would then be expected to decay into many-particle-many-hole configurations via normal pre-equilibrium cascades allowing emission of fast particles at any stage of equilibration. The classical heat transport equation

$$(4)\quad \frac{\partial}{\partial t}T(\vec{r},t) = \frac{1}{\rho c_p}\vec{\nabla}\cdot(\kappa\vec{\nabla}T(\vec{r},t))$$

for the temperature field $T(\vec{r},t)$, where ρ is the nuclear density, c_p the nuclear specific heat and κ the thermal conductivity, has been considered by Weiner et al[23] and applied to particle emission in damped reactions by Gottschalk et al[24]. High-energy α particles emitted in the reaction $^{58}Ni+^{160}$ at 6 MeV/u[25] have been claimed as evidence for such an emission mechanism.

Experimental information or theoretical predictions on

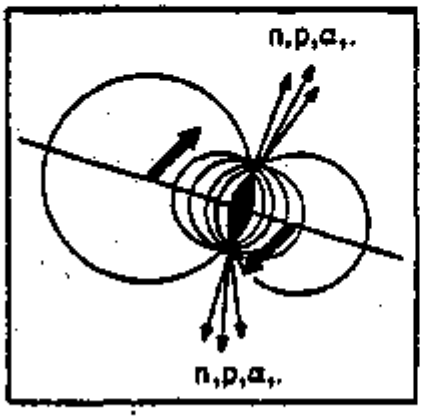

FIGURE 5. Decay of a "Hot Spot"

particle branching ratios and dependence on the bombarding energy are not available for this mechanism. Particle spectra are expected to be characterized by high-energy tails for particles emitted early in the equilibration process. Angular distributions should be peaked forward and backward of the light-fragment reaction angle, with the forward peak corresponding to the highest lab energies.

D. Particle Emission in Neck Rupture

At the final stages of the reaction, particles may be emitted during the rupture of the neck that has presumably been formed in the reaction. Such a process is known from fission studies[26], where long-range α particles are observed to accompany fission with a relatively low ($<10^{-4}$) probability.

Emission probabilities are expected to depend on the fragments' kinetic energies at the instant of scission and their deformations. Particle branching ratios are not well known from fission studies, but α-particle emission is expected to be a relatively significant channel. Particles are presumably produced with relatively low initial kinetic energies by such a mechanism and are emitted in directions approximately perpendicular to the system's symmetry axis

(Fig. 6). The final kinetic energies of charged particles depend on the balance between the initial particle and fragment kinetic energies determining the effective Coulomb field and the duration of acceleration.

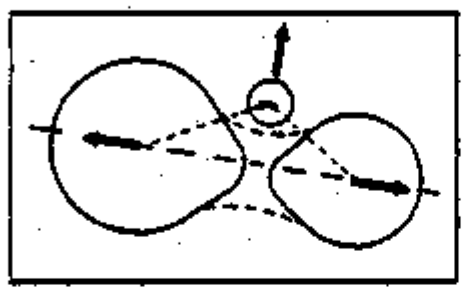

FIGURE 6, Particle emission in scission

Among the mechanisms of instantaneous particle emission discussed above, so far only breakup-induced processes appear to be experimentally well established[15-19,21] and are treated[20] in conventional quantal reaction theory. Other mechanisms still lack a profound theoretical basis or experimentally unambiguous verification.

While instantaneous emission may contribute to the total light-particle cross section associated with damped reactions, a majority of light particles is expected to be emitted from the highly excited final fragments at times sufficiently long to ensure their complete separation, full acceleration by the Coulomb field and complete equilibration of the excitation energy. Relevant time scales are plotted in Fig. 7 vs. the equilibrium nuclear temperatures. Damped-interaction times τ_{INT} as derived[27] for the reaction $^{165}Ho+^{56}Fe$ at E_{Lab}=476 MeV using a classical model are seen to range between $\sim 10^{-22}$ and several 10^{-21}sec for equilibrium temperatures up to 2.5 MeV attained in the reaction. They are compared to the much longer times $\tau_p \approx 5.10^{-23} \exp(13\ MeV/T)$ sec necessary[28], on the average, for particle evaporation from a compound nucleus. Of great importance for the evolution of a damped reaction and several

instantaneous emission processes is the thermal relaxation time τ_R, a time characteristic for the damping of a thermal distortion of nuclear matter at a specified temperature.

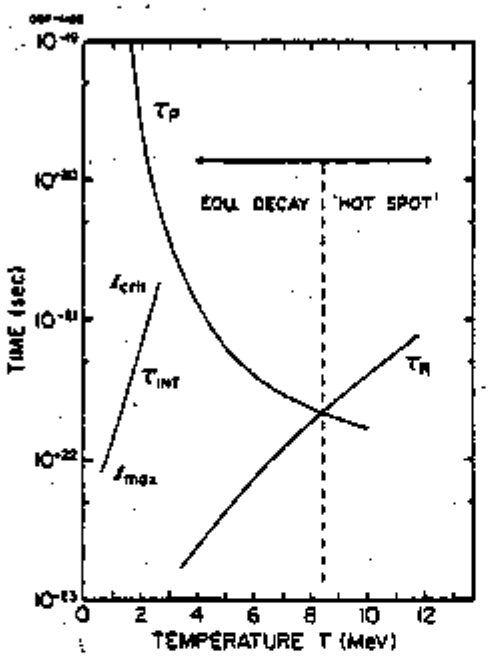

FIGURE 7, Characteristic time scales for the reaction $^{165}Ho + ^{56}Fe$

This time has been calculated[29] in a single-particle model to be given by the product of the nucleon transit time R/v_F, where R is the nuclear radius and v_F the Fermi velocity, and the number R/λ of nucleon-nucleon collisions:

$$(5) \quad \tau_R(T) \approx R^2/(v_F\lambda(T))$$

Here, the mean free path λ is temperature-dependent, because the exciton transition rates[11] are.

Obviously, for equilibrium temperatures accessible to damped reactions, thermal relaxation times are extremely short such that immediate response of the nuclear system is expected for relatively weak thermal distortions as may be imposed, for example, by the exchange of a nucleon. Only

for temperatures beyond 7-8 MeV are these relaxation times τ_R comparable to compound-nucleus evaporation times τ_p, and a significant probability for light-particle emission (pre-equilibrium emission in the normal notion) is expected at the early stages of the intranuclear cascade leading eventually to full equilibration of the thermal excitation energy remaining in the nuclei. However, whether or not the relation $\tau_R \ll \tau_{INT} \ll \tau_p$ between the various time scales is established in a damped reaction as depicted in Fig. 7 depends on crucial details of the energy dissipation mechanism, e.g. the presence or absence of localized zones of high temperature.

Studies concerned with the nature of dissipation and deexcitation mechanisms should then include the establishment of conditions associated with instantaneous or preequilibrium emission of light particles as revealed by the identity of these particles, their energy and angular distributions and their relation to the kinematic properties of the nuclear system. In addition, information on the damped reaction may be obtained from studying particle evaporation from the final fragments as exemplified in the following.

III. PARTICLE EVAPORATION FOLLOWING DAMPED NUCLEAR REACTIONS

As discussed above, particle evaporation occurs, on the average, long after the damped nuclear interaction has ceased but reveals various conditions of the intermediate system at scission time, such as fragment excitation, deformation and spin alignment. The statistical decay of the fully equilibrated system provides a powerful investigative tool because the dependence of this process on the nuclear properties is well known[30].

Particle branching ratios are determined by available phase space or (spin-dependent) level densities ρ according to

$$(6)\quad \Gamma_\nu(E^*,I) \sim (2s_\nu+1)\sum_{\ell_\nu=0}^{\infty}\sum_{J=|I-\ell_\nu|}^{I+\ell_\nu}(2J+1)$$

$$\int_0^{E^*-E_J-B_\nu} d\varepsilon_\nu\ \rho(E^*-E_J-B_\nu-\varepsilon_\nu)T_\nu(\ell_\nu,\varepsilon_\nu)$$

where the particle widths Γ_ν depend on excitation energy

E^* and spin I of the initial nucleus, the properties of the light particle given by spin s_ν, angular momentum ℓ_ν, kinetic energy ε_ν, binding energy B_ν and transmission coefficient T_ν. Properties of the final nucleus enter mainly via its yrast line E_J, the minimum excitation energy of levels at a given spin J. The energy spectrum $dN/d\varepsilon$ of particles in an evaporation chain is approximately given by[31]

$$(7)\quad dN/d\varepsilon \approx 2\langle M\rangle (\pi T_*^3)^{-1/2}\, \varepsilon^{5/11} \exp(-\varepsilon/T_*)$$

where $\langle M\rangle$ is the mean multiplicity and $T_*=(11/12)T$ an effective mean temperature, only slightly smaller than the temperature $T\approx(E^*/a)^{1/2}$ of the initial nucleus. The level density parameter a is approximately proportional to the nuclear mass: $a\approx A/8$.

The angular distributions of evaporation particles in the rest frame of a nucleus with spin I aligned perpendicular to its direction of motion ($\theta_{cm}=0$) is predicted[30] to be symmetric around $\theta_{c.m.}=\pi/2$:

$$(8a)\quad W(\theta_{c.m.}) \sim 1 + \frac{1}{3} mR^2 \frac{\hbar^2\langle I^2\rangle}{2\mathfrak{I}^2 T} P_2(\cos\theta_{c.m.}) \quad \text{for } \frac{\hbar^2 I\ell}{2\mathfrak{I}} \ll T$$

$$(8b)\quad W(\theta_{c.m.}) \sim 1/\sin\theta_{c.m.} \quad \text{for } \frac{\hbar^2 I\ell}{2\mathfrak{I}} \gg T$$

where m is the particle mass, R the radius of the nucleus, $\langle I^2\rangle$ its mean-square spin and $\mathfrak{I}$ its moment of inertia. In the limit of strong coupling between nuclear spin I and angular momentum ℓ of the emitted particle, the classical relation Eq. 8b for isotropic emission results. If the direction of the nuclear spin produced in a reaction is restricted, for example, to be perpendicular to the reaction plane selected by an experiment, the angular distribution of the emitted particles will be isotropic within this plane but vary with the out-of-plane angle $\phi_{c.m.}$ approximately according to

$$(9)\quad W(\phi_{c.m.}) \sim 1 + \frac{1}{2} \left(\frac{\hbar}{2\mathfrak{I}T}\right)^2 \langle I^2\rangle\langle \ell^2\rangle \cos^2\phi_{c.m.}$$

The mean squared angular momentum $\langle \ell^2\rangle$ carried away by a particle of kinetic energy ε

$$(10)\quad \langle \ell^2\rangle \sim m\, R^2(\varepsilon - V_c)/\hbar^2$$

is largest for fast, heavy particles, the measurement of which is then most sensitive to the size and alignment of the nuclear spin. For this reason, angular distributions of evaporated neutrons are only weakly dependent on spin alignment.

Laboratory intensity patterns of particles evaporated from fully accelerated fragments are quite conspicuous as demonstrated in Fig. 8 for neutron evaporation from final fragments from the reaction $^{165}Ho+^{136}Xe$ at E_{Lab}=1130 MeV.

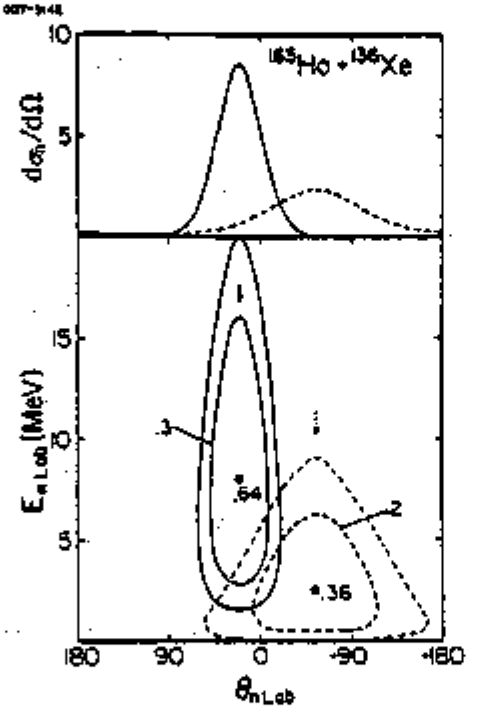

FIGURE 8, Cross section of neutrons from light (full curves) and heavy (dashed curves) fragments, plotted vs. lab angle and energy

In the calculation of the double-differential cross section $d^2\sigma/dE_n d\Omega$ plotted at the bottom of Fig. 8 vs. neutron lab energy E_{nLab} and emission angle θ_{nLab}, complete conversion of kinetic energy loss into intrinsic heat, establishment of thermal equilibrium before scission, and isotropic emission

in the rest frames of the fully accelerated fragments were assumed. Neutrons from the light fragment (full curves) are higher in energy and confined to a narrower angular range around the light-fragment emission angle (solid arrow) than those from the slow-moving heavy fragment. Obviously, there are kinematical regions allowing an unambiguous identification of the emitting fragment.

Because of the good separation, several kinds of information may be gathered for both reaction fragments separately: Experimental particle-fragment angular correlations may be used to determine the fragment's spin alignment (Eqs. 8, 9). The final fragment temperatures can be inferred from the particle energy spectra according to Eq. 7. Furthermore, the particle multiplicity distributions give a measure of the excitation distribution of the fragments.

If thermal equilibrium is reached during the reaction, the temperatures of light (L) and heavy (H) reaction partners are expected to be approximately equal: $T_H \approx T_L$. In contrast, if "hot spots" survive the reaction, $T_L > T_H$ may result. However, dynamical deformations developing during the reaction may lead to $T_L \neq T_H$, even if the system was thermalized at all times. In general, the total excitation energy $E^* = E_L^* + E_H^*$ will be smaller than the measured kinetic energy loss, because of the rotational energies acquired until scission occurs, that do not convert into intrinsic heat and are, subsequently, only partially removed by particle evaporation.

How strongly the moments of the particle multiplicity distributions are correlated with those of the excitation function may be demonstrated using a simplified evaporation model[32] neglecting spin effects. It is based on the assumptions that the energy $E^* - S_i$ available for evaporation, where S_i is the cumulative separation energy of i particles, is distributed among the particles with probabilities according to the particle energy spectra as given by a Maxwellian characterized by a mean temperature T. The probability W_i for emitting <u>at least</u> i particles from a nucleus at excitation energy E^* is easily calculated:

$$(10) \qquad W_i(E^*) = 1 - \left\{ \sum_{n=0}^{2i-3} \frac{1}{n!} \left(\frac{E^* - S_i}{T} \right)^n \right\} \cdot \exp\left[- \frac{E^* - S_i}{T} \right]$$

for $i \geq 2$. Trivially, $W_0(E^*) \equiv 1$, and $W_1(E^*) = \Theta(E^* - S_i)$. If $f(E^*)$ is the excitation energy distribution, one obtains for the particle multiplicity distribution

$$(11)\quad M(i) = \int_0^{\infty} dE^* \, f(E^*)[W_i(E^*) - W_{i+1}(E^*)]$$

Fig. 9a shows the calculated dependence of the mean neutron multiplicity <M> on the excitation energy E_i^* of each of the nuclei ^{165}Ho and ^{56}Fe. Binding energies were taken from the liquid-drop model corrected for shell effects. <M> is observed to be almost independent of the width of $f(E^*)$.

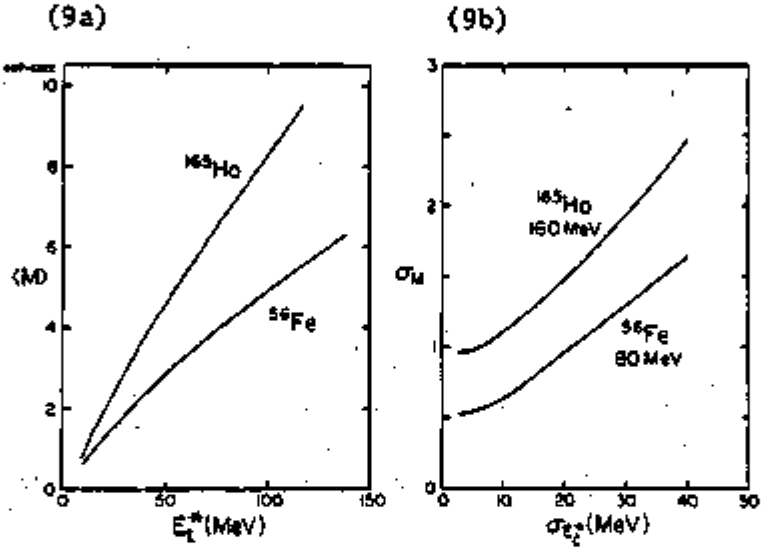

FIGURE 9, Correlation between mean values (a) standard deviations (b) of neutron multiplicity and excitation energy distributions

A similarly strong correspondence is observed between the standard deviations σ_M and σ_E^* of multiplicity and excitation distributions, respectively. This is illustrated in Fig. 9b for ^{165}Ho and ^{56}Fe nuclei at the indicated mean excitation energies.

These correlations are strongly dependent on the identity (A,Z) of the emitting nucleus, a dependence that can be amplified by considering relations between appropriate quantities corresponding to the two fragments of a damped reaction, where the total A and Z is fixed. For example, in Fig. 10 the ratio of the mean neutron multiplicities of Ho and Fe

fragments is plotted vs. the energy loss for the reaction $^{165}Ho+^{56}Fe$. The curves are labelled according to the A/Z ratio of the Fe fragment and its share of the total energy loss. The initial sharp drop at small energy losses is due to a threshold effect and depends on the binding energies and the width of the excitation function. For larger energy losses, a relatively constant value of the multiplicity ratio results that approaches the value of the mass ratio at very high temperatures: $\langle M_H\rangle/\langle M_L\rangle \rightarrow A_H/A_L$. In general, however, these two quantities are quite different.

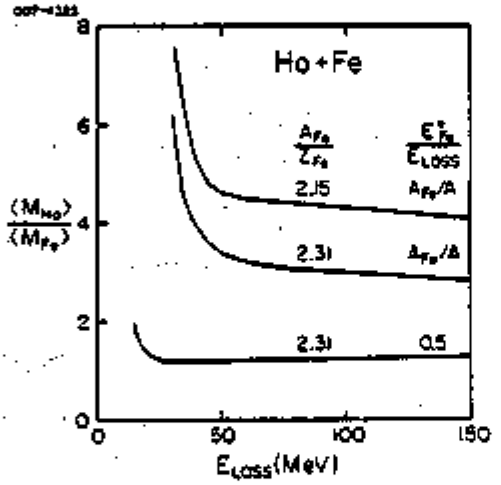

FIGURE 10, Ratio of mean neutron multiplicities from the reaction $^{165}Ho+^{56}Fe$ for different A/Z ratios and fractions E^*/E_{Loss} of the light fragment

IV. NEUTRON EMISSION IN THE DAMPED REACTIONS $^{165}Ho+^{56}Fe, ^{136}Xe$

The methods described in the preceding section were applied in a study[33] of neutron emission following the reaction $^{165}Ho+^{56}Fe$ addressing the questions:

(a) Is there direct or indirect evidence for instantaneous particle emission?

(b) Is thermal equilibrium achieved during the damped reaction?

(c) Is equilibration of the mass-to-charge asymmetry achieved?

A schematics of the experimental setup used in the fragment-neutron coincidence measurements is shown in Fig. 11.

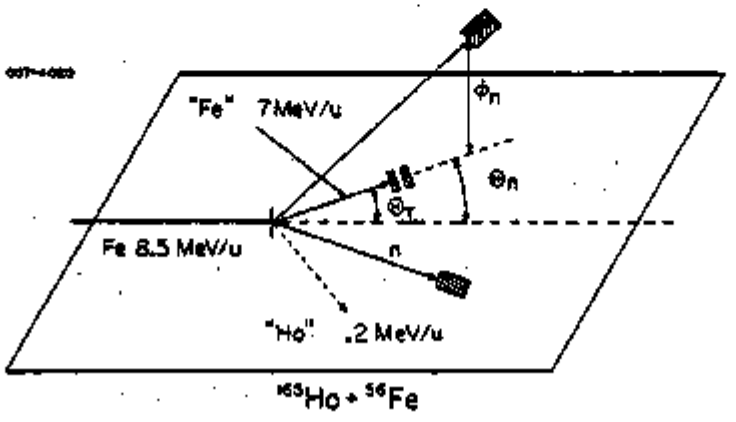

FIGURE 11, Schematic setup of fragment-neutron coincidence measurement

Six neutron detectors surrounded a thin-walled scattering chamber containing target and a solid-state telescope used to measure light reaction fragments and to provide a start signal for the neutron time-of-flight measurement. One of the neutron detectors was placed out of plane (θ_n=0°, ϕ=85°) to give an estimate of the out-of-plane anisotropy. The flight distance was ∿ 70 cm, and time resolutions of 1-1.5 nsec were achieved. Detection efficiencies were calculated[34], but verified by comparison with experiments[35].

Fig. 12 shows the resulting coincident laboratory neutron angular and energy distributions, for a fragment detection angle of θ_T=23°. The curves represent evaporation calculations with the code MBII[36] based on the assumptions that the kinetic energy loss was completely converted into excitation energy, that the system reached thermal equilibrium, and that isotropic evaporation occurred only after full acceleration of the fragments. Obviously, the experimental data are consistent with these assumptions: neutrons from the light fragment are emitted in a narrow cone around

its reaction angle and characterized by relatively high mean lab energies, while those associated with the heavy fragment are less focussed and less energetic. No positive evidence for any significant number of high-energy, forward-peaked neutrons was found that could have been attributed to instantaneous particle emission.

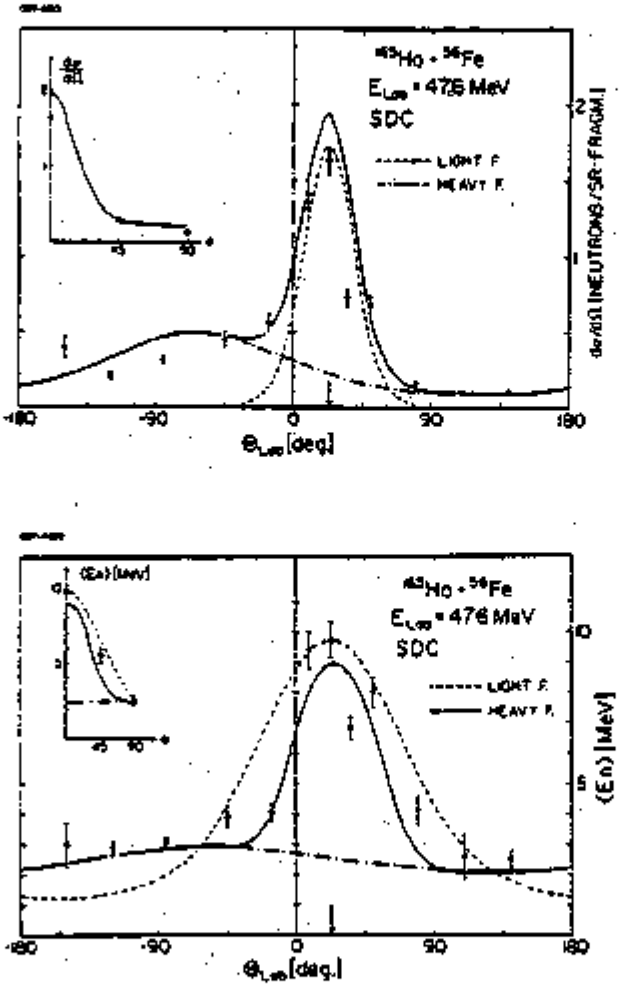

FIGURE 12, Laboratory angular distribution of neutron cross section (top) and mean energy (bottom). Curves are results of evaporation caculations

These assumptions were then used in an iterative, event-by-event analysis of the data as a suitable starting point for the transformation into the rest frames of the light and heavy fragments. Measurements at angles close to the reaction angles of the light and heavy fragments lead to predictions of neutron energy spectra at other angles, using the above assumptions, that can be compared to the data. In Fig. 13, neutron energy spectra in the rest frames of the light and heavy fragment, respectively, are plotted for a light-fragment detection angle θ_T=20°, averaged over fragment-Z values between 20 and 30 and energy losses greater than 36 MeV. As can be seen, the curves representing evaporation spectra, based on the assumptions discussed, reproduce the data very well both, with respect to spectral shape and absolute magnitude. There is again no positive evidence for high-energy neutron emission in addition to the evaporation process. Upper limits for such neutrons have to be placed around 5%.

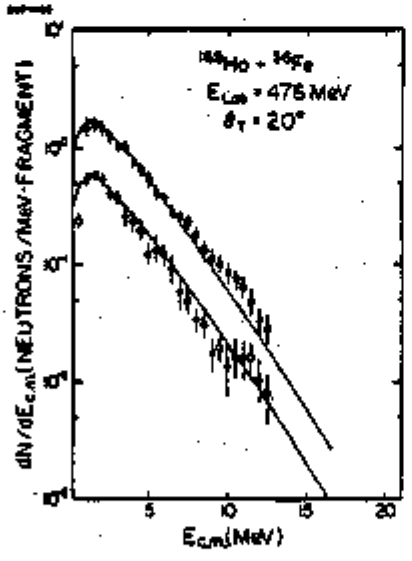

FIGURE 13, Center-of-mass neutron energy spectra from light (circles) and heavy (squares) fragments. Curves represent evaporation calculations

The assumption of isotropic neutron emission resulting in the calculations shown in Fig. 13 is consistent with measurements at all neutron angles within the reaction plane. However, results of the out-of-plane detector suggest a $\phi_{c.m.}=0°/90°$ anisotropy of 0.2±0.1. Although not very accurate, this measurement is consistent with fully aligned fragment spins (cf. Eq. 9) based on those transferred in a rolling or sticking situation, where anisotropies of 4% to 12% are expected.

In Fig. 14, the dependence of nuclear temperatures of the light (circles) and heavy (squares) fragments on the total kinetic energy loss is shown as obtained from the neutron spectra. As can be seen from Fig. 14, temperatures of light and heavy fragments are equal for each energy loss, indicating thermal equilibration within the interaction time τ_{INT}. Despite relatively large error bars, equal division of the excitation energy between the fragments corresponding to temperatures given by the dashed (L) and dashed-dotted (H) curves,

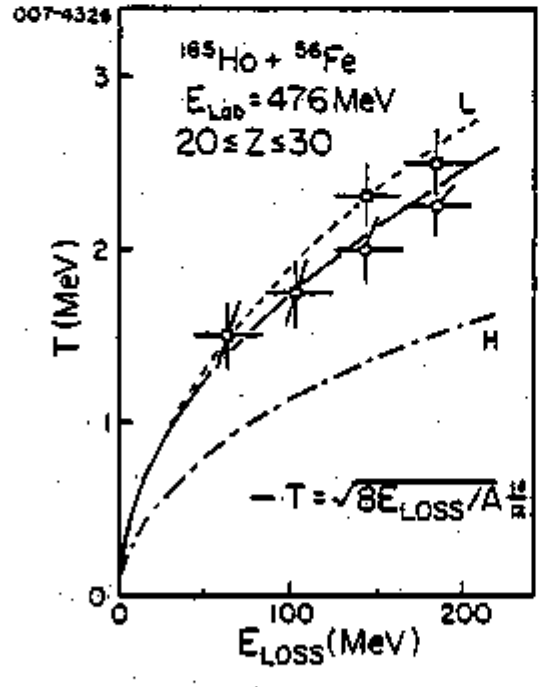

FIGURE 14, Final temperatures of light (circles) and heavy (squares) fragments. Dashed curves correspond to equal shares of the total excitation energy

can be ruled out. Estimates[27] for interaction times yield then upper limits for thermal relaxation times given in Table 1. Furthermore, from the agreement of data with the Fermi-gas equation of state (full curve in Fig. 14), it may be concluded that most of the kinetic energy dissipated in the reaction goes into intrinsic heat of the nuclei, with the exception of rotational energy estimated to be less than 15-18 MeV at all energy losses. This finding corroborates the lack of significant intensities of high-energy, non-evaporative neutrons.

TABLE 1 Relaxation times τ_R

E_{Loss}(MeV)	$\tau_R(10^{-22}$sec)
60	$\leq$ 2
100	$\leq$ 5
200	$\leq$ 20

Fig. 15 shows at the bottom the dependence of the measured neutron multiplicity M_n on the experimental Z of the fragment. Triangles connected by a dashed curve represent evaporation calculations using the code MBII[36], assuming thermal equilibrium, the composite system's ratio A/Z=2.38 for all fragments and angular-momentum dissipation according to the sticking limit. Good agreement between calculations and data is observed, except for Z values close to that of the projectile, where agreement is achieved upon relaxing the unrealistic sticking requirement. A discontinuity of the data at symmetry ($Z\approx 46$) is understood in terms of charged-particle evaporation from the light fragments.

Somewhat more instructive is the dependence of multiplicities and their ratio on the kinetic energy loss depicted in Fig. 16. As expected from calculations shown in Fig. 10, experimental values of the ratio M_H/M_L of the mean multiplicities exhibit an initial sharp decrease with increasing energy loss before reaching a relatively flat region. The latter is well described by evaporation calculations using MBII with a fragment A/Z ratio of 2.38 and fragment spins characterized by a linear approach to the rolling condition up to an energy loss of $\sim$ 130 MeV, whereafter rolling is

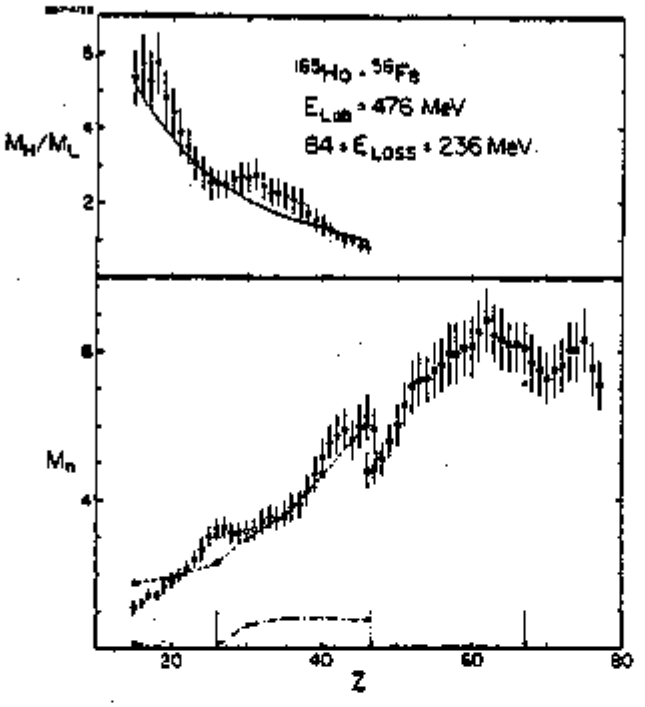

FIGURE 15, Neutron multiplicity (bottom) and multiplicity ratio vs. fragment Z. Triangles and dashed curve represent evaporation calculation. Crosses give predicted charged-particle multiplicity

always assumed. The bump occurring in the experimental M_H/M_L ratio around $E_{Loss} \sim 180$ MeV associated with a depression of the light fragment's multiplicity (circles in the bottom part of Fig. 16), may be due to dissipation of increasing fractions of the angular momentum. The sensitivity of the multiplicity ratio M_H/M_L to the A/Z ratio of the fragments is illustrated in the top part of Fig. 16 by open triangles corresponding to A/Z values given by the valley of β-stability. Detailed calculations for an energy loss of 100 MeV indicate a range $2.26 \leq A/Z \leq 2.38$ compatible with data.

The range of pre-evaporation A/Z values of the fragments yielding agreement between calculations and data is consistent with values where minima in the potential-energy surface

occur calculated from the droplet model including shell corrections. Fragment A/Z ratios are fairly well removed from those of projectile and target, and one might term this feature "equilibration" of the mass-to-charge asymmetry, which occurs at least at times as short as $(4-8)\cdot10^{-22}$sec. However, it should be realized that the fragment A/Z value is a dynamical quantity governed by the action of dynamically changing driving forces. Due to the lack of knowledge about these forces, an equilibrium A/Z value cannot be determined except via adoption of a model.

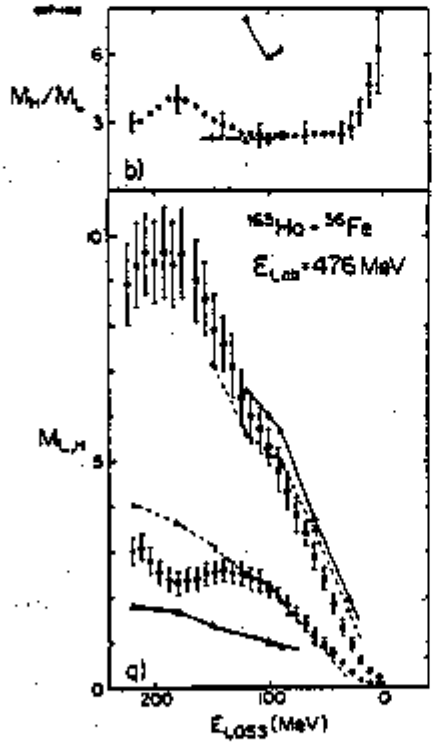

FIGURE 16, (a) Multiplicities of neutrons from light (circles) and heavy (squares) fragments vs. energy loss. (b) Multiplicity ratio. Open and full triangles represent evaporation calculations with different fragment A/Z ratios.

The most important findings of the study of neutron emission in the reaction $^{165}Ho+^{56}Fe$ described above are, as far as a preliminary analysis indicates, corroborated by a similar experiment on the reaction $^{165}Ho+^{136}Xe$ at E_{Lab}=1130 MeV. They can be summarized as follows:

(1) Kinetic energy dissipated in a damped reaction remains in the double-nucleus system and is converted mainly into intrinsic heat.

(2) Thermal equilibrium is reached within the interaction time. Relaxation times may be as short as 2.10^{-22}sec for relatively low energy losses but may be a factor of 10 longer than this for very large energy losses.

(3) No positive evidence is found for non-statistical high-energy neutrons. However, because of the large number of neutrons in the evaporation cascade, only a relatively high upper limit can be placed for such events, although a significant competition of these processes with other dissipation and deexcitation mechanisms can be ruled out.

(4) Based on a model-dependent definition, it is concluded that the mass-to-charge asymmetry also equilibrates during the interaction time. However, the corresponding relaxation times may, in reality, be much smaller than estimated values of $(4-8)\cdot10^{-22}$sec, since it takes the exchange of only a few nucleons to achieve A/Z equilibrium.

V. ENERGY DISSIPATION AND NUCLEON EXCHANGE

From the results presented in the preceding sections, one concludes that for nuclear reactions a few MeV/u above the barrier, the dissipation mechanism leads to a gradual heating of the nuclei involved to temperatures of the order 2-3 MeV. These temperatures are small compared to the Fermi energy $\epsilon_F \approx 37$ MeV, such that nuclear systems are expected to be well describable in terms of single-particle models. The s.p. occupation numbers $f(\epsilon)$ almost correspond to those of a degenerate Fermi gas of nucleons moving freely in the average potential. A relatively long nucleon mean free path λ, of the order of the nuclear radius R, leads one to expect the nucleus to respond as a whole to small perturbations such as imposed by the exchange of a nucleon between the interacting nuclei:

Experimental fragment mass distributions and their evolution with the energy loss suggest that many nucleons may be exchanged in a damped reaction on a similar time scale as applicable to energy dissipation. From light-ion reactions it is known that nucleon transfer induces kinetic energy loss

due to the difference in ground-state Q values and recoil effects. It is then natural to ask what fraction of the energy dissipated in damped reactions is due to the exchange process itself.

A classical model[1] developed earlier, was indeed able to explain most of the dissipated energy as being due to the recoil induced by nucleon exchange, at least for relatively high bombarding energies of > 3-4 MeV/u above the barrier. However, the observed systematic dependence of experimental correlations between energy loss and mass dispersion on the bombarding energy was not predicted by the model and induced suggestions of additional dissipation mechanisms, resulting in a mere parameterization of the data.

In this unsatisfactory situation, a relatively simple quantal transport model for energy dissipation and nucleon exchange introduced by Randrup[6,37] offered the chance for a more meaningful test of the basic mechanism. This model treats the interacting system as two almost degenerate Fermi-Dirac gases in communicating spherical containers. The current of nucleons transferred from nucleus A to nucleus B is given by

$$(12)\quad N_{BA} = \int d\varepsilon\, N'(\varepsilon)\, f^A[1 - f^B],$$

an integral over the bulk current $N'(\varepsilon)$ of nucleons from single-particle orbits at energy ε, accounting for the occupancy of these orbits in accordance with the Pauli principle. The occupation probabilities

$$(13)\quad f^A(\varepsilon, \vec{p}) = \left\{1 + \exp\left[(\varepsilon - \varepsilon_F - 1/2(F_{BA} - \vec{u}\cdot\vec{p}))/\tau\right]\right\}^{-1}$$

depend on the direction of the nucleon momentum $\vec{p}$ with respect to the relative velocity $\vec{u}$ of the two nuclei. ε_F is the mean and F_{BA} the difference of the two Fermi energies, τ is the nuclear temperature. $\omega_{BA} = F_{BA} - \vec{u}\cdot\vec{p} = -\omega_{AB}$ is the energy lost or gained in a transfer, depending on its direction. Averaging over the possible directions of the nucleon momenta in the Fermi surface yields an energy dissipation rate

$$(14)\quad -\dot{E} \approx \langle N_{BA}\omega_{BA} + N_{AB}\omega_{AB}\rangle_F \approx N'(\varepsilon_F)\left\{F_{BA}^2 + \frac{p_F^2}{4}\left(2u_n^2 + u_t^2\right)\right\}$$

where u_n and u_t are the velocity components normal and tangential, respectively, to the interface area of the two nuclei. Similarly, one obtains for the mass drift and diffusion coefficients

$$(15)\quad v_A = \langle N_{BA} - N_{AB} \rangle_F \approx N'(\varepsilon_F)\ F_{BA}$$

$$D_A = \langle N_{BA} + N_{AB} \rangle_F \approx N'(\varepsilon_F)\ \tau^*$$

respectively. Here $\tau^* = \tau\langle(\omega_{AB}/2\tau)\coth(\omega_{AB}/2\tau)\rangle_F$ denotes the energy region around the Fermi surface contributing to the transfer. This "effective temperature" τ^* depends on both, the dissipated and the kinetic energy still available, as is demonstrated in Fig. 17 showing the results of a dynamical calculation[37] for the reaction $^{209}Bi+^{136}Xe$ at two bombarding energies. For high energy losses, τ^* approaches the nuclear temperature τ with a rate depending on the bombarding energy.

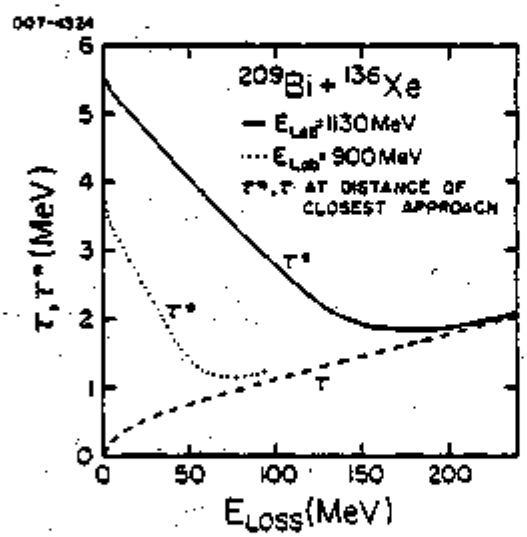

FIGURE 17, Effective temperature τ^* and nuclear temperature τ vs. energy loss, calculated for distance of closest approach.

Of interest to the classical model is the quantity $\alpha = -(\mu/m)\ d(\ln \Sigma)/d\sigma_A^2$, related to the slope of the experimental correlations $\Sigma_{Loss}(\sigma_A^2)$ exhibiting the previously unexplained bombarding-energy dependence. For systems with $F_{BA} \approx 0$, i.e. a negligible driving force, and peripheral collisions, Eqs. 14 and 15 predict a dependence

$$(16) \quad \alpha \approx \frac{T_F}{2\tau^*}$$

where T_F is the Fermi kinetic energy. This relation predicts an approximate universal bombarding-energy dependence of α for systems with $F_{BA} \approx 0$. Values of α increasing strongly with decreasing bombarding energy are predicted, a behavior observed experimentally. Different systems at similar bombarding energies per nucleon above the barrier exhibit different values of α to the extent that the corresponding values of F_{BA} differ.

The bombarding-energy dependence of the relation between nucleon exchange and energy dissipation as reflected by Eq. 16 is entirely due to the Fermion nature of the exchanged nucleon. The classical expressions derived recently are regained in the limit where the Pauli Principle is relaxed. Because the currents involved in the models are form factors, dynamical calculations were performed for a dinuclear system described by two spheres connected by a cylindrical neck. Conservative and dissipative forces as well as nucleon transport coefficients as given by this extension of the one-body transport model were used to describe an average dynamical path of the

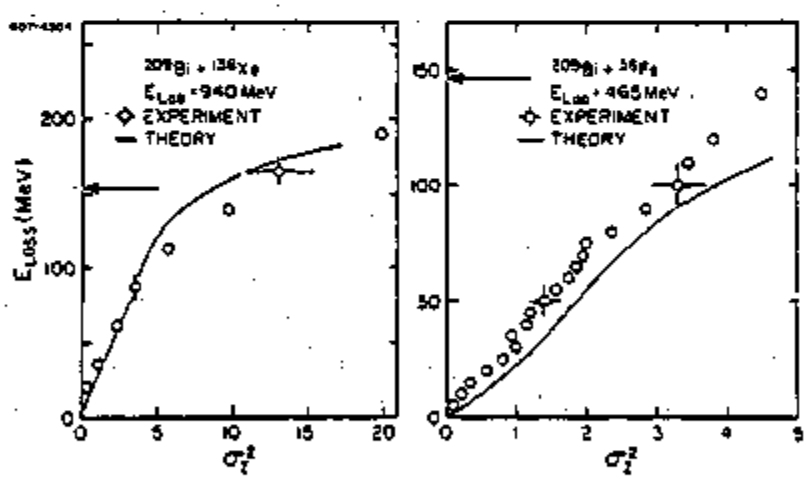

FIGURE 18, Comparison of results of dynamical calculations to experimental correlations $E_{Loss}(\sigma_t^2)$. Arrows denote initially available kinetic energy

system. Typical predictions of the model are compared in Figs. 18 and 19 to data on the reactions $^{209}Bi+^{136}Xe$ (940 MeV), $^{209}Bi+^{56}Fe$ (405 MeV) and $^{165}Ho+^{56}Fe$ (462 MeV), respectively. Similar calculations have been done for a variety of systems and bombarding energies yielding a satisfactory description of the data emphasizing the potential of the model and the necessity to consider quantal effects in damped nuclear reactions.

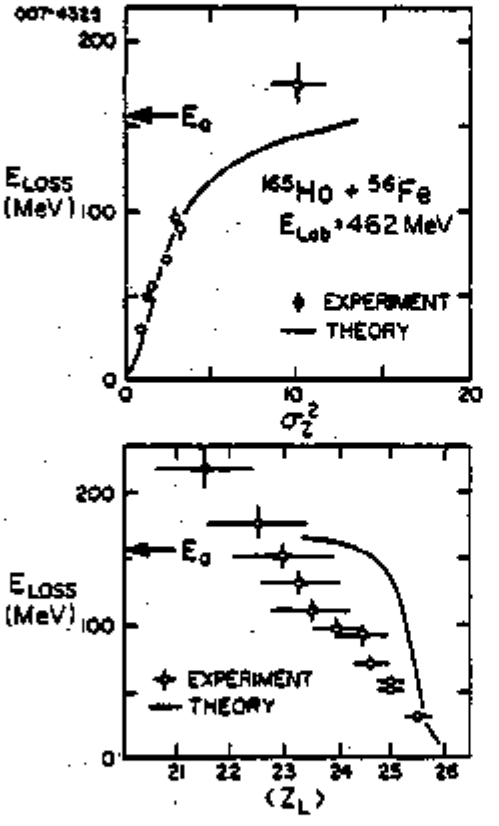

FIGURE 19, Comparison of dynamical calculations to data on correlations between energy loss and variance σ_Z^2 (top) and mean Z of light fragment (bottom)

By realizing that the quantity τ^* governing nucleon exchange is essentially a directional average of the current

of nucleons traversing the interface between the two interacting nuclei, it is, conceptually, relatively simple to extend the model to a consistent description of instantaneous nucleon emission. However, in order to account for absorption and refraction of the primary particles and ejection of secondary particles, the nuclear model has to be extended beyond the simple one-body limit to include the next higher approximation: two-body collisions.

VI. CONCLUSIONS

Studies of light-particle emission in damped nuclear reactions have proven to be a powerful tool in obtaining information about the reaction mechanism that is essential for its understanding and the development of reaction models. In particular, they offer the only experimental means known to date to investigate thermalization processes in nuclear matter and have provided the basis for the applicability of mean-field theories to damped reactions. Although the dissipation of relative kinetic energy occurs on a relatively fast time scale, nuclear modes have always sufficient time to adjust to the changing macroscopic conditions. Despite large amounts of dissipated energy, resulting nuclear temperatures are still small enough to prevent significant departure of the nuclear system from the one-body limit. There are indications, however, some of which will be discussed in other contributions to this symposium, for deviations of the nuclear interaction from this simplest model picture at bombarding energies higher than 6-10 MeV/u above the barrier. It can be expected that in this regime, measurements of the associated light particles will provide important evidence for a gradual breakdown of reaction mechanisms that successfully describe nuclear interactions at lower bombarding energies.

ACKNOWLEDGEMENT

This work was supported by the U.S. Department of Energy.

REFERENCES

1. W. U. Schröder and J. R. Huizenga, Ann. Rev. Nucl. Sci. 27, 465 (1977); V. V. Volkov, Phys. Rep. 44, 93 (1978).
2. P. Möller and J. R. Nix, Nucl. Phys. A272, 502 (1976); Nucl. Phys. A281, 354 (1977); Nucl. Phys. A296, 289 (1978).

3. W. Nörenberg and C. Riedel, Z. Physik A290, 335 (1979).
4. W. J. Swiatecki, Erice Lectures, Report LBL-8950 (1979).
5. M. Berlanger, A. Gobbi, F. Hanappe, U. Lynen, C. Ngô, A. Olmi, H. Sann, H. Stelzer, H. Richel and M. F. Rivet, preprint (1979).
6. J. Randrup, Nucl. Phys. A327, 490 (1979).
7. J. P. Bondorf, J. de Physique C5, 195 (1976); J. P. Bondorf, J. N. De, A. O. T. Karvinen, G. Fai and B. Jakobsson, Phys. Lett. 84B, 162 (1979); J. P. Bondorf, J. N. De, G. Fai, A. O. T. Karvinen, B. Jakobsson and J. Randrup, preprint NORDITA-79/27.
8. M. C. Robel, Ph.D. thesis, report LBL-8181 (1979).
9. D. H. E. Gross and J. Wilczyński, Phys. Lett. 67B, 1 (1977).
10. H. Machner, Phys. Lett. 86B, 129 (1979).
11. J. J. Griffin, Phys. Rev. Lett. 17, 478 (1966); M. Blann, Ann. Rev. Nucl. Sci. 25, 123 (1975).
12. W. U. Schröder, U. Jahnke, K. H. Lindenberger, G. Röschert, R. Engfer and H. K. Walter, Z. Physik 268, 57 (1974).
13. L. Westerberg, D. G. Sarantites, D. C. Hensley, R. A. Dayras, M. L. Halbert and J. H. Barker, Phys. Rev. C18, 796 (1978).
14. G. Baur and D. Trautmann, Phys. Rep. 25, 293 (1976).
15. H. C. Britt and A. R. Quinton, Phys. Rev. 124, 877 (1961).
16. R. K. Bhownik, E. C. Pollacco, N. E. Sanderson, J. B. A. England, and G. C. Morrison, Phys. Rev. Lett. 43, 619 (1979).
17. T. Inamura, M. Ishihara, T. Fukuda, T. Shimoda, and H. Hiruta, Phys. Lett. 68B, 51 (1977).
18. H. Yamada, D. R. Zolnowski, S. E. Cala, A. C. Kahler, J. Pierce and T. T. Sugihara, Phys. Rev. Lett. 43, 605 (1979).
19. K. Siwek-Wilczyńska, E. H. du Marchie van Voorthuysen, J. van Popta, R. H. Siemssen and J. Wilczyński, Phys. Rev. Lett. 42, 1599 (1979).
20. T. Udagawa, T. Tamura, T. Shimoda, H. Fröhlich, M. Ishihara, and K. Nagatani, Phys. Rev. C20, 1949 (1979).
21. A. Gamp, J. C. Jacmart, N. Poffé, H. Doubre, J. C. Roynette, J. Wilczyński, Phys. Lett. 74B, 215 (1978); A. Gamp, H. L. Harney, J. C. Roynette, E. Plagnol, H. Fuchs, H. Doubre, J. C. Jacmart and N. Poffé, report IPNO-PhN-79-13.
22. H. A. Bethe, Phys. Rev. 53, 675 (1938).
23. R. Weiner and M. Westrom, Nucl. Phys. A286, 282 (1977).

24. P. A. Gottschalk and M. Weström, Phys. Rev. Lett. 39, 1250 (1977).
25. H. Ho, R. Albrecht, W. Dünnweber, G. Graw, S. G. Steadman, J. P. Wurm, D. Disdier, V. Rauch and F. Scheibling, Z. Physik A283, 235 (1977).
26. R. Vandenbosch and J. R. Huizenga, Nuclear Fission (Academic Press, New York and London, 1973).
27. A. D. Hoover, J. R. Birkelund, D. Hilscher, W. U. Schröder, W. W. Wilcke, J. R. Huizenga, A. C. Mignerey, K. L. Wolf, H. F. Breuer and V. E. Viola, to be published.
28. R. G. Stokstad, Proceed. Conf. on Heavy-Ion Collisions, Fall Creek Falls, 1977, report CONF-770602.
29. A. Kind and G. Patergnani, Il Nuovo Ci. 10, 1375 (1953).
30. T. Ericson and V. Strutinski, Nucl. Phys. 8, 284 (1958); T. Ericson, Adv. Phys. 9, 425 (1960).
31. K. L. LeCouteur and D. W. Lang, Nucl. Phys. 13, 32 (1959); D. W. Lang, ibid. 53, 113 (1964).
32. J. D. Jackson, Can. Journ. Phys. 34, 767 (1956).
33. D. Hilscher, J. R. Birkelund, A. D. Hoover, W. U. Schröder, W. W. Wilcke, J. R. Huizenga, A. C. Mignerey, K. L. Wolf, H. F. Breuer and V. E. Viola, Jr., Phys. Rev. C20, 576 (1979).
34. R. E. Textor and V. V. Verbinski, ORNL-4160, 1968 (unpublished).
35. M. Drosg, Nucl. Instr. Methods 105, 573 (1972).
36. M. Beckerman and M. Blann, Univ. of Rochester report UR-NSRL-135 (1977).
37. W. U. Schröder, J. R. Birkelund, J. R. Huizenga, W. W. Wilcke and J. Randrup, to be published.

E. Experimental Summary of the International Symposium on Continuum Spectra of Heavy Ion Reactions

EXPERIMENTAL SUMMARY OF THE INTERNATIONAL SYMPOSIUM ON CONTINUUM SPECTRA OF HEAVY ION REACTIONS

JOHN R. HUIZENGA
Departments of Chemistry and Physics and
Nuclear Structure Research Laboratory
University of Rochester, Rochester, New York 14627

I. INTRODUCTION

Tom Sugihara impressed each of us in his introductory comments about the size, wealth and glorious virtues of Texas. Hence, it seems appropriate, speaking here in San Antonio, to illustrate in my first slide (Fig. 1)

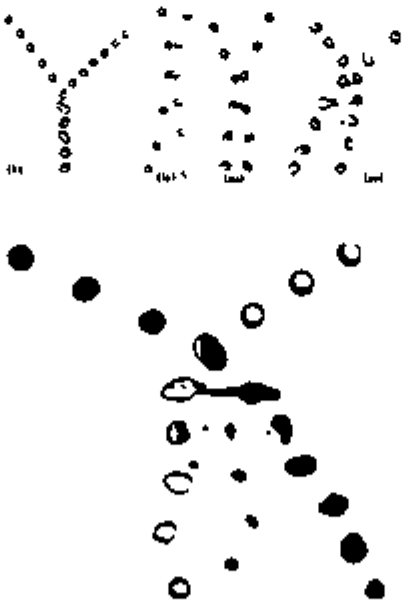

FIGURE 1, Collisions between water drops[1]

a reaction between two Texas-size nuclei, two water drops. At the top of (Fig. 1), the results of Brazier-Smith et al.[1] illustrate the similarity of collisions between water drops and heavy nuclei ranging from fusion, quasi-elastic to deep-inelastic or strongly-damped collisions. Inspection of the bottom part of (Fig. 1), where the time interval between the sequence of droplet pairs is constant, shows that approximately 60% of the translational energy is damped in this particular water-drop collision.

I find it impossible to summarize the many fine lectures of this symposium in 30 minutes. Hence, I've chosen to make a few remarks about topics covered in the invited and contributed papers under the following four categories: (1) properties of damped or deep-inelastic collisions at energies less than 5 MeV per nucleon above the Coulomb barrier; (2) emission of statistical light-particles in damped collisions; (3) emission of fast (non-statistical) particles in heavy-ion collisions; and, (4) heavy-ion fusion.

II. PROPERTIES OF DAMPED OR DEEP-INELASTIC COLLISIONS

As discussed in the talks of Gobbi[2], Schröder[3], Ngô[4], Rehm[5] and Specht[6], the well-known characteristic properties of these reactions are: (a) its binary nature; (b) the damping of a considerable amount of the initial kinetic energy and orbital angular momentum into internal energy and spin of each of the colliding nuclei - for some part of the cross section the final kinetic energy is even below the Coulomb energy of touching spheres, indicating that the nuclei are strongly deformed at the instant of separation; (c) angular distributions that are similar to those of a direct or relatively fast reaction; (d) the average charge and mass of the reaction products are close to those of the target and projectile, although during the interaction time there is an exchange of many nucleons between the colliding nuclei, the magnitude of which is corralated with the kinetic energy loss.

Each of these reaction features will be illustrated by a slide. (Fig. 2) demonstrates the binary nature of heavy-ion damped collisions. The distribution of the vector difference $|\vec{v}_1-\vec{v}_2|$ of the fission-fragment laboratory velocities, integrated over all other observables, is shown for the reactions of ^{208}Pb and ^{238}U projectiles on a ^{90}Zr target[6,7]. Hence, this figure clearly demonstrates the existence of an intermediate fissioning system as a "resonance". The quantity $\frac{1}{2}|\vec{v}_1-\vec{v}_2|^2$ times μ, the

reduced mass of the two fragments, determines the total fission-fragment kinetic energy in the rest frame of the intermediate nucleus. Kinematically complete experiments such as these have been performed on the three-body exit channels for a number of reactions at laboratory projectile energies of 7.5 MeV/u and show that the bulk of the events (> 99%) can be interpreted as sequential fission following a binary damped collision.

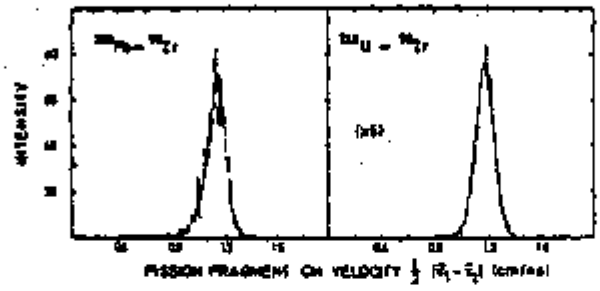

FIGURE 2. Distribution of the vector difference of fission-fragment laboratory velocities[6,7].

The large amount of energy damped in these heavy-ion collisions is illustrated in (Fig. 3) for the $^{209}Bi+^{136}Xe$ reaction at low bombarding energies[8]. The arrows represent the initial relative kinetic energies above the Coulomb barrier for the two cases, i.e. $E_{cm}-V_{Coul}$. One sees that the energy loss may exceed the initial kinetic energy by up to 150 MeV for the smaller bombarding energy, clearly demonstrating the importance of fragment deformations in damped collisions. The energy loss is the most important parameter for determination of the nature of a heavy-ion collision. As a function of energy loss, it is possible to obtain simple correlations with the first and second moments of various distributions. Some of these will be mentioned later.

The damping of angular momentum into intrinsic spin is illustrated in (Fig. 4) for the $^{238}U+^{86}Kr$ reaction[9]. The spin of the uranium-like fragment is plotted as a

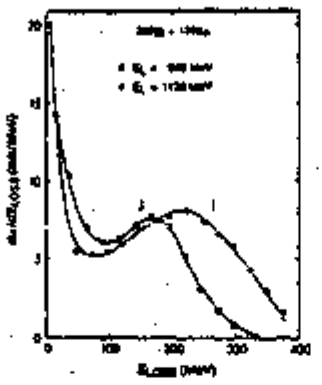

FIGURE 3, Energy loss spectra for damped collisions[8]

function of energy loss as inferred from sequential fission fragment angular correlation measurements with the Kr-like fragments. From this figure one sees that the spin of the uranium-like fragments increases sharply with energy loss reaching values of 45 ħ. This spin is known to be strongly

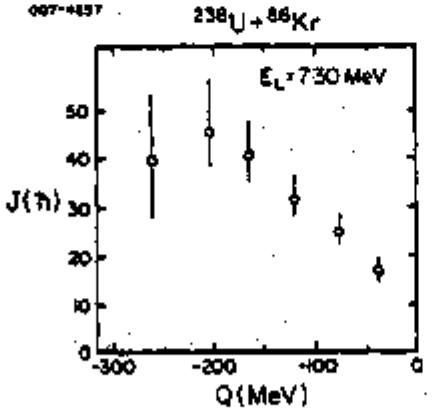

FIGURE 4, Spin of uranium-like fragments following damped collisions[9]

aligned, especially at the smaller energy losses. For some heavy-ion systems, it has been shown[10] that negative-angle scattering is associated with orbiting trajectories rather than a deflection function with a second rainbow near 0°. The spin of the deflection angle has been deduced from the circular polarization of the decay γ rays measured in coincidence with the ejectile[10,11].

The angular distribution of Xe-like reaction products measured for the $^{209}Bi+^{136}Xe$ reaction[12] at a laboratory energy of 1130 MeV is shown in (Fig. 5). This is a classic example of a sharply-focussed damped heavy-ion reaction for a system where the entire reaction cross section goes into this new process. In contrast to a reaction with orbiting trajectories and negative-angle scattering mentioned earlier, one sees for the reaction displayed in (Fig. 5) that Xe-like fragments are emitted on the average at $\theta_{cm} \approx 50°$, for all values of the energy loss. This focussing is due to a balance of the attractive nuclear forces and repulsive Coulomb forces giving a deflection function where the reaction angle is essentially independent of impact parameter. Raising or lowering the bombarding energy is expected to alter this balance of forces and change the deflection function as has been show for the $^{209}Bi+^{136}Xe$ reaction at 940 MeV[8]. It is also possible to change the deflection function from an orbiting type to a Coulomb-like type by

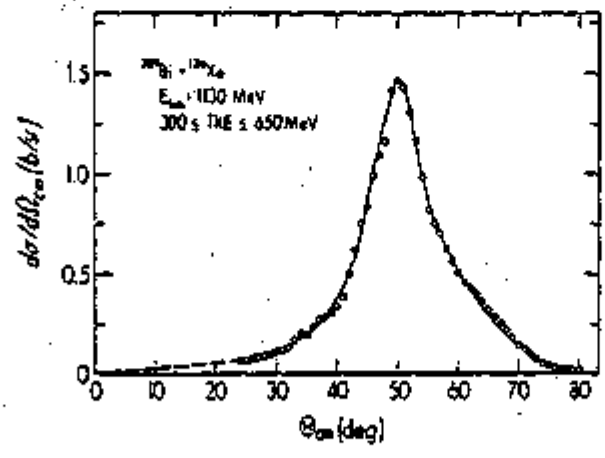

FIGURE 5, Angular distribution for xenon-like fragments following damped collisions[12]

keeping the ratio of the center-of-mass energy to the Coulomb energy, E_{cm}/V_{Coul}, fixed and to vary the product of the reaction charges, Z_pZ_T, thus changing substantially the absolute Coulomb force. This is illustrated in (Fig. 6) by the Wilczyński diagrams of two of the reactions shown in this series. The reactions $^{166}Er+^{86}Kr$ and $^{208}Pb+^{208}Pb$ were both performed at energies where $E_{cm}/V_{Coul}\approx 1.3$. Hence, when Z_pZ_T for these systems changes from 2448 to 6724 the deflection function changes from an orbiting to a Coulomb-like type.

The double-differential cross sections, $d^2\sigma/dEdZ$ and $d^2\sigma/dEdM$, are plotted in (Fig. 7) vs. the charge Z and mass M of the light fragment for the $^{110}Pd+^{208}Pb$ reaction[5,13] at E_{Lab}=1180 MeV. The results are shown for 30-MeV wide total-kinetic-energy bins. One sees that the fragment charge and mass distributions corresponding to a given energy bin are Gaussian in shape to a good approximation even though the bombarding energy is very low,

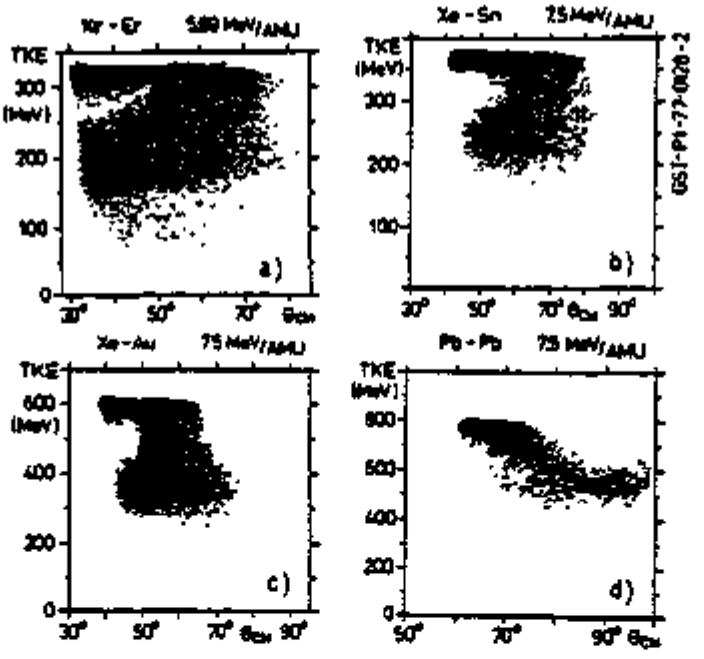

FIGURE 6, Wilczyński diagrams of four different reactions[2]

$(m/\mu)(E_{cm}-V_C)=\varepsilon_o=0.47$ MeV/u, and energy losses extend to some 150 MeV beyond the available kinetic energy for touching spherical nuclei. Hence, even at near barrier energies the mass and charge distributions remain nearly Gaussian as was first discovered for the $^{209}Bi+^{136}Xe$ reaction at higher energies[14,12,8].

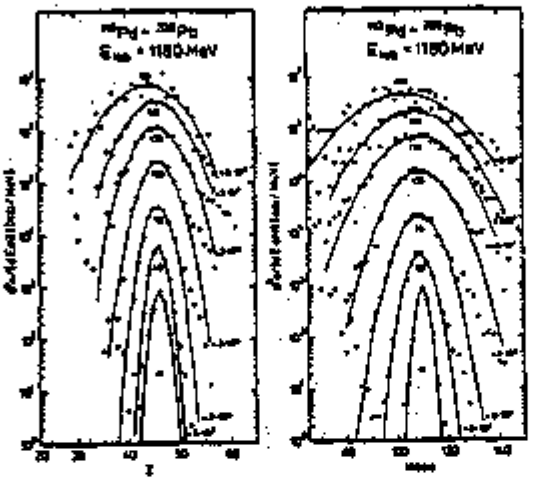

FIGURE 7. Fragment charge and mass distributions following damped collisions[5,13]

The experimental relationship between the second moments of the mass and charge distributions σ_A^2 and σ_Z^2, is a subject under active investigation[15,16,13] and reported in several papers[5,17-19] at this conference. The available data are summarized in (Fig. 8) as a function of E_{Loss} for the lighter reaction fragments. In this figure the variance ratios σ_A^2/σ_Z^2 for different systems and bombarding energies are normalized to the value $(A/Z)^2$ of the total system. One sees immediately that the relationship $\sigma_A^2=(A/Z)^2\sigma_Z^2$ (the dashed line in Fig. 8) is not valid in general. The systems in (Fig. 8) where the target and projectile have very different (A/Z) ratios have ratios $R=(\sigma_A/\sigma_Z)^2/(A/Z)^2$ much smaller than one for low energy losses and approach one only for large energy losses.

EXPERIMENTAL SUMMARY OF..

Another interesting feature can be seen for the $^{209}Bi+^{56}Fe$ data at very small energy losses where $(\sigma_A/\sigma_Z)^2$ increases as the energy loss decreases. These peripheral collisions enhance neutron exchange relative to proton exchange and may be indicative of the presence of a neutron skin. Dynamical calculations reproduce this trend[20]. When the bombarding energy is reduced to approximately 0.5 MeV per nucleon above the Coulomb barrier, ensuring that all collisions are distant or peripheral, the ratio R becomes considerably larger than unity, again indicating the relative enhancement of neutron exchange and the possible importance of a neutron skin. Although for a system like $^{166}Er+^{86}Kr$, where the A/Z values of the target and projectile are similar and the measured ratios R are unity[17], no data is available for the interesting region where the energy losses are less than 100 MeV.

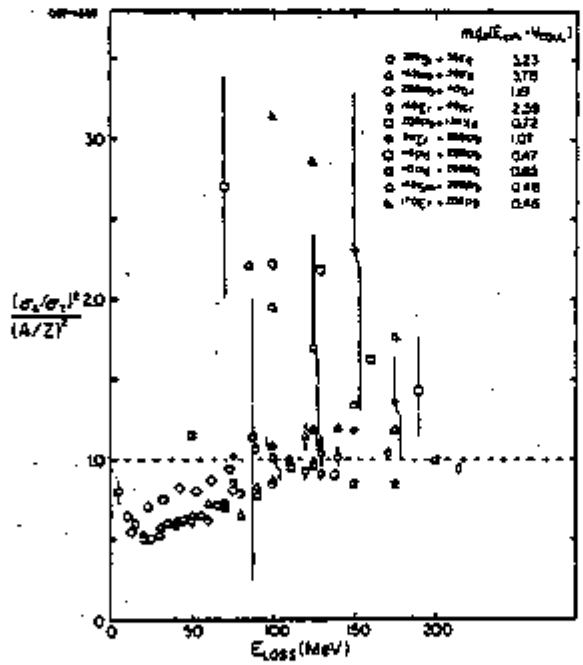

FIGURE 8, Ratios of the mass to charge variances divided by $(A/Z)^2$ as a function of E_{Loss}

The energy loss is the most important parameter for determining the nature of the heavy-ion collision. The well established correlation[21] between the energy loss and the second moment of the charge or mass distribution is illustrated in (Fig. 9) for the $^{209}Bi+^{136}Xe$ reaction[8] at two bombarding energies. In a phenomenological approach use has been made of the microscopic time scale provided by the nucleon exchange mechanism to give the dissipated energy as a function of the number N_{ex} of exchanged nucleons[12]

$$(1) \quad E_{Loss} = (E_{cm} - V_{Coul}) \left\{ 1 - \exp \left[- \alpha(m/\mu) \, N_{ex} \right] \right\}$$

In Eq. (1), the coefficient α conveys information on the character of the exchange process, m is the nucleon mass and μ the reduced mass of the dinuclear system. It is not in general possible to derive a simple and unique relation between N_{ex} and experimental observables such as the variances σ_A^2 and σ_Z^2 of fragment-A and-Z distributions. For simplicity, it is assumed that $N_{ex}=\sigma_A^2$ or, if only σ_Z^2 is available by $N_{ex}=(A/2)^2\sigma_Z^2$ where A and Z apply to the total system. Experimental information on the relationship between σ_A^2 and σ_Z^2 as a function of energy loss, shown in (Fig. 8), has already been discussed. As illustrated in

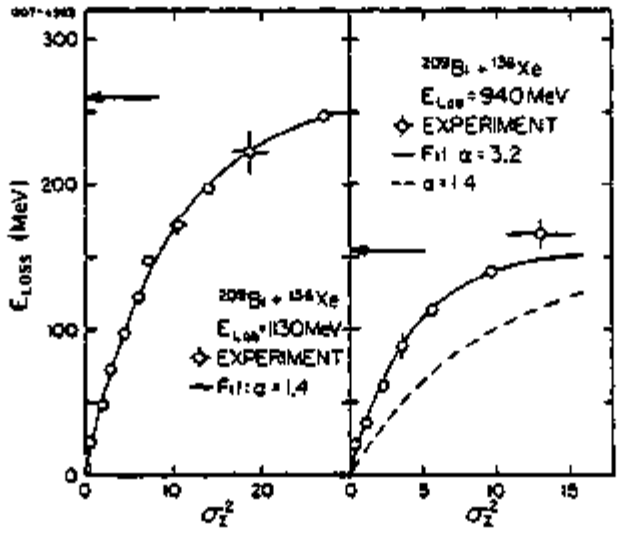

FIGURE 9, Correlation between the energy loss and variance of the fragment-Z distribution[8]

(Fig. 9), the classical model leads to a bombarding energy dependence for α, where α increases as the bombarding energy decreases.

The failure of the classical one-body dissipation model (see Eq. 1) to account for the variations of α with bombarding energy and reaction system has been attributed to shell structure[2] of the colliding nuclei but is expected, due to the neglect of the Fermion nature of the exchanged nucleons[3]. The simple quantal transport model for energy dissipation and nucleon exchange introduced by Randrup[22] treats the interacting system as two almost degenerate Fermi-Dirac gases. The current of nucleons in this quantal model depends on the occupancy of the single-particle orbits in accordance with the Pauli principle. Explicit account of these quantal restrictions of nucleon exchange gives a good reproduction of the various experimental data[3] and at the same time gives a natural microscopic explanation of the empirical correlation based on the extension of the classical one-body recoil formula to include shell structure.

Recent studies of the charge equilibration mode in deep-inelastic reactions have led to contradictory results[4]. Whereas initial results for symmetric systems appeared to exhibit quantal features[23], results from asymmetric systems have been interpreted in terms of a statistical behavior[24]. The different interpretations are based on the dependence of the variance of the charge distribution for <u>fixed final mass asymmetry</u> on E_{Loss}. The above data[23,24] along with more recent data[25] are compared in (Fig. 10). In order to keep the figure from becoming congested, only one or two representative A values are chosen for each reaction studied by the counter technique employing unit A and Z resolution[23,25]. The radiochemical data[24] for six different mass numbers were averaged to give the plotted points. In addition, the dependence of the variance of the charge distribution, $\sigma_Z^2(A)$, on excitation energy for fission[26] is illustrated in (Fig. 10). All of the counter data are similar, with $\sigma_Z^2(A)$ essentially independent of E_{Loss} for values of $E_{Loss} \geq 30$ MeV. If one interprets these results in terms of a relaxation time for the A/Z degree of freedom, this equilibration time is less than the interaction time associated with collisions where 30 MeV of kinetic energy is dissipated. Based on a classical model[27], this interaction time for the systems under consideration is approximately $(1\text{-}2)\times10^{-22}$sec. At present, there is no ready explanation for the very different results obtained for the $^{197}Au+^{132}Xe$ reaction data based on radiochemical

measurements in conjunction with unfolding procedures. One observes that the deduced variances for this system are much narrower than those observed for fission.

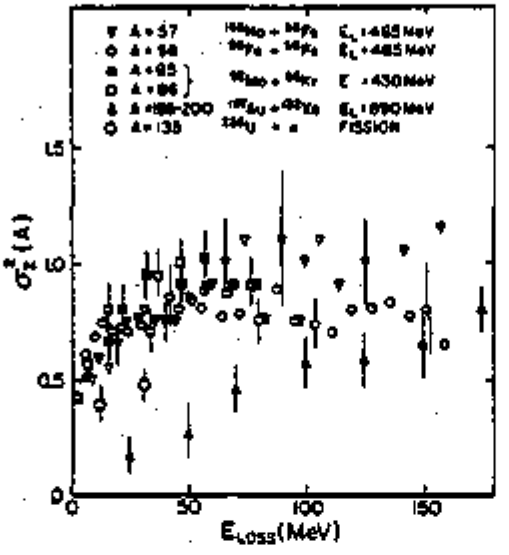

FIGURE 10, Dependence of the fragment-Z distribution for fixed A on the energy loss[4,23-26]

If one assumes the energy $\hbar\omega$ of a phonon corresponding to a collective charge-asymmetry oscillation is large compared to the thermodynamic temperature, as first postulated for the fission results[26] and more recently adopted for heavy-ion collisions[23], the variance of the charge distribution for fixed mass asymmetry is given by $\sigma_Z^2(A) = \hbar\omega/2C$. The quantities in this equation are defined in Ref. 4. The calculated variances, based on the quantal model are given in Table I. All of the calculated results except for the $^{197}Au+^{132}Xe$ reaction, are in qualitative agreement with the experimental results shown in (Fig. 10). The implication is that the quantum mechanical zero-point contribution dominates over the statistical fluctuations.

As already mentioned, one obtains a satisfactory description of the experimental correlations between E_{Loss} and the variance in the mass (or charge) distributions

TABLE I Variances $\sigma_z^2(A)$ based on quantal model

Reaction	$^{56}Fe+^{56}Fe$	$^{92}Mo+^{86}Kr$	$^{165}Ho+^{56}Fe$	$^{197}Au+^{132}Xe$
$\hbar\omega$ (MeV)	10.19	8.73	8.38	7.15
C (MeV)	7.08	4.56	4.82	2.66
$\sigma_z^2(A)$	0.72	0.96	0.87	1.34

when explicit account is taken of the quantal nature of nucleon exchange[3]. Hence, when Pauli blocking is included in these correlations, one concludes that nucleon exchange contributes the major part of the energy dissipation in heavy-ion collisions when the energy per nucleon above the Coulomb barrier is less than 5 MeV/u. It is of interest to determine the quantitative contribution of other energy loss processes including collective surface modes to the total energy dissipation. Is it possible to obtain experimental information on the excitation of these modes by the study of inclusive or exclusive spectra from heavy-ion reactions? It is well known that inclusive spectra from heavy-ion reactions contain structure. An example is the spectrum of ^{57}Co produced by the $^{56}Fe+^{56}Fe$ reaction[28] at E_{Lab}=465 MeV shown in (Fig. 11). Before one interprets this observed structure as due to high-energy giant resonances, one must eliminate the expected structure due to statistical processes[29] associated with the de-excitation phase of the damped reaction process (e.g. ^{57}Co fragments can arise from the decay of excited primary fragments of ^{58}Co, ^{58}Ni, ^{59}Cu, etc.). This structure produced by the various decay channels is illustrated in (Fig. 12) by the calculated spectrum of ^{41}Ca produced in the $^{40}Ca+^{40}Ca$ (E_{Lab}=400 MeV) reaction. The arrows correspond to the energies of the structure in the experimental spectrum[30] of ^{41}Ca. Recently, the experimental structure in the inelastic excitation of ^{16}O on ^{208}Pb at 20 MeV/nucleon has been interpreted in terms of direct excitation of giant resonances. Some of these assignments at energies where particle channels are open may well be incorrect as the structure may be due to statistical processes as discussed above.

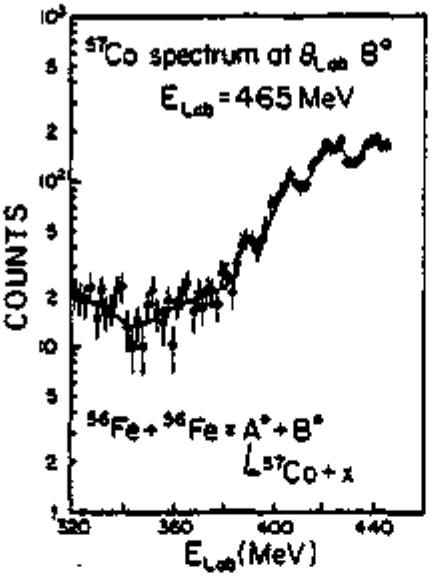

FIGURE 11, Experimental inclusive energy spectrum[28] of ^{57}Co

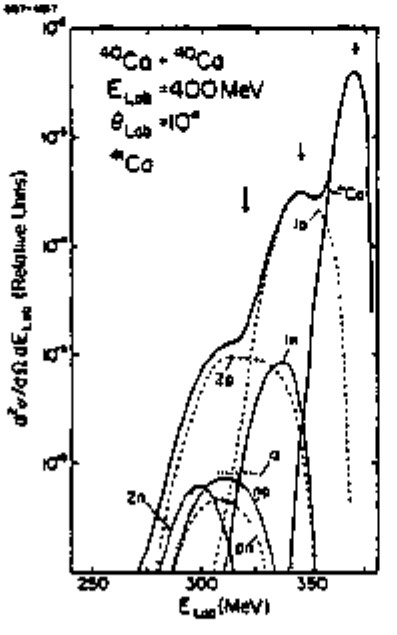

FIGURE 12, Calculated inclusive energy spectrum[29] of ^{41}Ca

EXPERIMENTAL SUMMARY OF..

III. EMISSION OF STATISTICAL LIGHT PARTICLES

Particle evaporation occurs on a slightly longer time scale than the damped reaction interaction times. From these statistical particles it is possible to infer information about the di-nucleus at the time of breakup such as the fragment excitation, deformation and spin alignment. In Table II examples of reactions are listed where only statistical particles of the types indicated are measured.

TABLE II Examples of reactions where only statistical particles are observed

Target	Proj.	E_{Lab}(MeV)	Particle	ϵ_o(MeV/u)	Com.	Ref.
^{150}Nd	^{20}Ne	175	n	4.7	(a)	32
^{58}Ni	^{40}Ar	280	α,p	4.3	(b)	33,4
^{165}Ho	^{56}Fe	465	n	3.8	(c)	34,3
^{165}Ho	^{136}Xe	1130	n	3.6	(d)	3
^{166}Er	^{86}Kr	675,600,495	n	3.2,2.3,1.1	(e)	35,17
^{nat}Se	^{40}Ar	201	α,p	2.1	(f)	36
^{197}Au	^{40}Ar	240	n	1.4	(g)	37,39
^{197}Au	^{63}Cu	400,365	n	1.3,0.8	(h)	38,4,39

(a) Neutrons were measured in coincidence with γ rays characteristic of specific evaporation residues. These neutrons show a temperature of about 2 MeV and there is no evidence for non-statistical n emission in the (^{20}Ne,Xn) reactions.

(b) The angular distributions and energy spectra of p and α particles are measured in coincidence with heavy fragments. All light particles are interpreted to be statistically evaporated by the fully accelerated fragments.

(c) Temperatures of projectile-like and target-like fragments are the same within experimental error. Pre-equilibrium neutron emission contributes less than 5%. A small out-of-plane neutron anisotropy is observed. The A/Z ratios of primary fragments are very different from projectile and target ratios.

(d) Results preliminary. Data analysis in progress.

(e) The excitation energy is shared between the fragments in proportion to their mass. Find no evidence for

preequilibrium neutrons within an experimental uncertainty of 10%.

(f) Measured inclusive spectra and angular distributions. Data interpreted in terms of statistical theory.

(g) Neutron multiplicity data interpreted as evidence for fragment deformation at separation.

(h) Excitation energy shared uniformly between all the nucleons of composite system. No evidence for preequilibrium neutrons.

The angular distributions of evaporated particles in the rest frame of an equilibrated nucleus is predicted[3] to be symmetric around $\theta_{cm}=90^{\circ}$. This is illustrated for the $^{nat}Se+^{40}Ar$ reaction[36] in (Fig. 13) where the angular distributions of the emitted α particles of different energy bins are shown to be symmetric around $\theta_{cm}=90^{\circ}$. Another criterion for equilibrium or statistical particle emission is shown in (Fig. 14) where the α particle spectra in coincidence with

(Fig. 13)

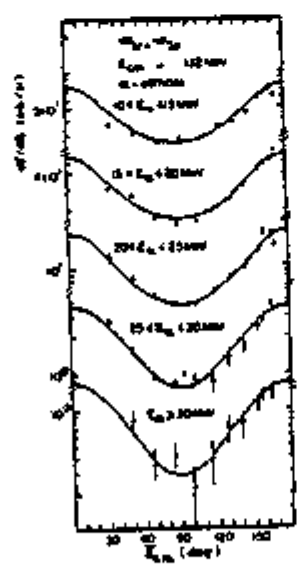

(Fig. 14)

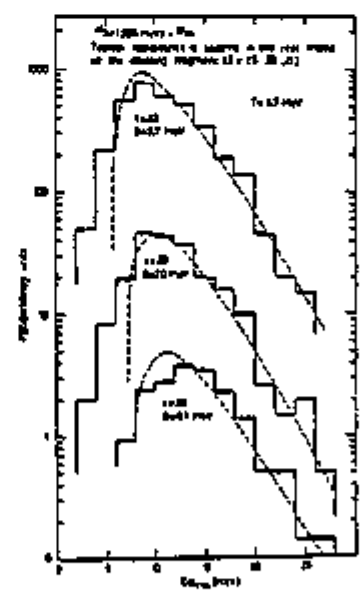

FIGURE 13, Alpha particle angular distributions[36]

FIGURE 14, Alpha particle energy spectra[33,4]

different fragments[33,4] are shown to be consistent with a single temperature of 2.7 MeV. The fragments observed in coincidence with the α particles originate from fusion-fission (Z=23) and deep inelastic events (Z=36).

In contrast to the above illustrations, the neutron channels is the most important for the de-excitation of very heavy systems. In a strongly damped collision the energy loss is given by

$$(2)\quad E_{Loss} = E_L^{DISS} + E_H^{DISS} = \sum_{i=n,p,\alpha,\gamma} \langle E_{i\nu} + B_{i\nu} \rangle M_{i\nu}$$

where $M_{i\nu}$, $E_{i\nu}$ and $B_{i\nu}$ are the multiplicity, kinetic energy and binding energy of particle i from fragment ν. At the time of fragment separation or scission,

$$(3)\quad E_L^{DISS} = E_L^{rot} + E_L^D + a_L^S \left(T_L^S\right)^2$$

$$(4)\quad E_H^{DISS} = E_H^{rot} + E_H^D + a_H^S \left(T_H^S\right)^2$$

where E_i^{rot}, E_i^D, a_i^S and T_i^S are the energy tied up in rotation, the energy in deformation, the level density parameter and temperature, respectively, at scission. After fragment separation (neglecting the change in E_i^{rot}), the excitation energies of the light and heavy fragments are

$$(5)\quad E_L^* \approx E_L^D + a_L^S \left(T_L^S\right)^2 \approx a_L T_L^2$$

$$(6)\quad E_H^* \approx E_H^D + a_H^S \left(T_H^S\right)^2 \approx a_H T_H^2$$

where a_i and T_i are the level density parameter and temperature, respectively, of the observed fragments. In general, $T_i > T_i^S$, $T_L \neq T_H$ and $E_H^*/E_L^* \neq A_H/A_L$. If one assumes the temperatures of the two fragments at scission are equal, $T_L^S = T_H^S$, and $a_i^S = A_i/\text{constant}$, it follows that if,

$$(7)\quad E_H^D / E_L^D = A_H / A_L \text{ , then } T_H = T_L > T_i^S$$

$$(8)\quad E_H^D / E_L^D > A_H / A_L \text{ , then } T_H > T_L > T_L^S$$

$$(9)\quad E_H^D / E_L^D < A_H / A_L \text{ , then } T_L > T_H > T_i^S$$

As discussed by several speakers [3,4,17,39] at this

conference, studies of the neutron multiplicities and spectra from fragments produced in strongly damped collisions are the most important probes to answer the question whether thermal equilibrium is achieved during a heavy-ion damped collision. However, the experiments measure T_L and T_H and do not give a direct measurement of T_L^S and T_H^S, the temperatures of the fragments at the time of separation or scission. The temperature T_i of the light Fe-like (open circles) and heavy Ho-like (solid squares) fragments are shown in (Fig. 15) for the $^{165}Ho+^{56}Fe$ reaction[34] as a function of energy loss. Within the experimental errors, the temperatures T_i of the two fragments are equal for all energy losses greater than 60 MeV. In order to deduce information on the temperatures T_i^S from the measured temperatures T_i, a model calculation is required. It turns out that if $T_L^S=T_H^S$, substantial deviation of the ratio E_H^D/E_L^D from A_H/A_L (see Eq. 7) is required in order to observe a statistically meaningful difference in T_H and T_L. For example, at E_{Loss}=145 MeV, a difference in T_H-T_L of 0.2 MeV requires E_H^D=20 MeV (when E_L^D=0). Hence,

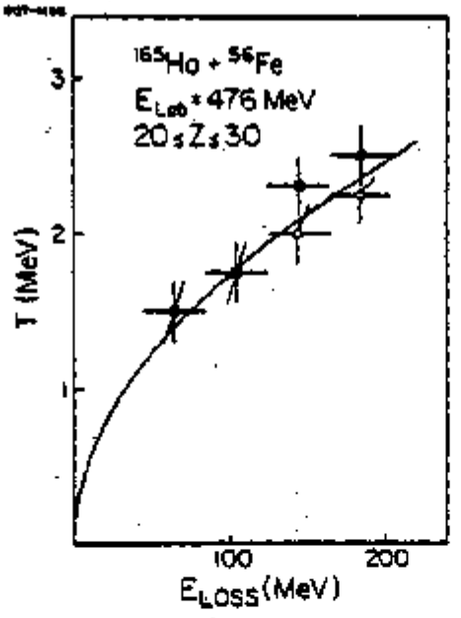

FIGURE 15, Nuclear temperatures of the Fe-like (open circles) and Ho-like (filled squares) fragments[34]

the temperature difference is quite insensitive to deformation energy when E_{Loss} is large. However, at small values of E_{Loss} information on the deformation energy at scission for damped reactions may be obtained if E_H^D/E_L^D is very different from A_H/A_L[37,39].

For the heavy-ion damped reactions listed in Table II, the various authors have concluded that the temperatures of the two reaction fragments are equal for each energy loss, indicating thermal equilibration on a time scale less than the interaction time. Estimates of the interaction time[27] based on a classical model give then upper limits for the thermal relaxation time of the intrinsic energy degree of freedom. For an E_{Loss} of 60 MeV (see Fig. 15), the relaxation is estimated to occur in less than 2×10^{-22}sec. For larger energy losses, the interaction times are longer and, hence, the upper limits on the experimental relaxation times are longer also.

The neutron multiplicity ratio (neglecting the energy carried away by γ rays in addition to E_i^{rot}) for damped reactions is given approximately by

$$(10)\quad \frac{M_H}{M_L} \approx \frac{E_H^*}{E_L^*} \frac{\langle E_n + B_n \rangle_L}{\langle E_n + B_n \rangle_H} \frac{\left[(\Gamma_p/\Gamma_n) + (\Gamma_\alpha/\Gamma_n) + 1\right]_L}{\left[(\Gamma_p/\Gamma_n) + (\Gamma_\alpha/\Gamma_n) + 1\right]_H}$$

where, in general, $M_H/M_L \neq A_H/A_L$. The neutron multiplicity ratios M_H/M_L for two reactions discussed in this conference are plotted in (Fig. 16) as a function of E_{Loss}. The experimental values of M_H/M_L for the $^{165}Ho+^{56}Fe$ reaction show a pronounced decrease with increasing E_{Loss}, as expected from an evaporation calculation, before reaching a relatively flat region where $M_H/M_L < A_H/A_L$. The multiplicity ratio is sensitive to the A/Z ratio of the reaction fragments as discussed previously[3], and indicates that the pre-evaporation A/Z values are well removed from those of the projectile and target. These data are consistent with calculations[20] based on a model where the A/Z value is a dynamical variable governed by the driving forces associated with the potential energy surface. If one associates the onset of the constant value of M_H/M_L with an "equilibration" of the energy degree of freedom and calculates from a classical model the interaction time associated with an $E_{Loss} \approx 30$ MeV, the relaxation of this mode is estimated to occur in less than $(1\text{-}2)\times10^{-22}$sec (for an E_{Loss}=30 MeV).

For the reactions and particles listed in Table II, no positive evidence has been found for emission of

non-statistical particles for either fusion or damped reactions. Hence, even for rather high heavy-ion bombarding energies, energy equilibrium is attained. A parameter that appears to determine the onset of non-statistical particle emission is the bombarding energy per nucleon above the Coulomb barrier, ϵ_0. On the basis of the data in Table II bombarding energies for heavy ions below about 5 MeV/u give only statistical particle emission. This conclusion is thought to be valid for reactions where projectile breakup or fragmentation doesn't contribute to the yield of the particles being studied. This qualification is necessary because light particles from projectile fragmentation can be emitted from some systems at bombarding energies much less than 5 MeV/u (e.g. projectiles like Li,d,C,N,O etc. see Table III).

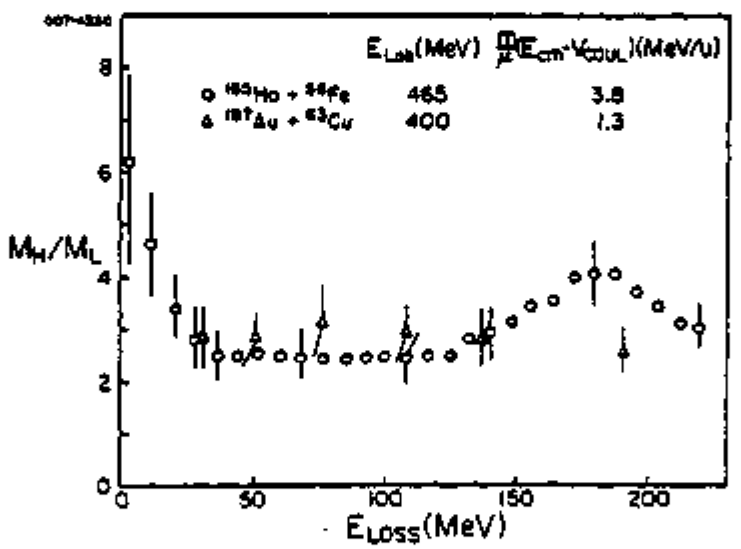

FIGURE 16, Neutron multiplicity ratios of heavy to light fragments as a function of E_{Loss}[3,4,34,38,39]

IV. EMISSION OF FAST (NON-STATISTICAL) PARTICLES

Nearly two decades ago in their classic paper on

particle emission, Britt and Quinton[40] reported a sizeable contribution of non-statistical protons (10% σ_R) and alpha (30% σ_R) particles for ^{12}C, ^{14}N and ^{16}O induced reactions on targets of ^{197}Au and ^{209}Bi at laboratory projectile energies of 10.5 MeV per nucleon. Since this time non-statistical particle emission has been reported for a large number of different reactions spanning a wide range of bombarding energies. Examples of heavy-ion reactions where some contribution of direct or non-statistical particles are observed are listed in Table III. Selected examples of light-ion induced reactions are included also in Table III for comparison. For example, for the $^{58}Ni+\alpha$ reaction at an energy of ϵ_o=7.8 MeV/u, six percent of the emitted protons are direct or non-statistical. This is an interesting case because almost the entire reaction cross section goes into proton emission. Hence, for this light-ion reaction non-statistical particle emission begins to occur for an energy somewhat above 5 MeV/u in excess of the Coulomb barrier discussed in section III (it is assumed that projectile fragmentation at this energy is still negligible for α particles).

TABLE III Fast (non-statistical) particles

Target	Projectile	E_{Lab}(MeV)	Particle	ϵ_o(MeV/u)	Com.	Ref.
^{209}Bi	$^{12}C, ^{16}O$	126,168	p,α	5.3	(a)	40
^{197}Au	$^{12}C, ^{14}N, ^{16}O$	126,147,168	α	5.5	(a)	40
^{58}Ni	α	42	p	7.8	(b)	41
^{103}Rh	^{14}N	121	p,α	5.2	(c)	42
^{209}Bi	$^{6}Li, ^{7}Li$	25-34	t,α	~0	(d)	43
^{27}Al	^{16}O	66	α	2.4	(e)	44
^{58}Ni	^{16}O	92,96	α	3.1,3.4	(f)	45
^{159}Tb	^{14}N	95	α	2.5	(g)	46
^{209}Bi	^{14}N	85,95	α	0.9,1.6	(h)	47
$^{197}Au, ^{208}Pb$	^{16}O	315,140	α	14.7,3.7	(i)	48
$^{232}Th, ^{209}Bi$ $^{120}Sn, ^{90}Zr$ ^{58}Ni	α	140	p,d, t,^{3}He	28.2-31.8	(j)	49, 50

JOHN R. HUIZENGA

Target	Projectile	E_{Lab}(MeV)	Particle	ϵ_o(MeV/u)	Com.	Ref.
^{158}Gd	^{12}C.	152	n	8.4	(k)	32
^{197}Au	^{32}S	373	α	5.5	(l)	51
Rare Earth	^{10}B, ^{12}C, ^{14}N ^{19}F, ^{20}Ne	75-166	p,d, t,α	3-7.6	(m)	52,53 54
^{160}Gd	^{12}C	90-200	α	3.8-14.6	(n)	55
^{197}Au	^{20}Ne	200-400	LI	6.2-18.7	(o)	56
^{197}Au	^{16}O	315	p	14.7	(p)	57
^{238}U	^{16}O	315	p,d, t,α, Li-O	14.0	(q)	58
^{93}Nb	^{40}Ar	400	α	6.6	(r)	59
^{nat}Ti	^{16}O	320	α	17.6	(s)	59,60
^{197}Au, ^{164}Dy, ^{154}Sm, ^{116}Sn	^{40}Ar	340	p,α	3.8-4.9	(t)	61, 62
$^{40,44,48}Ca$	^{16}O	100,142	n,α	4.3-6.9	(u)	63
^{91}Zr, ^{56}Fe, ^{12}C	^{16}O	208	p,d, t,α	9.8-11.8	(v)	64, 65
^{93}Nb	^{16}O	208	n	9.7	(w)	66
^{40}Ca	^{20}Ne	259	α, ^{16}O	10.8	(x)	67
^{40}Ca	^{16}O	135-304	^{12}C	6.4-17.0	(y)	68
^{58}Ni, ^{27}Al, ^{12}C	^{14}N	148	p,α	8.0-9.5	(z)	69
^{58}Ni	^{16}O	96	p,α	3.4	(aa)	70
^{27}Al	^{14}N	70,100	p,α	3.3-5.5	(bb)	71
^{27}Al	^{16}O	88	α	3.8	(cc)	72
$^{119,124}Sn$	α	109	n	23	(dd)	73
^{232}Th, ^{181}Ta, ^{93}Nb, ^{62}Ni, ^{27}Al	d	15,25.5	p	1-11.5	(ee)	74, 75

EXPERIMENTAL SUMMARY OF..

Target	Projectile	E_{Lab}(MeV)	Particle	ε_o(MeV/u)	Com.	Ref.
^{62}Ni	^{3}He	24.3,40.1	p,d	5.0,10.2	(ff)	74,
^{120}Sn	^{3}He	23.4	p,d	2.3		76
Light Targets	^{6}Li	34	d,t, ^{3}He,α	4.2-4.9	(gg)	77

(a) The cross sections for the emission of direct protons and direct alpha particles are reported to be approximately 10 and 30%, respectively, of the reaction cross sections.
(b) 6% of the protons emitted are direct and proton emission makes up essentially the entire reaction cross section.
(c) Sizeable yields of direct protons and alphas are reported.
(d) Projectile breakup makes up about 60% of the reaction cross section.
(e) Propose the reaction mechanism
$^{27}Al + ^{16}O \rightarrow [^{31}P]^* + ^{12}C \rightarrow ^{27}Al + \alpha + ^{12}C$
(f) α particles measured in coincidence with projectile-like reaction products. Pronounced forward peak of direct α particles.
(g) Gamma rays from the $^{159}Tb(^{14}N,\alpha,Xn)^{169-X}Yb$ reaction products were measured in coincidence with direct α particles emitted in the forward direction.
(h) $^{14}N(\alpha,Xn)$ and $^{14}N(2\alpha,Xn)$ reactions make up about 5% of the reaction cross section.
(i) Angular correlation measurements between fast α particles and projectile-like fragments $^{12,13,14}C$ and ^{14}N.
(j) The large-energy loss breakup processes account for about 40% of the total reaction cross section.
(k) Preequilibrium neutrons observed in coincidence with gamma rays from the $^{158}Gd(^{12}C,Xn)^{170-X}Yb$ reaction products (X=8 to 10) and the $^{158}Gd(^{12}C,\alpha\ Xn)^{166-X}Er$ reaction products (X=6 to 9).
(l) In-plane angular correlations between α particles and projectile-like residual nuclei (Z=5-22). Conclude that α emission originates from the region of the projectile which is facing the target nucleus during the collision.
(m) Charged particles are measured in coincidence with selected gamma rays used to identify the residual nuclei. The fast forward peaked charged particles result from projectile breakup and the remaining projectile mass fuses with the target. This process occurs for these heavy-ion projectiles with large cross sections.

JOHN R. HUIZENGA

(n) The energy dependence of the $^{160}Gd(^{12}C,\alpha)$ and $^{160}Gd(^{12}C,2\alpha)$ reactions are studied by means of $\alpha - \gamma$ coincidences. Also postulated the existence of the $(^{12}C,3\alpha)$ reaction. Cross sections for these reactions are large (up to 50% σ_{Reac}).

(o) Excitation functions measured for various light ions formed in breakup of ^{20}Ne projectiles. Evidence for nucleon exchange following projectile breakup.

(p) Inclusive p spectra extend up to very high energy and correspond to an effective temperature of about 12 MeV. Data are fit with a pre-equilibrium model with an initial exciton number of 25.

(q) Fast light particles are measured in coincidence with two fission fragments. Central and peripheral collisions are distinguished by the momentum transferred to the target residue as deduced from the angle between coincident fission fragments. The high energy light-ion spectra from both types of collisions have an effective temperature of 13 MeV.

(r) Fast α-particle component has a multiplicity of 0.3±0.1.

(s) Sizeable yield of fast (non-equilibrium) α particles. The multiplicity of beam velocity α particles in coincidence with fission-like residues is 0.4±0.1. Large component of beam velocity α particles in coincidence with projectile-like fragments also. In addition, a second component has two maxima in emission probability separated by a minimum in the direction of the projectile-like fragment.

(t) Direct p and α particle yields in terms of the percentage of the reaction cross section are, respectively, 5 and 11 (^{197}Au), 14 and 25 (^{164}Dy), 19 and 36 (^{154}Sm), and 11 and 32 (^{116}Sn).

(u) Reported substantial component of pre-equilibrium α emission as well as n emission.

(v) Light-ion spectra extend far beyond the E/A of the incident projectile at forward angles. The cross sections for the fast particles are large and depend only weakly on the target mass. At 8° the cross sections of protons with energies above 13 MeV are 335, 440 and 460 mb/sr, respectively for targets of ^{12}C, ^{56}Fe and ^{91}Zr.

(w) Preliminary evidence for a component of fast neutrons.

(x) Measured the coincident spectra of α and ^{16}O particles as a function of particle detection angles. Considerable yield concentrated along the Q=0 line which corresponds to the transition without exciting the target ^{40}Ca, thus implying the direct breakup of ^{20}Ne.

EXPERIMENTAL SUMMARY OF..

(y) Investigation of the interplay between transfer and projectile breakup processes. The breakup process becomes more important as the bombarding energy is increased.
(z) Made coincident measurements between light ions and alpha particles. A proposed possible interpretation of the data is that of fast direct α-emission followed by a deep-inelastic reaction between the remnants of the projectile and the target. Large cross section for direct α-emission (~ 50% σ_R).
(aa) Report three kinds of processes including deep-inelastic breakup of the projectile-like fragments and target-like fragments.
(bb) Coincident measurements between alpha particles (and proton) and projectile-like fragments (and evaporation residues). Report "direct" α particles with cross section of 50% σ_R.
(cc) Angular correlations between α particles and projectile-like fragments. The most important reaction mechanism is the sequential α decay from excited states of ^{16}O. This result differs from that reported by Harris et al.[5] who emphasize the sequential α-decay from excited ^{31}P.
(dd) In the Sn $(\alpha,\alpha'n)$ reaction, the α' and n particles were measured in coincidence. States in the continuum region of 10-40 MeV were populated leading to forward emission of fast pre-equilibrium neutrons and isotropic emission of slow evaporation neutrons. The giant quadrupole resonance decays by emitting both types of neutrons.
(ee) Total deuteron break-up yield is as large as 50% of the reaction cross section. The break-up cross section varies with target mass as $A^{1/3}$. The ratio of the break up cross section to the reaction cross section is rather constant with energy.
(ff) Measured ^3He breakup into p + d.
(gg) Light particle spectra were measured for the collisions of ^6Li with $^{12,13,14}C$, ^{16}O, ^{27}Al and ^{28}Si target nuclei.

During this conference a large amount of data have been presented on fast (non-statistical) particle emission from heavy-ion reactions (see e.g. Fig. 17). A number of reaction mechanisms have been proposed to account for these particles[3]. A sampling of the papers will reveal their origin to be due to projectile breakup, fragmentation, Fermi jets (or PEPS), hot spots, incomplete fusion, massive transfer, pre-equilibrium emission, neck rupture, etc. Hence it is too

early to systematize the different types of reaction mechanisms producing these fast particles. At some risk of over simplification, however, I do wish to group in a qualitative way some of the experimental results into categories of different reaction mechanisms. It is important to remember, of course, that the light particles from a particular reaction may be associated with several reaction mechanisms.

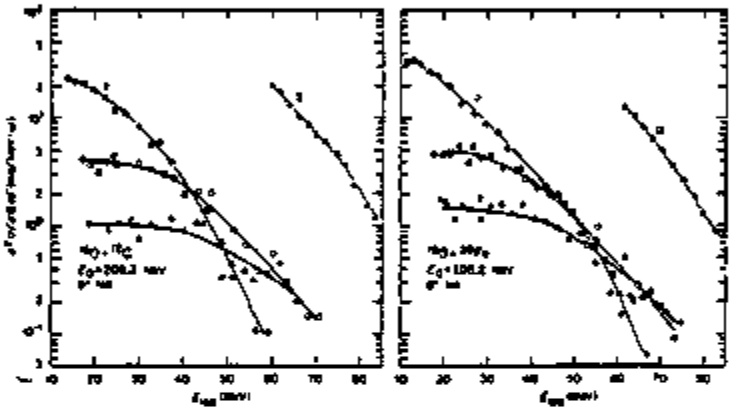

FIGURE 17. Energy spectra of Z = 1 and 2 particles[64]

A. Projectile Breakup or Fragmentation

Considerable evidence for a projectile breakup type of reaction mechanism has been presented for a large range of projectile types and energies. The spectra of these breakup particles are discussed in Ref. 3. The energy spectra are usually bell-shaped with mean energies decreasing with increasing emission angle from a maximum associated with a velocity near the beam velocity. The width reflects the momentum distribution of the particle inside the nucleus. The differential cross section increases sharply as the angle decreases and there is some evidence for a maximum[54] in the angular distribution for $\theta > 0^\circ$ (see Fig. 18). This process may be divided into elastic and inelastic breakup.

1. Elastic Breakup - both components of the projectile

emerge in their ground states and leave the target in its ground state also. Examples of this process are

(11) $^{40}Ca + {}^{20}Ne(E_{Lab}=259\ MeV)$[67] = $^{40}Ca(gs) + {}^{16}O(gs) + \alpha$

(12) $^{27}Al + {}^{16}O(E_{Lab}=88\ MeV)$[72] = $^{27}Al(gs) + {}^{12}C(gs) + \alpha$

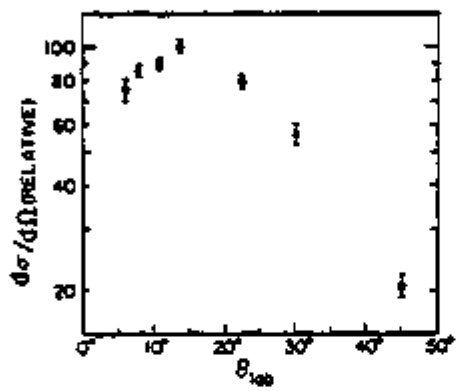

FIGURE 18, Angular distribution of 25-40 MeV α particles coincident with ^{164}Yb γ rays following the $^{159}Tb(^{14}N,\alpha 5n)^{164}Yb$ reaction at 115 MeV[54].

The reaction given in Eq. 11 is illustrated in (Fig. 19) where the events under discussion lie along the line in the figure. This general category of projectile breakup is relatively unimportant.

2. Inelastic Breakup - (a) Both projectile fragments emerge - in this process both components of the projectile emerge after collision although one or both of the initial fragments and target are excited. The initial projectile fragments may be altered by secondary breakup or nuclear exchange processes. Examples of this type of reaction with projectiles and energies above the Coulomb barrier are: α(30 MeV/u)[49,50], ^{14}N(8-10 MeV/u)[69], ^{32}S(5.5 MeV/u)[51], ^{16}O(14.7 MeV/u)[48] and ^{16}O(18 MeV/u)[59,60]. Coincidence

measurements of the projectile-like fragment and the light particles are reported in these studies. For example, in the experiments reported by Sanderson[69], light (Z=1 and 2) and heavy (Z=3-8) ejectiles are measured. These results may be interpreted in terms of ^{14}N breakup where the lighter (Z=1 or 2) ejectile emerges directly whereas the heavier ejectile interacts first with the target via a deep-inelastic process. An unusual projectile breakup process reported[2] at this conference is that of ^{86}Kr in the $^{166}Er+^{86}Kr$ reaction where the ^{86}Kr laboratory energy was 1040 MeV.

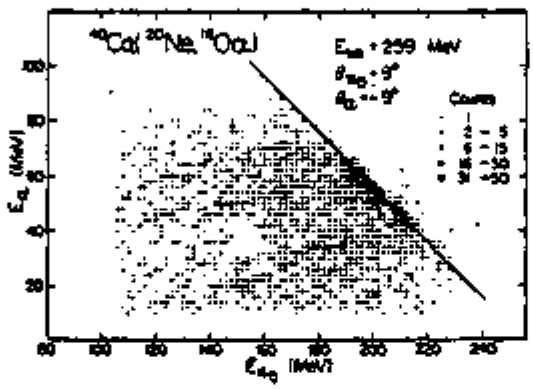

FIGURE 19. Two-dimensional spectra in laboratory system. Solid line indicates Q=0 locus[67]

(b) Only part of projectile emerges - some component or subset of the projectile nucleons interacts strongly with the target and fuses while the remaining projectile component emerges (however, this latter component may be altered by nucleon exchange or secondary breakup). This category includes the "massive transfer" and "incomplete fusion" processes. Examples of this type of reaction are numerous where the energy is defined by ϵ : $^{6,7}Li$(<0.5 MeV/u)[43], ^{14}N(~1 MeV/u)[47], ^{10}B to ^{19}F(3-8 MeV/u)[46,52,53], ^{12}C(4-15 MeV/u)[55], ^{16}O(14 MeV/u)[58] and α(30 MeV/u)[49,50].

An unusual aspect of the breakup process is the wide range of energies at which it occurs. Projectiles like d and Li breakup very easily while α-particle breakup is important only at relatively high energies. Hence,

non-statistical particles can arise for some projectiles at very low bombarding energies. For example, in the case of ^{6,7}Li induced reactions on ^{209}Bi at energies near the Coulomb barrier, projectile breakup accounts for 60% of the reaction cross section[43]. Hence, this source of non-statistical particles is not considered in the criterion for fast particle emission established in section III (see Table II).

A recent technique[46,52-55] whereby particular reaction channels are identified via particle-α coincidence measurements are especially important for channels such as RE(HI, yXn) where y is a charged particle with Z=1 or 2 and RE is a rare-earth target. Such coincidence studies of high-energy, light charged particles with near beam velocities and γ rays representative of specific exit channels have provided a clear demonstration for the remaining part of the projectile fusing with the target, in many cases with large cross sections. For example, the reaction channels (^{12}C,αXn) and (^{12}C,2αXn) on a ^{160}Gd target make up a substantial fraction of the reaction cross section, where the emerging α particles have, on the average, the velocity of the beam[55]. At laboratory ^{12}C bombarding energies above 15 MeV/u the (^{12}C,3α) reaction becomes important. Therefore, energetic heavy-ion projectiles like ^{12}C have a very high probability for breakup producing a multiparticle beam and making reaction mechanism studies very difficult to interpret.

Another interesting technique[78], first developed for light-ion reactions, that gives information on the momentum transfer by measuring the correlation angle between fission fragments is useful for the study of heavy-ion reactions. Recently, energetic light particles have been measured in coincidence with two outgoing fission fragments which result from the ^{238}U+^{16}O (E_{Lab}=315 MeV) reaction[58]. Central and peripheral collisions were defined by two different correlation angle bins, the larger correlation angles corresponding to the peripheral collisions. Light particle spectra measured at 14° in coincidence with events in these two correlation-angle bins are shown in (Fig. 20). The temperatures of the two groups of light-particle spectra are the same, corresponding to a spectral shape proportional to exp(-E/T) with T=13 MeV. This result would not be too surprising if the light particles arise from projectile breakup in both correlation-angle bins, with the magnitude of this angle simply reflecting a different fraction of the projectile mass fusing with the target.

The α particle breakup reaction has been thoroughly studied for 140-MeV α particles on a series of

targets[49,50,79,80] and accounts for 40% of the total reaction cross section. The dominant breakup process ($\geq$ 90%)

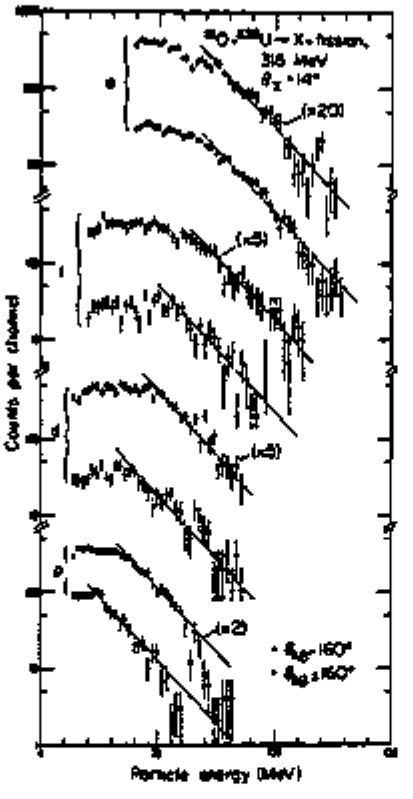

FIGURE 20. Light-particle spectra measured at a laboratory angle of 14° in coincidence with fission fragments for two correlation angle bins[58].

at these bombarding energies results in a fusion of a subset of the projectile nucleons resulting in either evaporation or non-statistical (including pre-equilibrium particle emission, secondary fragmentation, etc.) emission of particles from the residual nucleus, but leaves the remaining subset of projectile nucleons to continue with essentially their initial momentum prior to interaction. The experimental

α-particle breakup cross sections[49] into the ^{3}He-n channel at θ_{Lab}=13° for five target nuclei, divided by $A^{1/3}$, are shown in (Fig. 21). Information on the breakup or fragmentation of heavy-ion projectiles is usually far less complete than that presented above for α particles of 140 MeV, and points up the desirability of more detailed experimental studies on heavy-ion breakup.

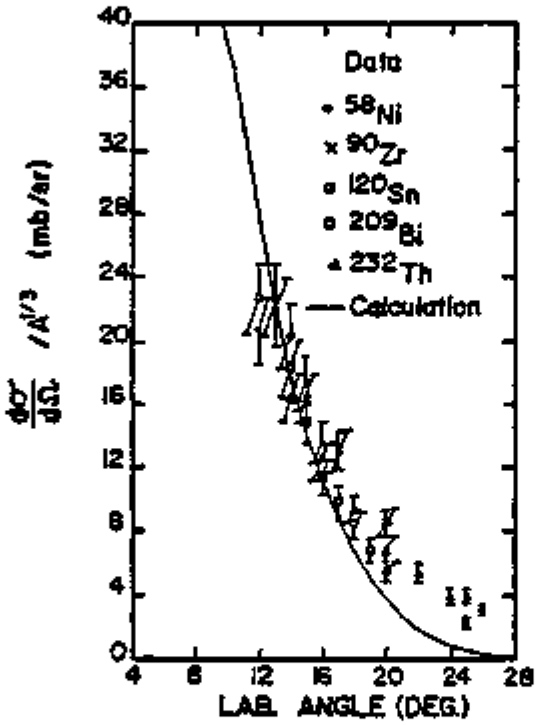

FIGURE 21, Experimental α-particle breakup cross sections[49] into the ^{3}He-n channel at θ_{Lab}=13°, divided by $A^{1/3}$. The α particle bombarding energy is 140 MeV.

B. Preequilibrium Particles (Hot Spots, Fermi Jets.....)

The composite system is excited by the addition of part or all of the projectile. However, the energy and

momentum of the absorbed nucleons are distributed over a few particle-hole states in the composite system. The $^{58}Ni+\alpha$ reaction[41] (ε_0=7.8 MeV/u) is a typical light-ion reaction in this category. Approximately 6% of the protons are preequilibrium or non-statistical in origin (and essentially the entire reaction cross section goes into proton emission).

Preequilibrium neutrons have been observed for the $^{158}Gd+^{12}C$ (E_{Lab}=152 MeV) reaction[32] (see Fig. 22) at an energy of 8.4 MeV/u above the Coulomb barrier, an energy comparable to the above light-ion reaction. The technique employed in this experiment utilizes n-γ coincidence measurements to identify selected exit channels as described earlier. The reaction mechanism responsible for these fast neutrons is unclear. Bondorf et al.[81] ascribe these

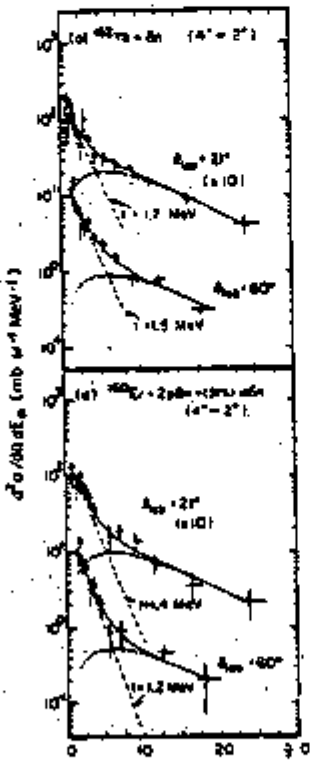

FIGURE 22, Spectra of neutrons[32] in coincidence with indicated gamma transition for 152-MeV ^{12}C on ^{158}Gd

neutrons to Fermi jets. These neutrons may be preequilibrium in origin also or they may arise from projectile breakup. Much more work is required to settle this question.

The inclusive proton spectra from the $^{197}Au(^{16}O,p)X$ reaction[57] at a projectile laboratory energy of 315 MeV, corresponding to an energy of 14.7 MeV/u above the Coulomb barrier, have been interpreted in several ways. Preequilibrium emission analysis leads to an initial exciton number of 25. The data are also consistent with emission from a source moving with a velocity of about 0.1c in the laboratory. These inclusive spectra have nearly the same temperatures as the light particle spectra from the previously discussed $^{238}U+^{16}O$ reaction at the same energy where the light particles are measured in coincidence with fission fragments gated into two correlation angle bins. This may be a clue that in both reactions the light particles result mainly from projectile breakup processes and are not giving information on the heavy-ion nuclear reaction mechanism.

As shown in Table III, non-statistical particles have been reported for a large number of heavy-ion reactions. Evidence for light-particle emission arising from heavy-ion breakup processes is substantial (see section IV.A), however, the relative importance of other reaction mechanisms, such as those discussed in this section, for producing non-statistical light particles is still not well established and a subject needing much more study.

C. Particle Emission from Neck Rupture

Although such particles are well known to be associated with fission[26], no definite evidence exists for this source of particles from deep-inelastic reactions.

V. HEAVY-ION FUSION

In papers[82,83] presented to this conference, it is reported that the statistical properties of the compound nucleus are important for determining the fusion cross sections of light heavy-ion reactions. The concept of a "statistical yrast line" is introduced that runs nearly parallel to the yrast line with an additional energy ΔQ. The model then assumes that fusion occurs only for those values of the angular momentum where the energy exceeds that of the "statistical yrast line". The quantity ΔQ is an open parameter. Values of maximum fusion cross sections calculated with this model for ΔQ=10 MeV are

plotted as triangles in (Fig. 23) (this theory does not predict the energy at which the cross section is a maximum, therefore, the present calculations have been made at the energy where the experimental fusion cross section is a maximum). The maximum experimental cross sections for the same reactions are shown as solid circles.

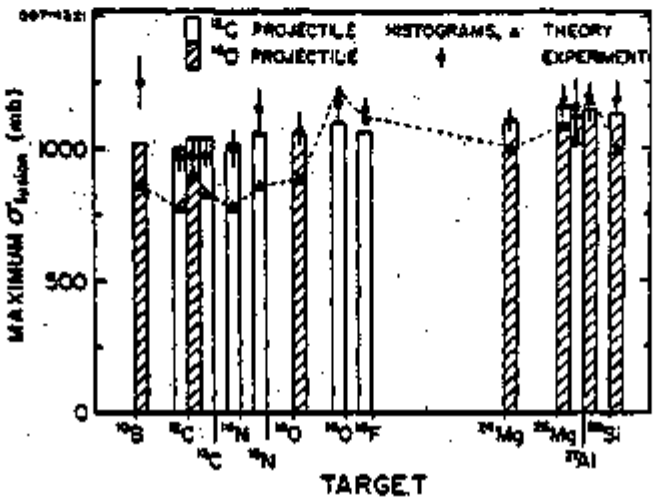

FIGURE 23, Comparison of calculated and experimental maximum fusion cross sections. The histograms are calculated with a one-body dissipation model[84,85] and the triangles are calculated with a model[82,83] that includes the "statistical yrast line"

The histograms represent the results of the calculation for fusion cross section maxima by a very different model that depends on entrance channel criteria. This latter model[84,85] is based on the classical motion of the nuclei in a potential field, including the nuclear proximity potential[86], and dissipative forces based on the one-body friction of Randrup[87]. The comparison of the fusion cross sections for target-projectile systems involving lp-shell and 2s-1d shell nuclei with this classical model is

discussed elsewhere[88,89].

The classical model based on entrance channel criteria gives better overall agreement with experiment than does the very different model based on compound nucleus properties. Hence, the conclusion[82] that the fusion cross section at high energies is essentially determined by the "statistical yrast line" of the compound nucleus is not established by the present comparison with experimental data. Neither model reproduces some of the data such as the cross section for the $^{10}B+^{16}O$ reaction.

It is well known that fusion cross sections for heavy projectile-target systems are considerably larger than those predicted from the liquid drop model[85]. These observations need not indicate that the liquid drop limits are too low, but rather that interaction times for these higher angular momenta, which have potential pockets, are so long that there is considerable relaxation of the mass asymmetry degree of freedom[85,88,89]. In addition, the lifetimes of these trajectories are long enough to produce a nearly $1/\sin\theta$ angular distribution of the "fission fragments". The lifetimes of these dinuclear systems (a type of molecular resonance) in the window of ℓ values between the liquid drop critical ℓ value and the last ℓ value with a potential pocket (larger ℓ values lead to deep-inelastic processes) may well be long enough for light-particle emission to occur before "fission". This may be a source of the evaporation-like charged particles with a temperature of about 2.5 MeV observed for the $^{197}Au+^{40}Ar$ (E_{Lab}=340 MeV) reaction[90,61]. A rotation time for this system with a typical angular momentum in the above window is 8×10^{-21} sec. The time required for the evaporation of a particle with a temperature of 2.5 MeV [$\tau\approx0.5\times10^{-22}\exp(13/T)$] is approximately 9×10^{-21} sec. Hence, times of the order of the particle evaporation time are required to explain the experimental "fission fragment" angular distributions and suggests that particle emission may well occur from the dinuclear system with its reduced Coulomb potential due to deformation.

VI. CONCLUSIONS

1. Dissipative heavy ion collisions cover a whole range of angular momentum values between direct peripheral events and "fusion" events. For very heavy systems these collisions make up almost the entire reaction cross section. Lighter systems sometime allow the study of narrow ℓ bins.

2. Damped or deep-inelastic collisions are a binary

process. Three-body events are due to sequential fission.

3. The identity of projectile and target is essentially preserved in a damped heavy-ion collision. Drift in charge and mass is small for heavy systems.

4. Large amounts of kinetic energy and orbital angular momentum may be dissipated, the magnitudes of these quantities depend on the relative motion and the intrinsic motion and quantal nature of the exchanged nucleons.

5. A strong alignment and polarization of the intrinsic angular momentum is observed (except for the fully relaxed events of heavy systems).

6. The energy loss is the most important experimental parameter for determining the nature of the collision. As a function of the energy loss, one obtains simple correlations with the first and second moments of various distributions.

7. The relationship between the variance in the charge and mass distributions depends on the dynamical driving force and σ_A^2/σ_Z^2 may be smaller or larger than $(A/Z)^2$ depending on the dinuclear system and the energy loss. There is some evidence that peripheral collisions show a neutron skin effect.

8. Pauli blocking plays an important role in the correlation between the energy loss and the variance of the charge or mass distribution, and strongly influences the average energy loss per nucleon exchanged. Nucleon exchange is the dominant mode of energy loss.

9. The variance in the charge distribution for fixed mass asymmetry, $\sigma_Z^2(A)$, is constant for energy losses above approximately 30 MeV for all systems, except the $^{197}Au+^{132}Xe$ reaction, indicating the possible importance of quantal effects.

10. Measurements of light-particle spectra (mostly neutrons) indicate that the reaction partners from a damped collision have the same temperatures over a range of energy losses. Hence, one infers equilibration of the energy between the two reaction partners.

11. Intrinsic degrees of freedom including energy dissipation and A/Z equilibration are relaxed on a time scale less than 2×10^{-22} sec (this is determined from a classical model for an energy loss of about 30 MeV, for larger energy losses the upper time limit is increased).

12. For bombarding energies less than 5 MeV per nucleon above the Coulomb barrier, particle emission is predominately evaporation (neglecting reactions where breakup occurs at low energy). The parameter $\varepsilon_0=(m/\mu)(E_{cm}-V_{Coul})$ puts the light and heavy ion reactions on the same footing even

though very large amounts of energy may be dissipated in some heavy-ion collisions.

13. Identifiaction of giant resonances in heavy ion reactions by spectral structure is severely hampered when particle emission channels are open.

14. As the bombarding energy increases beyond 5 MeV per nucleon above the Coulomb barrier, nonstacistical particle emission sets in and total thermalization of the energy is no longer valid.

15. Projectile breakup is a well established source of fast nonstatistical light particles and becomes a dominant reaction mechanism already at bombarding energies of 15 MeV per nucleon. Hence, the projectile breakup process complicates severely heavy-ion reaction mechanism studies at energies in excess of 15 MeV per nucleon.

16. Evidence of fast nonstatistical particles from mechanisms other than projectile breakup, such as fireball emission, hot spots, Fermi jets etc. is not well established. Much additional work is required in order to characterize these mechanisms.

17. Fusion cross section can be reasonably well reproduced by very different models based on entrance channel limitations to compound nucleus limitations.

ACKNOWLEDGEMENT

This work is supported by the U.S. Department of Energy. The author thanks his colleagues J. R. Birkelund, D. Hilscher, W. U. Schröder and W. W. Wilcke for many helpful discussions.

REFERENCES

1. P. R. Brazier-Smith et al., Proc. Roy. Soc. London A326, 393 (1972).
2. A. Gobbi, proceedings of this conference (1979).
3. W. U. Schröder, proceedings of this conference (1979).
4. C. Ngô, proceedings of this conference (1979).
5. E. Essel, K. Hartel, P. Kienle, H. J. Körner, K. E. Rehm, R. E. Segel, P. Sperr and W. Wagner, proceedings of this conference (1979).
6. H. Specht, proceedings of this conference (1979).
7. D. V. Harrach et al., Phys. Rev. Lett. 42, 1728 (1979); P. Glässel, Phys. Rev. Lett. 43, 1483 (1979).
8. W. W. Wilcke et al., Phys. Rev. C, to be published.
9. R. Vandenbosch, Phys. Rev. C20, 171 (1979).
10. W. Trautmann, proceedings of this conference (1979).

11. W. Trautmann et al., Phys. Rev. Lett. 39, 1062 (1977).
12. W. U. Schröder et al., Phys. Rep. 45, 301 (1978).
13. K. E. Rehm et al., preprint (1979).
14. W. U. Schröder et al., Phys. Rev. Lett. 36, 514 (1976).
15. Y. Eyal et al., Phys. Rev. Lett. 42, 826 (1979).
16. H. Breuer et al., Phys. Rev. Lett. 43, 191 (1979).
17. Y. Eyal, proceedings of this conference (1979).
18. H. Breuer et al., proceedings of this conference (1979).
19. U. Arit et al., proceedings of this conference (1979).
20. W. U. Schröder et al., unpublished results.
21. J. R. Huizenga et al., Phys. Rev. Lett. 37, 885 (1976).
22. J. Randrup, Nucl. Phys. A307, 319 (1978); A327, 490 (1979).
23. M. Berlanger et al., Z. Phys. A291, 133 (1979).
24. J. Poitou et al., preprint (1979).
25. H. Breuer et al., proceedings of this conference; and unpublished data.
26. R. Vanbenbosch and J. R. Huizenga, Nuclear Fission, (Academic Press, 1973), see Chapter XI B.
27. W. U. Schröder et al., Phys. Rev. C16, 623 (1977).
28. A. C. Mignerey et al., proceedings of this conference; and unpublished results.
29. D. Hilscher et al., Phys. Rev. C20, 556 (1979).
30. N. Frascaria et al., Phys. Rev. Lett 39, 918 (1977).
31. P. Doll et al., Phys. Rev. Lett. 42, 366 (1979).
32. L. Westerberg et al., Phys. Rev. C18, 796 (1978)
33. R. Babinet et al., preprint (1979).
34. D. Hilscher et al., Phys. Rev. C20, 576 (1979).
35. Y. Eyal et al., Phys. Rev. Lett. 41, 625 (1978).
36. J. Galin et al., Phys. Rev. C9, 1113 (1974).
37. M. Dakowski et al., preprint (1979).
38. B. Tamain et al., preprint IPNO-RC-79-02 (1979).
39. B. Tamain, proceedings of this conference (1979).
40. H. C. Britt and A. R. Quinton, Phys. Rev. 124, 877 (1961).
41. R. W. West, Phys. Rev. 141, 1033 (1966).
42. J. Galin et al., Phys. Rev. C9, 1126 (1974).
43. H. Freieslehen et al., Phys. Rev. C10, 245 (1974).
44. J. W. Harris et al., Phys. Rev. Lett. 38, 1460 (1977).
45. H. Ho et al., Z. Physik, A283, 235 (1977).
46. T. Inamura et al., Phys. Lett. 68B, 51 (1977).
47. T. Nomura et al., Phys. Rev. Lett. 40, 694 (1977).
48. C. K. Gelbke et al., Phys. Lett. 71B, 83 (1977).
49. J. R. Wu et al., Phys. Rev. Lett. 40, 1013 (1978).
50. R. Koontz et al., proceedings of this conference (1979).

51. A. Gamp et al., Phys. Lett. 74B, 215 (1978).
52. D. R. Zolnowski et al., Phys. Rev. Lett. 41, 92 (1978).
53. H. Yamada et al., Phys. Rev. Lett. 43, 605 (1979).
54. A. C. Kahler et al., proceedings of this conference (1979).
55. K. Siwek-Wilczyńska et al., Phys. Rev. Lett. 42, 1599 (1979).
56. H. Homeyer et al., Proceedings of the Symposium on Heavy Ion Physics from 10 to 200 MeV/amu, Brookhaven National Laboratory, July 16-20 (1979).
57. T. J. M. Symons et al., LBL Report 8379 (1979).
58. T. C. Awes et al., Phys. Lett. 87B, 43 (1979).
59. H. Ho et al., Proceedings of Symposium on Deep-Inelastic and Fusion Reactions with Heavy Ions, Berlin, (1979).
60. P. Gonthier et al., proceedings of this conference (1979).
61. M. F. Rivet et al., proceedings of this conference (1979).
62. H. Delagrange et al., Phys. Rev. Lett. 43, 1490 (1979).
63. S. Wald et al., proceedings of this conference (1979).
64. C. W. Fulmer et al., proceedings of this conference (1979).
65. J. B. Ball et al., Phys. Rev. Lett. 40, 1698 (1978).
66. R. L. Ferguson et al., proceedings of this conference (1979).
67. E. Takada et al., proceedings of this conference, p. 34 (1979).
68. E. Takada et al., proceedings of this conference, p. 35 (1979).
69. N. E. Sanderson et al., proceedings of this conference (1979).
70. J. C. Adloff et al., proceedings of this conference (1979).
71. R. Billerey et al., proceedings of this conference (1979).
72. M. Sasagase et al., proceedings of this conference (1979).
73. K. Okada et al., proceedings of this conference (1979).
74. J. Bisplinghoff et al., proceedings of this conference (1979).
75. J. Pampus et al., Nucl. Phys. A311, 141 (1978).
76. J. Bisplinghoff et al., Nucl. Phys. A269, 147 (1976).
77. A. Cunsolo et al., proceedings of this conference (1979).
78. W. J. Nicholson and I. Halpern, Phys. Rev. 116, 175 (1959).

79. J. R. Wu et al., Phys. Rev. C20, 1284 (1979).
80. R. W. Koontz et al., Phys. Rev. Lett. 43, 1862 (1979).
81. J. P. Bondorf et al., NORDITA preprint 79/27 (1979).
82. S. M. Lee et al., proceedings of this conference (1979).
83. T. Matsuse et al., proceedings of this conference (1979).
84. J. R. Birkelund et al., Phys. Rev. Lett. 40, 1123 (1978).
85. J. R. Birkelund et al., Phys. Rep. 56, 107 (1979).
86. J. Blocki et al., Ann. Phys. (NY) 105, 427 (1977).
87. J. Randrup, Ann. Phys. (NY) 112, 356 (1978).
88. J. R. Huizenga et al., Proceedings of the Symposium on Heavy Ion Physics from 10 to 200 MeV/amu, Brookhaven National Laboratory, July 16-20 (1979).
89. J. R. Birkelund et al., Proceedings of Symposium on Deep-Inelastic and Fusion Reactions with Heavy Ions, Berlin (1979).
90. J. M. Alexander, proceedings of this conference (1979).

F. Bombarding Energy Dependence of the $^{209}Bi + ^{136}Xe$ Reaction

Bombarding Energy Dependence of the $^{209}Bi + ^{136}Xe$ Reaction

W.W. Wilcke, J.R. Birkelund, A.D. Hoover,
J.R. Huizenga and W.U. Schröder

Departments of Chemistry and Physics and
Nuclear Structure Research Laboratory
University of Rochester, Rochester
New York 14627 U.S.A.

V.E. Viola, Jr.

Department of Chemistry
University of Maryland, College Park
Maryland 20742 U.S.A.

K.L. Wolf, A.C. Mignerey

Argonne National Laboratory
Argonne, Illinois 60439 U.S.A.

ABSTRACT:

A previous study of the strongly damped reaction $^{209}Bi + ^{136}Xe$ at 1130 MeV has been extended to the lower bombarding energy of 940 MeV. With the same experimental technique, angular, energy and atomic charge distributions and their correlations have been measured. The angular distribution of the reaction products is sideways peaked, but less strongly focussed than at the higher bombarding energy. The energy spectrum extends far below the Coulomb energy calculated for touching spherical ions, indicating large deformations of the final fragments. The charge distributions are Gaussians approximately centered around the initial fragmentation. Examination of the correlations between experimental observables confirms that the energy loss parameter is the most suitable quantity to describe the time evolution of the reaction. The relationship between energy loss and the width of the charge distribution is studied to gain information on the contribution of the nucleon exchange process to the total dissipated energy. The bombarding energy dependence of this relationship suggests that the Pauli blocking of occupied single particle levels is an important effect, leading to a smaller dispersion of the fragment Z-distribution for a given energy loss than expected from a classical theory. A quantitative analysis establishes the nucleon exchange as the dominant mechanism for the dissipation of kinetic energy. With the aid of a phenomenological model a decomposition of the reaction cross section in

partial waves is performed. Classical trajectory calculations assuming spherical ions are compared to an empirically determined deflection function, energy loss and interaction times. These calculations do not provide a consistent description of the experimental results, since the energy loss is systematically underestimated. From the interaction times and widths of the charge distributions an angular momentum dependent proton number diffusion coefficient $D_Z(\ell)$ is derived, which shows a pronounced saturation behavior for angular momenta less than 2/3 of the grazing angular momentum. The total probability for sequential fission of the target-like fragment is determined to be 30% for all inelastic events. A simple model is presented which allows calculation of this probability on the basis of known fission properties of heavy elements.

[NUCLEAR REACTIONS $^{209}Bi + ^{136}Xe$, E_{Lab} = 940 MeV; measured $\sigma(\theta, E, Z)$; strongly damped reaction; deduced correlations, interaction times, transport-coefficients; comparison to trajectory calculations; yield of sequential fission.]

I. INTRODUCTION

The reaction $^{209}Bi + ^{136}Xe$ has been studied previously[1] at a bombarding energy of E_{Lab} = 1130 MeV as a typical example of a strongly damped reaction. The use of such a heavy system has several advantages: Strongly damped collisions are by far the dominant reaction mechanism and allow, therefore, the study of the reaction over a wide range of impact parameters: from grazing collisions to nearly central impacts. Thus the correlations between observable quantities such as dissipated kinetic energy, reaction angle and the charge distribution of the final reaction fragments can be studied much more readily than for light systems, where only a comparatively narrow window of impact parameters leads to strongly damped events.[2]

It has been shown in the previous study,[1] that the degree of kinetic energy dissipation is the most useful parameter to characterize the time development of strongly damped reactions. Therefore, it is a natural extension of this investigation to change the bombarding energy and thus the amount of kinetic energy available for dissipation. This paper reports on a detailed study of the system $^{209}Bi + ^{136}Xe$ at a bombarding energy of E_{Lab}=940 MeV, an energy of 1.4 times the Coulomb energy of touching spheres.

In the following section, the experimental procedures are described briefly. Results on elastic scattering, angular, charge and energy distributions for the Xe and Bi-like reaction products are discussed in Section III. In Section IV the implications of the experimental results for the understanding of the

reaction mechanism are discussed. Special attention is given to the importance of nucleon exchange as a mechanism of energy dissipation and to the importance of the Pauli principle for an understanding of the correlation between the widths of the element distributions and the degree of energy damping. In Section V a model is presented to calculate the observed yield of sequential fission of the Bi-like fragments. A summary can be found in Section VI.

II. EXPERIMENTAL PROCEDURE AND DATA REDUCTION

The experiments were performed at the LBL SuperHILAC accelerator. Targets of 235 $\mu g/cm^2$ ^{209}Bi on carbon backings were bombarded with 940-MeV ^{136}Xe ions. The beam energy was determined with four independent detector systems calibrated with α and ^{252}Cf fission sources. The result was 940 MeV, with a statistical uncertainty of 12 MeV, allowing for a pulse height defect of 51 MeV according to the procedure of J.B. Moulton et al.[3,4,5]. The reaction products were detected in two ΔE - E silicon surface barrier detector telescopes and one silicon detector. The thicknesses of the two ΔE detectors were 14.3 and 9.6 μm, respectively. The telescopes subtended angles of 0.5° and 1.0° in the reaction plane. Two monitor counters, placed out of plane at fixed forward angles monitored the beam intensity and allowed for dead-time corrections. The beam was defined by two pairs of slits outside the chamber and one pair of cleanup slits at its entrance. Permanent magnets and 160 $\mu g/cm^2$ thick Ni foils protected the detectors from delta electrons generated by the beam.

The electronic setup was very similar to the one described in Ref. 1, and included pileup circuitry and a system allowing a determination of the system dead-time, taking into account the pulsed character of the HILAC beam. All data were recorded on magnetic tape in an event-by-event mode.

In Figure 1 are shown examples of the laboratory energy spectra taken with the singles detector. The spectrum at θ_L = 24° shows an intense elastic peak at 838 MeV, a broad bump of

strongly damped events centered at 600 MeV and a second small bump at 450 MeV which is due to sequential fission of the heavy, Bi-like fragments, which are also scattered to forward angles for large negative reaction Q-values. In the two-dimensional $\Delta E - E$ spectra the two groups of fragments are well separated.

At $\theta_L = 38°$ the elastic peak is still dominant and has a low-energy tail smoothly joining the strongly damped, Xe-like fragments centered around 550 MeV. The Bi-like fragments show up at this angle as a bump located around 420 MeV, whereas the sequential fission events are not distinguishable from other events in the one-dimensional spectrum. At $\theta_L = 43°$, very close to the quarter-point angle, the spectrum shows the same components as at $\theta_L = 38°$. For larger angles the spectra are dominated by the recoil nuclei.

Since elastic scattering events were not resolved from those with small energy losses, a standard peak was defined at forward scattering angles and subtracted from the spectra taken at angles in the vicinity of the quarter point. This procedure has been used extensively in the analysis of heavy ion elastic scattering.[6]

The experimental $\Delta E - E$ distributions were converted into $Z - E$ distributions using the tables of Northcliffe and Schilling[7], renormalized to the experimental stopping power of Xe-ions in Si. A constant mass-to-charge ratio of $A/Z = 2.52$ was assumed to convert the measured fragment

charge into fragment mass, necessary to perform kinematical calculations. Since ^{136}Xe and ^{209}Bi both have this mass-to-charge ratio, no change in the A/Z ratio is expected to occur during the interaction. The Z-E distributions were transformed into the center-of-mass system for 26-MeV wide bins of the asymtotically measured center-of-mass total kinetic energy, E, using the experimentally established fact that strongly damped reactions at low bombarding energies are essentially of a binary nature[2], except for light-particle evaporation from the highly excited fragments. The reduction in kinetic energy of the fragments in the laboratory system due to the evaporation of neutrons was corrected for. Details of this calculation can be found in Ref. 1. Further corrections were applied for the energy loss in the target and Ni foils and for the pulse-height defect in the detectors.

For angles up to the quarter point, the heavy, Bi-like fragments could easily be distinguished from the light fragments, because they occupy a well defined region in the Z-E plane. For larger angles, Xe-like fragments with very large Z-transfer, merge with the Bi-like fragments, and the separation between the fragments is not quite as unambiguous. However, the uncertainty in the reaction cross section introduced by this overlap is not large. Since a sizeable fraction of the heavy fragments is expected to undergo sequential fission, the yield of Bi-like reaction products is of interest. Because there is no simple way to discriminate the elastic recoil events from heavy reaction products, due to insufficient Z and E resolution, the elastic

recoils were accounted for by determining the cross section of elastically scattered Bi from the measured Xe angular distribution and subtracting it from the total yield of heavy fragments.

III. EXPERIMENTAL RESULTS AND DISCUSSION

A. Elastic scattering and the reaction cross section

The elastic scattering was investigated in order to obtain information on the bombarding energy dependence of the total reaction cross section σ_R, the strong absorption radius R_{SA} and an optical model potential suitable to describe the scattering.

Figure 2 shows the ratio of elastic-to-Rutherford cross section in the center-of-mass-system. Compared to the experiment at 1130 MeV bombarding energy, the quarter point angle is shifted backwards to $\theta_{cm} = 70.2°$, and the slope of the angular distribution at the quarter point is smaller.

The data were analyzed using two models: the semi-quantal model of Fresnel scattering[8] and a one-channel optical model. The reaction parameters deduced are compiled in Table I. In a simple version of the Fresnel model the transmission coefficients are approximated by a step function: $T_\ell = 1$ for $\ell \leq \ell_g$ and $T_\ell = 0$ for $\ell > \ell_g$, where ℓ_g represents the grazing angular momentum. Since this sharp-cutoff model is known to produce large oscillations of the ratio $d\sigma_{EL}/d\sigma_{RUTH}$ forward of the quarter point angle, it was refined[9] by introducing a finite transition region in ℓ-space of width $\Delta\ell$. The broken curve in Fig. 2

indicates the prediction of this model for $\Delta\ell = 16$. Although the overall agreement with the data is reasonable, the relatively gradual fall-off of the data cannot be reproduced by the Fresnel model, regardless of the width $\Delta\ell$ chosen. It is nottoo surprising that the Fresnel model does not fit the present experimental data at 940 MeV as well as the data taken at 1130 MeV, because it is known[8] that diffractive models lose their validity for bombarding energies close to the Coulomb barrier.

Nevertheless, the present experiment still allows extraction of a meaningful value for the grazing angular momentum ℓ_g, where the transmission coefficient assumes the value 3/4, via the relation

$$\theta_{1/4} = 2 \cdot \arctan\,[\eta/(\ell_g + 1/2)] \qquad (3.1)$$

and of the total reaction cross section

$$\sigma_R = \frac{\pi}{k^2}\,(\ell_g + 1/2)^2\,\left[1 + 2\,\frac{\Delta\ell}{\ell_g + 1/2} + \frac{\pi^2}{3}\left(\frac{\Delta\ell}{\ell_g + 1/2}\right)^2\right] \qquad (3.2)$$

Here, η is the Coulomb parameter and k the asymptotic wave number. The values obtained are $\ell_g = 383$ and $\sigma_R = 2.2$b, very similar to the results derived from the simple version of the Fresnel model ($\ell_g = 383$, $\sigma_R = 2.1$b). From these values an interaction radius of $R_{INT} = 15.5$ fm is deduced. This radius is slightly larger than that deduced for the same system at 1130 MeV bombarding energy (15.1 fm). An optical model calculation was performed to check the dependence of the deduced interaction radius on the type of analysis made. A standard Woods-Saxon nuclear potential was used to generate the elastic angular distributions with the optical model code GENOA.[10]

A set of parameters which fit the 1130 MeV data very well produced results which missed the experimental quarter point by several degrees. A two-parameter search on the radii determined values which are considerably larger than the starting values. The strong absorption radius R_{SA} defined by

$$kR_{SA} = \eta + [\eta^2 + \ell_g(\ell_g + 1)]^{1/2} \qquad (3.3)$$

was found to be 15.5 fm, which is consistent with an increase of the interaction radius at the lower bombarding energy. There is some confirmation of this tendency from other analyses of heavy ion elastic scattering[6,11].

These findings illuminate the well known difficulty in defining a unique and energy independent optical potential for very heavy ion reactions. Therefore, no further attempt was make to search for a set of more suitable optical-model parameters. For the further analysis the grazing angular momentum as extracted with the modified Fresnel model was employed in order to be consistent with Ref. 1.

B. Angular, charge and energy distributions of the Xe-like reaction fragments.

The angular distribution of the light reaction products in the laboratory system is shown in Fig. 3. Similar to the 1130 MeV experiment, the cross section is focussed around an angle slightly forward of the quarter point angle. The integration of the data yields an experimental total reaction cross section of $\sigma_R = (2.1 \pm 0.1)$ barns, in good agreement with the analysis of the elastic scattering data. Towards forward and

backward angles the cross section drops quickly, and the data are consistent with vanishing cross section at $\theta = 0^{\circ}$, indicating that no negative-angle scattering (orbiting) occurs. This is not surprising since orbiting should become less pronounced with decreasing bombarding energy and increasing product $Z_p \cdot Z_T$[2,12].

In Fig. 4 the angular distribution is shown in the center-of-mass system for all events with a total kinetic energy E between 260 and 546 MeV. Since elastic scattering corresponds to an energy of 569 MeV, most of the quasielastic events have been excluded. Compared to the 1130 MeV experiment, the angular distribution is skewed and extends further backwards, indicating that the nearly perfect angular focussing at 1130 MeV is not an intrinsic feature of the reaction $^{209}Bi + ^{136}Xe$, but has to be viewed as the coincidental result of a delicate balance between nuclear, Coulomb and centrifugal forces, which is destroyed at other bombarding energies.

The Z-distribution of the Xe-like fragments is shown in Fig. 5, integrated over the same range of total kinetic energies. The weak asymmetry is due to a slight shift of the centroid of the Z-distribution towards higher Z for decreasing energies. The bump around $Z = 41$ is caused by a weak contamination with sequential-fission products of Bi-like fragments, which could not be separated completely from the highly damped events. The correlation of the Z-distribution with the energy loss parameter will be discussed later.

In Fig. 6 the energy loss spectrum is shown for the two bombarding energies under study. The arrows indicate the

initially available kinetic energies above the Coulomb barrier as calculated assuming spherical ions separated by the strong interaction radius. The data show clearly that a large fraction of the reaction cross section cannot be explained without assuming strong deformations of the fragments at the time of breakup. This is especially important at the low bombarding energy where 800 mb, (or 40%) of the total reaction cross section, correspond to final kinetic energies below the Coulomb barrier, as compared to 500 mb (or 20%) for the 1130 MeV experiment.

It should be pointed out that the cross section for very low energy losses (below 20 MeV) is not very well known due to insufficient experimental energy resolution. It was not possible to determine whether the cross section is rising monotonically in the quasielastic region, or reaches a maximum around 10 MeV energy loss. In the present paper, a montonic increase of $d\sigma/dE_{Loss}$ with decreasing energy loss has been assumed in the quasielastic region.

C. Angular distribution of the Bi-like fragments

In contrast to the experiment at 1130 MeV, it was possible in the present experiment to observe the heavy Bi-like fragments simultaneously with the light fragments over a wide angular range. The heavy fragments appear as a well separated island in the ΔE versus E distributions for all but the largest angles, where the fringes of the light and heavy fragment Z distribution

start to overlap. It was not possible to make a reliable Z-identification for the slow Bi-like fragments and, therefore, no conversion into the center-of-mass system was performed. However, the angular distribution of the inelastically scattered heavy fragments was obtained indirectly. This was done by subtracting the number of elastically scattered Bi ions, as determined from the measured angular distribution of the Xe ions, from the total number of Bi-like fragments for a given angle.

The resulting angular distribution of the Bi-like reaction products in the laboratory system is shown in Fig. 7. The pronounced asymmetry is due to a kinematic effect: the light reaction fragments are strongly focussed into a narrow angular region, but with rising energy loss the corresponding heavy fragments are scattered to smaller angles. The long tail towards forward angles is, therefore, due to very strongly damped events.

The integrated cross section of the Bi-like fragments is only (1.5 ± 0.4)b, which is 30% smaller than the reaction cross section deduced from the light fragments. This difference can be explained by subsequent fission of the Bi-like reaction fragments in 30% of all non-elastic events. A discussion of this number with respect to known fission properties of elements near Bi is deferred to section V.

D. Qualitative correlations of observables with fragment charge and kinetic energy loss

In Ref. 1 the importance of the energy loss parameter $E_{Loss} = E_{cm} - E$ is discussed in detail for the description of the strongly damped reaction between ^{136}Xe and ^{209}Bi at 1130 MeV. A knowledge of the energy loss determines the associated angular - and Z-distributions, whereas a selection of either Z or the scattering angle does not determine uniquely the other observables. This significance of the energy loss as a parameter characterizing the reaction is confirmed in the present experiment. In Fig. 8 the double-differential cross section $d^2\sigma/d\bar{Z}dE$ is plotted on a logarithmic scale vs. the total kinetic energy of the fragments. The events are sorted into 3-Z unit wide bins, the centroids of which are indicated at the spectra. The arrows indicate Coulomb energies calculated for spherical reaction products, assuming spheres touching at the strong absorption radius. It is obvious from Fig. 8 that multiple proton pickup and stripping reactions lead to rather similar energy loss spectra, confirming that the charge of the light fragment is certainly not a suitable quantity to characterize a given strongly damped event. (The small difference in the shape of the spectra for the $\bar{Z} = 42$ and the $\bar{Z} = 63$ bins is at least partly due to the contamination of the former bin with sequential fission events). A variation from the results of the experiment at 1130 MeV, however, is represented by the relative positions of the maxima in the spectra relative to the calculated Coulomb

barriers. Whereas the maximum of the yield is always located at energies above the Coulomb barrier for $42 \leq Z \leq 63$ at 1130 MeV bombarding energy, this is a feature not corroborrated for most Z-bins in the present experiment. This emphasizes even more strongly the importance of considering deformations or neck degrees of freedom in understanding the low energy data.

Similar to the energy-loss distributions, the angular distributions depend strongly on the atomic number of the fragment, but the correlation is not unique. This is shown in Fig. 9, where the double-differential cross section $d^2\sigma/d\Omega_{cm}\, dZ$ is plotted for the same Z-bins as in Fig. 8. The angular distributions of fragments near the projectile Z are strongly peaked, but the spectra for either very low or very high Z values of the light fragments look similar. In contrast to the findings obtained in the 1130 MeV experiment, the maxima of the angular distributions do not remain centered around $\theta_{cm} = 64°$, where the quasielastic cross section has a maximum, but are shifted steadily to larger angles with increasing magnitude of the charge transfer. A discussion of these results will be given in section IV.

Since a large net charge transfer is related to a large energy loss, it is expected that the maxima in the double-differential cross section $d^2\sigma/d\Omega \cdot dE$ move to larger angles with increasing energy loss. This can indeed be seen in the Wilczyński plot[13] (Fig. 10), showing contour lines of the cross section in the E vs θ_{cm} plane. The ridge of damped events, starting out at $\theta_{cm} = 64°$, moves backwards with decreasing E,

whereas it was found to be parallel to the E-axis in the 1130 MeV experiment. Qualitatively, this result is due to the lower angular momentum for a given impact parameter in the 940 MeV experiment. The Coulomb deflection towards backward angles is more pronounced, and the rotation towards forward angles during the nuclear interaction time is less for smaller angular momenta.

The angular distributions integrated over all Z for a given E bin, i.e. cuts of the Wilczyński plot parallel to the θ_{cm} axis, are shown in Fig. 11. The reaction cross section is sideways peaked for all E values, and no indication of orbiting, such as enhancement of the cross section at forward angles, is visible. The dominant feature of the angular distribution is the increase of its width with increasing energy loss, suggesting that longer reaction times are associated with higher energy losses.

The charge distributions $d^2\sigma/dEdZ$ of the Xe-like fragments as a function of the final total kinetic energy are shown in Fig. 12. It is obvious that the data can be described rather well by Gaussian distributions as indicated by the solid curves. The width of the Z distribution is seen to increase strongly with increasing energy loss, suggestive of a diffusion mechanism where the time available for the diffusion process increases monotonically with increasing energy loss.[14] The width of the 558-MeV bin is mostly due to the experimental Z resolution of about 3 Z-units. The following analysis accounts

for this intrinsic width by assuming an additive law of the variances σ_Z^2.

In agreement with the 1130 MeV experiment, the centroids of the charge distributions stay close to the charge of Xe and drift only very slowly towards mass symmetry. Experimental results for the cross section, the variance σ_Z^2 and the centroid $\langle Z \rangle$ of the fragment charge distributions are collected in Table III for 26-MeV wide E bins.

The relationship between the variance σ_Z^2 and the energy loss is plotted in Fig. 13 for the two bombarding energies. For energy losses up to 100 MeV the two curves are indistinguishable within the experimental errors, but then the energy loss rises less fast for a given increase in σ_Z^2 at the lower bombarding energy. This is to be expected, since there is much less kinetic energy $E_{cm} - V_C$ available at the lower bombarding energy. However, it is surprising that this energy limit, calculated assuming spherical nuclei and indicated by the horizontal arrows, does not show up more distinctly in the experimental data. This fact can again be interpreted as an indication of a strong dynamical deformation of the system, evolving continuously with increasing interaction time.

The dominant role of the energy loss parameter is made obvious by Fig. 14, where the FWHM of the charge distributions is plotted as a function of energy loss and scattering angle. The horizontal lines represent the fits to the angle-integrated data as shown in Fig. 12. It is obvious that there is no correlation between the scattering angle and the width of the charge

distribution for any given energy loss.

Fig. 15 shows the contour lines of $d^3\sigma/dZd\Omega dE$ in a series of Wilczyński plots for 3-Z-unit wide bins. Since the statistical accuracy of triple-differential cross sections is not very high, one has to assign large uncertainties to the contour lines, especially for the Z bins far away from Xe. As can be seen from Fig. 15, positive and negative charge transfers lead to approximately the same shape of the Wilczyński plot. However, a slight influence of the Coulomb barrier calculated for spherical systems may be seen in the fact that the center of the distributions for large positive charge transfers ($\Delta Z>6$) is systematically at higher TKE values than for the corresponding negative charge transfers. In addition, the total cross sections for the positive charge transfer is systematically somewhat higher because the Z distribution is slightly skewed to large Z values (Fig. 5) due to the weak drift towards charge equilibrium.

IV. IMPLICATIONS OF THE BOMBARDING-ENERGY DEPENDENCE FOR THE REACTION MECHANISM OF STRONGLY DAMPED COLLISIONS

A. Correlations between total kinetic energy loss and mass diffusion

The understanding of the mechanism of strongly damped collisions of a few MeV/u has progressed to a stage where the gross features of the reaction are well established. Strongly damped collisions are basically binary processes, where the orbital angular momentum ℓ_i in the entrance channel is the governing parameter for the evolution of a particular collision.

The mean values of the kinematic observables for a given ℓ_i (such as scattering angle, energy loss, angular momentum) follow the laws of classical mechanics assuming conservative potentials and phenomenological friction forces.[12,14,15] The second moments of the observables can be described in terms of quantal[15,16] and statistical fluctuations[17], the latter ones arising from the exchange of nucleons between the two colliding nuclei. This microscopic flux of nucleons, responsible for the observed charge and mass transfer, can also account for a considerable fraction of the observed energy loss, because of the momentum transfer[18] by the nucleons crossing the boundary between the moving heavy ions.

The dissipation of kinetic energy by this mechanism may be described by a friction force $\vec{F}$, which in a classical model can be written as

$$\vec{F} = j(2u_r\hat{e}_r + u_t\hat{e}_t) \qquad (4.1)$$

where u_r and u_t are the radial and tangential components of the relative velocity $\vec{u}$ of the two colliding nuclei, and j is the one-sided mass flux of exchanged nucleons. For a completely open window of area A permitting an unrestricted flux of particles, j is given by $j = n_o A$, where $n_o = \rho\bar{v}/4$ is the static one-sided bulk flux, $\bar{v}$ is the average velocity of nucleons and ρ is the mass density of nuclear matter. Here and in the following paragraphs, it is assumed that the magnitude of $\vec{u}$ is small compared with $\bar{v}$.

The exchange of nucleons gives rise to a finite width of the mass and charge distribution due to the statistical nature of this exchange. The random-walk theory relates the variance σ_A^2 of the mass distribution to the total number N of exchanged nucleons by

$$\sigma_A^2 = N \tag{4.2}$$

where N is given by the time integral of the total particle flux (left and right) 2j/m integrated over the interaction time τ associated with the collision. In the same way the total energy loss is given by a time integral of the kinetic energy loss rate $-\frac{dT}{dt}$:

$$E_{Loss} = -\int_o^\tau \frac{dT}{dt}\, dt \tag{4.3}$$

with $$-\frac{dT}{dt} = \vec{F}(t)\cdot\vec{u}(t) = j(t)\cdot(2u_r^2 + u_t^2),$$

where $T = 1/2\ \mu\vec{u}^2$ is the instantaneous kinetic energy of the relative motion of the nuclei in the center-of-mass system and $\vec{F}(t)$ is the friction forces defined in Eq. 4.1.

For peripheral reactions the radial component of the velocity $\vec{u}$ is much smaller than the tangential component. Thus one may neglect u_r and write

$$\frac{dT}{dt} = - j(t) \cdot u_t^2 = - j(t) \cdot \frac{2}{\mu} T(t) \qquad (4.4)$$

Differentiating Eq. (4.2) with respect to t gives

$$\frac{dN}{dt} = \frac{d\sigma_A^2}{dt} = \frac{2j(t)}{m} \qquad (4.5)$$

Thus one can express dt in terms of $d\sigma_A^2$, as has been suggested by Schröder et al[1].

Inserting Eq. (4.5) into Eq. (4.4) results in the differential equation

$$\frac{dT(t)}{T(t)} = - \frac{m}{\mu} d\sigma_A^2 = - \frac{m}{\mu} \left(\frac{A}{Z}\right)^x d\sigma_Z^2 \qquad (4.6)$$

where the mass and charge variances have been related by

$$\sigma_A^2 = \left(\frac{A}{Z}\right)^x \sigma_Z^2 \qquad (4.7)$$

Here, x = 1 and x = 2 represent the extreme assumptions of totally uncorrelated and totally correlated proton and neutron exchange[19], respectively. These terms refer to the distribution of reaction products in the N-Z plane. The contour lines of constant cross section are circles in the former and straight lines in the latter case.

The solution of the differential equation (4.6) is given by

$$\ln(T_o/T) = \frac{m}{\mu} \left(\frac{A}{Z}\right)^x \sigma_Z^2 \qquad (4.8)$$

where $T_o = E_{cm} - V_c$ and $T = E_{cm} - V_c - E_{Loss}$ are the kinetic energies in the entrance and exit channels. Thus this model predicts a linear relationship between $\ln (T_o/T)$ and σ_Z^2, with a slope given by $\frac{m}{\mu} (\frac{A}{Z})^x$. In Fig. 16 the experimental data are shown for the reaction at 940 and 1130 MeV. It is seen that the data indeed follow straight lines for both bombarding energies and not too high energy losses. This experimental observation may be regarded as an indication for energy dissipation and the proton exchange to be of statistical nature and to occur on the same time scale. The above simple classical model, however, fails to explain the observed bombarding-energy dependence of the slope, and the value for the slope as given by Eq.(4.8) is too small compared to the experimental results, as can be seen from Table IV. It has been suggested by Randrup[18,20] and Schröder et al.[21] that the effect of the Pauli principle plays an important role in the calculation of nucleon exchange. Only those nucleons close to the Fermi surface can participate in the exchange, and thus the flux of nucleons through the window is reduced by a factor $1/\alpha$ as compared to the classical value. Accordingly, the variance σ_A^2 of the mass distribution, which is given by Eq. 4.2, is reduced by the Pauli principle. It can be proven[21], however, that the total energy loss rate is not affected by the reduction of the flux, since each transferred nucleon carries on the average a larger amount of momentum than in the classical case, since only fast nucleons close to the Fermi surface can be exchanged. It has been shown,[18] that drift coefficients including both the rate of energy loss and the net mass transfer are not affected by the inclusion of the

Pauli principle in a theory which is based on one-body transition operators.

Since the quantum-mechanical treatment leads to a variance σ_A^2 that is smaller than the value expected classically but does not affect the energy loss rate, the classical expression for the slope has to be multiplied with the factor α to account for the quantum-mechanical reduction of the nucleon flux. Moreover, the importance of the Pauli blocking is expected to depend strongly on the relative velocity of the two ions, since the relative momentum displaces the Fermi momentum spheres of the two nuclei in k-space and opens up otherwise inaccessible parts of the phase space, thus reducing the impact of the Pauli principle on the mass dispersion for higher bombarding energies. Therefore, the slope for a bombarding energy of 1130 MeV is predicted to be smaller than for 940 MeV, in accordance with experiment. A more quantitative comparison of the quantal theory with experimental data has to await a complete dynamical calculation taking into account the velocity-dependent blocking and has, in addition, to account for the correlation between neutron and proton exchange.

An estimation of the reduction of the flux, however, can be made by considering the displacement of two Fermi spheres of equal radius k_F by the momentum k, corresponding to the relative motion of the two nuclei. If one assumes $k_F >> k$, a simple geometrical calculation of the ratio α of the total volume occupied by nucleons in k-space to that where the two spheres do not overlap yields the relation,

$$\alpha = \frac{2}{3}\frac{k_F}{k} = \frac{2}{3}\left(\frac{\mu \cdot T_F}{m(E_{cm} - V_c)}\right)^{1/2} \qquad (4.9)$$

Here $T_F = 37$ MeV is the Fermi kinetic energy in nuclear matter and μ/m is the reduced mass number of the dinuclear system. Since nucleon exchange is restricted to those parts of phase space where the two Fermi spheres do not overlap, Eq. (4.9) gives approximately the reduction of the flux from its classical value and, therefore, also the increase of the slope as compared to Eq. (4.8). Inserting the parameters from Table I for the 940 MeV and 1130 MeV experiments into Eq. (4.9) one obtains theoretical values of $\alpha = 3.0$ and 2.3, respectively. In Table IV, the experimental values for the slopes α are compared to the predicted ones, assuming either totally correlated or uncorrelated nucleon exchange. It can be seen from this comparison that the assumption of correlated nucleon exchange (i.e. $\sigma_A^2 = (A/Z)^2\,\sigma_Z^2$) and introduction of Pauli blocking leads to a reasonable agreement with the experimental data. This simple calculation of the blocking, however, leads to a bombarding energy dependence of α that is too weak compared to the data. For a more realistic calculation, such effects as the variation of the wave number along a trajectory, the influence of a non-zero nuclear temperature and of the driving forces in the A-Z plane have to be included. It was the aim of this discussion, however, to demonstrate that the experimental data indicate the importance of Pauli blocking in nucleon exchange processes.[22] In addition, it should be pointed out that further simultaneous measurements of the mass and charge distributions would be very helpful to

disentangle the effects of the proton-neutron correlations from those due to the Pauli-blocking on the function $\sigma_Z^2(E_{Loss})$. Only then will it be possible to decide whether the nucleon exchange process alone can account for the large energy losses observed or if additional energy dissipation mechanisms such as shape degrees of freedom have to be included. A recent experimental study[23] of the reaction $^{208}Pb + ^{136}Xe$ at a very low bombarding energy ($E_{cm} - V_c \approx 40$ MeV) indicates that for this system the correlation between σ_A^2 and σ_Z^2 is given by the correlated limit ($x = 2$). If this result holds also for the system $^{209}Bi + ^{136}Xe$ at the higher bombarding energies studied here, then most of the observed energy loss up to 150 MeV can be accounted for by the nucleon exchange mechanism. This point will be further discussed in Section IV C.

B. Angular momentum decomposition

A procedure described in Ref. 1 was used to extract an angular-momentum scale from the data. For this purpose, a monotonic relationship between the angular momentum in the entrance channel and the total kinetic energy loss was assumed, neglecting fluctuations predicted[24] to be of particular importance for central collisions. Using the relation

$$\frac{d\sigma}{d\ell} = \pi\lambda^2(2\ell + 1)\, T_\ell \qquad (4.10)$$

between cross section and angular momentum, a one-to-one relationship between the experimental energy loss spectrum $d\sigma/dE_{Loss}$ and $d\sigma/d\ell$ can be established.[25] The transmission coefficients

T_ℓ may be taken either from the sharp-cutoff model or the optical model fit to the elastic scattering data. In the following analysis the latter were taken. The results of this analysis are shown in Fig. 17 and the first 3 columns in Table V. As can be seen, there is a nearly linear relationship between ℓ and E_{Loss} for both bombarding energies.

The above ℓ scale is used in conjunction with the angle θ_{max}, giving the location of the cross-section maximum (cf. Table III), to construct an experimental deflection function $\theta(\ell)$. The results for the two bombarding energies are shown in Fig. 18. As was already obvious from the Wilczynski plot, the ridge of maximum cross section for the 940-MeV data moves to larger scattering angles with decreasing impact parameter, qualitatively similar to a Coulomb deflection function. However, there is still a considerable angle $\Delta\theta$, by which the double-nucleus system rotates to forward angles before it breaks apart,[14] as can be seen from a comparison with the sum θ_c of the Coulomb deflection angles in entrance and exit channels. Details of the calculation can be found in Refs. 1 and 25. The labels NS and S indicate the extreme cases of a non-sticking and sticking contact of the nuclear surfaces during the interaction time. In the latter case 23% of the angular momentum ℓ_i in the entrance channel is converted into intrinsic spin of the colliding nuclei. In the non-sticking case, the final orbital angular momentum ℓ_f is the same as in the entrance channel. The interaction time is calculated as

$$\tau(\ell_i) = \Delta\theta(\ell_i) \cdot \mathcal{J}(\ell_i)/\hbar\,\ell_f \qquad (4.11)$$

and J represents the appropriate moment of inertia for the non-sticking and sticking case, for which the following values were taken:

$$J_{NS} = \mu \cdot R_{INT}^2 \tag{4.12}$$

$$J_S = \mu R_{INT}^2 + \frac{2}{5} (M_p R_p^2 + M_T R_T^2) \tag{4.13}$$

The interaction times thus deduced as a function of ℓ_i are given in columns 5 and 9 of Table V. The results for the non-sticking model are shown in Fig. 19. At both bombarding energies the interaction times increase approximately exponentially with decreasing orbital momentum. Thus the lifetimes can be parameterized as:

$$\tau(\ell_i) = \begin{cases} 1.53 \cdot 10^{-20} \exp(-\ell_i/80)\,\text{sec} & E_L = 940\ \text{MeV} \\ 2.18 \cdot 10^{-20} \exp(-\ell_i/84.8)\,\text{sec} & E_L = 1130\ \text{MeV} \end{cases} \tag{4.14}$$

As can be seen, the slopes are comparable for both bombarding energies, but for a given ℓ_i the interaction time is about twice as long for the higher bombarding energy. For a given impact parameter, the interaction times are nearly the same for both energies.

C. Classical trajectory calculations

The phenomenological analysis presented in the previous section allowed the extraction of the scattering angle θ_{cm}, the total kinetic energy loss E_{Loss} and the interaction time τ as functions of the angular momentum ℓ_i. The same quantities can be obtained as the result of classical dynamical calculations. In the following, a model[26] with four degrees of freedom is

discussed. The time-dependent distance r of the centers of the spherical nuclei, the angle Θ between the line connecting them and the beam axis, and the angles of rotation Θ_T and Θ_p of the two spheres were determined by the following equations of motion:

$$\mu\ddot{r} = \frac{-\partial V_C}{\partial r} - \frac{\partial V_N}{\partial r} + \mu r\dot{\theta}^2 - f_r(r)\,\dot{r}$$

$$\mu r^2\dot{\theta} = \ell = \ell_i - J_T - J_p$$

$$\dot{J}_T = -C_T\left(\frac{r}{C_T + C_p}\right)^2 f_\theta(r)\,[C_T(\dot{\theta}_T - \dot{\theta}) + C_p(\dot{\theta}_p - \dot{\theta})] \qquad (4.15)$$

$$\dot{J}_p = -C_p\left(\frac{r}{C_T + C_p}\right)^2 f_\theta(r)\,[C_T(\dot{\theta}_T - \dot{\theta}) + C_p(\dot{\theta}_p - \dot{\theta})]$$

Here ℓ_i, J_T and J_p are the orbital angular momenta in the entrance channel and the spins of the target and projectile, respectively. The quantities μ, C_T and C_p are the reduced mass of the system and the radii of projectile and target, as taken from Myers' systematics.[27] In order to solve the above equation, the Coulomb potential V_C, the nuclear potential V_N, the radial friction form factor $f_r(r)$ and the tangential friction form factor $f_\theta(r)$ have to be specified. The Coulomb potential proposed by Bondorf, Sobel and Sperber[14] for heavy ions was taken for all calculations. For the nuclear potential the proximity potential,[28] a modified version of the proximity potential[20] and the Krappe-Nix potential[12] were chosen. In the modified version of the proximity potential derived from the consideration that the maximum nuclear density is limited to the nuclear bulk value,

the repulsive hard core of the normal proximity potential is absent. The proximity potentials were used in conjunction with the proximity friction force given by Randrup,[18] which is essentially due to the mechanism described in section 4.1. The Gross friction force[12] with radial and tangential strength parameters of $k_r = 2.5 \cdot 10^{-26}$ and $k_t = 10^{-28}$ sec fm^2 MeV^{-3} was used in connection with the Krappe-Nix potential.

Fig. 20 shows the results of the classical calculations solving Eqs. (4.15) in comparison with the data (full symbols) obtained from the partial-wave analysis. The lowest part of Fig. 20 depicts the deflection function. The general trend of a Coulomb-dominated behavior is reproduced about correctly, but the theoretical calculations show too much structure due to the Coulomb and nuclear rainbows, and the modified proximity potential leads to fusion for $\ell_i < 150$, which appears to be unphysical.

The uppermost part of Fig. 20 shows the interaction times as a function of ℓ_i. Here the interaction time in the calculation is defined as that period of time, where the distance between the centers of the two is smaller than the interaction radius. The calculations using the soft proximity and the Krappe-Nix potentials qualitatively reproduce the results of the phenomenological analysis, whereas the hard core of the standard proximity potentials yields much shorter interaction times for $\ell_i < 250$.

The middle part of Fig. 20 shows E_{Loss} as a function of ℓ_i. It is obvious that all three calculations fail to reproduce the

large energy losses observed. To a large extent this is due to the fact that no shape-degrees of freedom were incorporated into the calculations, so that the available energy above the Coulomb barrier is an upper limit for the energy which can be dissipated. The importance of deformations is demonstrated by the fact that events with a total kinetic energy as low as 270 MeV have been observed. This energy corresponds to the Coulomb repulsion of two spherical Bi and Xe ions 23.6 fm apart and is close to the lowest E-value (280 MeV) observed at 1130 MeV bombarding energy and comparable to the predicted[29] mean kinetic energy (300 MeV) released by fission of a fictitious compound system (Xe + Bi). This may indicate that the highest energy losses occurring in a strongly damped collision are not determined by the details of the reaction mechanism, but by the same properties of nuclear matter which govern the snapping of the neck in fission.

The importance of surface degrees of freedom (vibration[30] or forming of a neck[21]) is less obvious for more peripheral collisions. Fig. 20 shows that calculations for spherical ions understimate the energy loss as compared with phenomenological analyses for all ℓ-values. Inclusion of a neck degree of freedom strongly enhances the energy loss even for large impact parameters, but it appears premature to conclude from this comparison that deformations are important for peripheral collisions.

D. Transport coefficients derived from the phenomenological model

In the framework of a diffusion model,[17] the time evolution of an observable x such as the charge transfer $\Delta Z = Z - Z_o$ in the reaction is governed by the Fokker-Planck equation

$$\frac{\partial}{\partial t} P(x,t) = \frac{-\partial}{\partial x} [v_x(x,t) \cdot P(x,t)] + \frac{\partial^2}{\partial x^2} [D_x(x,t) \cdot P(x,t)] \quad (4.15)$$

where v_x and D_x are the drift and diffusion coefficient, respectively. For constant transport coefficients the solution of Eq. (4.15) is a Gaussian

$$P(x,t) = (4\pi D_x \cdot t)^{-1/2} \cdot \exp[-(x - v_x t)^2/(4D_x t)] \quad (4.16)$$

where the variance and the centroid of the distribution are given by $\sigma_x^2 = 2D_x \cdot t$ and $x_o = v_x t$, respectively. As discussed in section IV. A, however, there is no reason to expect the transport coefficients to be time-independent, since the exchange of nucleons certainly depends strongly on the relative distance between the two nuclei. Time-dependent transport coefficients still lead to Gaussian solutions, however, if they do not depend explicitly on the variable x. The experimental Gaussian shape of the Z distributions shown in Fig. 12 indicates therefore only that the charge drift coefficient v_z and the diffusion coefficient D_Z are very weakly dependent on the fragment charge Z. The experimentally measured variance can then be written as

$$\sigma_Z^2 = 2 \int_0^\tau D_Z(t) \cdot dt \equiv 2 \bar{D}_Z \cdot \tau \quad (4.17)$$

where a time-averaged diffusion coefficient $\bar{D}_Z$ has been defined by introducing the interaction time τ. Since the latter has been extracted from the data using the phenomenological procedure described in section 4.2, it is possible to determine the experimental value of the time-averaged diffusion coefficient $\bar{D}_Z$. Since the interaction time τ as well as the width σ_Z^2 are strongly dependent on the impact parameter, it is expected that these diffusion coefficients are functions of the angular momentum in the entrance channel: $\bar{D}_Z = \bar{D}_Z(\ell_i)$. Assuming the non-sticking model for the derivation of the interaction times, the two curves shown in Fig. 21 are obtained using Eq. (4.17). For both bombarding energies, the diffusion coefficient rises quickly with decreasing ℓ for angular momenta close to the grazing ℓ, but reaches a plateau for intermediate and low ℓ values. As has been pointed out in Ref. 1, this behavior might be attributed to the presence of the conservative and radial friction forces, which limit the interpenetration depth of the two colliding ions over a wide range of ℓ values. Thus the size of the window between the ions which largely determines the flux of nucleons and hence the diffusion coefficient remains rather constant for $\ell < 0.7 \cdot \ell_g$.

The saturation values of the diffusion coefficients D_Z are $1.1 \cdot 10^{22}$ sec^{-1} and $0.6 \cdot 10^{22}$ sec^{-1} for the high and low bombarding energy, respectively. It is not surprising that for the lower energy D_Z is smaller, since the Pauli blocking of nucleon exchange is more effective and, in addition, the trajectories for a given impact parameter penetrate less deeply, thus reducing the size of the window for nucleon exchange.

An inspection of Fig. 12 shows that the centroids of the charge distributions drift slightly towards symmetry with increasing energy loss. Drift and diffusion coefficients are related by the Einstein relation to the driving force $\partial U/\partial Z$ and the nuclear temperature T:

$$\frac{\Delta Z}{\sigma_Z^2} = \frac{\bar{v}_t \cdot \tau}{2\bar{D}_Z \cdot \tau} = - \frac{1}{2T} \frac{\partial}{\partial Z} U(Z) \ . \qquad (4.18)$$

The model-independent experimental ratio $\Delta Z/\sigma_Z^2$ is approximately constant and equal to 0.21 ± 0.1 for energy losses up to 120 MeV and decreases steadily beyond 120 MeV. If the temperature T is given by the intrinsic temperature of the nucleus[31], which is related, in a Fermi gas model, to the total excitation energy E^* by

$$aT^2 = E^* \approx E_{Loss} \qquad (4.19)$$

where a is the level density parameter of the combined system, then the magnitude of the right hand side of Eq. (4.18) is large for grazing collisions, which are characterized by a small loss of kinetic energy provided the driving force is not too small. Therefore, a very fast, non-diffusive energy-loss mechanism has been postulated[32], which would heat the system to a high temperature before the diffusion starts and thus explain the experimentally observed small drift.

The inclusion of the Pauli principle in the description of the nucleon exchange processes, however, gives a better account of the experimental ratios $\Delta Z/\sigma_Z^2$ without the necessity to introduce additional dissipation mechanisms. The quantum mechanical

treatment[20] reveals that the quantity T entering in Eq. (4.18) is merely a measure of the phase space available for nucleon exchange and equal to the nuclear temperature only in a certain limit. As has been discussed in Section IV. A, the relative motion of the colliding nuclei opens otherwise inaccessible parts of the phase space and has therefore similar effects as a non zero temperature. To estimate which intrinsic temperature T^* is equivalent to a given relative momentum k, one may assume that a spherical shell of thickness $2T^*$ and mean radius k_F with $T_F = \hbar^2 k_F^2/2m$ contributes to nucleon exchange between two hot nuclei at rest. This shell has a thickness $\Delta k = k_1 - k_2$ in k-space given by:

$$2T^* = \frac{\hbar^2}{2m}(k_1^2 - k_2^2) = \frac{\hbar^2 k_F}{m}\Delta k \ . \qquad (4.20)$$

The ratio of the volume of this shell to the total volume is equated to $1/\alpha$ where α is determined by Eq. (4.9), giving

$$\frac{4\pi\, k_F^{\,2}\,\Delta k}{4\pi\, k_F^{\,3}/3} = \frac{3}{2}\frac{k}{k_F} \qquad (4.21)$$

and yielding $\Delta k = (1/2)k$. Inserting Δk into Eq. (4.20) defines an "effective temperature" T^* for intrinsically cold nuclei colliding with a relative momentum k per nucleon:

$$T^* = \frac{\hbar^2}{4m} k \cdot k_F = \frac{1}{2}\left[\frac{m(E_{cm} - V_C)}{\mu} \cdot T_F\right]^{1/2} . \qquad (4.22)$$

Inserting the parameters of Table I yields an effective temperature of 4.1 MeV for the present experiment (940 MeV) in the limit of grazing collisions. A more refined calculation by Schröder et al. leads to a value of 3.5 MeV.

In order to compare this result with the experiment, it is necessary to obtain an estimate of the static driving force $\partial U/\partial Z$. It can be calculated for spherical nuclei approximately from the liquid-drop masses of the two fragments and the Coulomb, centrifugal and nuclear potentials. Evaluating the total potential at the strong-absorption radius for grazing collisions yields a driving force of about -1 MeV/Z-unit, depending somewhat on the details of the calculation. Inserting this value and the effective temperature into Eq. (4.18), one obtains a theoretical value of 0.14 for $\Delta Z/\sigma_Z^2$. This value is in qualitative agreement with the experiment, therefore, the inclusion of the Pauli principle readily explains the low value of the drift measured in these experiments without the necessity of introducing an additional energy loss mechanism.

It should be noted that nucleon exchange is a fast mechanism in the sense that most of the energy loss associated with nucleon exchange happens during the approach phase of the reaction, where the relative momentum k is high and therefore the energy loss rate is large. Thus there is less of a qualitative discrepancy between models with high initial energy loss such as the one proposed by Gross et al.[12] and the diffusion model than is frequently assumed.

V. YIELD OF SUBSEQUENT FISSION

As has been discussed in Section III. V, there is evidence for sequential fission of the excited Bi-like fragments in approximately 30% (f=0.30) of all non-elastic events. In the following section, a simple formalism will be discussed, which allows this fraction to be calculated using known fission properties of heavy elements. The

basis of the formalism is a study of the energy dependence of the ratio of neutron to fission width, Γ_n/Γ_f. Assuming the evaporation model description for Γ_n and the Bohr-Wheeler formula for Γ_f[33], and adopting a Fermi gas expression for the level densities entering these models, one obtains the following expression for the excitation energy dependence of Γ_n/Γ_f:

$$\frac{\Gamma_n}{\Gamma_f} = \frac{4A^{2/3}\, a_f(E^* - B_n)}{k_o\, a_n(2a_f^{1/2}(E^* - E_f)^{1/2} - 1)} \times \exp\left(2a_n^{1/2}(E^* - B_n)^{1/2} - 2a_f^{1/2}(E^* - E_f)^{1/2}\right) \quad (5.1)$$

where $k_o = \hbar^2/2mr_o^2 = 9.8$ MeV, B_n is the neutron binding energy, E_f is the effective fission barrier, a_n the level density parameter at equilibrium, and a_f is the level density parameter at the saddle point. Using a compilation[33] of values for B_n, E_f and a_n/a_f as measured for low excitation energies E^* for 15 nuclei between Lu and U, it is possible to extrapolate Γ_n/Γ_f to the high excitation energies observed in strongly damped collisions.

Since Γ_f/Γ_n shows a very steep, exponential dependence on the excitation energy, it is possible to associate with the condition $\Gamma_n=\Gamma_f$ a critical excitation energy E^*_{CT}, constituting a rather sharp boundary between the regimes of deexcitation by neutron emission and by fission. In Fig. 22 calculated values of E^*_{CT} are plotted as open circles vs. the atomic number Z. An approximately linear relationship between E^*_{CT} and Z results, given by:

$$E^*_{Crit}(Z) = \begin{cases} 808 - 8.9 * Z \text{ MeV} & Z < 91 \\ 6 \text{ MeV} & Z \geq 91 \end{cases} \quad (5.2)$$

The filled rhomboids indicate measured values for E_{crit} [34,35,36]. It can be seen that there is good agreement between the existing meacurements and the extrapolations. In deducing Eq. (5.2) the dependence of E^*_{cr} on A has been removed by averaging over the broad isotopic distribution of a given element produced in a strongly damped collision.

The effect of angular momentum on the fission probability can be taken into account by renormalizing the values of $E^*_{cr}(Z)$ for the angular-momentum-dependent fission barrier and neutron binding energy[33]. Hence, the inclusion of a nuclear angular momentum J leads to a modification of Eq. (5.2), where the critical energy E^*_{cr} now depends on both Z and J.

$$E^*_{cr}(Z,J) = \begin{cases} E^*_{cr}(Z) \cdot (1-J^2/6400) & J \leq 80\hbar \\ 0 & J > 80\hbar \end{cases} . \qquad (5.3)$$

Alternatively, Eq. (5.3) can be interpreted as a definition of a critical atomic number $Z_{cr}(E^*,J)$ for each given excitation energy and spin, such that all elements with $Z > Z_{cr}$ decay by fission.

From the measured charge distribution of the Xe-like fragments the distribution of the heavy fragments can easily be deduced assuming that charged-particle evaporation is not an important process. Thus the centroid of the heavy fragment-Z distribution is given by

$$\langle Z \rangle_H = Z_T + Z_p - \langle Z \rangle_L \qquad (5.4)$$

and the variances σ_Z^2 corresponding to heavy and light fragments are equal.

In addition, assuming a model for the relation between E_{Loss} and the amount of angular momentum transferred into intrinsic spin - such as the non-sticking or sticking models - the two-dimensional surface $Z_{cr}(E^*,J)$ can be reduced to a one-dimensional function $Z_{cr}(E^*)$. The excitation energy E^* can be obtained from E_{Loss}, since the division of the available excitation energy occurs approximately proportional to the masses of the fragments[31,37] For a Gaussian charge distribution, the cross section $\sigma_{SF}(E^*)$ for sequential fission can then be calculated by integrating the charge distribution from $Z_{cr}(E^*)$ upwards:

$$\Delta\sigma_{SF}(E^*) = \frac{\Delta\sigma_R(E^*)}{\sigma_Z(E^*)\sqrt{2\pi}} \int_{Z_{cr}(E^*)}^{\infty} \times \exp\left\{\frac{-(Z - \langle Z\rangle_H(E^*))^2}{2\sigma_Z^2}\right\} dZ \ . \qquad (5.5)$$

In Eq. (5.5) $\Delta\sigma_R(E^*)$ is the reaction cross section for a particular E-bin. The total probability f for sequential fission is obtained by summing $\Delta\sigma_{SF}$ for all excitation energies. The results are compiled in Table VI for the non-sticking model and for a more realistic J-distribution where $J(\ell_i)$ was parameterized by

$$J(\ell_i) = J_o(\ell_i)\left(1 + \exp\frac{\ell_i - \ell_o}{A}\right)^{-1} \qquad (5.6)$$

and

$$J_o(\ell_i) = \ell_i\left(1 - \frac{J_{NS}}{J_S}\right)J_T(J_T + J_p)^{-1} \qquad (5.7)$$

Here, J_o is the spin transfer to the heavy fragment in the

sticking limit, and values of ℓ_o = 283 and A = 45 were estimated from Ref. 30.

The effect of charged-particle evaporation was studied by reducing $\langle Z \rangle_H$ arbitrarily by one Z-unit before integrating Eq.(5.5). It was seen that the results are not sensitive to the assumptions entering the calculation, and the theoretical values compare favorably with the experimental result. For the 1130-MeV data sequential fission of the heavy fragments is predicted to occur with about 50% probability. In Fig. 23 the cross section $d\sigma_{SF}/dE_{Loss}$ is shown for sequential fission as a function of E_{Loss} for the 940 MeV data as calculated from Eq. (5.5).

VI. CONCLUSIONS

The study of the reaction $^{209}Bi + ^{136}Xe$ at a bombarding energy of E_{Lab} = 940 MeV allowed, in connection with a previous experiment performed at E_{Lab} = 1130 MeV, a detailed investigation of the bombarding energy dependence of strongly damped reactions and, in addition, confirmed conclusions drawn from the previous experiment. The angular distribution of the reaction products is characteristic for a fast peripheral process and is strongly dominated by the repulsive Coulomb force, although a considerable rotation of the dinuclear system is observable.

The element distributions of the reaction products for different energy losses are Gaussian and consistent with a diffusion model employing diffusion coefficients that are independent of the atomic number Z. These diffusion coefficients are dependent on the impact parameter for grazing collisions and constant for more central collisions.

The study of the relation between the dissipation of kinetic

energy and the width of the charge distribution as a function of the bombarding energy indicates that a classical description of nucleon exchange is not valid. Instead, consideration of the blocking of the nuclear orbitals available for nucleon transfer due to the Pauli principle is essential for an understanding of this relationship as well as of the ratio between charge drift and diffusion. In a simple model, the degree of blocking is inversely proportional to the momentum per nucleon of the relative motion and thus most effective for collisions at low bombarding energies. Further, more refined dynamical calculations including this blocking effect will be necessary to understand quantitatively the experimental results and to decide whether or not energy dissipation due to statistical nucleon exchange can account completely for the large amounts of dissipated energy observed or if additional energy loss mechanisms have to be included. Further simultaneous measurements of mass and Z distributions at different bombarding energies of selected systems will be helpful, because of a strong and characteristic velocity dependence of these processes.

ACKNOWLEDGEMENT

This work was supported by the U.S. Department of Energy. The authors express their gratitude for the hospitality extended to them at the Lawrence Berkeley Laboratory, Berkeley. Particular thanks are due to Dr. M. Zisman for his efficient and continuous support during the experiments and to H. Grunder and the operating staff of the SuperHILAC accelerator. Use of the facilities of the Nuclear Structure Research Laboratory supported by a grant from the National Science Foundation is acknowledged.

REFERENCES

1. W.U. Schröder, J.R. Birkelund, J.R. Huizenga, K.L. Wolf, and V.E. Viola, Jr., Phys. Rep. 45, 301 (1978).
2. W.U. Schröder and J.R. Huizenga, Ann. Rev. Nucl. Sci. 27, 465 (1977).
3. J.B. Moulton, J.E. Stephenson, R.P. Schmitt, and G.J. Wozniak, Nucl.Instr. Meth. 157, 325 (1978); H. Essel, P. Sperr, K. Hartel, P. Kienle, H.J. Körner, K.E. Rehm and W. Wagner, (to be published).
4. S.B. Kaufman, E.P. Steinberg, B.D. Wilkins, J. Unik, A.J. Gorski, and M.J. Fluss, Nucl. Instr. Meth. 115, 47 (1974).
5. Recent measurements using 780 MeV Xe ions were consistent with the large pulse height defect described in Ref. 3.
6. J.R. Birkelund, J.R. Huizenga, H. Freiesleben, K.L. Wolf, J.P. Unik, and V.E. Viola, Jr., Phys. Rev. C13, 133 (1976), and references cited therein.
7. L.C. Northcliffe and R.F. Schilling, Nucl. Data, Sect. A7, 233 (1970).
8. W.E. Frahn and R.H. Venter, Ann. Phys. 24, 243 (1963); W.E. Frahn, Phys. Rev. Lett. 26, 568 (1971) and Ann. Phys. 72, 524 (1972).
9. W.E. Frahn, Nucl. Phys. A302, 267 (1978).
10. F.G. Perey, unpublished report.
11. C. Olmer, M. Mermaz, H. Buenerd, C.K. Gelbke, D.L. Hendrie, J. Mahoney, D.K. Scott, M.H. Macfarlane, and S.C. Pieper, Phys. Rev. C18, 205 (1978).
12. D.H.E. Gross and H. Kalinowski, Phys. Rep. 45, 175 (1978).
13. J. Wilczyński, Phys. Lett. B47, 484 (1973).

14. J.P. Bondorf, M.I. Sobel, and D. Sperber, Phys. Rep. C15, 83 (1974).

15. R.A. Broglia, C.M. Dasso, and Aa. Winther, Phys. Lett. 53B, 301 (1974); H.H. Deubler and K. Dietrich, Phys. Lett. 56B, 241 (1975); Nucl. Phys. A277, 493 (1977); J.N. De, F. Beck, D.H.E. Gross, and H. Kalinowski, Z. Phys. A277, 385 (1976).

16. D. Agassi, C.M. Ko, and H.A. Weidenmüller, Ann. Phys. 107, 140 (1977); Ann. Phys. 117, 237 (1979); Ann. Phys. 117, 407 (1979); H. Hofmann and P.J. Siemens, Nucl. Phys. A257, 464 (1976).

17. W. Nörenberg, Phys. Lett. B52, 289 (1974); Z. Phys. A274, 241 (1976); A276, 84 (1976); S. Ayik, B. Silvermann, and W. Nörenberg, Z. Phys. A277, 299 (1976); Z. Phys. A279, 145 (1976); S. Ayik, G. Wolschin, and W. Nörenberg, Z. Phys. A286, 271 (1978); C. Riedel, G. Wolschin, and W. Nörenberg, Z. Phys. A290, 47 (1979).

18. J. Randrup, Ann. Phys. 112, 356 (1978); J. Błøcki, Y. Boneh, J.R. Nix, J. Randrup, M. Robel, A.J. Sierk, and W.J. Swiatecki, Ann. Phys. 113, 330 (1978).

19. F. Beck, M. Dworzecka, and H. Feldmeier, Z. Phys. A289, 113 (1978); Y. Eyal, G. Rudolf, I. Rode, and H. Stelzer, Phys. Rev. Lett. 42, 826 (1979); J. Barette, P. Braun-Munzinger, C.K. Gelbke, M.L. Harvey, H.E. Wegner, and B. Zeidman, Nucl. Phys. A299, 147 (1978); P. Braun-Munzinger and J. Barette, Nucl. Phys. A299, 161 (1978); B. Gatty, D. Guerreau, M. Lefort, X. Tarrago, J. Galin, B. Cauvin, J. Girard, and H. Nifenecker, Nucl. Phys. A253, 511 (1975); H. Breuer, B. G. Glagola,

V.E. Viola, K.L. Wolf, A.C. Mignerey, J.R. Birkelund, D. Hilscher, A.D. Hoover, J.R. Huizenga, W.U. Schröder, W.W. Wilcke, Phys. Rev. Lett. 43, 791 (1979).

20. J. Randrup, Nucl. Phys. A307, 319 (1978); Nucl. Phys. A327 490 (1979).

21. W.U. Schröder, J.R. Birkelund, J.R. Huizenga, W.W. Wilcke, and J. Randrup, Phys. Rev. Lett. 44, 30 (1980).

22. It should be stressed that the interpretation of the quantity α has changed as compared to Ref. 1. In the purely classical treatment of Ref. 1 the nucleon exchange mechanisms could explain only a fraction of the observed energy loss, and α was introduced to describe the effect of an ad hoc postulated non-exchange energy loss mechanism.
Now, with the inclusion of quantal effects the nucleon exchange process is found responsible for the majority or possibly all of the observed energy loss, and α is interpreted as the ratio of the classical to the quantal flux of exchanged nucleons. If future results should indicate, that non-exchange processes do contribute to the energy loss, then α would have to be interpreted as the sum of this ratio and the contribution from the non-exchange process.

23. H. Essel, K. Hartel, W. Henning, P. Kienle, H.J. Körner, K.E. Rehm, P. Sperr, W. Wagner, and H. Spieler, Z. Phys. A289, 265 (1979).

24. G. Wolschin and W. Nörenberg, Phys. Rev. Lett. 41, 691 (1978); A. Olmi, H. Sann, D. Pelte, Y. Eyal, A. Gobbi,

W. Kohl, V. Lynen, G. Rudolf, H. Stelzer, and R. Bock, Phys. Rev. Lett. 41, 688 (1978). A particular model [H. Esbensen et al., Phys. Rev. Lett. 41, 296 (1978)] where the entire energy loss is due to surface vibrations leads to sizeable fluctuations even for peripheral collisions.

25. W.U. Schröder, J.R. Birkelund, J.R. Huizenga, K.L. Wolf, and V.E. Viola, Jr., Phys. Rev. C16, 623 (1977).

26. J.R. Birkelund, J.R. Huizenga, J.N. De and D. Sperber, Phys. Rev. Lett. 40, 1123 (1978).

27. W.D. Myers, Nucl. Phys. A204, 465 (1973).

28. J. Błocki, J. Randrup, W.J. Swiatecki and C.F. Tsang, Ann. Phys. 105, 427 (1977).

29. V.E. Viola, Jr., Nucl. Data Sect. A1, 391 (1966).

30. R.A. Broglia, C.M. Dasso, G. Pollarolo, and A. Winther, Phys. Rev. Lett. 41, 25 (1978).

31. D. Hilscher, J.R. Birkelund, A.D. Hoover, W.U. Schröder, W.W. Wilcke, J.R. Huizenga, A. Mignerey, K.L. Wolf, H.F. Breuer, and V.E. Viola, Jr., Phys. Rev. C20, 576 (1979).

32. C. Ngô, J. Péter, B. Tamain, M. Berlanger, and F. Hanappe, Nucl. Phys. A267, 181 (1976).

33. R. Vandenbosch and J.R. Huizenga, Nuclear Fission, Academic Press, New York and London, 1973.

34. U. Lynen, Y. Civelekoglu, A. Olmi, H. Sann, D. Pelte, A. Gobbi, G. Rudolf, H. Stelzer, and R. Bock, ADE. Conf. 78-007-001, Hirschegg, Austria, 1978.

35. L.G. Moretto, Proceedings of Hakone Conf. September, 1977, Japan.

36. M. Rajagopalan, L. Kowalski, D. Logan, M. Kaplan, J.M. Alexander, M.S. Zisman, and J.M. Miller, Phys. Rev. C19, 54 (1979).

37. Y. Eyal, A. Gavron, I. Tserruya, Z. Fraenkel, Y. Eisen, S. Wald, R. Bass, G.R. Gould, G. Kreyling, R. Renfordt, K. Stelzer, R. Zitzmann, A. Gobbi, U. Lynen, H. Stelzer, I. Rode, and R, Bock, Phys. Rev. Lett. 41, 625 (1978).

TABLE I. A comparison of the reaction parameter for the system $^{209}Bi + ^{136}Xe$ at two bombarding energies.

Quantity	940 MeV	1130 MeV	Units
E_{Lab}	940	1130	MeV
E_{cm}	569	684	MeV
$\theta_{1/4}$(lab)	43.5°	33°	deg
$\theta_{1/4}$(c.m.)	70.1°	54°	deg
μ (reduced mass)	82.4	82.4	$\bar{u}$
k_∞ (wave number)	47.37	51.94	fm^{-1}
η (Coulomb-parameter)	268.4	244.8	-
R_{INT} (Fresnel)	15.5	15.1	fm
ℓ_g (Fresnel exp.$\theta_{1/4}$)	383	480	$\hbar$
σ_R (" " ")	2.06	2.70	b
σ_R (exp)	2.09	2.80	b
R_{SA} (optical model)	15.5	15.2	fm
V_C (R_{INT})	416	428	MeV
$T_o = E_{c.m.} - V_C(R_{INT})$	152	256	MeV
$[E_{c.m.} - V_C(R_{INT})]/u$	1.86	3.11	MeV/u
peak in $d\sigma_R/d\Omega$(lab)	39.5°	30°	deg
peak in (c.m.)	64.5°	50°	deg

TABLE II. The angular distribution of the Xe-like fragments in the C-M system, integrated over all Z and all E values between 260 and 545 MeV. This accounts for 80% of the reaction cross section. The unit of the table entries is mb/sr.

	+0°	+1°	+2°	+3°	+4°	+5°	+6°	+7°	+8°	+9°
40°	-	-	-	-	10	15	22	25	28	33
50°	39	52	65	74	94	126	159	178	182	200
60°	317	408	505	865	1046	1033	994	921	859	783
70°	760	655	617	556	489	438	386	348	309	276
80°	256	240	231	203	172	164	159	158	149	130
90°	121	112	93	73	61	50	42	37	30	25

The charge distribution of the Xe-like fragments, integrated over angle, $40^\circ \leq \theta_{cm} \leq 100^\circ$, and E values between 260 and 545 MeV. The units of the table entries are mb/Z-unit. The (*) indicates contamination with sequential fission events.

Z	+0	+1	+2	+3	+4	+5	+6	+7	+8	+9
40	6*	6*	6*	8*	9*	9*	11	14	18	29
50	44	64	121	194	224	229	190	148	108	80
60	62	45	36	26	17	12	6	4	2	1

TABLE III. $^{209}Bi + ^{136}Xe$ at E_L = 940 MeV (E_{cm} = 569 MeV)
The first E window is 23 MeV wide, all others 26 MeV. The variance σ_Z^2 is corrected for the experimental Z resolution. The total cross section accounted for amounts to 1.96 barns. θ_{max} is the angle, where $d\sigma/d\Omega_{cm}$ has its maximum in the C-M system for each E bin.

Bin #	<E> MeV	$<E_{loss}>$ MeV	σ_Z^2	<Z>	dσ/dE mb/MeV	θ_{max} deg
12	558	12	0.4 ± 0.2	54 ± 0.1	14.2	64
11	533	35	1.2 ± 0.3	54.3 ± 0.3	10.4	64
10	507	61	2.3 ± 0.4	54.5 ± 0.5	7.1	66
9	481	87	3.6 ± 0.4	55.1 ± 0.5	6.1	67
8	455	113	5.7 ± 0.8	55.6 ± 0.7	6.3	68
7	429	139	9.7 ± 1.5	55.9 ± 0.7	7.2	69
6	403	165	13.0 ± 2.5	56.0 ± 1.0	7.8	70
5	377	191	19.9 ± 3.3	56.3 ± 1.0	7.1	72
4	351	217	29 ± 7	56.8 ± 1.0	5.2	72
3	325	243	39 ± 15	57.0 ± 1.5	3.1	76
2	299	269			1.7	76
1	273	295			0.9	

TABLE IV. Comparison of experimental and theoretical slopes, $\frac{m}{\mu}\left(\frac{A}{Z}\right)^{x}\alpha$, from the linear relation of $\ln(T/T_o)$ vs. σ_Z^2 for the $^{209}Bi + ^{136}Xe$ reaction at bombarding energies of 940 and 1130 MeV. This slope is a measure of the fraction of energy loss associated with nucleon exchange. The quantity μ/m is the reduced mass number of the dinuclear system, $T_o = E_{cm} - V_C$ and $T = E_{cm} - V_C - E_{Loss}$. The values of $x = 1$ and $x = 2$ represent extreme assumptions of uncorrelated and correlated proton and neutron exchange, respectively. For the classical model $\alpha = 1$ (see Eq. 4.8). For the quantal model (see text) α is calculated approximately by Eq. 4.9 and always has a numerical value larger than one.

E_{Lab} (MeV)	Experimental Slope (see Fig. 16)	Classical Slope		Quantal Slope	
		x=1	x=2	x=1	x=2
940	0.25	0.03	0.08	0.09	0.23
1130	0.11	0.03	0.08	0.07	0.17

TABLE V. The results of the angular momentum decomposition.

			Non-sticking model			Sticking model			
Bin #	$\langle E_{Loss} \rangle$	$\langle \ell_i \rangle$	$\Delta\Theta$	τ	$\bar{D}_Z$	$\langle \ell_f \rangle$	$\Delta\Theta$	τ	$\bar{D}_Z$
	MeV	$\hbar$	deg	10^{-22}sec	10^{22}sec^{-1}	$\hbar$	deg	10^{-22}sec	10^{22}sec^{-1}
12	12	376	7.5	1.2	0.17	288	14.9	3.8	0.05
11	35	340	13.6	2.4	0.26	261	21.2	6.0	0.10
10	61	314	16.8	3.1	0.37	241	24.4	7.5	0.15
9	87	294	20.3	4.0	0.44	225	27.9	9.1	0.20
8	113	273	24.4	5.2	0.54	209	31.8	11.2	0.25
7	139	249	29.4	6.9	0.70	191	36.6	14.2	0.34
6	165	219	36.5	9.8	0.67	168	43.1	19.0	0.34
5	191	184	46.9	14.9	0.67	141	52.9	27.7	0.36
4	217	150	60.6	23.7	0.61	115	65.7	42.2	0.34
3	243	122	66.4	31.9	0.61	94	70.6	55.8	0.35
2	269	102	73.3	42.1		78	76.8	72.6	
1	295	90				69			

TABLE VI. Probability $f = \sigma_{SF}/\sigma_R$ for sequential fission of the heavy (Bi-like) fragments.

Bombarding energy (MeV)	940	1130
Experiment	0.30 ± 0.15	-
NS Model	0.32	0.49
Realistic J-distribution	0.37	-
NS Model and charged particle evap.	0.27	-

FIGURE CAPTIONS

Fig. 1. Laboratory energy spectra of the reaction products taken at the angles indicated.

Fig. 2. The experimental ratio $d\sigma_{EL}/d\sigma_{RUTH}$ of the elastic- to Rutherford cross section as a function of the center of mass scattering angle is compared to calculations using the generalized Fresnel model (dashed curve) and an optical model (solid curve).

Fig. 3. Laboratory angular distribution of the light, Xe-like reaction products. The curve is to guide the eye.

Fig. 4. Center-of-mass angular distribution of the reaction cross section for events with total kinetic energies in the indicated range. This distribution accounts for 80% of the total reaction cross section.

Fig. 5. The Z distribution of projectile-like fragments integrated over the indicated angle and TKE range. The low-Z wing of the distribution is slightly affected by incompletely removed events from sequential fission of the heavy fragment.

Fig. 6. The energy-loss spectrum of the $^{209}Bi + ^{136}Xe$ reaction for 940 MeV and 1130 MeV bombarding energy. The energy-loss E_{Loss} is defined as the difference between the center-of-mass asymptotic kinetic energies in the entrance and exit channels. The arrows indicate the available kinetic energy in the entrance channel

Fig. 7. Laboratory angular distribution of the heavy, target-like reaction products. The curve is intended to guide the eye.

Fig. 8. Center-of-mass energy spectra for 3-Z units wide bins. The centroid of each bin is indicated for each curve. The arrows represent Coulomb energies for spherical fragments. The curves are arbitrarily displaced along the ordinate.

Fig. 9. Angular distribution of the damped reaction cross section as a function of the fragment Z.

Fig. 10. Double-differential cross section $d^2\sigma/(dEd\Omega)$ plotted as a contour diagram (Wilczyński plot) in the TKE-versus-scattering-angle plane.

Fig. 11. Angular distribution for 26-MeV-wide TKE bins, integrated over the Z-range indicated. The centroid energy for each bin is given at each curve.

Fig. 12. Fragment Z distributions plotted as a function of the total kinetic energy indicated at the curves. The TKE bins are 26 MeV wide. The curves represent Gaussian fits. The distribution at the bottom corresponds to elastically scattered Xe-ions and illustrates the experimental Z resolution. The arrow labeled FF indicates contamination with sequential fission of target-like fragments.

Fig. 13. Experimental correlation between E_{loss} and the variance σ_Z^2 of the fragment charge distribution for two bombarding energies. The insert shows the same data on a larger scale.

Fig. 14. The width (FWHM) of the fragment Z distribution is plotted versus the reaction angle for various bins of the total kinetic energy. The horizontal lines represent fits to the angle-integrated Z-distributions as shown in Table III.

Fig. 15. Triple-differential cross sections $d^3\sigma/(dZd\Omega)$ plotted as contour diagrams with the atomic number of the fragment as parameter. $\Delta Z = Z - 54$ is the difference between the centroid of each Z bin and the atomic number of Zenon.

Fig. 16. The variance σ_Z^2 of the charge distribution is plotted versus the logarithm of the ratio T_o/T of the available kinetic energy in the entrance and exit channel. The slope of the resulting linear dependence is a measure for the contribution of the momentum transfer by nucleon exchange to the total observed kinetic energy loss.

Fig. 17. Correlation between the angular momentum in the entrance channel and the loss of total kinetic energy. The decomposition of the cross section into partial waves assumed a monotonic relation between angular momentum and kinetic energy loss.

Fig. 18. The average experimental deflection functions for 940 and 1130 MeV is compared to the sum of the Coulomb deflections in the entrance and exit channels for the non-sticking and sticking models at 940 MeV bombarding energy.

Fig. 19. The angular momentum dependent interaction times for 940 and 1130 MeV bombarding energy.

Fig. 20. The experimentally deduced deflection function, total kinetic energy loss and interaction time as a function of the angular momentum are compared to classical trajectory calculations, using potential and friction form factors as indicated. No deformations are taken into account.

Fig. 21. Average proton number diffusion coefficients $D_Z(\ell_i)$ as a function of the angular momentum for two bombarding energies. The curves are to guide the eye.

Fig. 22. A systematic relationship between the atomic number Z and excitation energy E^*, where fission width Γ_f and neutron width Γ_n are equal. The straight line is a fit to the data and separates the $Z - E^*$ plane into the domains of deexcitation by neutron emission and by fission, respectively.

Fig. 23. The cross section $d\sigma_{SF}/dE$ for sequential fission of the heavy, Bi-like fragment as a function of the total kinetic energy loss at 940 MeV bombarding energy. The broken curve indicates the total reaction cross section $d\sigma_R/dE$, as deduced from the Xe-like fragments.

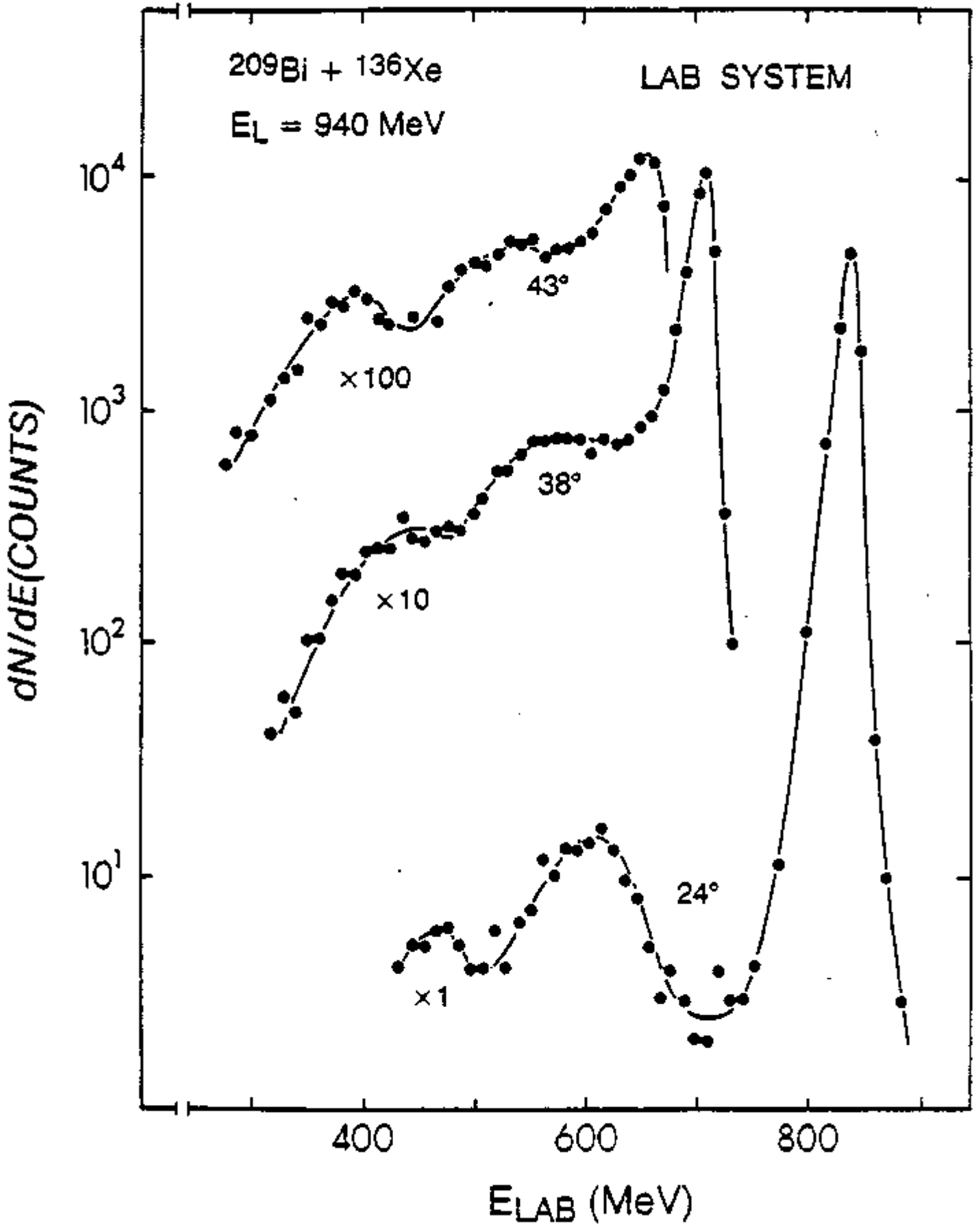
209Bi + 136Xe
EL = 940 MeV
LAB SYSTEM
43°
38°
24°
×100
×10
×1
dN/dE(COUNTS)
ELAB (MeV)

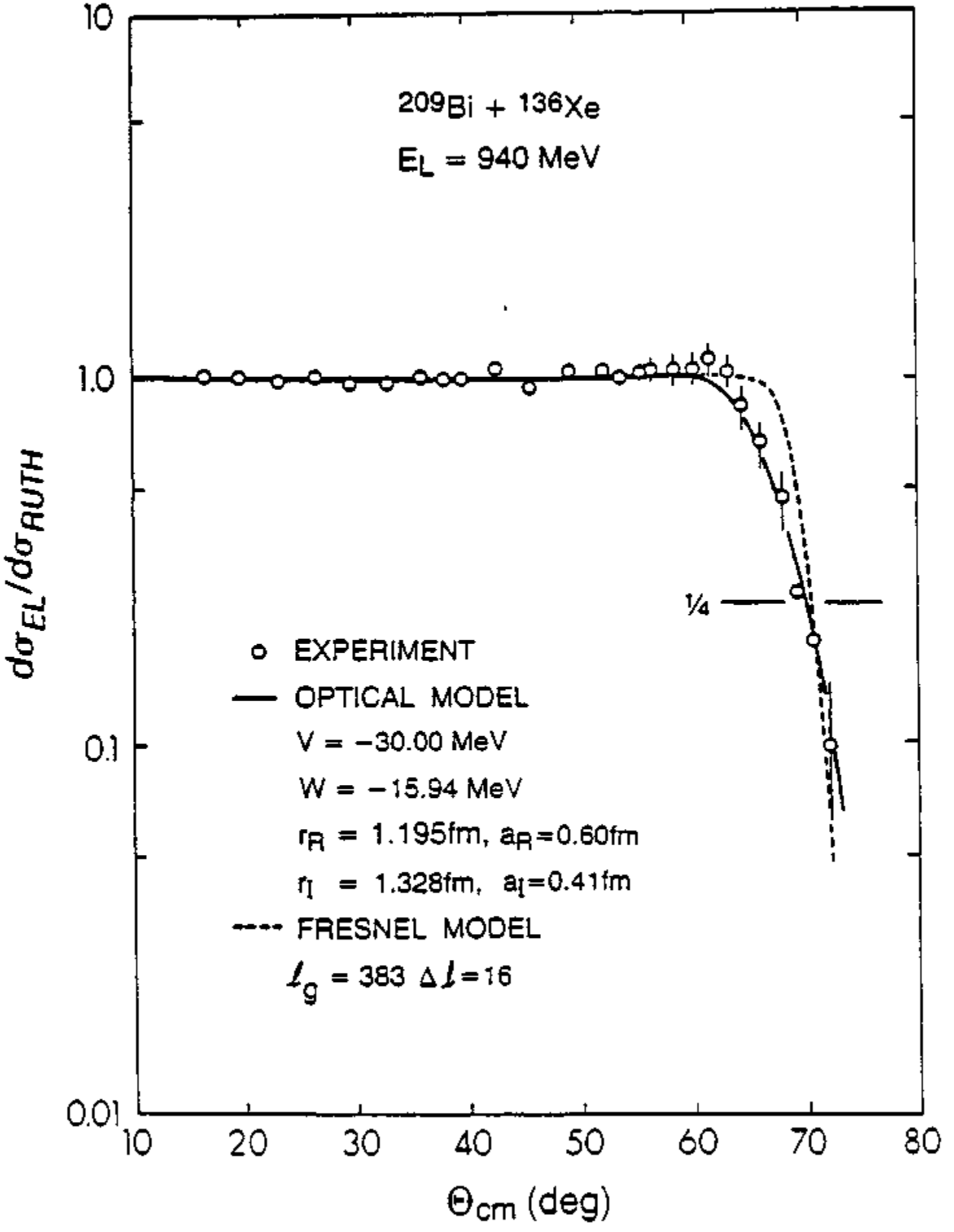
10
1.0
0.1
0.01
$d\sigma_{EL}/d\sigma_{RUTH}$
$^{209}Bi + ^{136}Xe$
E_L = 940 MeV
¼
o EXPERIMENT
— OPTICAL MODEL
V = −30.00 MeV
W = −15.94 MeV
r_R = 1.195fm, a_R=0.60fm
r_I = 1.328fm, a_I=0.41fm
---- FRESNEL MODEL
ℓ_g = 383 $\Delta\ell$=16
10 20 30 40 50 60 70 80
Θ_{cm} (deg)

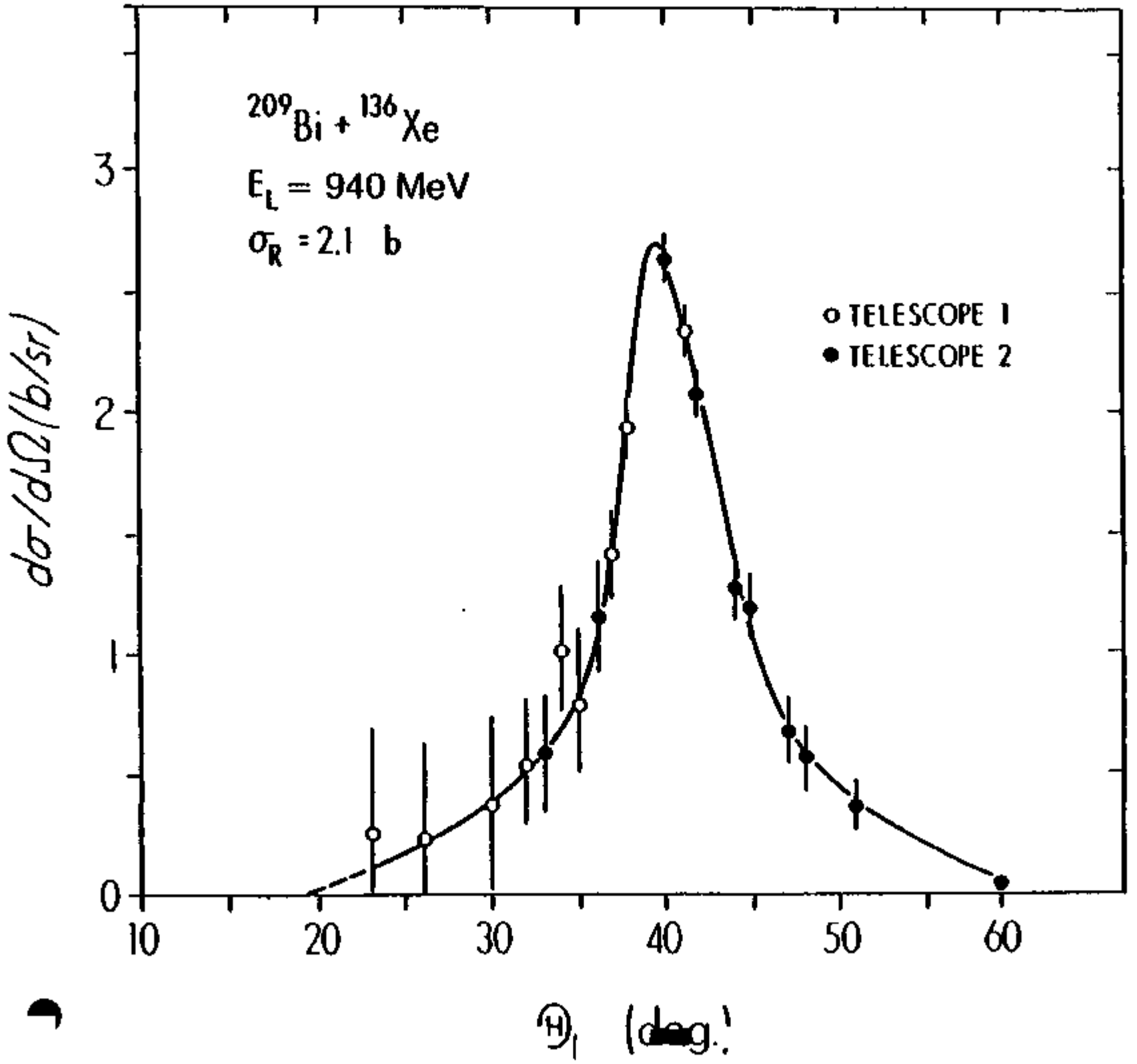
$^{209}Bi + ^{136}Xe$
$E_L = 940$ MeV
$\sigma_R = 2.1$ b
o TELESCOPE 1
• TELESCOPE 2
$d\sigma/d\Omega$(b/sr)
0
1
2
3
10
20
30
40
50
60
Θ_l (deg.)

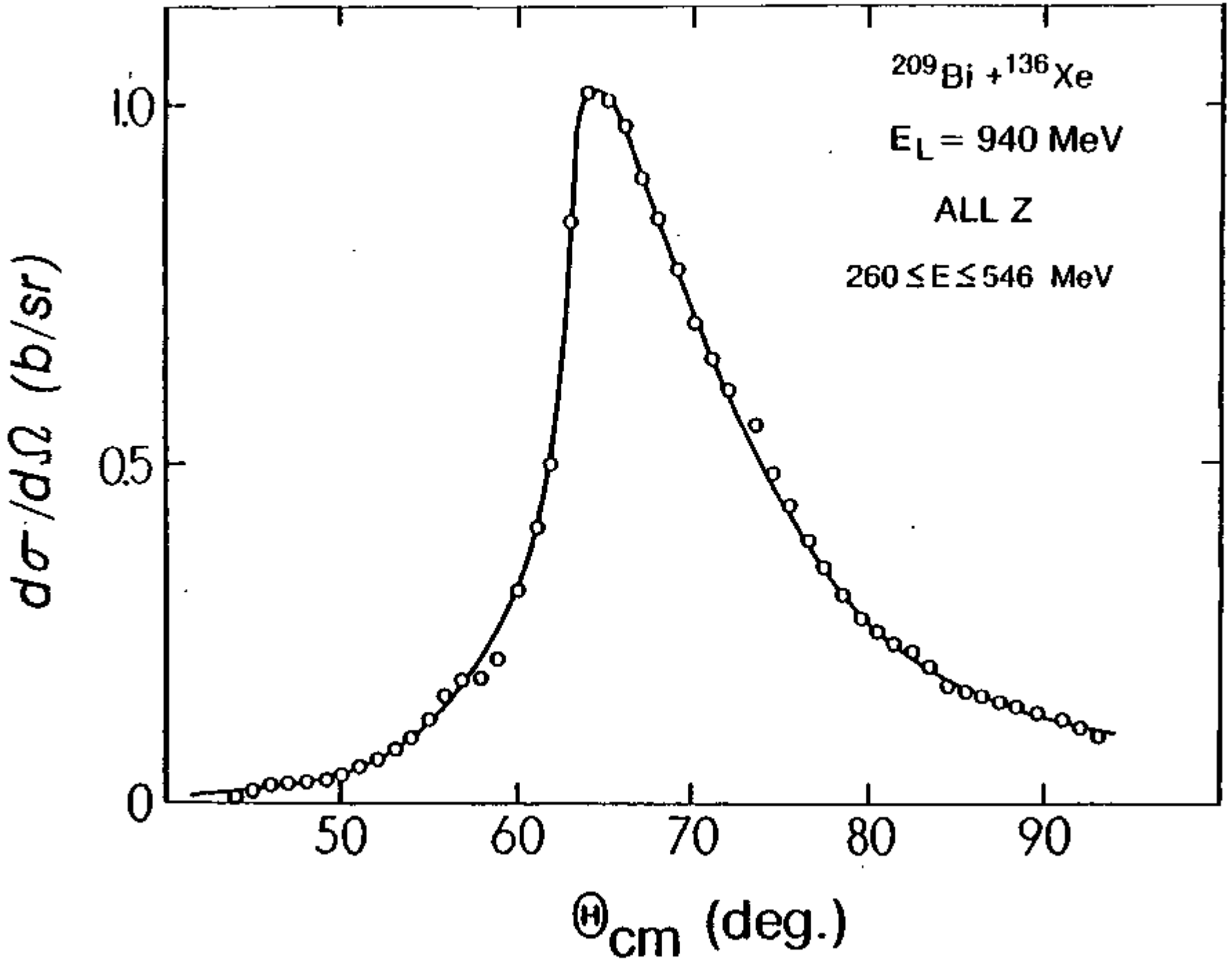
$^{209}Bi + ^{136}Xe$
$E_L = 940$ MeV
ALL Z
$260 \leq E \leq 546$ MeV
$d\sigma/d\Omega$ (b/sr)
1.0
0.5
0
50
60
70
80
90
Θ_{cm} (deg.)

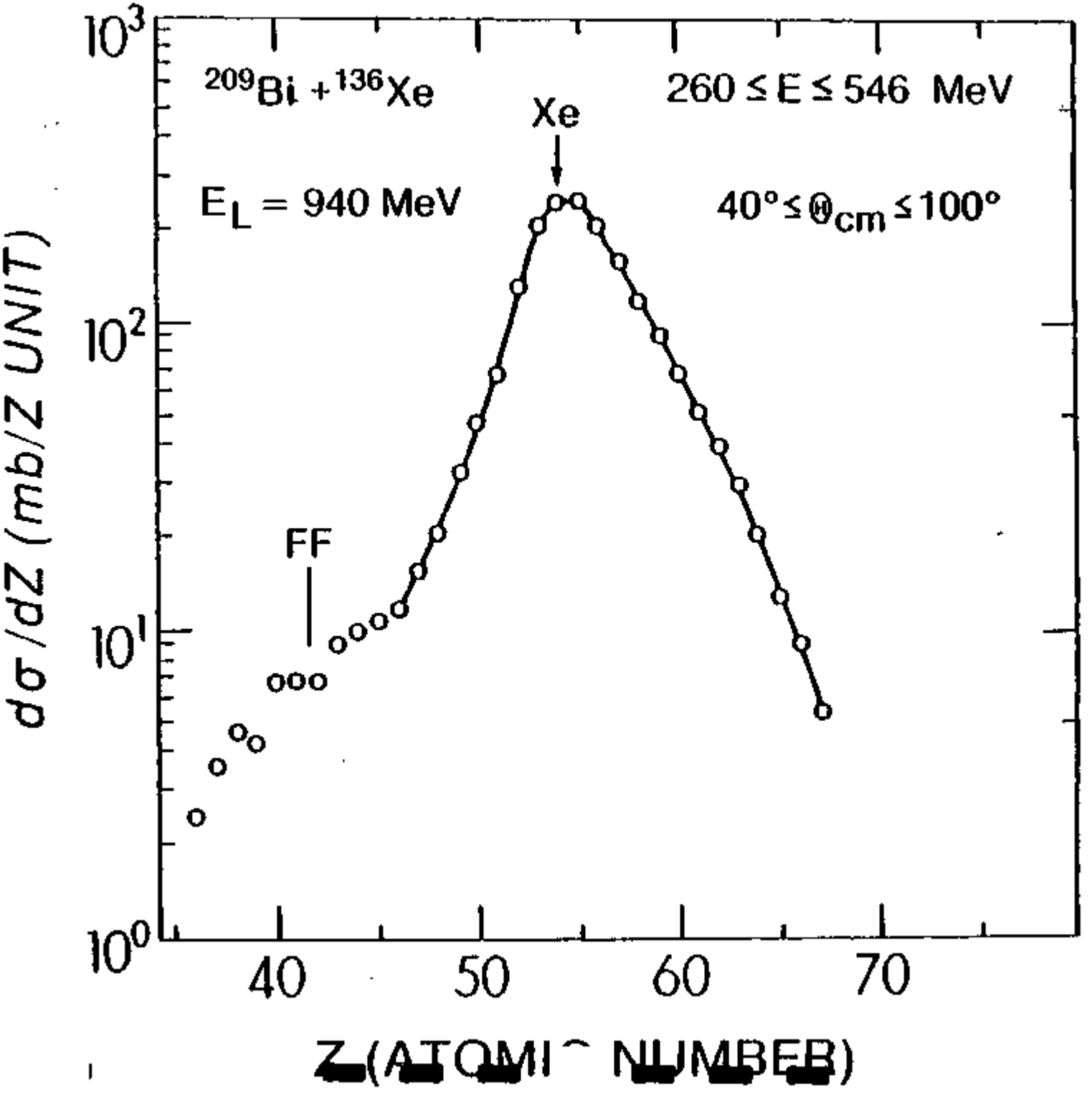
$^{209}Bi + ^{136}Xe$
260 ≤ E ≤ 546 MeV
Xe
E_L = 940 MeV
40° ≤ θ_{cm} ≤ 100°
FF
$d\sigma/dZ$ (mb/Z UNIT)
10^3
10^2
10^1
10^0
40
50
60
70
Z (ATOMIC NUMBER)

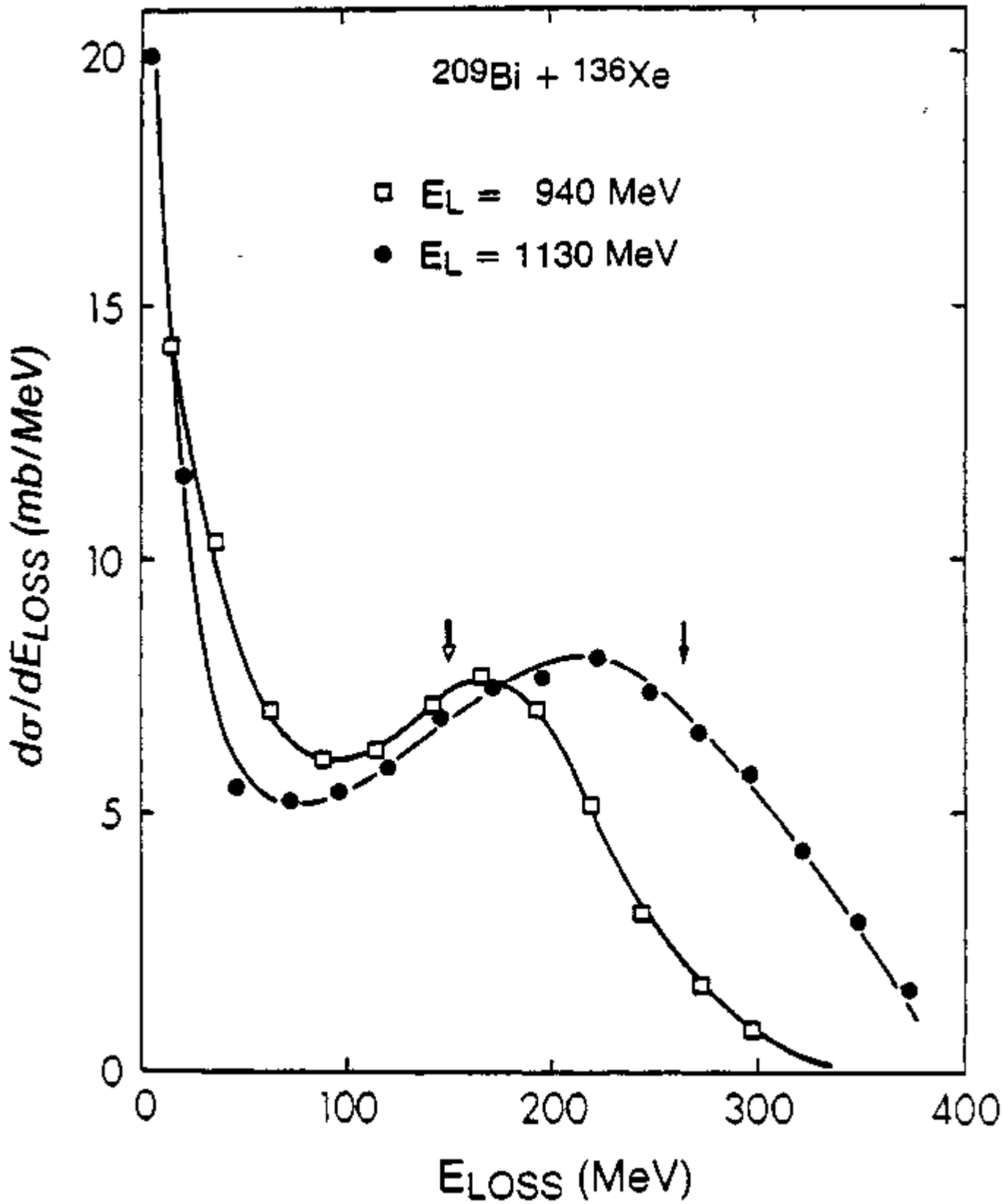
$^{209}Bi + ^{136}Xe$
E_L = 940 MeV
E_L = 1130 MeV
$d\sigma/dE_{LOSS}$ (mb/MeV)
E_{LOSS} (MeV)
0
5
10
15
20
0
100
200
300
400

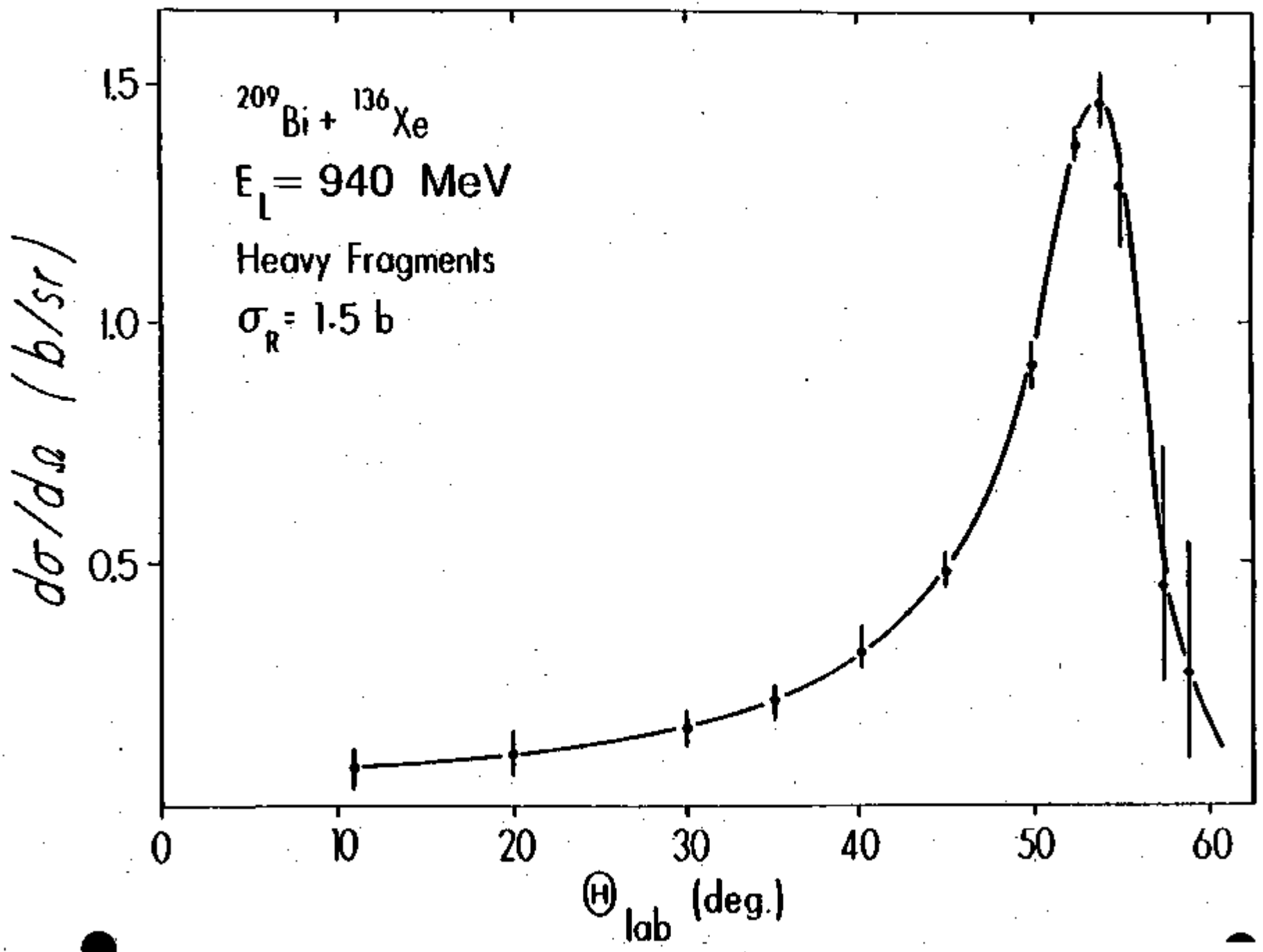
$^{209}Bi + ^{136}Xe$
$E_L = 940$ MeV
Heavy Fragments
$\sigma_R = 1.5$ b
$d\sigma/d\Omega$ (b/sr)
1.5
1.0
0.5
0
10
20
30
40
50
60
Θ_{lab} (deg.)

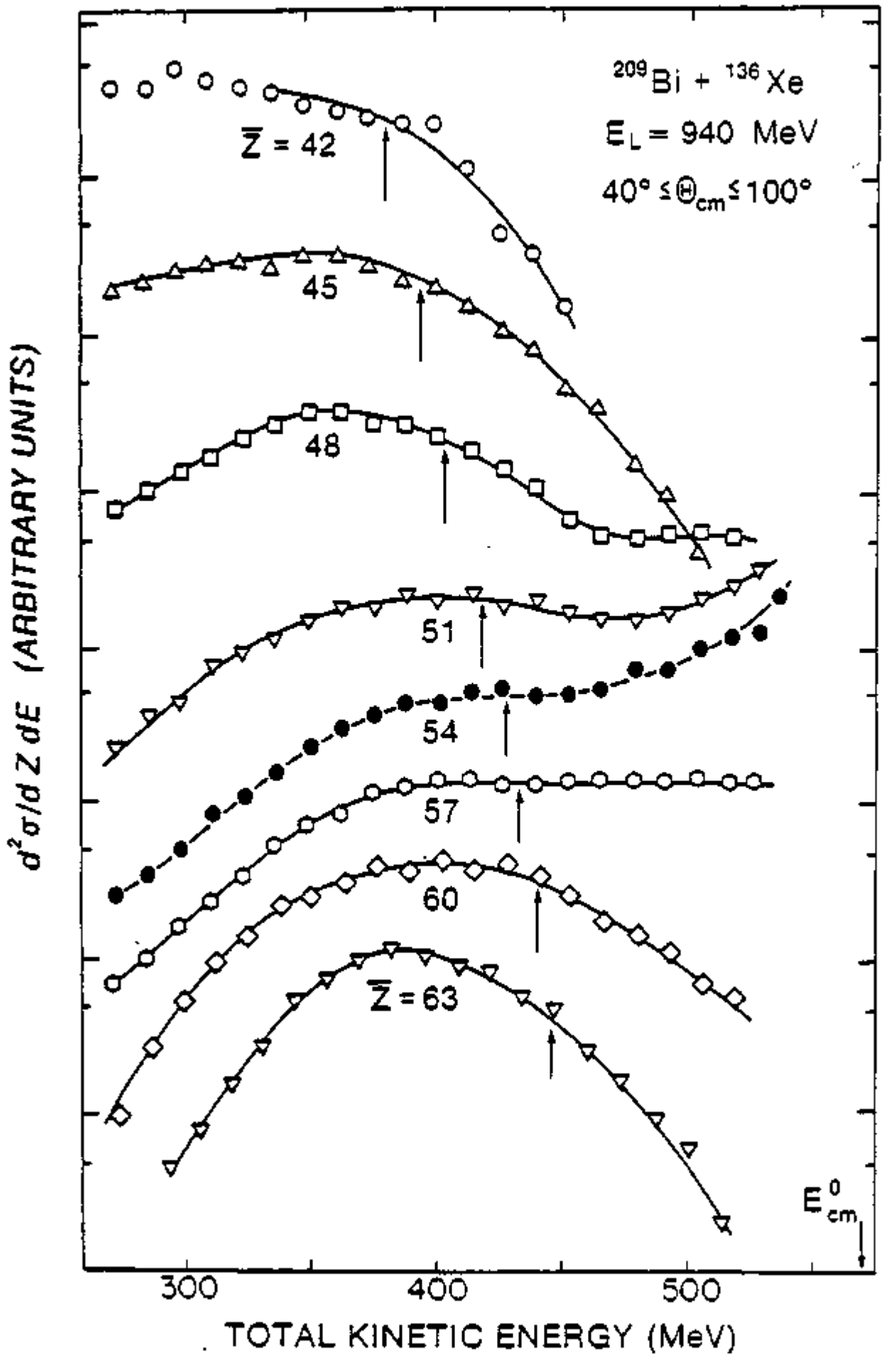
$^{209}Bi + ^{136}Xe$
$E_L = 940$ MeV
$40° \leq \Theta_{cm} \leq 100°$
$\bar{Z} = 42$
45
48
51
54
57
60
$\bar{Z} = 63$
E^0_{cm}
$d^2\sigma/dZ\,dE$ (ARBITRARY UNITS)
300
400
500
TOTAL KINETIC ENERGY (MeV)

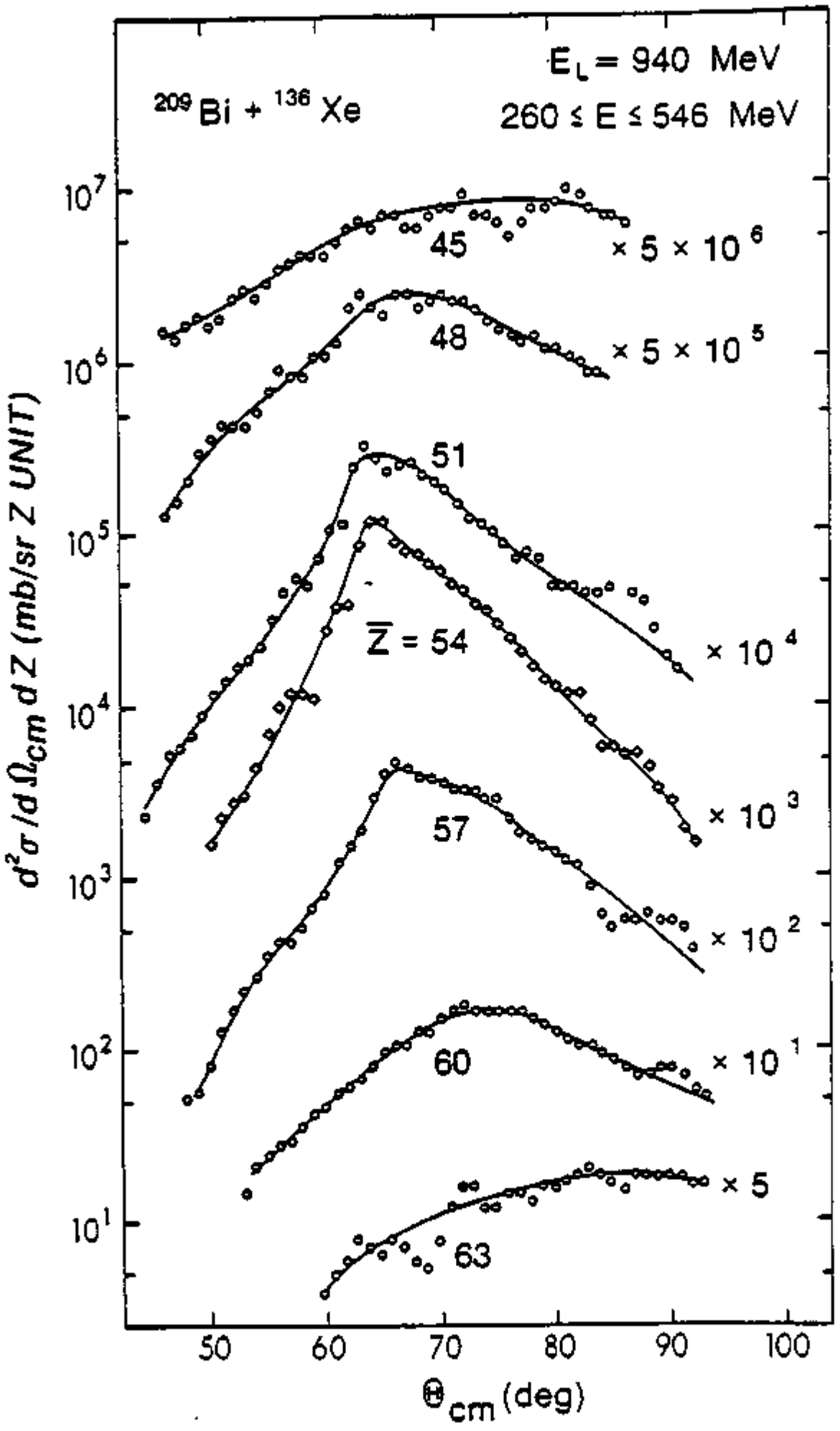
E_L = 940 MeV
^{209}Bi + ^{136}Xe
260 ≤ E ≤ 546 MeV
45
× 5 × 10^6
48
× 5 × 10^5
51
× 10^4
$\bar{Z}$ = 54
× 10^3
57
× 10^2
60
× 10^1
× 5
63
$d^2\sigma/d\Omega_{cm}\,dZ$ (mb/sr Z UNIT)
Θ_{cm} (deg)

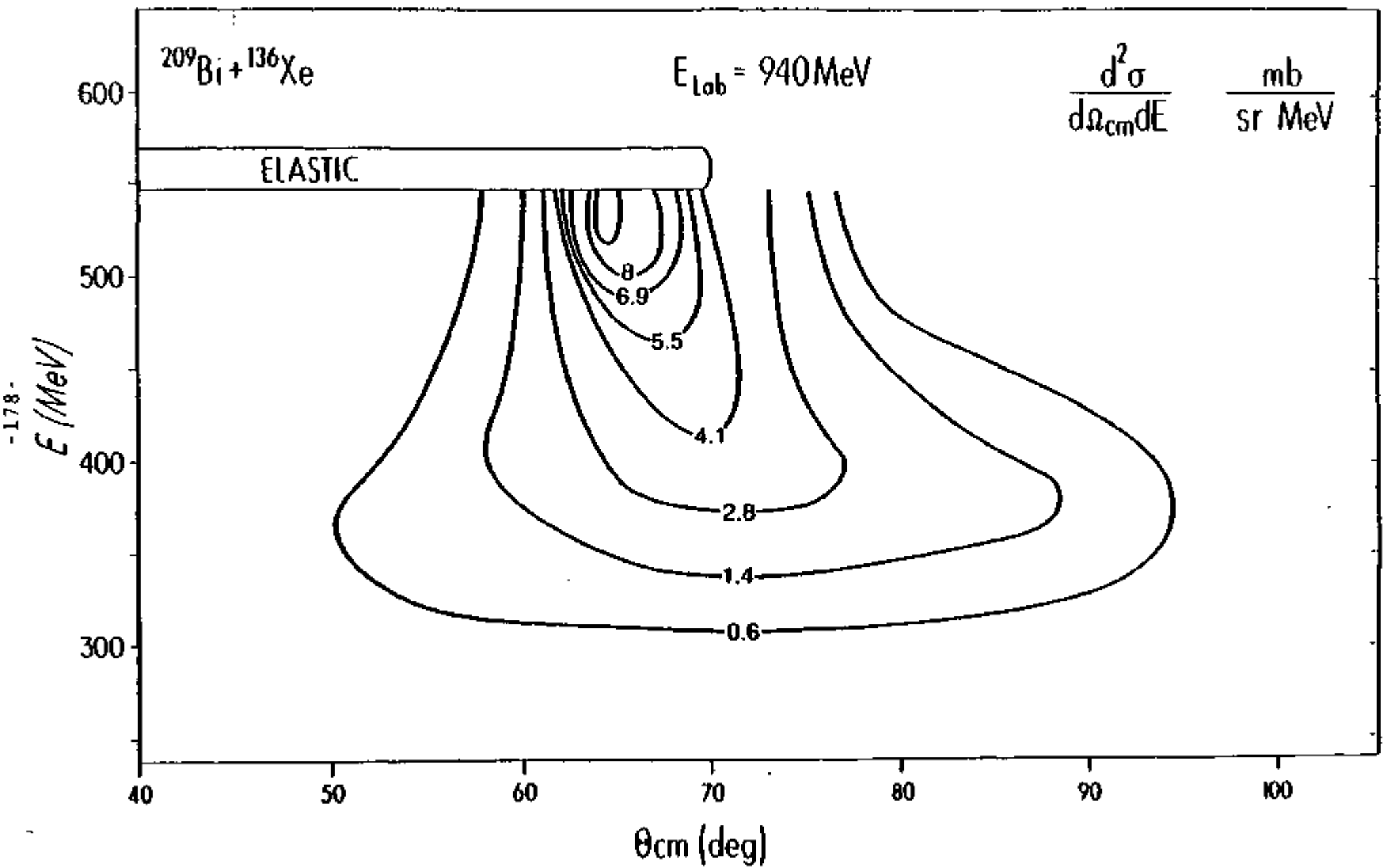
$^{209}Bi + ^{136}Xe$
E_{Lab} = 940MeV
$\frac{d^2\sigma}{d\Omega_{cm}dE}$ $\frac{mb}{sr\ MeV}$
ELASTIC
8
6.9
5.5
4.1
2.8
1.4
0.6
600
500
400
300
E (MeV)
40
50
60
70
80
90
100
θcm (deg)

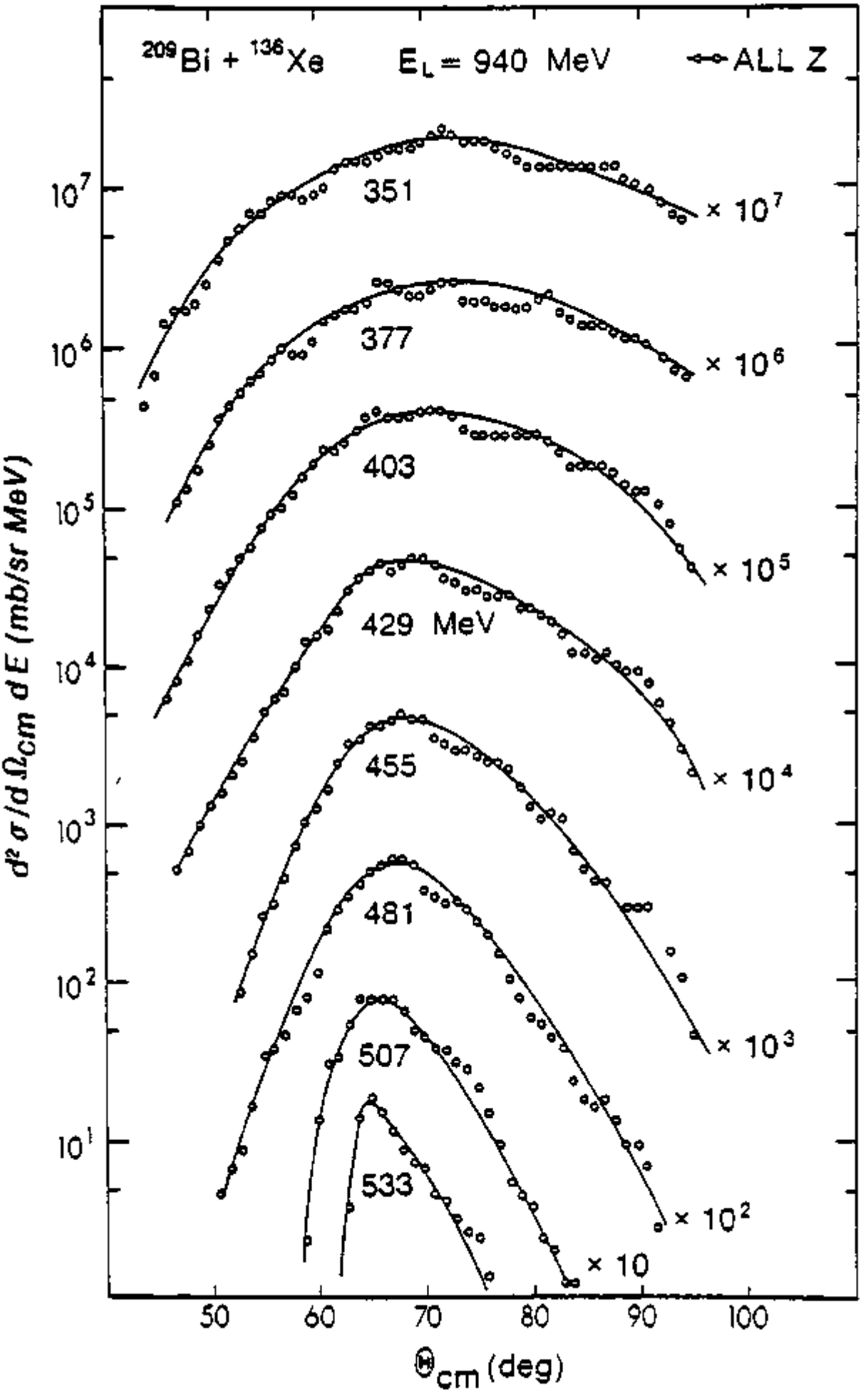
$^{209}Bi + ^{136}Xe$ $E_L = 940$ MeV ALL Z
351
377
403
429 MeV
455
481
507
533
$\times 10^7$
$\times 10^6$
$\times 10^5$
$\times 10^4$
$\times 10^3$
$\times 10^2$
$\times 10$
10^7
10^6
10^5
10^4
10^3
10^2
10^1
$d^2\sigma/d\Omega_{cm}\, dE$ (mb/sr MeV)
50
60
70
80
90
100
Θ_{cm} (deg)

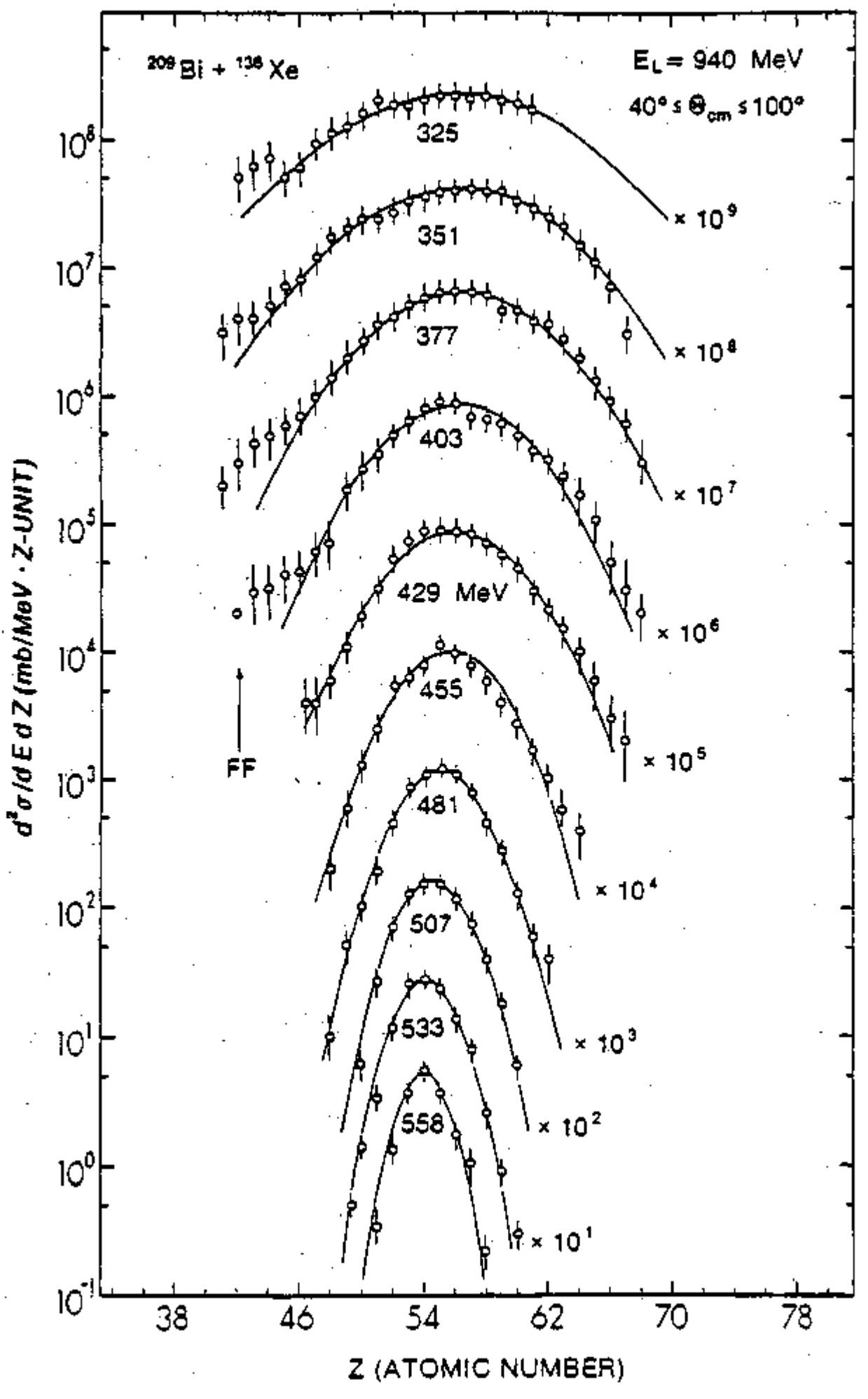
$^{209}Bi + ^{136}Xe$
$E_L = 940$ MeV
$40° \leq \Theta_{cm} \leq 100°$
325
351
377
403
429 MeV
455
481
507
533
558
FF
$\times 10^9$
$\times 10^8$
$\times 10^7$
$\times 10^6$
$\times 10^5$
$\times 10^4$
$\times 10^3$
$\times 10^2$
$\times 10^1$
$d^2\sigma/dE\,dZ$ (mb/MeV · Z-UNIT)
Z (ATOMIC NUMBER)
38
46
54
62
70
78

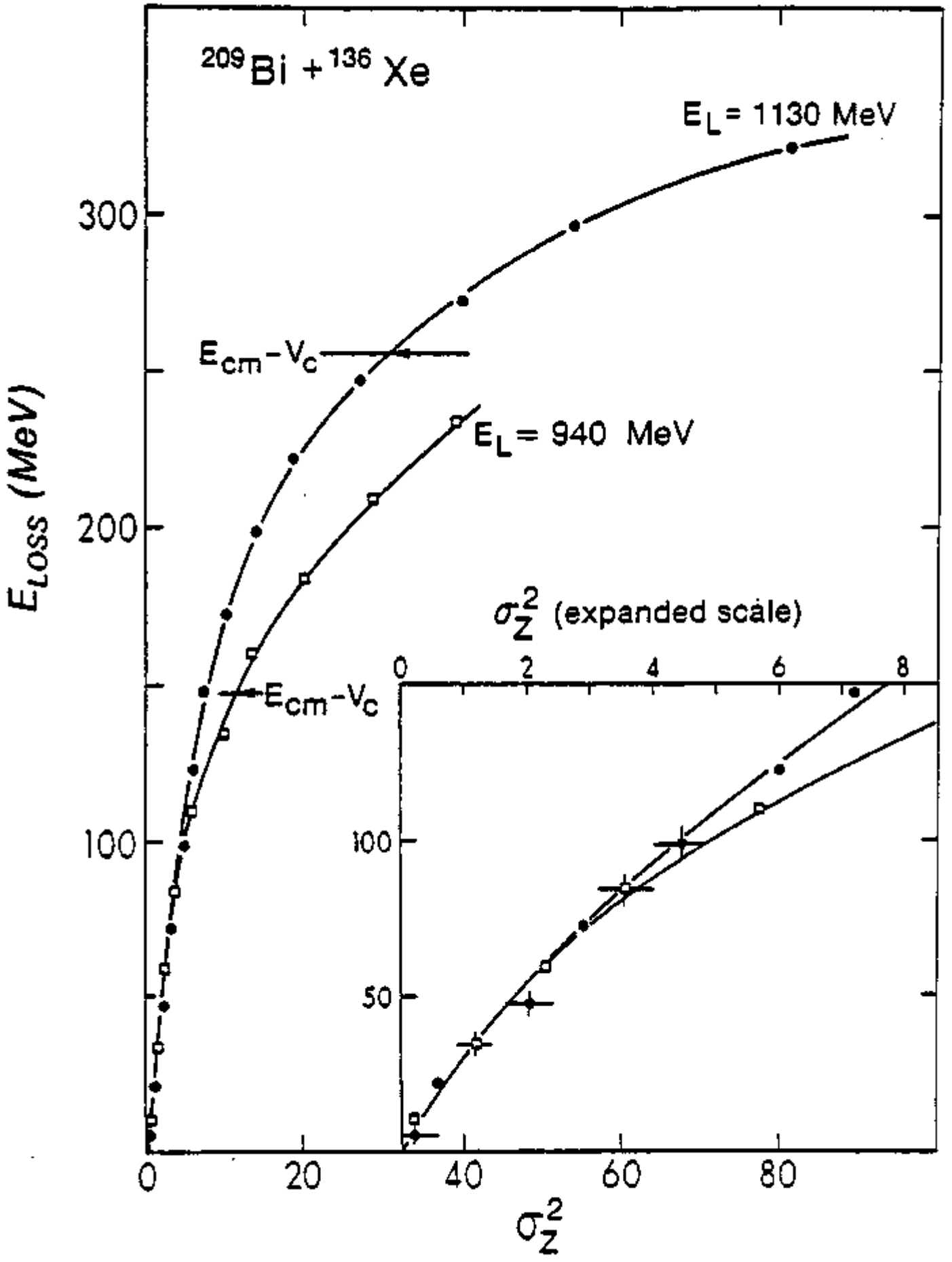
$^{209}Bi + ^{136}Xe$
E_L = 1130 MeV
$E_{cm}-V_c$
E_L = 940 MeV
E_{LOSS} (MeV)
300
200
100
0
20
40
60
80
σ_Z^2
σ_Z^2 (expanded scale)
0
2
4
6
8
$E_{cm}-V_c$
100
50

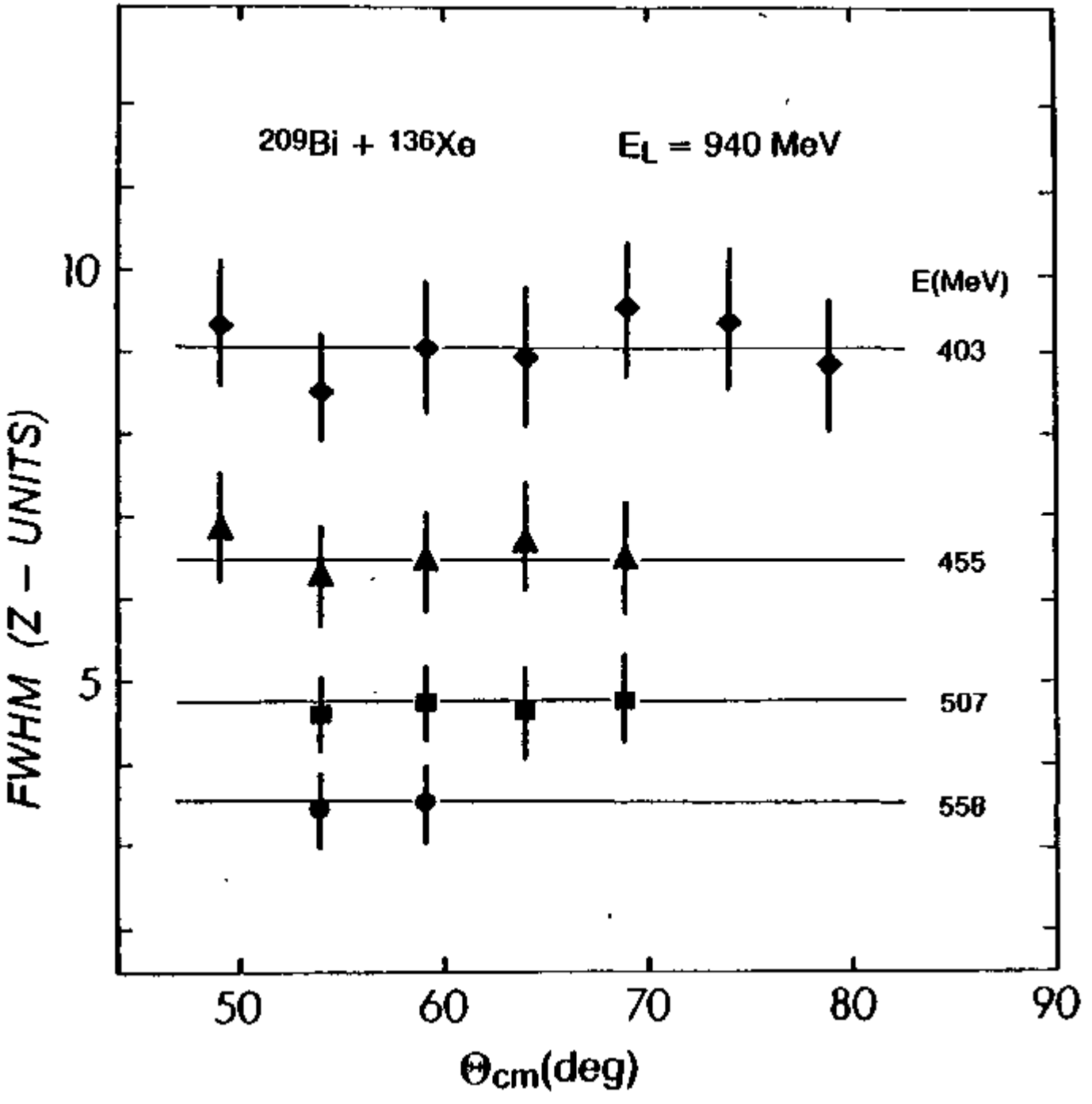
209Bi + 136Xe
EL = 940 MeV
E(MeV)
403
455
507
558
10
5
FWHM (Z – UNITS)
50
60
70
80
90
Θcm(deg)

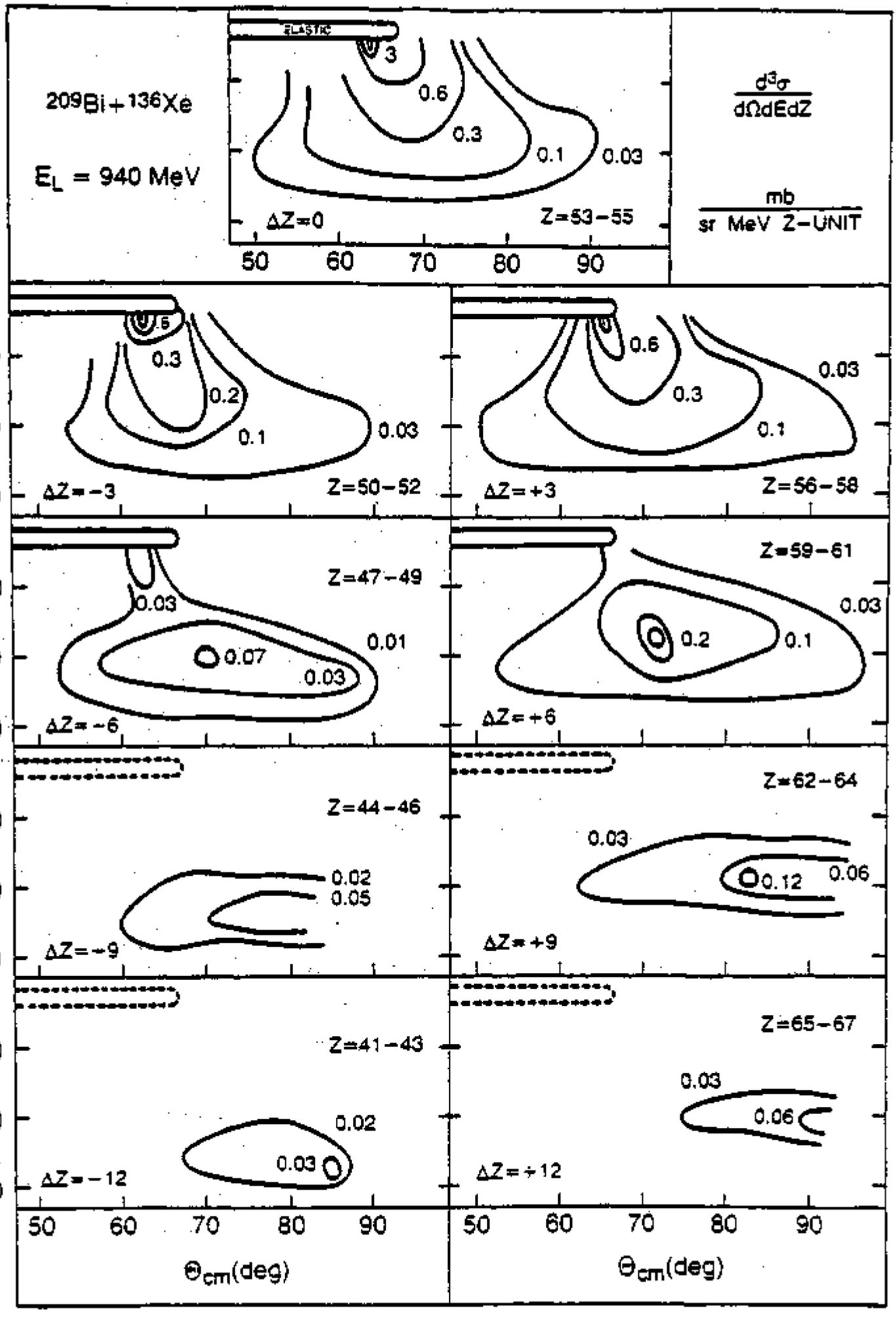
209Bi+136Xe
EL = 940 MeV
d3σ / dΩdEdZ
mb / sr MeV Z-UNIT
ELASTIC
ΔZ=0
Z=53-55
ΔZ=-3
Z=50-52
ΔZ=+3
Z=56-58
ΔZ=-6
Z=47-49
ΔZ=+6
Z=59-61
ΔZ=-9
Z=44-46
ΔZ=+9
Z=62-64
ΔZ=-12
Z=41-43
ΔZ=+12
Z=65-67
Θcm(deg)
Θcm(deg)

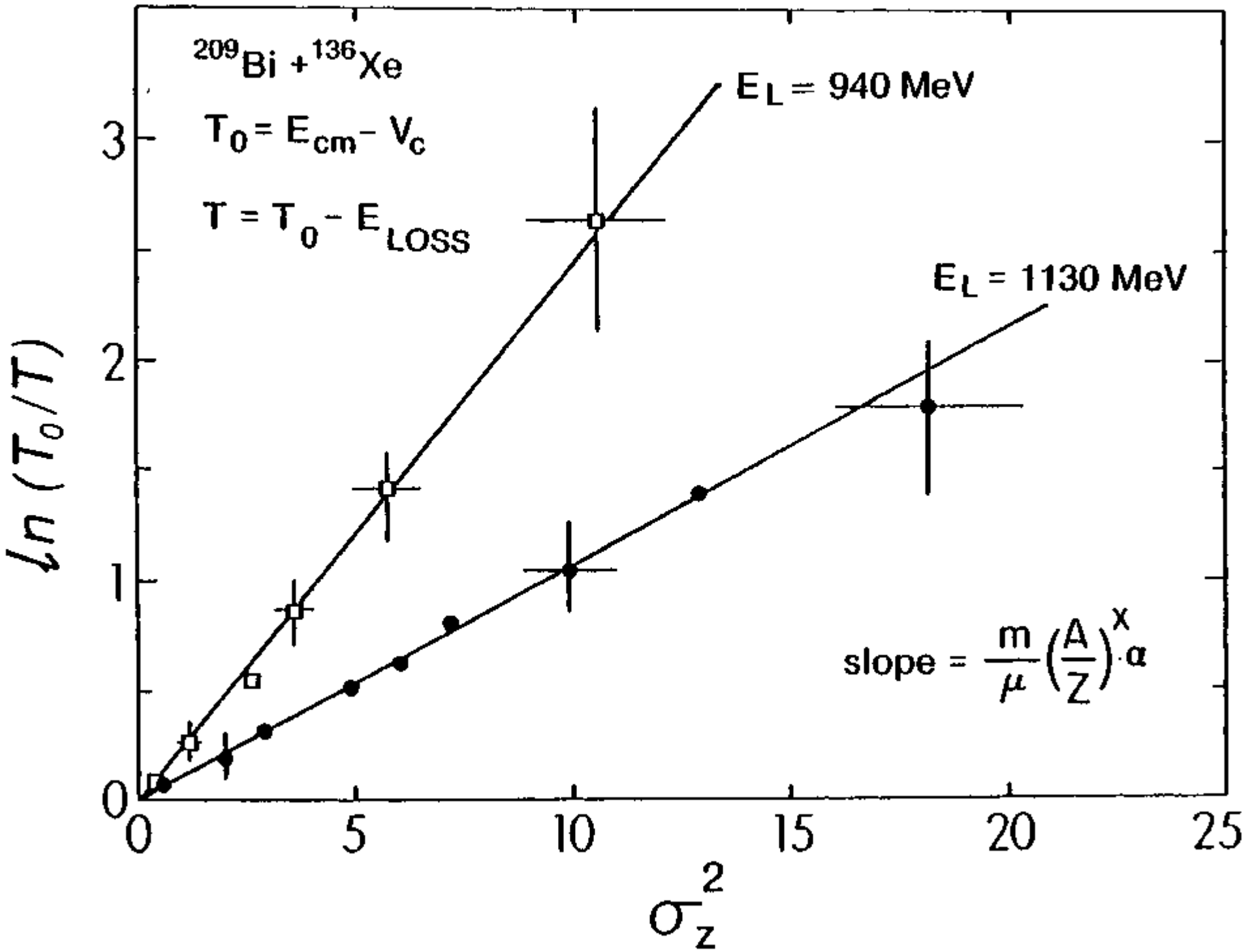
$^{209}Bi + ^{136}Xe$
$T_0 = E_{cm} - V_c$
$T = T_0 - E_{LOSS}$
E_L = 940 MeV
E_L = 1130 MeV
slope = $\frac{m}{\mu}\left(\frac{A}{Z}\right)^x \alpha$
$ln\,(T_0/T)$
σ_z^2
0
1
2
3
0
5
10
15
20
25

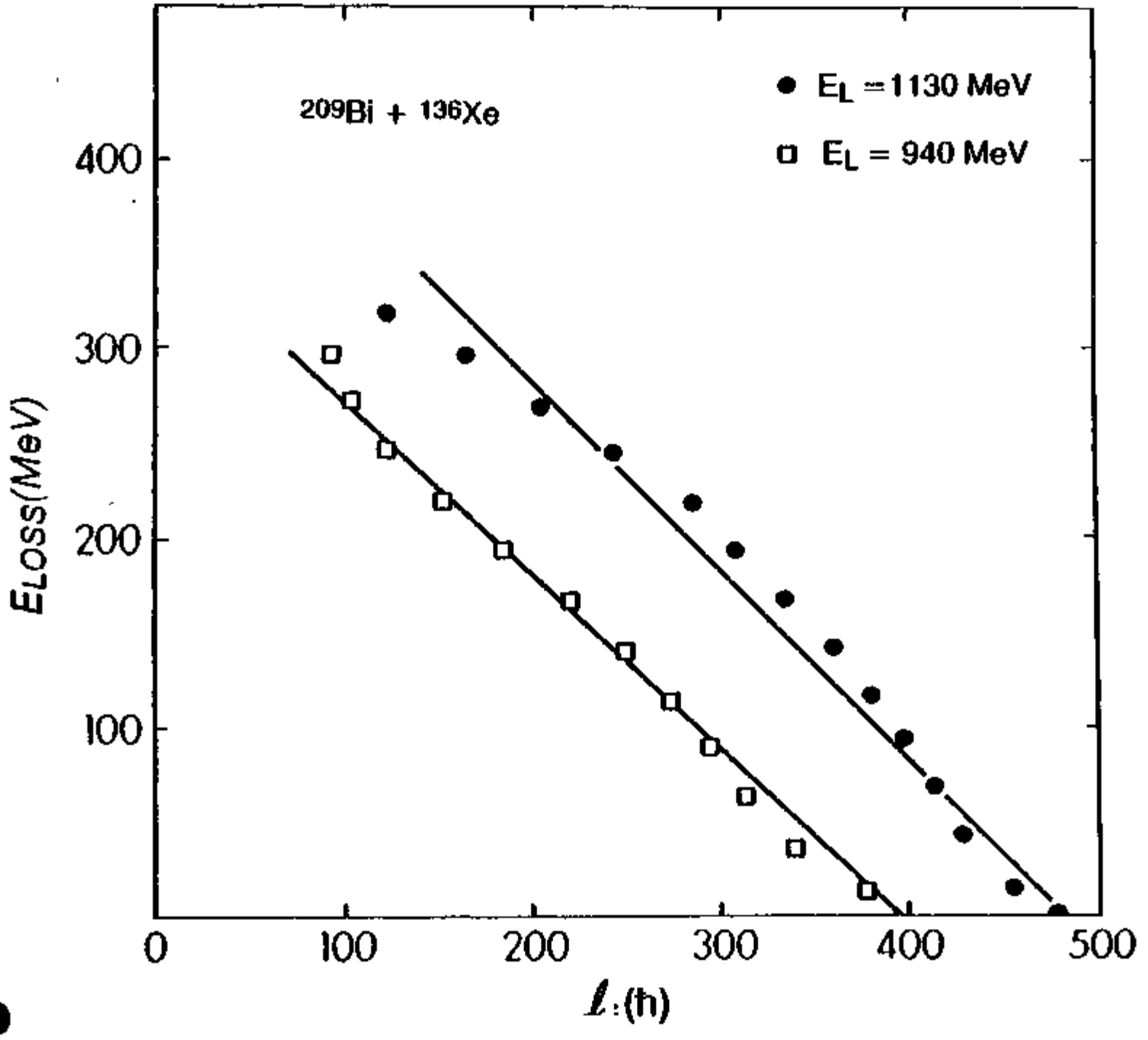
^{209}Bi + ^{136}Xe
E$_L$ = 1130 MeV
E$_L$ = 940 MeV
E$_{LOSS}$(MeV)
400
300
200
100
0
100
200
300
400
500
ℓ:(ħ)

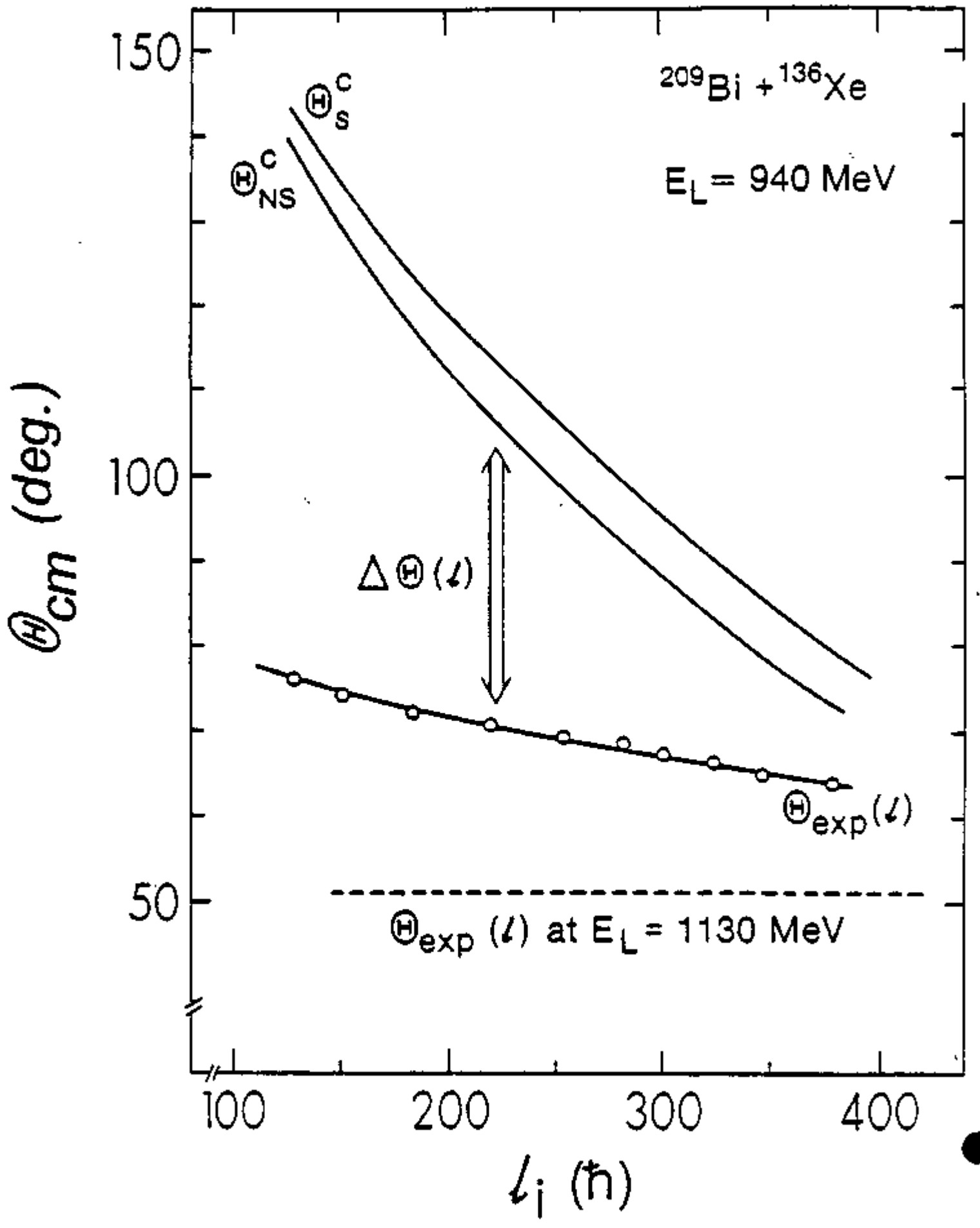
150
100
50
$^{209}Bi + ^{136}Xe$
$E_L = 940$ MeV
Θ^c_S
Θ^c_{NS}
$\Delta\Theta(\ell)$
$\Theta_{exp}(\ell)$
$\Theta_{exp}(\ell)$ at $E_L = 1130$ MeV
Θ_{cm} (deg.)
100
200
300
400
ℓ_i ($\hbar$)

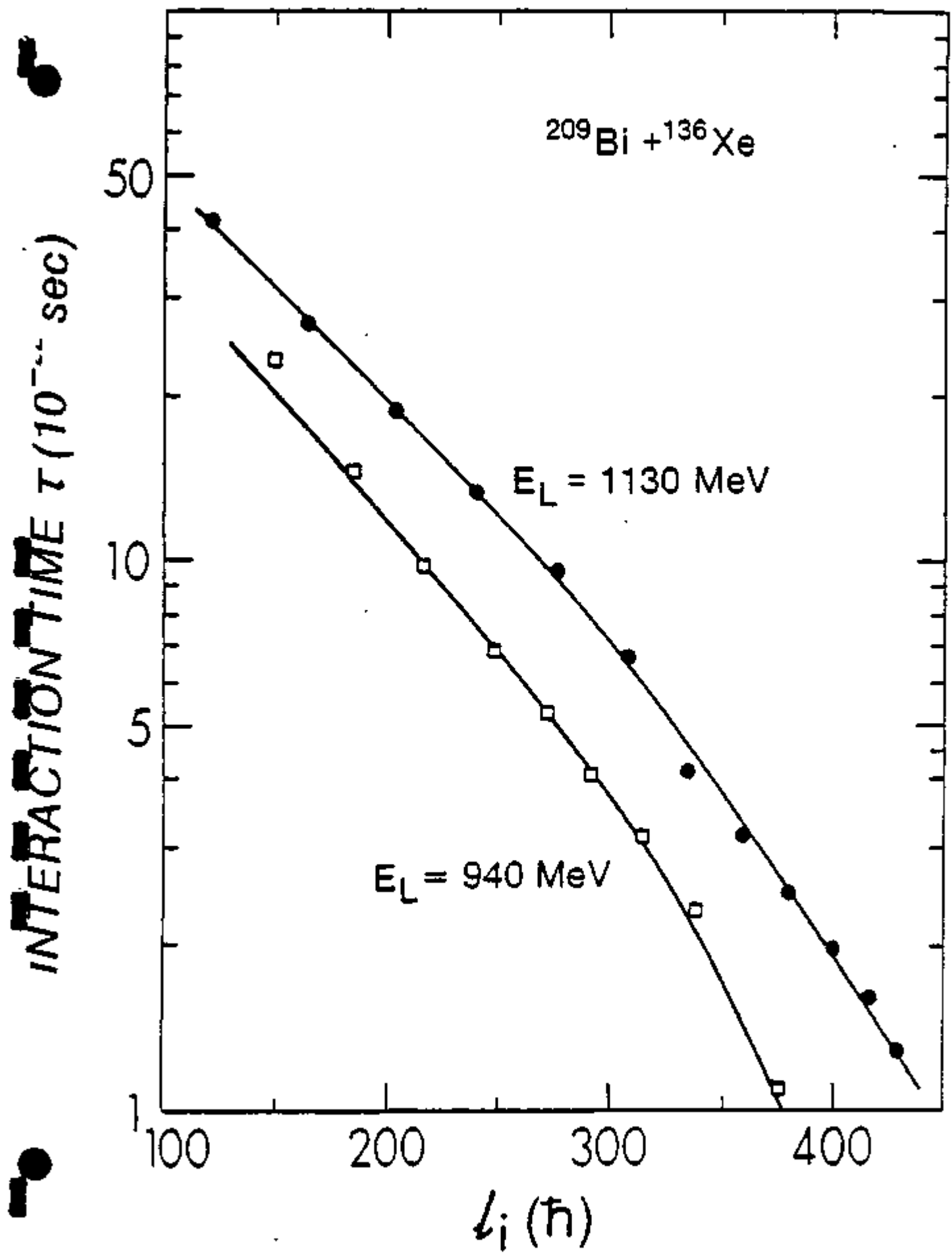
$^{209}Bi + ^{136}Xe$
E_L = 1130 MeV
E_L = 940 MeV
INTERACTION TIME τ (10⁻²² sec)
50
10
5
1
100
200
300
400
l_i (ħ)

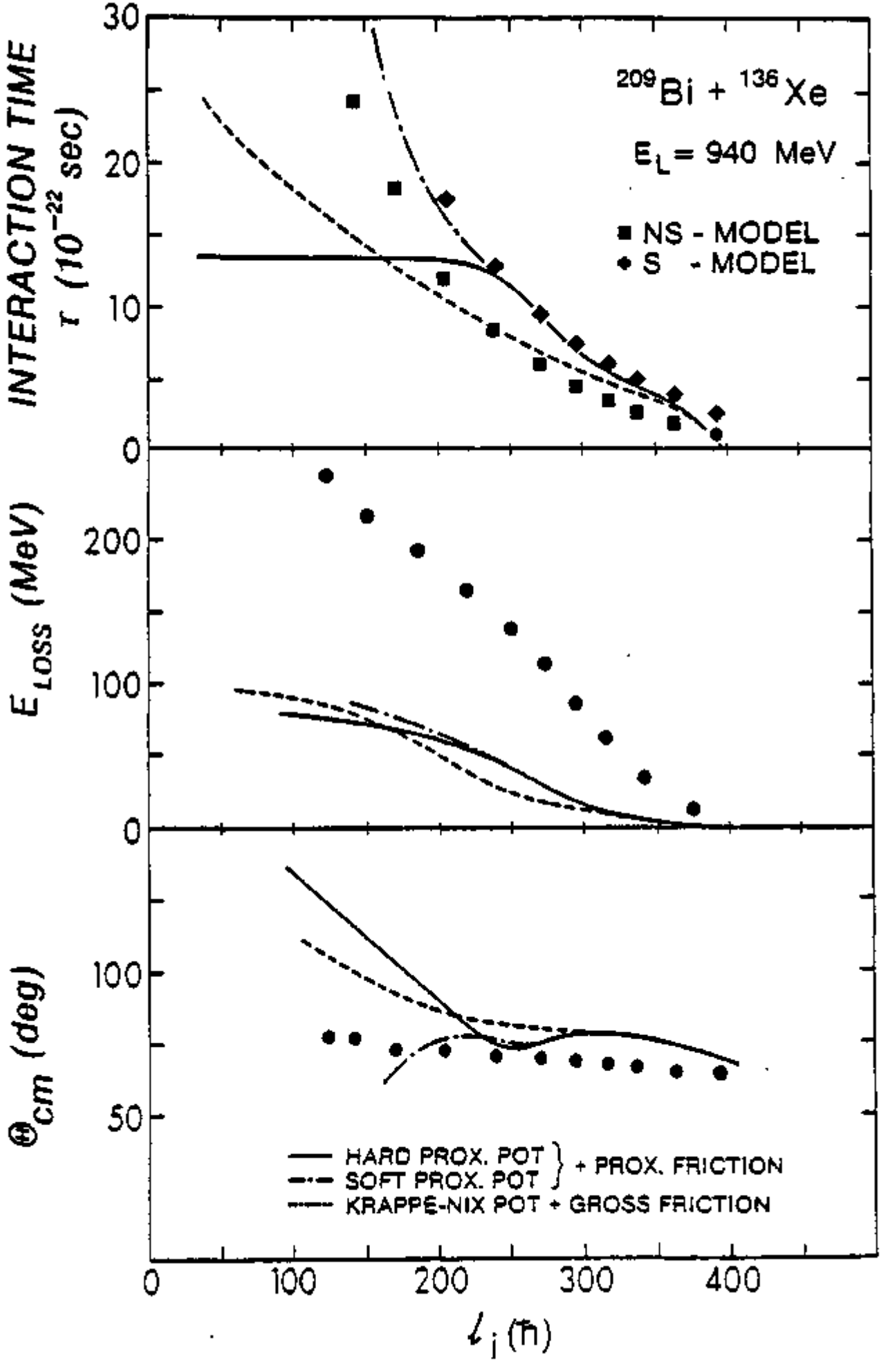
INTERACTION TIME
τ (10⁻²² sec)
30
20
10
0
^{209}Bi + ^{136}Xe
E$_L$ = 940 MeV
NS - MODEL
S - MODEL
E$_{LOSS}$ (MeV)
200
100
0
Θ$_{cm}$ (deg)
100
50
HARD PROX. POT
SOFT PROX. POT
} + PROX. FRICTION
KRAPPE-NIX POT + GROSS FRICTION
0
100
200
300
400
l$_j$ (ħ)

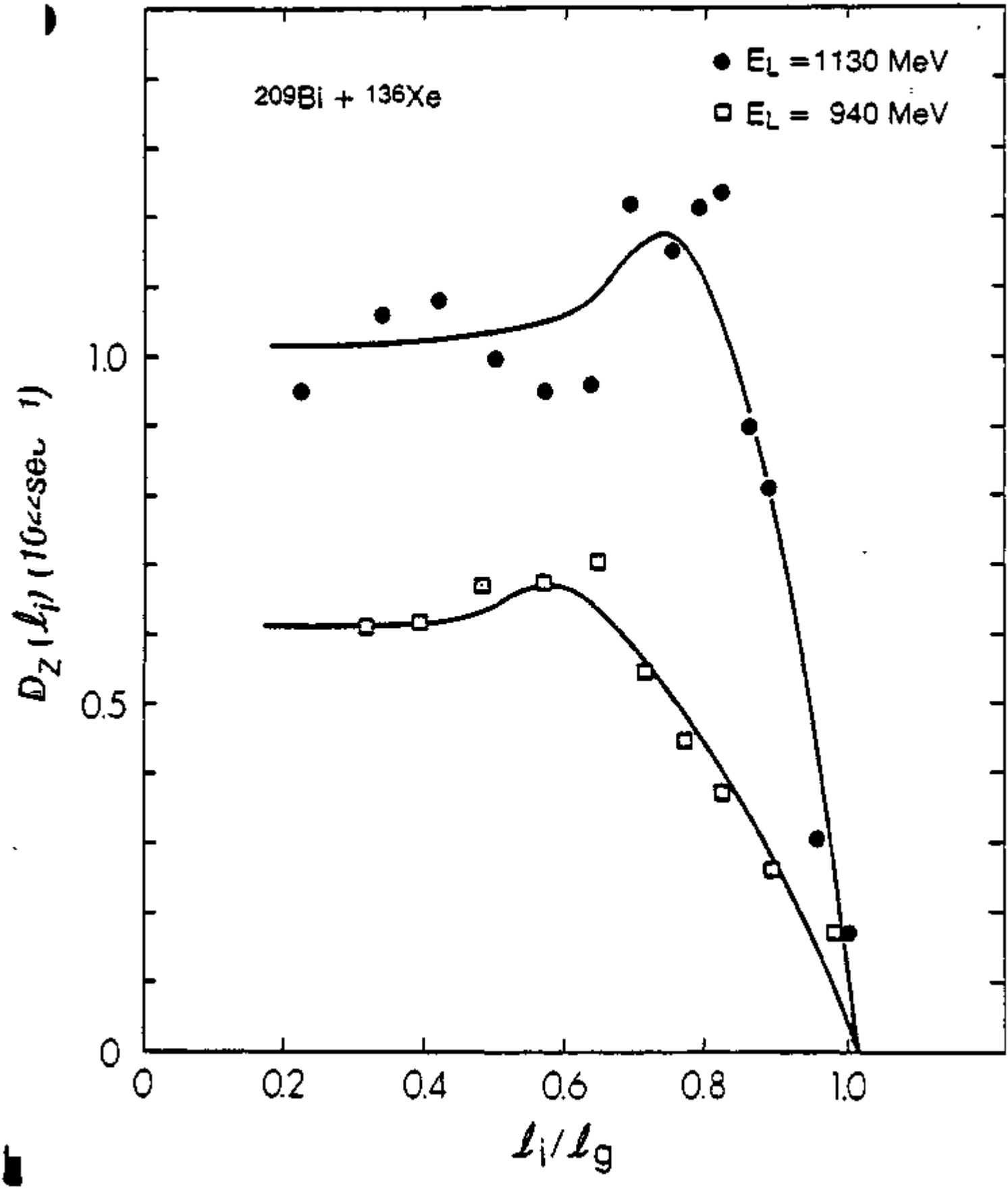
209Bi + 136Xe
E_L =1130 MeV
E_L = 940 MeV
1.0
0.5
0
0
0.2
0.4
0.6
0.8
1.0
D_Z (l_i) (10<sec)
l_i/l_g

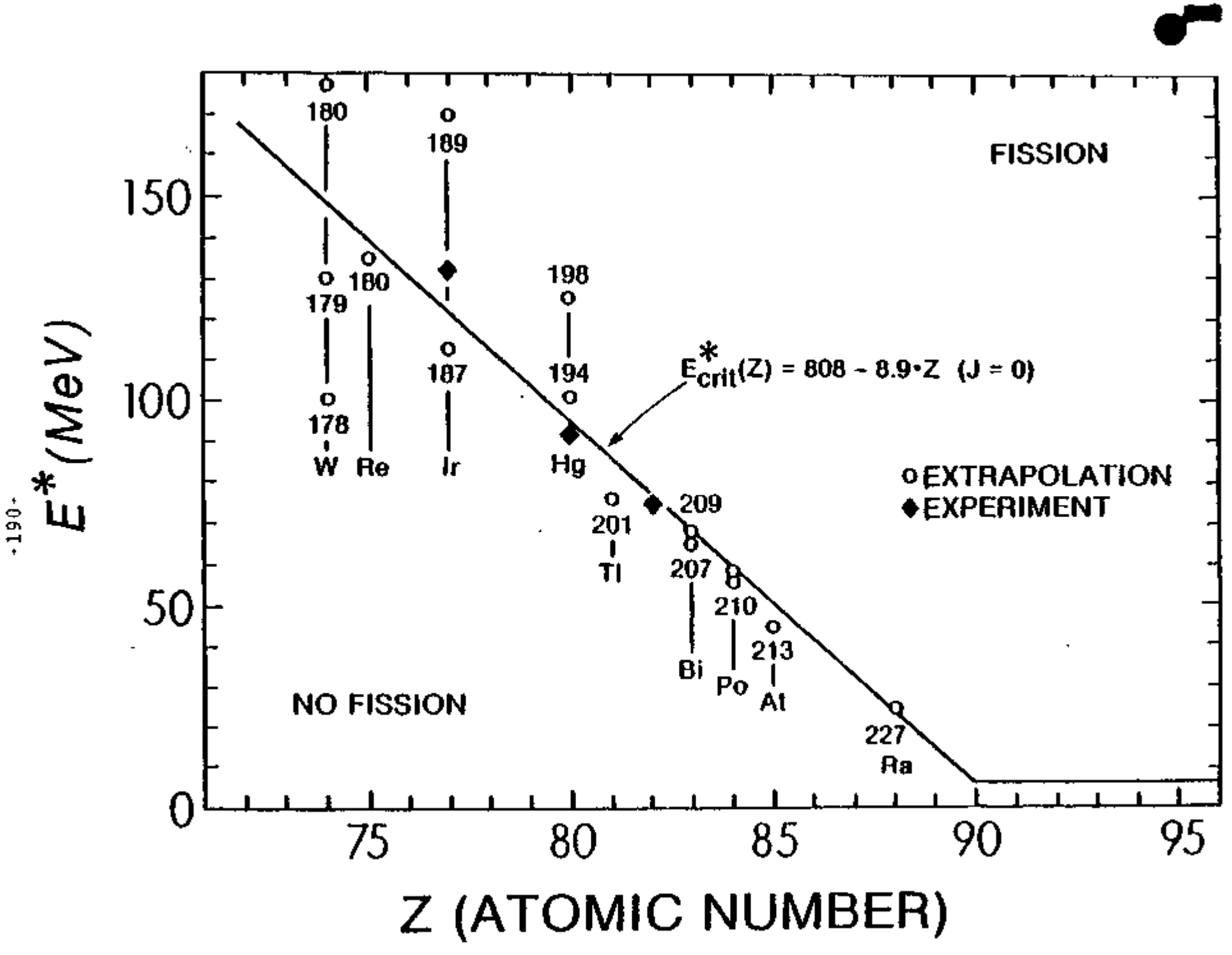
FISSION
NO FISSION
$E^*_{crit}(Z) = 808 - 8.9 \cdot Z$ (J = 0)
o EXTRAPOLATION
◆ EXPERIMENT
180
189
179
180
198
187
194
178
W
Re
Ir
Hg
201
Tl
209
207
Bi
210
Po
213
At
227
Ra
150
100
50
0
75
80
85
90
95
E^* (MeV)
Z (ATOMIC NUMBER)

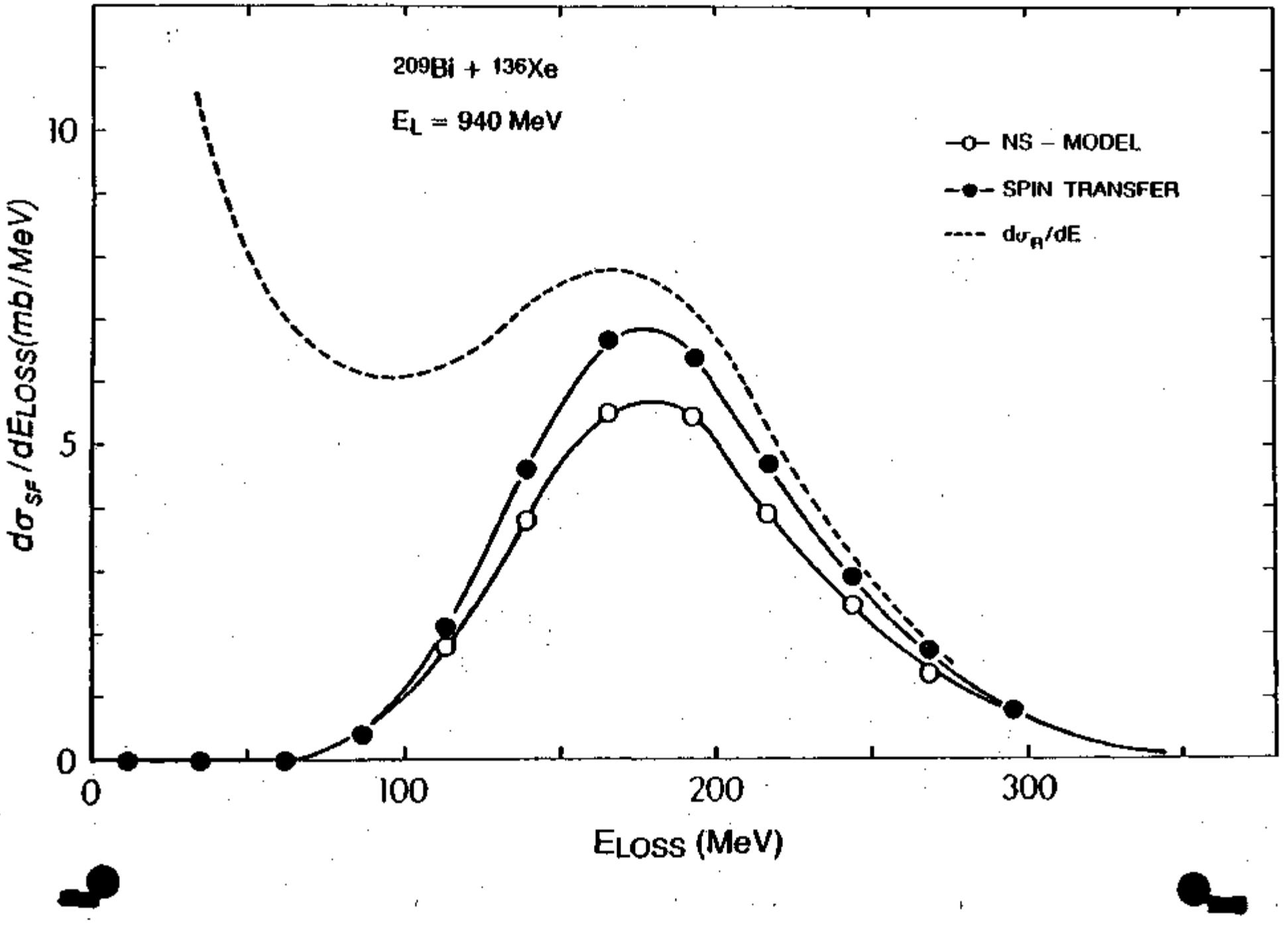
^{209}Bi + ^{136}Xe
E_L = 940 MeV
NS – MODEL
SPIN TRANSFER
$d\sigma_R/dE$
$d\sigma_{SF}/dE_{LOSS}$(mb/MeV)
E_{LOSS} (MeV)
0
5
10
0
100
200
300

G. Can the Z = 104-107 Spontaneous Fission Activities be Explained by Actinide Production in Damped Collisions?

CAN THE Z = 104-107 SPONTANEOUS FISSION ACTIVITIES BE EXPLAINED BY ACTINIDE PRODUCTION IN DAMPED COLLISIONS?

V.E. Viola, Jr. and A.C. Mignerey
Department of Chemistry and Cyclotron Laboratory
University of Maryland
College Park, MD 20742

H. Breuer
Department of Physics and Cyclotron Laboratory
University of Maryland
College Park, MD 20742

K.L. Wolf and B.G. Glagola
Chemistry Division
Argonne National Laboratory
Argonne, IL 60439

and

W.W. Wilcke, W.U. Schröder, J.R. Huizenga,
O. Hilscher* and J.R. Birkelund
Departments of Chemistry and Physics and
Nuclear Structure Research Laboratory
University of Rochester
Rochester, NY 14627

*On leave from Hahn-Meitner-Institut fur Kernforschung Berlin GmbH,
D-1000 Berlin 39, West Germany

ABSTRACT

Results of recent nuclear reaction studies on the $^{209}Bi + ^{56}Fe$ system are analyzed in order to investigate the cross sections for production of spontaneously fissioning species with $90 < Z < 100$. This reaction is nearly identical to those used as the basis for identification of new elements with Z = 104 -107, reported to be spontaneous fission emitters. Evidence is presented which indicates that actinide elements are formed with primary yields of the order of millibarns in strongly-damped collisions of 464 MeV ^{56}Fe with ^{209}Bi. Although strongly depleted by fission competition, final yields of possible spontaneous fission activities $^{240f-244f}Am$, $^{234-238}Cf$ and $^{242-246}Fm$ are calculated to be of the order of nanobarns. These results suggest that the spontaneous fission activities observed in similar reactions may be due at least in part to fission decay of actinide elements rather than elements with Z = 104 -107.

[NUCLEAR REACTIONS $^{209}Bi(^{56}Fe,X)$, E = 464 MeV; measured σ for discrete Z and A for Fe-like fragments; deduced primary and final yields for Z = 90 - 100 partners with SF half-lives in ms-to-s range.]

In studies of reactions induced by Ti, V, Cr, Mn and Fe ions on Tl, Pb and Bi targets, Oganessian and co-workers[1-4] have reported evidence for the discovery of several isotopes of the elements with Z = 104 -107. All of these species have been identified as spontaneous fission (SF) emitters with characteristic half-lives either in the range of 1-10 milliseconds or a few seconds. Atomic number identification has relied upon the assumption that the observed parent nuclide is produced by complete fusion of target and projectile, followed by equilibration via neutron emission to the ground state. Cross sections of the order of 0.1-1 nanobarn or less are associated with these products. A summary of the targets and projectiles used in the experiments of Ref. 1-4 and the reported half-lives of the Z = 104-107 products is presented in Table I.

A particularly striking aspect of these studies[1-4] has been the spontaneous fission half-life systematics for element 104. The reported half-lives exhibit a very weak dependence on even neutron number for N = 150 -156, whereas for lighter even-Z elements the half-lives decrease by 2-3 orders of magnitude for each additional pair of neutrons from N = 152-156.

Recently, our group[5] has performed counter experiments in order to investigate the nuclear reaction mechanisms which characterize a similar reaction, $^{209}Bi + ^{56}Fe$. It is the purpose of this paper to discuss the implications of these results on the work of Refs. 1-4. The measurements involved determination of cross sections as a function of energy loss for Fe-like fragments using a ΔE-E time-of-flight system that provided discrete mass and atomic number identification[5]. Self-supporting targets of ~500 $\mu g/cm^2$ metallic bismuth were bombarded with 464-MeV ^{56}Fe ions from the Lawrence Berkeley Laboratory SuperHILAC accelerator. From the binary nature of the damped collision process[6] it is thus possible to infer the yields of the primary heavy recoil nuclei. In addition the fusion-fission cross section has

been measured, which permits evaluation of the contribution of fusion processes in these reactions.

Of particular relevance to the question of the source of the spontaneous fission activities reported in Refs. 1-4 are the following results from our studies:

(1) The nucleon diffusion process in damped collisions induced by ^{56}Fe ions favors a Z-drift in which protons are preferentially transferred from the projectile to the target, reulting in a net mass drift in the same direction. This serves to enhance the yields of actinide products. It is expected that other projectiles in the Ti-Fe region will exhibit this same behavior.

(2) For damped reactions the yield of heavy reaction products is determined primarily by the choice of target nucleus, since the target represents the injection point for the nucleon diffusion process. The major additional factor which influences the product yields is the neutron-excess (N-Z) of both target and projectile.

(3) The fusion-fission cross section is found to be about 500 mb for the ^{209}Bi + ^{56}Fe reaction at bombarding energies of 385 and 480 MeV. Despite the reduced reaction cross sections expected at lower energies and the high fissility of such composite nuclei, this result leaves open the possibility of forming evaporation residues for reactions of this type although with very small cross sections. In Refs. 1-4 it is assumed that the observed SF activities are the products of complete fusion reactions in which a compound nucleus is formed, followed by de-excitation via neutron and gamma emission. No account is taken of the large (>70%) fraction of dampled collisions in reactions of this type or of the constraints imposed by the maximum liquid drop angular momentum ($\ell_{LD} \sim 60\ \hbar$) for nuclei in the Z~104 region[7]. Based on this latter point, it is expected that the maximum in the excitation function for true compound nucleus fromation in reactions of this type should be about

150 mb.

In view of the first two points listed above, it is of interest to examine the possibility of forming known spontaneous fission emitters with Z<104 with half-lives in the millisecond and second range by means of damped collisions in the $^{209}Bi + ^{56}Fe$ reaction, where detailed nuclear reaction data are now available. Known candidates for such products are the spontaneous fission isomers of americium (Z = 95) and ground state SF activities of fermium (Z = 100). In addition the unknown isotopes $^{234-238}_{98}Cf$ are estimated to have half-lives in the 1 ms -1 sec range with possible significant SF branching ratios. Other possibilities may also exist since the strongly damped products populate a large number of unknown neutron-deficient nuclei with Z > 90. In Table II the measured properties of the Am and Fm isotopes and the estimated properties of the Cf isotopes of interest here are listed. In estimating the SF half-lives, t_{SF}, for Cf isotopes, a systematic dependence of log t_{SF} on neutron number that is intermediate between curium and fermium SF behavior has been assumed. If Fm-like SF systematics are assumed for Cf, half-lives 10^2 -10^5 times shorter result; Cm-like SF systematics lead to half-lives much longer than those in Table II.

In Fig. 1 the experimental charge distribution for projectile-like fragments formed in the bombardment of ^{209}Bi with 464-MeV ^{56}Fe ions is shown. The charge resolution in these experiments was FWHM <0.8 Z units, whereas the mass resolution was FWHM <0.7 mass units. The primary charge distribution is assumed to be identical to the experimental charge distribution since charged-particle emission has been determined to be negligible in this reaction.[5] It is apparent that significant yields of Z = 9-19 products (corresponding to Z = 100-90 primary heavy partners) can be produced in damped collisions. The mass- , angle- and energy-integrated cross sections for Z = 90-100 primary yields are tabulated in Table III, assuming the reaction is

binary in nature. Table III constitutes the basis for the absolute yields quoted below. Another possible source of fragments with comparable Z values in these reactions is projectile breakup, which has been reported for heavy-ion collisions at higher bombarding energies.[8] On the basis of the continuous transition from Z = 26 to much lower Z values in the Z yields shown in Fig. 1, it is concluded that projectile breakup is not a dominant source of such fragments. In addition it should be pointed out that light element target contaminants such as oxygen cannot contribute to the observed yields in these experiments since the angle of measurement was substantially larger than the grazing angle for possible competing reactions; e.g., $^{16}O(^{56}Fe,^{52}Cr)^{20}Ne$.

Figure 2 shows a plot of the most-probable value of the fragment atomic number, $\overline{Z}$, versus the most probable mass number, $\overline{A}$, for the primary fragments. (The A results are corrected for neutron evaporation as described in Refs. 5 and 10). The N/Z ratio of the most probable light fragments is found to approach unity ($\overline{N}/\overline{Z} \approx 1.1$) for the lowest Z values, indicating the influence of the ground state mass surface on the nucleon diffusion process. For example, for Z = 14 a value of $\overline{A}$ = 29.5 is found, corresponding to a most-probable complementary product for Am with $\overline{A}$ = 235.5. A similar analysis leads to $\overline{A} \approx 242$ for Cf and $\overline{A} \approx 245$ for Fm. Gaussian distributions were assumed to describe the mass and energy distributions of the products. Analysis of the fragment mass distribution data for fixed Z in the range $9 < Z < 19$ yields an average value for the variance of the mass distribution of σ_A^2 (Z) $\approx$ 3.0, based on rather poor statistics. This value is somewhat smaller than that for the more probable Z values near Fe, where one finds a nearly constant value of σ_A^2 (Z) $\approx$ 4.0 for energy losses greater than 30-40 MeV. For the purpose of these calculations we have used σ_A^2 (Z) = 3.0 as a lower limit on the variance and σ_A^2 (Z) = 4.0 as an upper limit.

Primary mass yields for $^{240-244}Am$, $^{234-238}Cf$ and $^{242-246}Fm$ isotopes are listed in Table IV. The energy loss (E_{loss}) distribution for Z = 14 is found to have a most probable E_{loss} value of 240 MeV and a FWHM of about 40 MeV. This energy distribution and the ground state masses of Liran and Zeldes[9] were used to determine the excitation energies of the primary fragments. With respect to the ground state Q-values, Qgg, it is important to stress that these values are highly negative for the reactions of interest here (e.g., for production of ^{240}Am, Qgg = -137 MeV). As a consequence, even for rather large values of projectile energy loss, diffusion processes which transfer a large net number of nucleons yield products which are formed in relatively low states of excitation. If it were not for this fact, the final yields discussed below would be much smaller.

Although the primary yields of Am, Cf and Fm isotopes are found to be quite substantial compared to the cross sections of 1 nb or less reported for the Z = 104-107 spontaneous fission emitters[1-4], fission competition during de-excitation of the primary fragments strongly depletes these yields. In order to estimate the final cross sections, we have calculated the probabilities for de-excitation as a function of E_{loss}, assuming neutron emission and fission are the major decay channels. The excitation energy of the primary fragments was assumed to be determined by the energy loss (divided according to the mass ratio of the fragments[10]) and the calculated Qgg-values. The neutron-to-fission decay widths, Γ_n/Γ_f, tabulated by Vandenbosch and Huizenga[11], were used to estimate fission probabilities at all stages of the de-excitation process, which was followed using standard statistical methods[12] to determine the final fragment yields. No attempt was made to include an angular momentum dependence in the estimation of Γ_n/Γ_f for the following reasons: (1) because of the very low fission barriers for the actinide elements, the effect of angular momentum on Γ_n/Γ_f is much less pronounced than

in lighter systems where barriers are much larger, and (2) most of the yield of heavy fragments which survive fission de-excitation comes from the smallest E_{loss} values in the fragment kinetic energy distribution, where the transferred angular momentum is smallest.

The yields were then integrated over all E_{loss} values and are tabulated in Table IV. For Am isotopes the choice of σ_A^2 (Z) influences the final product yields strongly since the isotopes of interest are on the high A tail of the mass yield curve. For Cf and Fm products the results are only weakly dependent on σ_A^2 (Z) since the peaks of the primary product distributions nearly coincide with the isotopes of interest. Hence, an average is quoted.

It is observed in Table IV that interesting amounts of the $^{240-4}$Am isotopes are formed in damped collisions. However, the possibility that the Am fission isomers may constitute at least part of the observed SF activities depends strongly on the branching ratio for population of the isomeric states relative to the ground state. If a value of 5×10^{-4} is assumed for this ratio, which is consistent with formation of the isomeric states in light-ion-induced reactions, then the final yields will be depleted to rather low levels as shown in Table IV. On the other hand, the highly stretched configuration that characterizes the scission point in strongly damped processes may serve to enhance the relative population of the fission isomeric states if they are formed in low states of excitation. In this case, the higher mass variance σ_A^2 (Z) = 4.0 may be adequate to yield measurable cross sections for the Am fission isomers in reactions of the type ^{209}Bi + ^{56}Fe. If the lower limit for σ_A^2 (Z) of 3.0 is valid, it would appear less favorable for producing the Am SF isomers, unless the population of the fission isomer states is quite large.

As far as the isotopes of Cf and Fm are concerned, the yields of the primary fragments are depleted strongly due to fission competition during

de-excitation. The calculated final yields are quite sensitive to assumptions concerning the fission barriers, which determine the behavior of Γ_n/Γ_f for these very neutron-deficient nuclei. If direct extrapolation of the Γ_n/Γ_f systematics for Cf and Fm of Ref. 11 is employed in these calculations, then the cross sections for $^{234-238}Cf$ and $^{242-244}Fm$ are estimated to be of the order of tens of picobarns or less. If, on the other hand, the fission barriers in this region are influenced by the N = 126 closed shell, as is predicted by shell-corrected fission barrier calculations[13], then larger values of Γ_n/Γ_f are predicted. In our estimates we have assumed Γ_n/Γ_f values intermediate between these two extremes. In this case significant amounts of $^{234-238}Cf$ and $^{242-246}Fm$ isotopes result (Table IV).

Although the calculated final cross sections are subject to considerable uncertainties, depending on the input assumptions, we have attempted to use parameters which represent a compromise between possible extremes. For example, the calculated final product cross sections can be enhanced from one-to-three orders of magnitude by means of the following modifications:

(1) Instead of using a Gaussian function to describe the energy loss, a distribution that is skewed toward low values of E_{loss} would be more consistent with the experimental data for higher Z values, where better statistical definition of these distributions exists,

(2) Excitation energy division between the two fragments has been assumed to be a unique value defined by $E_1^*/E_2^* = A_1/A_2$; a more realistic assumption would be to use a statistical distribution of excitation energies about this mean[10], and

(3) An alternative method for dividing the excitation energy between the light and heavy fragments would be to calculate this division on the basis of shell-dependent level density parameters rather than using a uniform value of A/8 MeV^{-1}.

All of these modifications would increse the relative yields of low excitation-energy heavy fragments, which have a greatly enhanced survival probabilities due to fewer stages of neutron-fission competition in their de-excitation. In this regard it should be reiterated that all of the final yields for each nucleus listed in Table IV come from the low E_{loss} tail of the energy-loss distribution, well below the most probable E_{loss} value.

One major additional factor must be considered in this evaluation. That is, the bombarding energies in the experiments of Oganessian et al.[1-4], were approximately 2-3 MeV/nucleon lower than that for which the $^{209}Bi + ^{56}Fe$ data used in this analysis were obtained. Although data with simultaneous Z and A identification are not available as a function of bombarding energy for the $^{209}Bi + ^{56}Fe$ system, studies of very heavy ion reactions near the Coulomb barrier by Rehm et al[14] demonstrate that substantial nucleon exchange occurs in near-barrier reactions, although with somewhat lower primary cross sections. Nonetheless, due to the much lower excitation energies associated with near-barrier reactions, the depletion of the primary yields due to fission competition during fragment de-excitation should be greatly reduced. Since fission competition is responsible for the large depletion factors between the primary and final yields in these calculations, it is not unreasonable to expect that equivalent or enhanced final product yields may accompany lower-energy bombardments.

In conclusion, evaluation of results from studies of the $^{209}Bi + ^{56}Fe$ reaction indicate that neutron-deficient isotopes of the actinide elements are produced with primary cross sections of the order of millibarns via multiple nucleon transfer processes in damped collisions. Peak primary yields correspond approximately to the lightest known isotopes for each element, as shown in Fig. 1. Based on estimates of neutron-fission competition in the de-excitation of the primary products, it is concluded that $^{234-238}Cf$,

$^{242-246}Fm$ and perhaps $^{240f-244f}Am$ spontaneous fission emitters may be produced with final yields of the same order of magnitude as those reported for elements Z = 104-107 by Oganessian et al[1-4]. These measurements further indicate that at least 70% of the total reaction cross section goes into damped reactions. The remaining cross section can be accounted for by fusion-fission processes, which for the most part involve angular momenta in excess of the critical value for a rotating liquid drop of $\ell_{LD} \approx 60\hbar$ for this system[7]. Hence, the probability for formation of completely energy-equilibrated compound nuclei in this reaction is expected to be small, even before fission competition is considered in the de-excitation of such species. For these reasons it is suggested that before the results of Oganessian et al.[1-4] can be accepted as evidence for new elements with Z = 104-107 and for a major anomaly in SF half-life systematics, a more unique atomic number identification of the products of these reactions must be performed.

The authors wish to acknowledge conversations with Dr. M. Nitschke concerning these results. We also wish to thank Dr. M. S. Zisman and the staff of the LBL SuperHILAC for their assistance in the performance of these experiments. This work was supported by the U. S. Department of Energy.

REFERENCES

1. Yu. Ts. Oganessian, Yu. P. Tretyakov, A. S. Iljinov, A. G. Demin, A. A. Pleve, S. P. Tretyakova, V. M. Plotko, M. P. Ivanov, N. A. Danilov, Yu. S. Korotkin and G. N. Flerov, JETP Letters 20, 265 (1974).

2. Yu. Ts. Oganessian, A. G. Demin, A. S. Iljinov, S. P. Tretyakova, A. A. Pleve, Yu. E. Penionzhkevich, M. P. Ivanov and Yu. P. Tretykova, Nucl. Phys. A239, 157 (1975).

3. G. M. Ter-Akopyan, A. S. Iljinov, Yu. Ts. Oganessian, O. A. Orlova, G. S. Popeko, S. P. Tretyakova, V. I. Chepigin, B. V. Shilov and G. N. Flerov, Nucl. Phys. A255, 509 (1975).

4. Yu. Ts. Oganessian, A. G. Demin, N. A. Danilov, G. N. Flerov, M. P. Ivanov, A. S. Iljinov, N. N. Kolesnikov, B. N. Markov, V. M. Plotko and S. P. Tretyakova, Nucl. Phys. A273, 505 (1976).

5. H. Breuer, B. G. Glagola, V. E. Viola, K. L. Wolf, A. C. Mignerey, J. R. Birkelund, D. Hilscher, A. D. Hoover, J. R. Huizenga, W. U. Schröder and W. W. Wilcke, Phys. Rev. Lett. 43, 191 (1979).

6. K. L. Wolf and C. T. Roche, Proc. Symp. Macroscopic Features of Heavy-Ion Collisions, Argonne Nat'l Lab. Report ANL/PHY-76-2, Vol. I, 295 (1976).

7. S. Cohen, F. Plasil and W. Swiatecki, Ann. of Phys. 82, 557 (1974).

8. A. Olmi, U. Lynen, J. B. Natowitz, M. Dakowksi, P. Doll, A. Gobbi, H. Sann, H. Stelzer, R. Bock and D. Pelte, Gesellschaft für Schwerionenforschung Report GSI-79-17 (1979).

9. S. Liran and N. Zeldes, Atomic and Nucl. Data Tables, 17, 431 (1976).

10. D. Hilscher, J. R. Birkelund, A. D. Hoover, W. U. Schröder, W. W. Wilcke, J. R. Huizenga, A. C. Mignerey, K. L. Wolf, H. Breuer and V. E. Viola, Phys. Rev. C20, 576 (1979).

11. R. Vandenbosch and J. R. Huizenga, Proc. Int. Conf. Peaceful Uses Atomic Energy, 15, 284, United Nations, Geneva (1958).

12. R. Vandenbosch and J. R. Huizenga, Nuclear Fission (Academic Press) 216 (1974).

13. W. D. Myers and W. J. Swiatecki, Nucl. Phys. 81, 1 (1966); Auk. Phys. 36, 343 (1967).

14. A. C. Mignerey et al., to be published.

15. K. E. Rehm, H. Essel, K. Hartel, P. Kienle, H. J. Körner, R. E. Segel, P. Sperr and W. Wagner, Z. Physik A239, 119 (1979); H. Essel, K. Hartel, W. Henning, P. Kienle, H. J. Körner, K. E. Rehm, P. Sperr, W. Wagner and H. Spieler, Z. Physik A289, 265 (1979).

15. V. E. Viola, J. A. Swant and J. Graber, Atomic and Nucl. Data Tables 13, 35 (1974); V. E. Viola and G. T. Seaborg, J. Inorg. Nucl. Chem. 28, 697 (1966).

TABLE I

Summary of target and projectile types used in assignment of spontaneous fission activities of Refs. 1-4. Bombarding energies were in the range 240-300 MeV. Also listed are the reported products (half-lives in parenthesis).

Projectiles: $^{48,50}Ti$, ^{51}V, $^{52,54}Cr$, ^{55}Mn, ^{58}Fe

Targets: $^{203,205}Tl$, $^{206-208}Pb$, ^{209}Bi

Products:

$^{253}104$(2s) $^{254}104$(0.5ms) $^{255}104$(4s) $^{256}104$(5ms) $^{258}104$(11ms) $^{260}104$(<25ms)

$^{257}105$(4s)

$^{259}106$(7ms)

$^{261}107$(2ms)

TABLE II

Measured and predicted (in brackets) decay properties of Am, Cf and Fm activities with half-lives in the range of 1 ms or 1s (t_{SF} = partial half-life for spontaneous fission; t_α = partial half-life for alpha decay). Alpha decay half-lives were derived according to Ref. 15.

	^{240}fAm	^{242}fAm	^{244}fAm
t_{SF}	0.9ms	14ms	1.0ms

	^{234}Cf	^{236}Cf	^{238}Cf	^{240}Cf
t_{SF}	(1μs-200ms)	(1ms-100s)	(2s-2h)	(2h-20d)
t_α	(200μs)	(5ms)	(300ms)	1ms

	^{242}Fm	^{244}Fm	^{246}Fm
t_{SF}	0.8ms	3ms	1.2 s

TABLE III

Cross sections for actinide element primary yields derived from projectile-like fragment yields in the reaction ^{209}Bi + 464-MeV ^{56}Fe, as described in text.

Z	σ(mb)
90	62
91	40
92	24
93	18
94	13
95	10
96	10
97	6
98	4
99	4
100	4

TABLE IV

Primary and calculated final product cross sections (in nanobarns) for possible millisecond and second spontaneous fission activities of Am, Cf and Fm isotopes produced in the reaction of 464-MeV ^{56}Fe with ^{209}Bi. Parameters of the calculation are described in the text. The Am fission isomer yields assume a fission isomer branching ratios of 5×10^{-4}, consistent with that measured in fission isomer synthesis with light ions.

	Primary Yield (nanobarns)		Final Yield (nanobarns)	
	$\sigma_A^2(Z) = 3.0$	$\sigma_A^2(Z) = 4.0$	$\sigma_A^2(Z) = 3.0$	$\sigma_A^2(Z) = 4.0$
^{240f}Am	8×10^4	2×10^5	0.7	30
^{240f}Am			-	0.02
^{242}Am	2×10^3	2×10^4	0.5	20
^{242f}Am			-	0.01
^{244}Am	20	500	0.1	5
^{244f}Am			-	0.003
^{234}Cf	300		0.02	
^{236}Cf	1×10^4		0.1	
^{238}Cf	1×10^5		0.3	
^{242}Fm	2×10^5		0.05	
^{244}Fm	6×10^5		0.10	
^{246}Fm	6×10^5		0.05	

FIGURE CAPTIONS

Figure 1 - Plot of elemental (Z) yields of damped reaction products for 464-MeV ^{56}Fe + ^{209}Bi. Upper curve is for all Z; lower curve shows the data for $6 < Z < 20$ on an expanded scale.

Figure 2 - Plot of most probable projectile-like fragment mass, $\overline{A}_p$, as a function of most probable element charge, $\overline{Z}_p$, for primary fragments as derived from the data of Ref. 5. Right-hand and upper scales refer to complementary heavy partner with mass "$\overline{A}_t$" and charge "$\overline{Z}_t$", assuming a binary reaction mechanism.

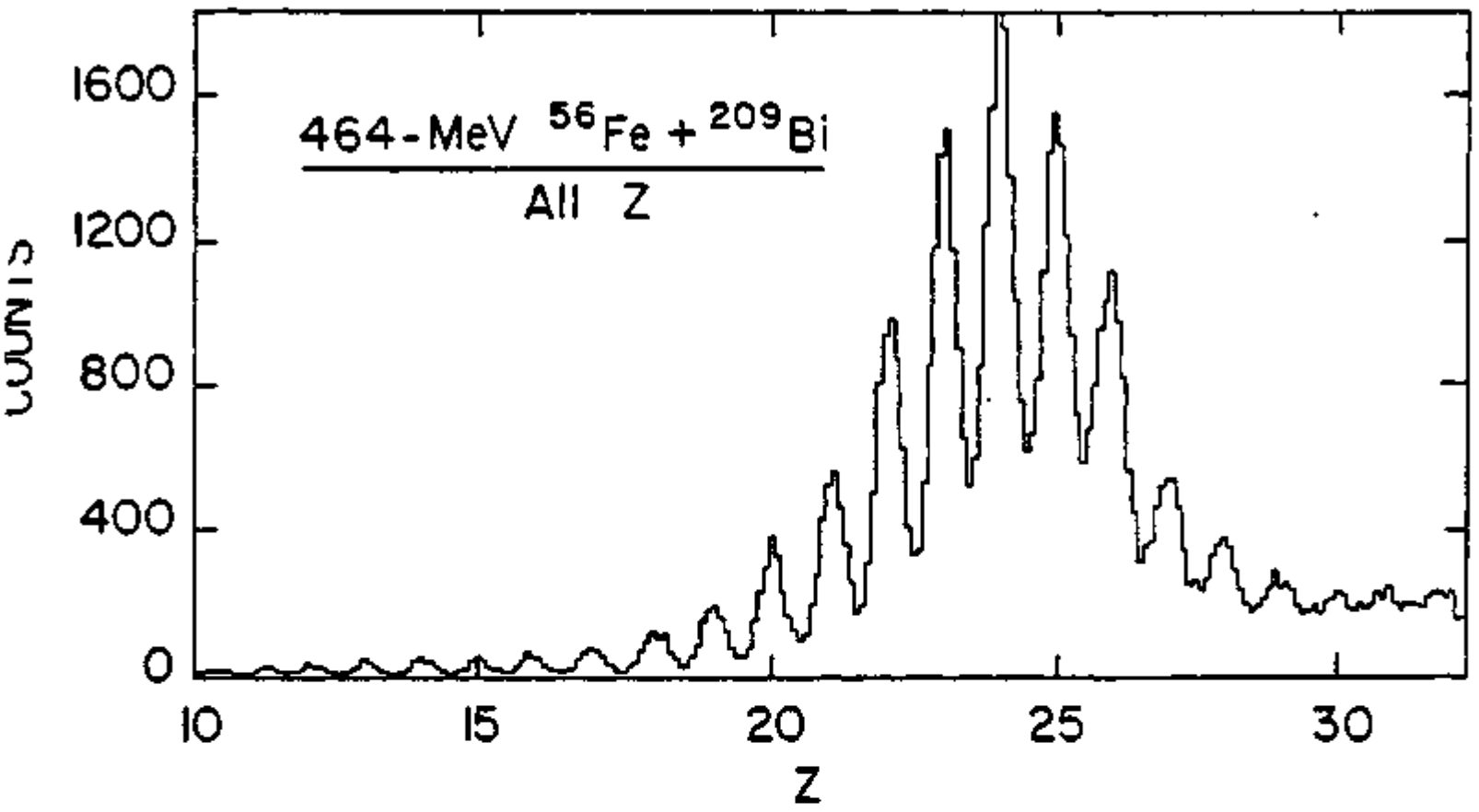
464-MeV $^{56}Fe + ^{209}Bi$
All Z
COUNTS
1600
1200
800
400
0
10
15
20
25
30
Z

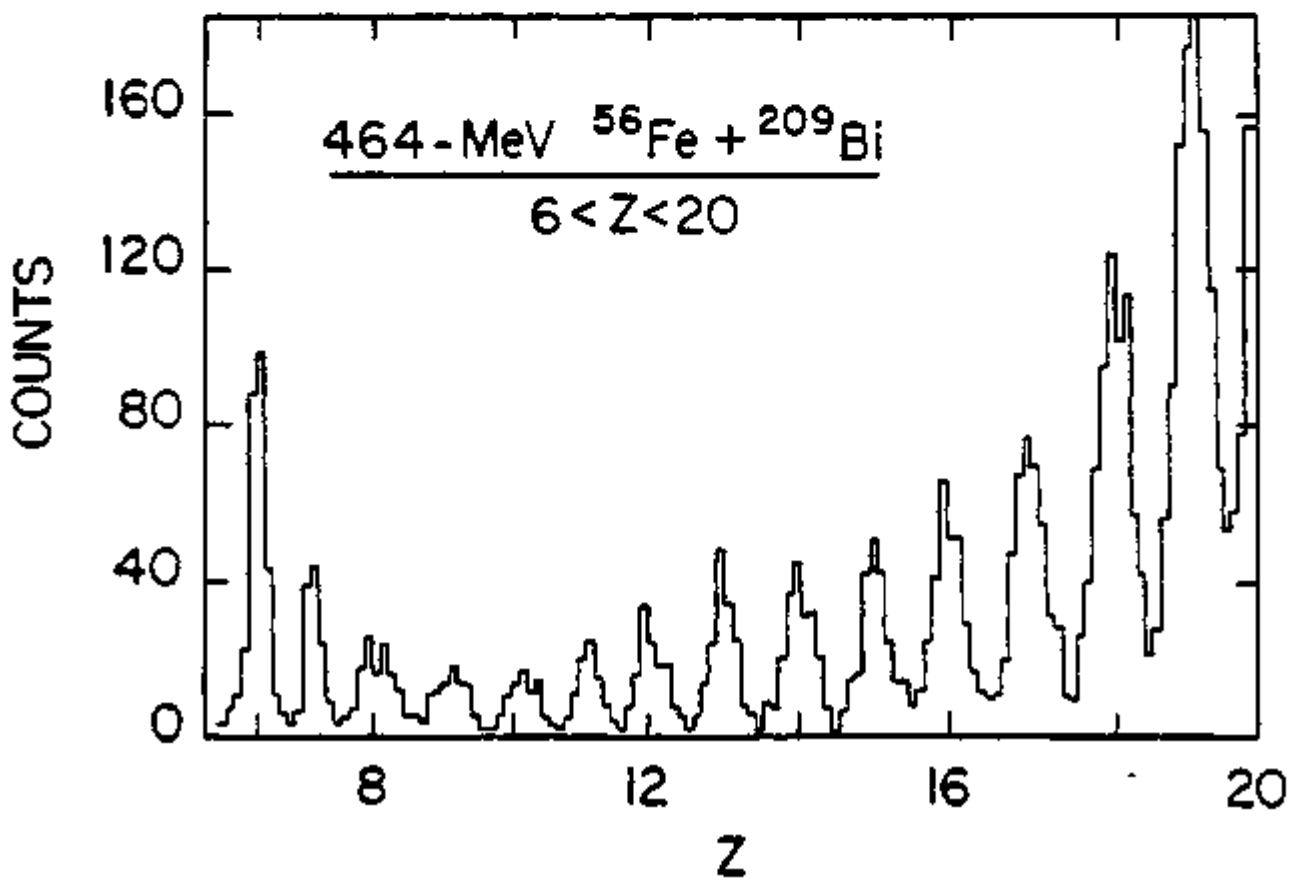
464-MeV $^{56}Fe + ^{209}Bi$
6<Z<20
COUNTS
160
120
80
40
0
8
12
16
20
Z

Figure 1

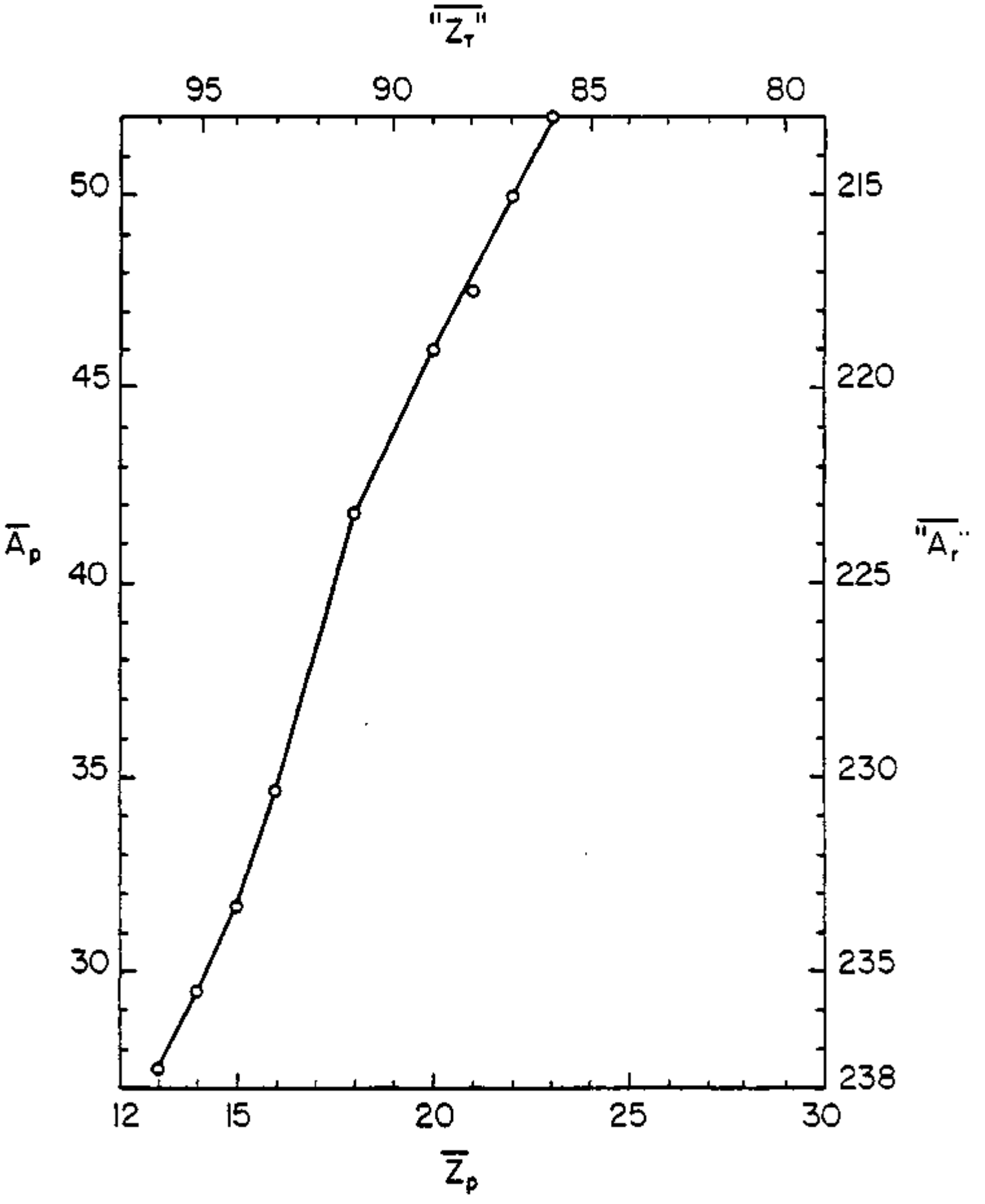
"$\overline{Z_T}$"
95
90
85
80
50
45
40
35
30
215
220
225
230
235
238
$\overline{A_p}$
"$\overline{A_r}$"
12
15
20
25
30
$\overline{Z_p}$

Figure 2

H. The Dependence of Isobaric Charge Distributions on Energy Loss and Mass Asymmetry in Damped Collisions

THE DEPENDENCE OF ISOBARIC CHARGE DISTRIBUTIONS ON ENERGY LOSS AND MASS ASYMMETRY IN DAMPED COLLISIONS

A.C. Mignerey and V.E. Viola, Jr.
Department of Chemistry and Cyclotron Laboratory
University of Maryland
College Park, Maryland 20742

H. Breuer
Department of Physics and Cyclotron Laboratory
University of Maryland
College Park, Maryland 20742

K.L. Wolf and B.G. Glagola
Chemistry Division
Argonne National Laboratory
Argonne, Illinois 60439

and

J.R. Birkelund, D. Hilscher,* J.R. Huizenga,
W.U. Schröder and W.W. Wilcke
Departments of Chemistry and Physics and
Nuclear Structure Research Laboratory
University of Rochester
Rochester, New York 14627

*Permanent address: Hahn-Meitner-Institut für Kernforschung,
D-1000, Berlin 39, West Germany

Abstract

Fragment yields for specific Z and A have been measured for projectile-like fragments produced in the reaction of 8.3 MeV/u ^{56}Fe ions with targets of ^{56}Fe, ^{165}Ho and ^{238}U. Analyses of the variances of the isobaric charge distributions $\sigma_Z^2(A)$ reveal that a saturation value of $\sigma_Z^2(A) \approx 0.8$ is reached within the first 30-50 MeV of energy loss. For the variances of the isotopic mass distributions we find a saturation value of $\sigma_A^2(Z) \approx 3.0\text{-}4.0$, which is reached after about 60-80 MeV of energy loss. The data are compared with N/Z equilibration models which invoke quantal and satistical fluctuations, based on the symmetry term in the liquid drop mass formula.

In order to gain a more microscopic understanding of the processes whereby energy is dissipated in damped collisions, yields of individual projectile-like fragments have been measured as a function of energy loss for ^{56}Fe-induced reactions. A series of target nuclei ranging from ^{56}Fe to ^{238}U has been studied, thus providing information on the effects of mass asymmetry and target-projectile N/Z ratios in the entrance channel. Such data ($d^3\sigma/dAdZdE$) provide a much more detailed view of the evolution of the nucleon exchange process than previously possible. Of particular current interest is the explanation of the fragment isobaric charge distributions, which define the charge equilibration (N/Z) degree of freedom. This process is believed to be one of the fastest relaxation modes in damped collisions.[1] Hence, from studies of this type one hopes to derive a clearer picture of the very early stages of the target-projectile interaction mechanisms which subsequently evolve toward statistical equilibrium.

Recently the subject of isobaric charge distributions has received considerable attention, both experimentally[2,3] and theoretically.[4-11] Due to uncertainties in correcting the experimental distributions for particle emission from the primary fragments, the principal focus of these investigations has been on the variances of the distributions, which are only slightly sensitive to these effects. Two sets of experimental data for systems in which damped collisions dominate the total reaction cross section have been reported prior to the present work. In counter studies of a nearly mass-symmetric system,

430 MeV ^{86}Kr + $^{92,98}Mo$, Berlanger et al,[2] found that the variances in the isobaric charge distributions, $\sigma_Z^2(A)$, increased rapidly with increasing energy loss up to $E_{Loss} \approx 30$ MeV and then remained constant at a value of $\sigma_Z^2(A) \approx 0.8$ thereafter. In these measurements a mass resolution of only 1.5 u was attained, leaving some uncertainties in the derivation of the experimental variances for individual mass numbers. In contrast a radiochemical study by Poitou et al,[3] involving the mass-asymmetric 890-MeV ^{132}Xe + ^{197}Au system produced quite different results. The variances were reported to increase monotonically up to an excitation energy of 150 MeV and in addition the data were characterized by smaller values of $\sigma_Z^2(A)$ (≈ 0.2-0.8). Despite the definite Z and A identification in these experiments, their interpretation is complicated by the problems of energy resolution and the assumptions employed in the complex data reduction procedures required to unfold the $d^3\sigma/dAdZdE$ data.

In this letter we present isobaric charge distribution data obtained with counter techniques which provided discrete Z and A identification of all projectile-like fragments. The measurements were performed at the Lawrence Berkeley Laboratory SuperHILAC accelerator with 8.3 MeV/u ^{56}Fe ions incident on targets of ^{56}Fe, ^{165}Ho and ^{238}U. Hence, we have studied target-projectile systems ranging from symmetric to very asymmetric combinations under identical experimental conditions. In each case the energy in excess of the Coulomb barrier, E_{cm}-V_c, is the same within 10 percent. Fragment mass and charge distributions were measured at angles near the grazing angle with a

ΔE-E time-of-flight counter telescope; data on the gross features of the ^{56}Fe, ^{165}Ho and ^{209}Bi reactions with ^{56}Fe have been reported previously.[12] In the most recent measurements a Z resolution (FWHM) of ≤ 0.8 units and an A resolution of ≤ 0.7 units were obtained for the fragments over a 200 MeV range in E_{Loss}. In Fig. 1 we show a representative mass distribtuion for Z = 24 fragments measured for the $^{56}Fe + ^{238}U$ reaction.

In Fig. 2 the isobaric charge variances are shown for two systems at 8.3 MeV/u bombarding energy: (1) $^{56}Fe + ^{56}Fe$ for all masses from A = 52 to 58 and (2) $^{56}Fe + ^{165}Ho$ for all masses from A = 52 to 57. Similar results are found for the ^{238}U target. The data shown in Fig. 2 are the fragments observed in the detectors without corrections for particle emission or detector resolution. If corrections are made for particle evaporation from the primary fragments, assuming division of the excitation energy according to A_1/A_2, the values of $\sigma_Z^2(A)$ remain essentially unchanged. However, no information is available on the spread in excitation energy about this average excitation energy. If this spread is large, somewhat smaller values of $\sigma_Z^2(A)$ may result for the primary fragments. It should be pointed out that for the projectile-like fragments observed with Ho and U targets, the observed most probable mass for each element lies on the neutron-rich side of beta-stability. Hence, for the primary fragments only neutron emission is important. For the $^{56}Fe + ^{56}Fe$ system charged particle emission is also possible; we estimate this effect on the data will decrease the $\sigma_Z^2(A)$ values by less than 10%.

The significant result of this study is that all the isobaric charge distributions are very similar and nearly independent of target-projectile mass asymmetry (A_1/A_2) or total mass ($A_1 + A_2$). The variances are observed to saturate within the first 30-50 MeV of energy loss and thereafter remain constant at $\sigma_Z^2(A) \approx 0.9$ up to energy losses in excess of 150 MeV. As an example of the similarity in the variances, if one averages all experimental $\sigma_Z^2(A)$ values for each isobar over an energy range from 50-150 MeV for the data of Fig. 2 and corrects for the experimental resolution, an average value of $\sigma_Z^2(A) = 0.75\pm0.08$ is found for the ^{56}Fe target, $\sigma_Z^2(A) = 0.85\pm0.10$ for the ^{165}Ho target, and $\sigma_Z^2(A) = 0.72\pm0.10$ for the ^{238}U target. The average slope $\sigma_Z^2(A)$ versus E_{Loss} is found to be consistent with zero for energy losses greater than 50 MeV. In this respect our data are similar to those of Berlanger *et al.*,[2] but show an energy-loss dependence different from that reported by Poitou *et al.*[3]

Examination of the first 50 MeV of energy loss in Fig. 3 suggests that the approach to saturation in the variances depends on the system studied. Although this feature of the data is less well-defined, it indicates that the amount of energy dissipation required to reach the saturation value for $\sigma_Z^2(A)$ increases with increasing Z and A of the composite system. Such an effect may provide a self-consistent explanation for the differences between the data reported here and in Ref. 2 and those of Ref. 3; however, more extensive data as a function of bombarding (excitation) energy are needed before a rigorous

comparison of all these systems can be made.

Analysis of the isotopic mass variances, $\sigma_A^2(Z)$, produces similar results. For charges near that of the projectile, all systems yield a nearly uniform saturation value of $\sigma_A^2(Z) \approx 3.0\text{-}4.0$, which is reached, however, only after an energy loss of about 60-80 MeV. Thus it appears that approximately twice as much energy must be dissipated in order to saturate the variances for the mass degree of freedom as for the charge degree.

In an attempt to explain these results a simple model has been proposed that is based on treatment of the neutron-excess (N-Z) degree of freedom in terms of an harmonic oscillator analogy.[2,4,5] This oscillator (assumed to have a constant collective frequency ω) is coupled to the intrinsic degrees of freedom of the system which are assumed to constitute a heat bath of temperature T. Two extreme predictions for $\sigma_Z^2(A)$ arise from this model, depending on the relative magnitude of the oscillator phonon energy $\hbar\omega$ compared to T:

(1) If $\hbar\omega >> T$, then $\sigma_Z^2(A)$ is predicted to be a constant related to the stiffness coefficient, C, of the mode by $\sigma_Z^2(A) = \hbar\omega/2C$. In this case the charge fluctuations are of the quantal type and ω represents the frequency of the underlying collective mode.

(2) If $\hbar\omega << T$, then $\sigma_Z^2(A)$ varies directly with the nuclear temperature $\sigma_Z^2(A) = T/C$. In this case one is dealing with statistical fluctuations.

The $^{86}Kr + {}^{92,98}Mo$ results have been interpreted[2] in terms of a quantal picture with $\hbar\omega \approx 8.5$ MeV. On this basis the

authors of Ref. 2 have suggested that the out-of-phase vibration of the neutron and proton distributions, i.e., the giant isovector dipole resonance, is an important factor in determining N/Z equilibration and energy damping in the early phase of damped collisions. On the other hand the ^{132}Xe + ^{197}Au support a model based on statistical fluctuations which then readily couple to the slower degrees of freedom, well known to be described by statistical transport models.[13] By modifying the quantal fluctuation model to include dynamical considerations,[4,6] a slightly better fit to both of above sets of the data can be obtained; however, this cannot be achieved with self-consistent values of $\hbar\omega$ for the two pairs of target projectile combinations. The variance data of Refs. 2 and 3 are difficult to reconcile in another sense; because the symmetry term in the liquid drop mass surface plays an important role in defining the widths of the Z distributions, one expects the ^{132}Xe + ^{197}Au system to exhibit intrinsically larger values of $\sigma_Z^2(A)$ than ^{86}Kr + $^{92,98}Mo$. Just the reverse is observed. Another suggested interpretation[5] of these data is that mass-symmetric systems exhibit quantal fluctuations and asymmetric systems behave statistically. Our data show no evidence for such behavior.

In order to compare these data with the predictions for quantal and statistical fluctuations, in Fig. 3 we have plotted the average of the isobaric charge variances for the data of Fig. 2 at each energy loss as a function of E_{Loss}. The theoretical curves have been calculated assuming[4] $\hbar\omega = 78/C(A_1^{1/3} + A_2^{1/3})$ MeV and C = 7.1 MeV, 4.8 MeV and 4.2 MeV

for the $^{56}Fe + ^{56}Fe$, $^{165}Ho + ^{56}Fe$ and $^{238}U + ^{56}Fe$ systems, respectively. The agreement of the saturation values with the quantal fluctuation extreme is good for both the $^{165}Ho + ^{56}Fe$ and $^{56}Fe + ^{56}Fe$ systems. However, before attributing this correspondence to the isovector giant dipole resonance, it should be cautioned that the underlying feature of this theory is the liquid drop mass equation, for which the parabolic dependence on Z for a given set of isobars is well known. Hence, these experimental results may simply be a consequence of liquid drop energetics. In addition, it should be noted that the initial increase of the variances with energy loss is inconsistent with instantaneous increase predicted by the simple quantal model discussed above. More realistic quantal calculations[9] qualitatively reproduce the observed energy dependence of $\sigma_Z^2(A)$ for the earlier data of Refs. 2 and 3. Recently, Brosa[10] has shown that the data of Refs. 2 and 3 can be described with a single-particle model, while Samaddar and Sobel[11] have explained the rapid equilibration of the N/Z ratio in damped collisions in terms of both a diffusion and a collective model. Thus, although the data presented here are consistent with the quantal calculations, this agreement does not necessarily confirm the existence of quantal fluctuations.[10] It would be interesting to have a quantitative prediction of these widths based on a microscopic transport theory.

In conclusion, these measurements with discrete Z and A identification demonstrate that the isobaric charge variances in damped collisions saturate very rapidly ($E_{Loss} < 50$ MeV).

In addition, it is shown that target-projectile mass asymmetry has little effect on the limiting value of the observed variances. On the other hand, the dependence of $\sigma_Z^2(A)$ on energy loss below 50 MeV suggests that saturation may be achieved more slowly as the Z and A of the composite system increases. Our results are in general agreement with the predictions of the quantal fluctuation model and imply values of $\hbar\omega \cong 7\text{-}10$ MeV for the associated oscillator mode. Equivalently, one can attribute the results to constraints imposed by the parabolic nature of the isobaric mass surface. Other explanations may also exist.[8,10,11] Under any circumstances the data demonstrate the very rapid equilibration of the isobaric charge degree of freedom and suggest that studies of this type are important to the understanding of the earliest stages of damped collision processes.

This research was supported by the U.S. Department of Energy. The authors wish to thank Dr. M.S. Zisman and the staff at the Lawrence Berkeley Laboratory SuperHILAC for their cooperation in performing these measurements.

References

1. B. Gatty, D. Guerreau, M. Lefort, J. Pouthas, X. Tarrago, J. Galin, B. Cauvin, J. Girard, H. Nifenecker, Z. Physik A273, 65 (1975) and Nucl. Phys. A253, 511 (1975).
2. M. Berlanger, A. Gobbi, F. Hanappe, U. Lynen, C. Ngo, A. Olmi, H. Sann, H. Stelzer, H. Richel and M.F. Rivet, Z. Physik A291, 133 (1979).
3. J. Poitou, R. Lucas, J.V. Kratz, W. Brüchle, H. Gaggeler, M. Schädel and G. Wirth, Phys. Lett. 88B, 69 (1979).
4. H. Hoffman, C. Gregoire, R. Lucas and C. Ngo, Z. Physik A293, 229 (1979).
5. L.G. Moretto, J. Sventek and G. Mantzouranis, Phys. Rev. Lett. 42, 563 (1979).
6. L.G. Moretto, C.R. Albiston and G. Mantzouranis, Phys. Rev. Lett. 44, 924 (1980).
7. U. Brosa and H.J. Krappe, Z. Phys. 284, 65 (1978).
8. U. Brosa, preprint (1979).
9. E.S. Hernandez, W.D. Myers, J. Randrup and B. Remaud, LBL Report LBL-9761 (1979).
10. U. Brosa and D.H.E. Gross, preprint (1979).
11. S.M. Samaddar and M.I. Sobel, Phys. Lett. 82B, 191 (1979).
12. H. Breuer, B.G. Glagola, V.E. Viola, K.L. Wolf, A.C. Mignerey, J.R. Birkelund, D. Hilscher, A. Hoover, J.R. Huizenga, W.U. Schröder and W.W. Wilcke, Phys. Rev. Lett. 43, 191 (1979).
13. W. Nörenberg, Z. Phys. A274, 241 (1975) and A276, 84 (1976); H. Hoffman and P.J. Siemens, Nucl. Phys. A257, 165 (1976);

D. Agassi, C.M. Ko and H.A. Weidenmüller, Ann. Phys. 107, 140 (1977).

Figure Captions

Figure 1. Plot of mass distribution for Z = 24 fragments obtained for $^{56}Fe + ^{238}U$ reaction at 8.3 MeV/u. Fragments cover an energy range of $20 \leq E_{Loss} \leq 200$ MeV.

Figure 2. Plot of isobaric charge variances for
(a) $^{56}Fe + ^{56}Fe$ for A = 52-58 and
(b) $^{56}Fe + ^{165}Ho$ for A = 52-57 as a function of E_{Loss}.

Figure 3. Comparison of average $\sigma_Z^2(A)$ values for data in Fig. 2 and ^{238}U, corrected for experimental resolution, as a function of E_{Loss} with predictions of theory for quantal fluctuations (solid line) and statistical fluctuations (dashed line) as described in text.

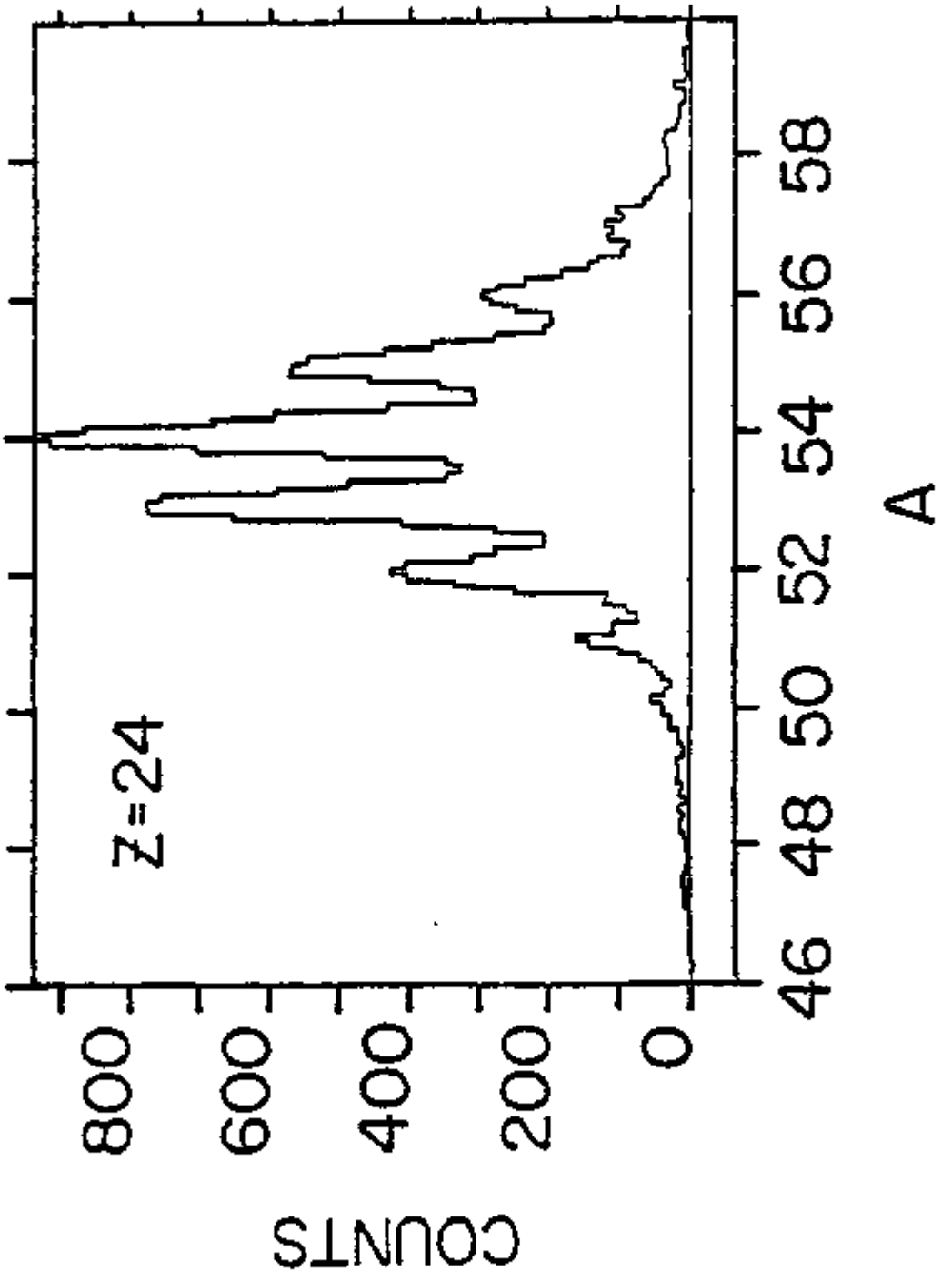

Figure 1

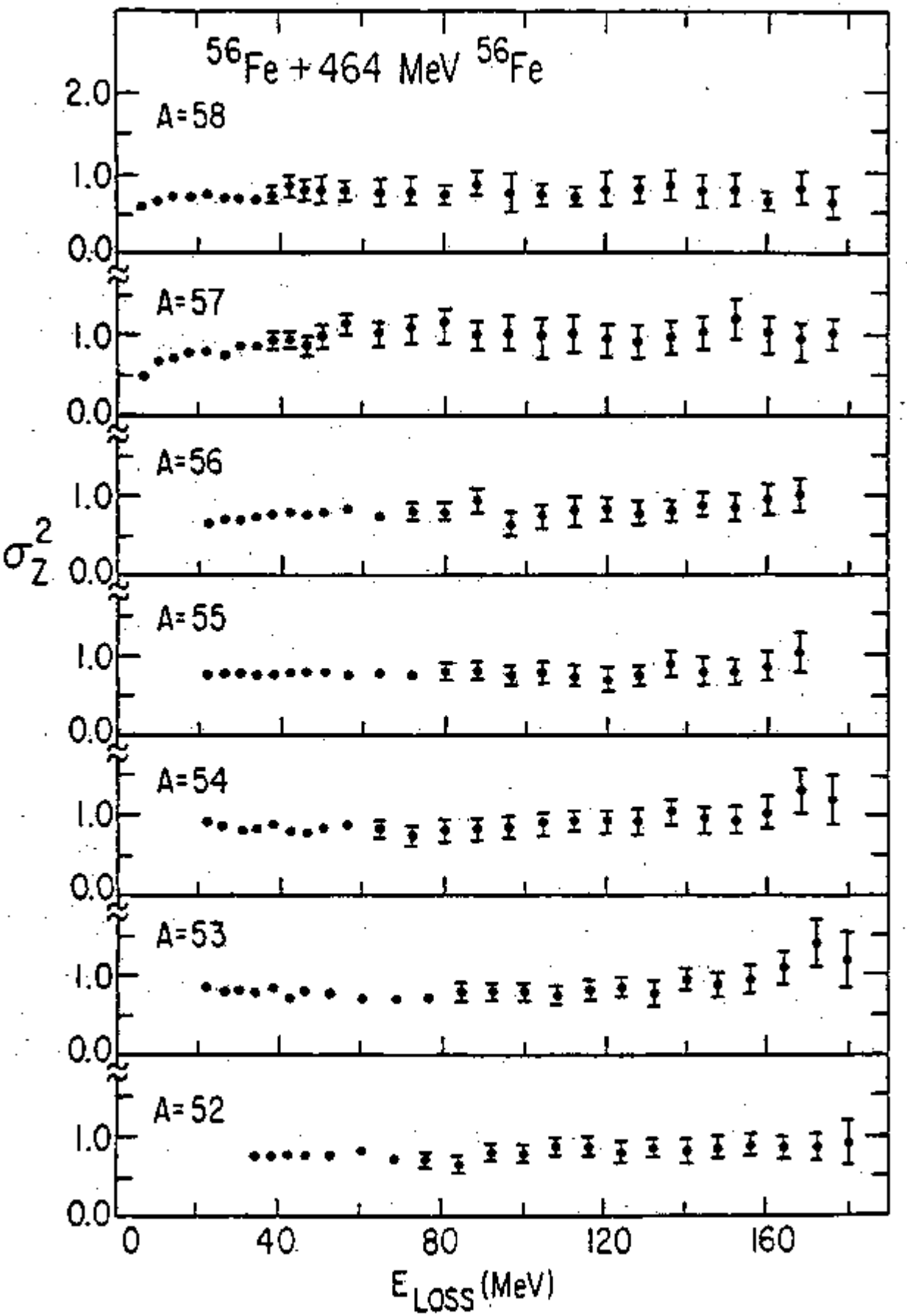
^{56}Fe + 464 MeV ^{56}Fe
A=58
A=57
A=56
A=55
A=54
A=53
A=52
2.0
1.0
0.0
σ_Z^2
0
40
80
120
160
E_{LOSS} (MeV)

Figure 2a

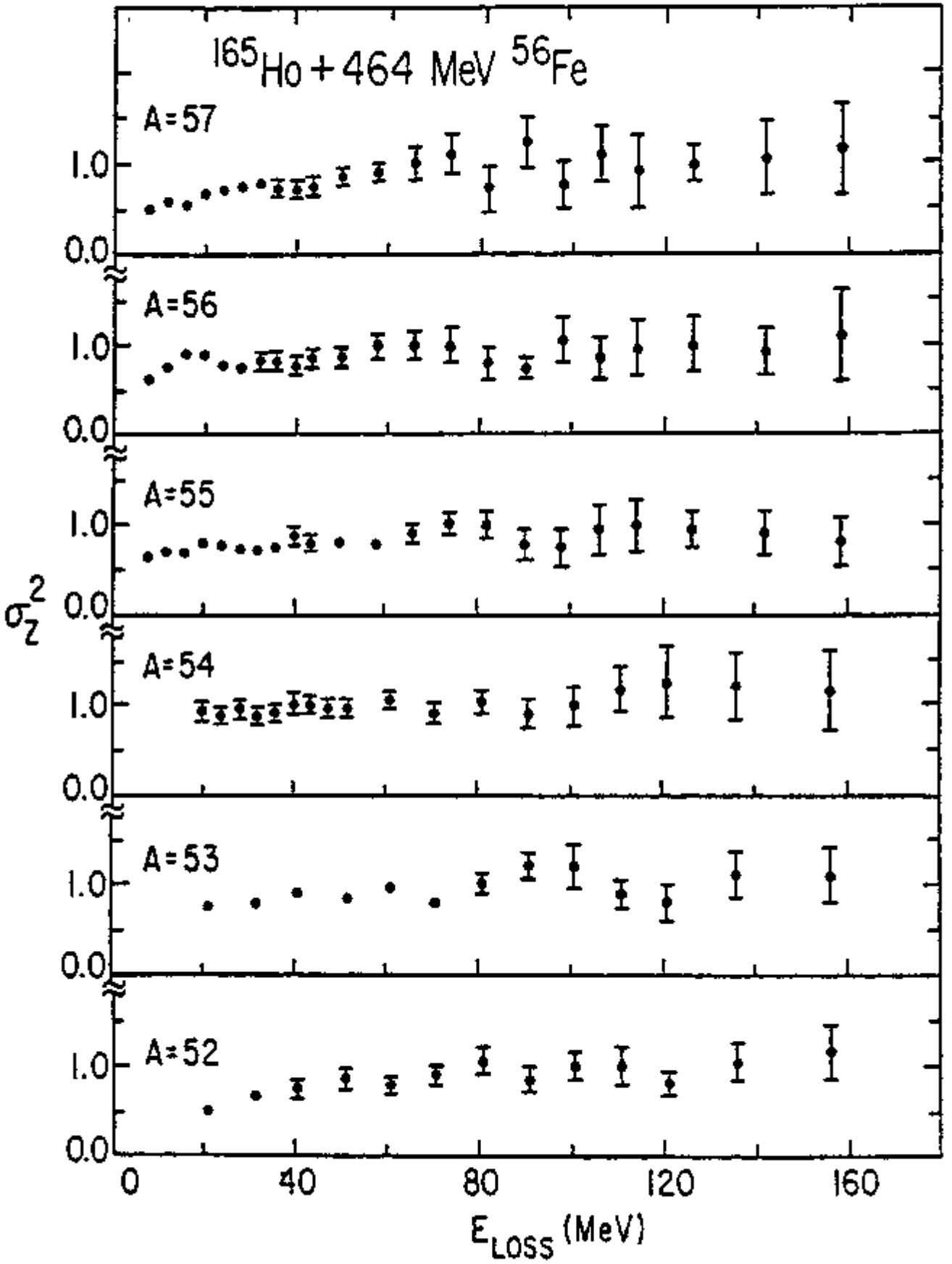
^{165}Ho + 464 MeV ^{56}Fe
A=57
A=56
A=55
A=54
A=53
A=52
1.0
0.0
σ_Z^2
0
40
80
120
160
E_{LOSS} (MeV)

Figure 2b

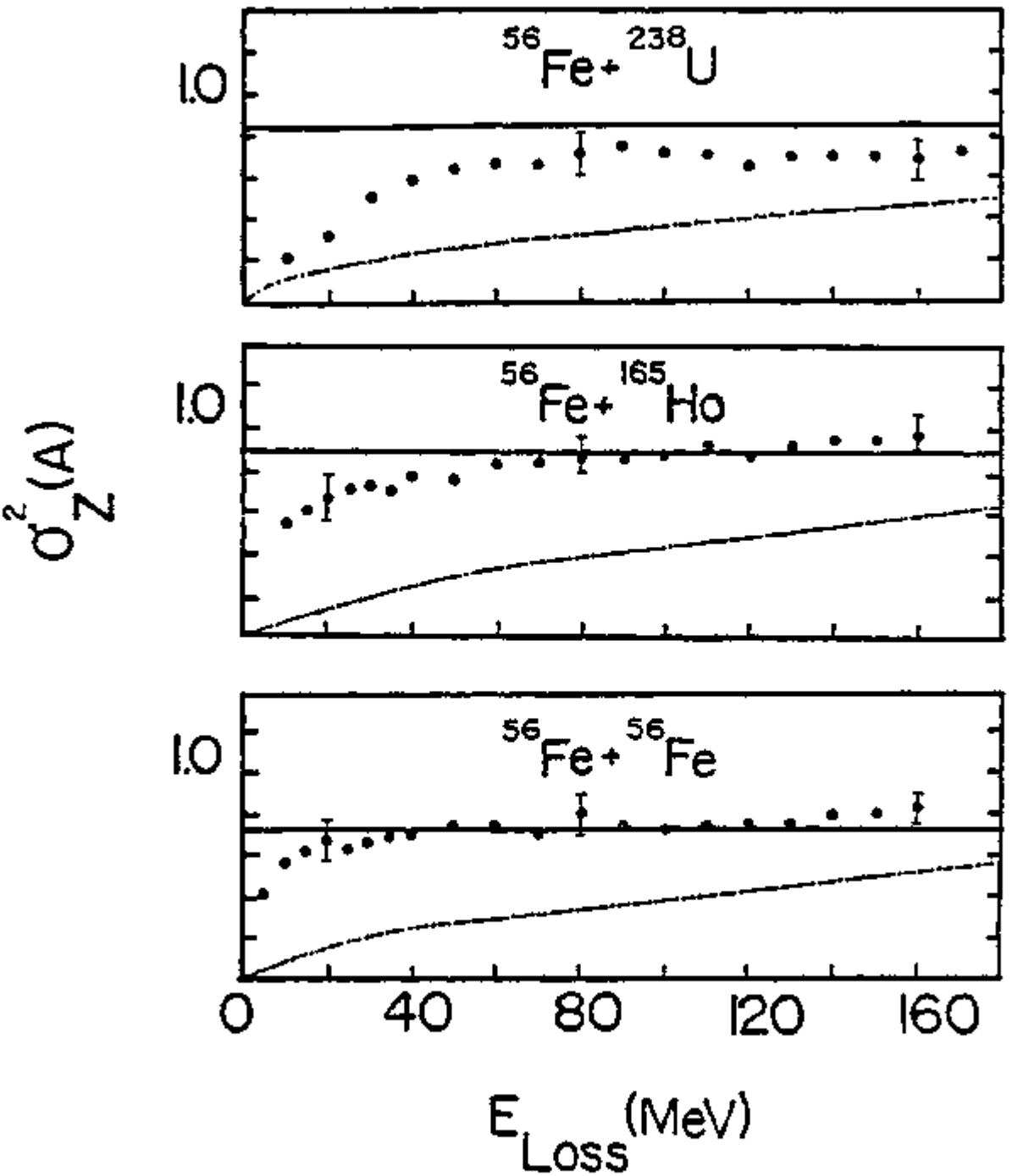
$^{56}Fe + ^{238}U$
$^{56}Fe + ^{165}Ho$
$^{56}Fe + ^{56}Fe$
1.0
1.0
1.0
$\sigma^2_Z(A)$
0
40
80
120
160
E_{Loss} (MeV)

Figure 3

I. Production of Neutron-Excess Nuclei in ^{56}Fe-Induced Reactions

PRODUCTION OF NEUTRON-EXCESS NUCLEI IN ^{56}Fe-INDUCED REACTIONS

H. Breuer
Department of Physics and Astronomy and
Cyclotron Laboratory
University of Maryland
College Park, Maryland 20742

K.L. Wolf and B.G. Glagola
Chemistry Division
Argonne National Laboratory
Argonne, Illinois 60439

K.K. Kwiatkowski, A.C. Mignerey and V.E. Viola
Department of Chemistry and
Cyclotron Laboratory
University of Maryland
College Park, Maryland 20742

and

W.W. Wilcke, W.U. Schröder, J.R. Huizenga,
D. Hilscher* and J. Birkelund
Departments of Physics and Chemistry and
Nuclear Structure Research Laboratory
University of Rochester
Rochester, New York 14627

*Permanent address: Hahn-Meitner-Institut für Kernforschung,
D-1000, Berlin 39, West Germany

Abstract

The observation of new neutron-rich isotopes of $^{52-53}$Sc, $^{54-55}$Ti, ^{56}V, and $^{58-59}$Cr produced in damped collisions of 8.3 MeV/u ^{56}Fe ions with ^{238}U and ^{209}Bi is reported. Tentative identification for ^{56}Ti, $^{57-58}$V, ^{60}Cr, ^{61}Mn and ^{63}Fe is also presented.

Studies of product mass and charge distributions have demonstrated that the nucleon-exchange process in damped heavy-ion collisions is strongly influenced by the N/Z ratio of the composite system.[1-3] Consequently, in reactions between projectiles and targets which differ sifnificantly in their N/Z ratios, the lighter products tend to be neutron-rich, while the heavy partners are neutron-deficient. This feature of damped collisions can thus serve as a useful means of synthesizing nuclides far from stability[4-6] with yields comparable to or greater than those obtained with relativistic heavy ions.[7,8]

In this letter we report identification of seven previously unobserved nuclides: $^{52-53}$Sc, $^{54-55}$Ti, ^{56}V and $^{58-59}$Cr. In addition, tentative identification of six additional nuclides (^{56}Ti, $^{57-58}$V, ^{60}Cr, ^{61}Mn and ^{63}Fe) is reported.

The experiments were performed at the Lawrence Berkeley Laboratory SuperHILAC accelerator. Self-supporting targets of ^{209}Bi and ^{238}U of thicknesses approximately 500 $\mu g/cm^2$ were bombarded with 8.3 MeV/u ^{56}Fe ions. Projectile-like reaction products were identified with a ΔE-E time-of-flight semiconductor detector telescope consisting of a 17 μm ΔE detector and a 100 μm E detector. The ΔE detector was placed 18 cm and the E detector 118 cm from the target. Data were taken at two angles separated by 5° near the grazing angle for each target. Fast-timing signals were obtained from a timing system of the Sherman-Roddick[9] design which yielded a resolution of 80-100 psec under experimental conditions for elastically-scattered ^{56}Fe ions.

The data reported in this letter are for the $^{238}U + ^{56}Fe$ system, for which greater statistics were obtained, although similar results are observed for the $^{209}Bi + ^{56}Fe$ system.[1,4] For the data reported here a Z-resolution of $\Delta Z = 0.84$ Z units (FWHM) was obtained and the A-resolution was $\Delta A = 0.65$ u (FWHM) for fragments in the $50 \leq A \leq 60$ region.

In Fig. 1 the relative mass yeilds for fragments with $21 \leq Z \leq 26$ are shown for the $^{238}U + ^{56}Fe$ system at 40 degrees in the laboratory system. Arrows indicate the expected centroids of each A value in the spectrum which has not been previously identified. The problem of possible contamination of the mass spectrum for a given element due to high-yield nuclides of neighboring Z and A was given particular attention in the data analysis procedures. First, since most of the yields for the new nuclides reported here were from strongly damped events, energy gates were chosen to eliminate quasi-elastic products. These gates corresponded to $90<E_{Loss}<180$ MeV for Z = 21; $60<E_{Loss}<150$ MeV for Z = 22-24, and $50<E_{Loss}<140$ MeV for Z>24. Then, in order to minimize possible leak-through of events of the same A from the next higher Z in the charge distribution, a Z-window of ±0.3 Z units about the charge centroid was established as a second criterion for acceptable events. Based on calculations which assume that the experimental peak shape is a gaussian function, this procedure establishes a limit of less than three percent for contamination due to the tails of the peak for the next higher Z.

In Table I the new nuclides identified in this study are

listed along with the net number of observed counts. In determining the net counts for each nuclide, only events which occurred within ±0.3 A units of the mass centroid were accepted. These values were further corrected by subtracting the calculated contribution due to possible leak-through of events from higher Z isobars. The quoted errors include contributions from both counting statistics and the background subtraction. Each net count represents 4.4μb/sr of differential cross section, as determined from comparison with elastic scattering. Total production cross sections for each nuclide listed in Table I were estimated from measurements of the cross section, $d\sigma/dE$, as a function of energy loss for the $^{209}Bi + ^{56}Fe$ reaction at 8.3 MeV/u, where complete angular distribution measurements have been made.[4] For these data a nearly constant value of $d\sigma/dE \approx 6$ mb/MeV is found over a broad range of energy loss. It is assumed that the $^{238}U + ^{56}Fe$ system exhibits similar behavior at this bombarding energy. The quoted cross sections derived from this procedure are believed to be accurate to within a factor of two.

The validity of the Z and A assignments for each new nuclide reported here was determined on the basis of the statistical and spectral criteria established in Ref. 10. Nuclides for which $N-\Delta N>10$ have been given an A classification and appear to be clearly identified. Seven such nuclides are identified in our spectra. Nuclides for which $N>10$ but $N-\Delta N<10$ have been given a B classification and require further statistical or spectral definition. However, based on their

production cross sections, these should be readily observable.

In summary, the identification of seven new isotopes is reported: $^{52-53}Sc$, $^{54-55}Ti$, ^{56}V and $^{58-59}Cr$. In addition, tentative evidence is found for ^{56}Ti, $^{57-58}V$, ^{60}Cr, ^{61}Mn and ^{63}Fe. The cross sections for production of these nuclides are of the order of 0.1-to-1 millibarn, indicating that the production of neutron-excess isotopes in damped collisions is a viable means of synthesizing nuclei far from stability in significant yields.

This research was supported by the U.S. Department of Energy. We wish to acknowledge Claude Ellsworth of LBL for fabricating the ^{238}U targets and M.S. Zisman of LBL for his assistance with these experiments.

References

1. H. Breuer et al., Phys. Rev. Lett. 43, 191 (1979).
2. Y. Eyal et al., Phys. Rev. Lett. 42, 126 (1979).
3. B. Gatty et al., Nucl. Phys. A253, 511 (1975).
4. V.E. Viola, Jr., University of Maryland Report ORO-5172-13, August (1979).
5. A.G. Artukh et al., J. de Physique 32, 129 (1971).
6. P. Auger et al., Z. Phys. A289, 255 (1979).
7. T.J.M. Symons et al., Phys. Rev. Lett. 42, 40 (1979).
8. G.D. Westfall et al., Phys. Rev. Lett 43, 1859 (1979).
9. I.S. Sherman, R.G. Roddick and A.F. Metz, IEEE Trans. Nucl. Sci. 15, 500 (1968).
10. J.D. Bowman et al., Phys. Rev. C9, 836 (1974); G.W. Butler et al., Phys. Rev. Lett. 38, 1380 (1977).

Table I

Nuclide	Counts	σ(mb)	Classification*
^{52}Sc	30±8	0.5	A
^{53}Sc	19±6	0.3	A
^{54}Ti	74±11	1.0	A
^{55}Ti	24±7	0.3	A
^{56}Ti	13±5	0.2	B
^{56}V	107±12	1.3	A
^{57}V	27±7	0.3	B†
^{58}V	12±4	0.1	B
^{58}Cr	74±10	0.9	A
^{59}Cr	28±6	0.3	A
^{60}Cr	10±4	0.1	B
^{61}Mn	14±4	0.2	B
^{63}Fe	13±4	0.2	B

* A = $(N-\Delta N)>10$

B = $N>10$; $(N-\Delta N)<10$

† spectrum poorly defined

Figure Captions

Figure 1. Mass spectra for Z = 21-26 fragments observed in bombardment of ^{238}U with 8.3 MeV/u ^{56}Fe ions. Arrows indicate expected mass centroids for previously unknown nuclides. The anomalously strong peak for ^{56}Fe is due to elastic scattering effects.

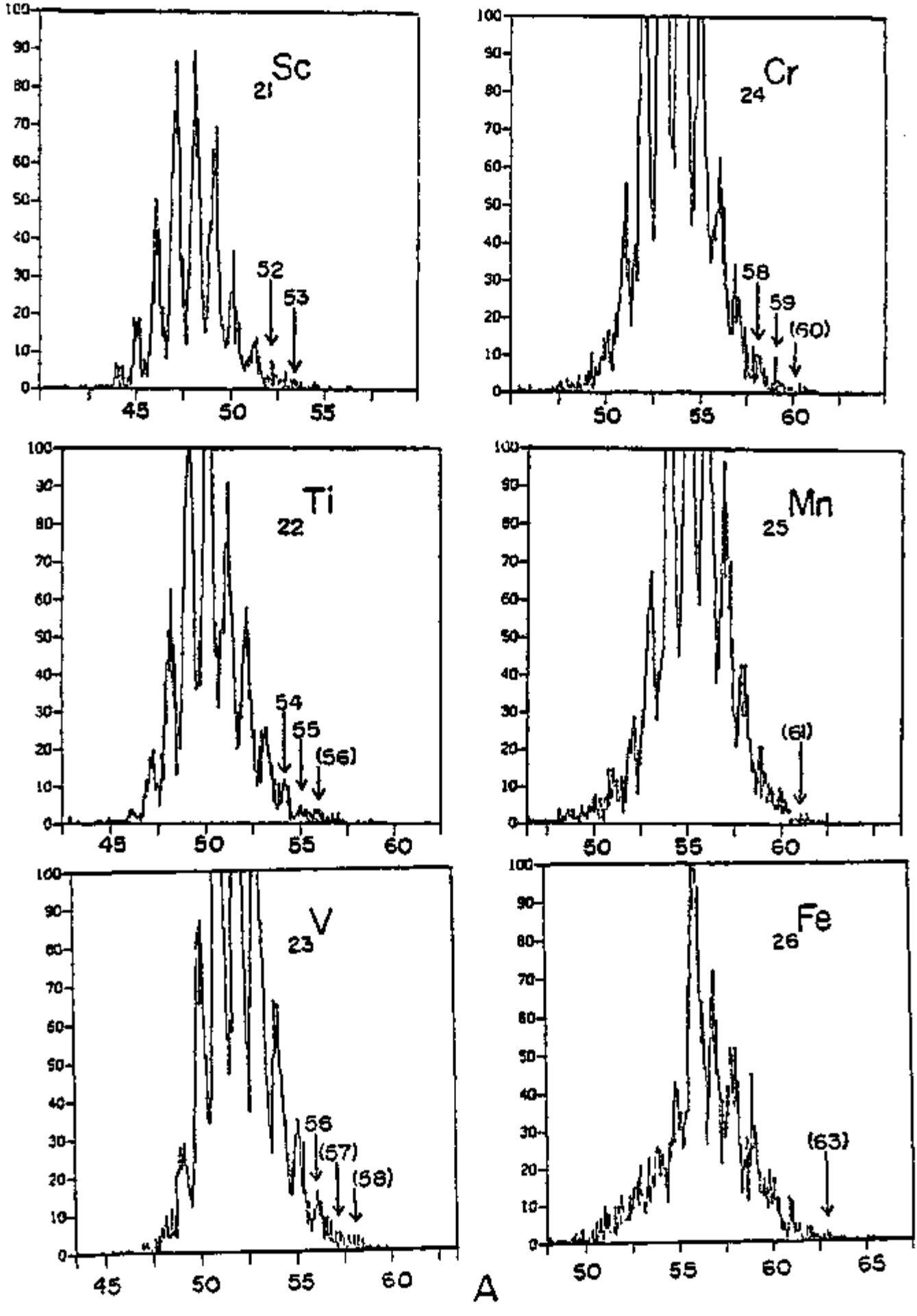
COUNTS
21Sc
52
53
24Cr
58
59
(60)
22Ti
54
55
(56)
25Mn
(61)
23V
56
(57)
(58)
26Fe
(63)
A

Figure 1

IV. PUBLICATIONS AND ACTIVITIES

A. Articles

H. Breuer, B.G. Glagola, V.E. Viola, K.L. Wolf, A.C. Mignerey, J.R. Birkelund, D. Hilscher, A.D. Hoover, J.R. Huizenga, W.U. Schröder and W.W. Wilcke
NUCLEON EXCHANGE AND A/Z EQUILIBRATION IN INTERACTIONS OF 8.3 MeV/u ^{56}Fe IONS WITH ^{56}Fe, ^{165}Ho AND ^{209}Bi
Phys. Rev. Lett. 43, 191 (1979).

D. Hilscher, J.R. Birkelund, A.D. Hoover, W.U. Schröder, W.W. Wilcke, J.R. Huizenga, A. Mignerey, K.L. Wolf, H. Breuer and V.E. Viola, Jr.
NEUTRON EMISSION FROM THE ^{165}Ho + ^{56}Fe REACTION AT 8.5 MeV/u
Phys. Rev. C20, 576 (1979).

D. Hilscher, J.R. Birkelund, A.D. Hoover, W.U. Schröder, W.W. Wilcke, J.R. Huizenga, A. Mignerey, K.L. Wolf, H.F. Breuer and V.E. Viola
STRUCTURE IN THE ENERGY SPECTRA OF THE FRAGMENTS PRODUCED IN DAMPED HEAVY-ION REACTIONS
Phys. Rev. C20, 556 (1979).

J.R. Huizenga, J.R. Birkelund, L.E. Tubbs, J.N. De and D. Sperber
FUSION REACTIONS AT HIGH ENERGIES
Proceedings of the Symposium on Heavy Ion Physics from 10 to 200 MeV/amu, Brookhaven National Laboratory, Report BNL-51115, Vol. 1, page 235-271 (1979).

W.U. Schröder, W.W. Wilcke, M.W. Johnson, D. Hilscher, J.R. Huizenga, J.C. Browne and D.G. Perry
EVIDENCE FOR ATOMIC MUON CAPTURE BY FRAGMENTS FROM PROMPT FISSION OF MUONIC ^{237}Np, ^{239}Pu and ^{242}Pu.
Phys. Rev. Lett. 43, 672 (1979).

J.R. Birkelund, L.E. Tubbs, J.R. Huizenga, J.N. De and D. Sperber
HEAVY-ION FUSION: COMPARISON OF EXPERIMENTAL DATA WITH CLASSICAL TRAJECTORY MODELS
Physics Reports 56, No. 3, 107-166 (1979).

J.R. Huizenga
HEAVY-ION REACTIONS: A NEW FRONTIER OF NUCLEAR SCIENCE
Proceedings of Symposium on Deep-Inelastic and Fusion Reactions with Heavy Ions, Berlin. Lecture Notes in Physics 117, 1-24 (1979), Springer-Verlag, Edited by W. von Oertzen.

D. Hilscher, J.R. Birkelund, A.D. Hoover, W.U. Schröder, W.W. Wilcke, J.R. Huizenga, A.C. Mignerey, K.L. Wolf, H.F. Breuer and V.E. Viola
NEUTRON EMISSION IN HEAVY ION REACTIONS
Proceedings of Symposium on Deep-Inelastic and Fusion Reactions with Heavy Ions, Berlin. Lecture Notes in Physics 117, 100-112 (1979), Springer-Verlag, Edited by W. von Oertzen.

J.R. Birkelund, L.E. Tubbs, J.R. Huizenga, J.N. De and D. Sperber
HEAVY-ION FUSION: A CLASICAL TRAJECTORY MODEL
Proceedings of Symposium on Deep-Inelastic and Fusion Reactions with Heavy Ions, Berlin. Lecture Notes in Physics 117, 294-311 (1979), Springer-Verlag, Edited by W. von Oertzen.

W.U. Schröder, J.R. Birkelund, J.R. Huizenga, W.W. Wilcke and J. Randrup
THE EFFECT OF PAULI BLOCKING ON EXCHANGE AND DISSIPATION MECHANISMS OPERATING IN HEAVY ION REACTIONS
Phys. Rev. Lett. 44, 308 (1980).

W.U. Schröder
LIGHT-PARTICLE EMISSION AS A PROBE OF DISSIPATION AND DEEXCITATION MECHANISMS IN HEAVY-ION REACTIONS
Proceedings of International Symposium on Continuum Spectra of Heavy Ion Reactions, San Antonio, Texas Dec. 3-5 (1979).

J.R. Huizenga
EXPERIMENTAL SUMMARY OF THE INTERNATIONAL SYMPOSIUM ON CONTINUUM SPECTRA OF HEAVY ION REACTIONS
Proceedings of International Symposium on Continuum Spectra of Heavy Ion Reactions, San Antonio, Texas Dec. 3-5 (1979).

W.U. Schröder, J.R. Birkelund, J.R. Huizenga, W.W. Wilcke and J. Randrup
MANIFESTATION OF THE QUANTUM-STATISTICAL NATURE OF EXCHANGE AND DISSIPATION MECHANISMS OPERATING IN DAMPED NUCLEAR REACTIONS
Proceedings of the International Workshop on Gross Properties of Nuclei and Nuclear Excitations VIII, Hirschegg, Austria, p. 92, January 14-19 (1980).

W.W. Wilcke, M.W. Johnson, W.U. Schröder, D. Hilscher, J.R. Birkelund, J.R. Huizenga, J.C. Browne and D.G. Perry
ACTINIDE MUONIC ATOM LIFETIMES DEDUCED FROM MUON-INDUCED FISSION
Phys. Rev. C21, 2019 (1980).

R.W. Atcher, A.M. Friedman, J.R. Huizenga, G.V.S. Rayudu, E.A. Silverstein and D.A. Turner,
MANGANESE-52m, A NEW SHORT-LIVED, GENERATOR-PRODUCED RADIONUCLIDE: A POTENTIAL GENERATOR FOR POSITRON TOMOGRAPHY
Journal of Nuclear Medicine, 21 565 (1980).

R.W. Atcher, A.M. Friedman and J.R. Huizenga
PRODUCTION OF ^{52}Fe FOR USE IN A RADIONUCLIDE GENERATOR SYSTEM
International Journal of Nuclear Medicine and Biology
7 75 (1980).

M. Kildir
ISOSPIN DEPENDENCE OF THE NUCLEAR LEVEL WIDTH IN THE COMPOUND NUCLEUS ^{30}P
Nucl. Phys. A340 117 (1980).

W.W. Wilcke, J.R. Birkelund, A.D. Hoover, J.R. Huizenga, W.U. Schröder, V.E. Viola, K.L. Wolf and A.C. Mignerey
BOMBARDING ENERGY DEPENDENCE OF THE ^{209}Bi + ^{136}Xe REACTION
Phys. Rev. C22, (1980) (in press).

J.R. Huizenga
DEEP INELASTIC HEAVY ION COLLISIONS
McGraw-Hill Yearbook of Science and Technology, (1980) (in press).

V.E. Viola, A.C. Mignerey, H. Breuer, K.L. Wolf, B.G. Glagola, W.W. Wilcke, W.U. Schröder, J.R. Huizenga, D. Hilscher and J.R. Birkelund
CAN THE Z=104-107 SPONTANEOUS FISSION ACTIVITIES BE EXPLAINED BY ACTINIDE PRODUCTION IN DAMPED COLLISIONS?
Phys. Rev. C22, (1980) (in press).

B. Ph.D. Thesis

"NEW RADIONUCLIDE GENERATOR SYSTEMS FOR USE IN NUCLEAR MEDICINE"
by Robert A.Atcher, Department of Chemistry
University of Rochester, January, 1980.

C. Contributed Papers at Professional Meetings

A.C. Mignerey, K.L. Wolf, J.R. Birkelund, D. Hilscher, W.U. Schröder, W.W. Wilcke, J.R. Huizenga, V.E. Viola and H. Breuer
NON-CLASSICAL EFFECTS IN THE REACTION 464-MeV ^{56}Fe + ^{56}Fe AND ^{165}Ho
Bull. Am. Phys. Soc. 24, 852 (1979).

A.C. Mignerey, K.L. Wolf, H. Breuer, B.G. Glagola, V.E. Viola, J.R. Birkelund, D. Hilscher, J.R. Huizenga, W.U. Schröder and W.W. Wilcke
STRUCTURE IN THE ENERGY SPECTRA OF DAMPED PRODUCTS FROM THE $^{56}Fe + ^{56}Fe$ REACTION
Proceedings of the International Symposium on Continuum Spectra of Heavy Ion Reactions, San Antonio, Texas, Dec. 3-5 (1979), page 2 of abstracts.

H. Breuer, A.C. Mignerey, B.G. Glagola, V.E. Viola, K.L. Wolf, J.R. Birkelund, D. Hilscher, J.R. Huizenga, W.U. Schröder and W.W. Wilcke
NUCLEON EXCHANGE AND A/Z EQUILIBRATION IN ^{56}Fe-INDUCED REACTIONS
Proceedings of the International Symposium on Continuum Spectra of Heavy Ion Reactions, San Antonio, Texas, Dec. 3-5 (1979), page 3 of abstracts.

V.E. Viola, H. Breuer, A.C. Mignerey, K.L. Wolf, B.G. Glagola, W.W. Wilcke, W.U. Schröder, J.R. Huizenga, D. Hilscher and J.R. Birkelund
PRODUCTION OF NUCLEI FAR FROM STABILITY IN ^{56}Fe-INDUCED REACTIONS
American Chemical Society Meeting, Houston, Texas, March 23-28 (1980).

W.U. Schröder, J.R. Birkelund, D. Hilscher, W.W. Wilcke, J.R. Huizenga, K.L. Wolf, H. Breuer, A.C. Mignerey and V.E. Viola
NEUTRON EMISSION IN THE STRONGLY DAMPED REACTION $^{136}Xe + ^{165}Ho$ AT 8.5 MeV/u
Deutsche Physikalische Gesellschaft E.V., München, Germany, March 17-23 (1980).

H. Breuer, K. Kwiatkowski, A.C. Mignerey, V.E. Viola, B.G. Glagola, K.L. Wolf, J.R. Birkelund, D. Hilscher, J.R. Huizenga, W.U. Schröder and W.W. Wilcke
CHARGE AND MASS EXCHANGE IN ^{56}Fe-INDUCED REACTIONS
Proceedings of the Workshop on Nuclear Dynamics, Granlibakken, Calif., March (1980), LBL-10688

W.W. Wilcke, W.U. Schröder, J.R. Huizenga, J.R. Birkelund and J. Randrup
BOMBARDING ENERGY DEPENDENCE OF NUCLEON EXCHANGE AND ENERGY DISSIPATION IN THE STRONGLY DAMPED REACTION $^{209}Bi + ^{136}Xe$
Proceedings of the Workshop on Nuclear Dynamics, Granlibakken, Calif., March (1980), LBL-10688

A.C. Mignerey, H. Breuer, V.E. Viola, K.L. Wolf, B.G. Glagola, W.W. Wilcke, W.U. Schröder, J.R. Huizenga and J.R. Birkelund
DOES PARTICLE EMISSION EXPLAIN THE STRUCTURE IN THE ENERGY SPECTRA FOR THE $^{56}Fe + ^{56}Fe$ REACTION?
Bull. Am. Phys. Soc. 25, 482 (1980).

V.E. Viola, H. Breuer, A.C. Mignerey, K. Kwiatkowski, K.L. Wolf, B.G. Glagola, J.R. Birkelund, D. Hilscher, J.R. Huizenga, W.U. Schröder and W.W. Wilcke
PRODUCTION OF NUCLEI FAR FROM STABILITY IN DAMPED COLLISIONS WITH ^{56}Fe PROJECTILES
Bull. Am. Phys. Soc. 25, 482 (1980).

H. Breuer, K. Kwiatkowski, A.C. Mignerey, V.E. Viola, K.L. Wolf, B.G. Glagola, J.R. Birkelund, J.R. Huizenga, W.U. Schröder and W.W. Wilcke
MASS AND CHARGE DISTRIBUTIONS IN THE $^{238}U + ^{56}Fe$ REACTION AT 470 MeV
Bull. Am. Phys. Soc. 25, 482 (1980).

A.D. Hoover, L.E. Tubbs, W.W. Wilcke, W.U. Schröder, J.R. Birkelund, J.R. Huizenga, D. Hilscher and H.J. Wollersheim
FUSION-FISSION FRAGMENTS FROM THE $^{165}Ho + ^{56}Fe$ REACTION
Bull. Am. Phys. Soc. 25, 483 (1980).

D. Invited Lectures

"DE-EXCITATION PROCESSES IN DAMPED HEAVY-ION REACTIONS"
American Chemical Society Meeting, Washington, D.C., September 9-14, 1979 (by W.U. Schröder).

"GRADUATE EDUCATION AT THE UNIVERSITY OF ROCHESTER"
Fudan University, Shanghai, China,
September 17, 1979 (by J.R. Huizenga).

"HEAVY-ION FUSION"
Fudan University, Shanghai, China,
September 20, 1979 (by J.R. Huizenga).

"HEAVY-ION STRONGLY DAMPED COLLISIONS"
Fudan University, Shanghai, China,
September 20, 1979 (by J.R. Huizenga).

"HEAVY-ION REACTIONS: FUSION"
Lanchow University, Lanchow, China,
September 22, 1979 (by J.R. Huizenga).

"HEAVY-ION REACTIONS: STRONGLY DAMPED COLLISIONS"
Institute of Modern Physics, Lanchow, China,
September 23, 1979 (by J.R. Huizenga).

"RESEARCH AT THE UNIVERSITY OF ROCHESTER'S NUCLEAR STRUCTURE RESEARCH LABORATORY"
Institute of Atomic Energy, Peking, China,
September 27, 1979 (by J.R. Huizenga).

"HEAVY-ION REACTIONS: FUSION"
Institute of Atomic Energy, Peking, China,
September 27, 1979 (by J.R. Huizenga).

"HEAVY-ION REACTIONS: STRONGLY DAMPED COLLISIONS"
Peking University, Peking, China,
September 30, 1979 (by J.R. Huizenga).

"ARE SINGLE PARTICLE EFFECTS FUNDAMENTAL TO DAMPED NUCLEAR REACTIONS"
Nuclear Structure Seminar, University of Rochester,
October 4, 1979 (by W.U. Schröder).

"REACTION PHENOMENA IN NUCLEAR COLLISIONS BETWEEN ^{56}Fe AND ^{165}Ho"
Physical Chemistry Seminar, University of Rochester,
October 22, 1979 (by A.D. Hoover).

"HEAVY-ION REACTIONS: A NEW FRONTIER OF NUCLEAR SCIENCE"
Meitner-Hahn Lecture, Hahn-Meitner Institute,
Berlin, Germany,
October 23, 1979 (by J.R. Huizenga).

"HEAVY-ION FUSION: A CLASSICAL TRAJECTORY MODEL"
Symposium on Deep-Inelastic and Fusion Reactions with Heavy-Ions, Hahn-Meitner Institute, Berlin, Germany,
October 25, 1979 (by J.R. Birkelund).

"NEW RADIONUCLIDE GENERATOR SYSTEMS FOR USE IN NUCLEAR MEDICINE"
Physical Chemistry Seminar, University of Rochester,
November 7, 1979 (by R.A. Atcher).

"MUON CAPTURE IN THE ACTINIDES"
Nuclear Structure Seminar, University of Rochester,
November 8, 1979 (by W.W. Wilcke).

"LIGHT PARTICLE EMISSION AS A PROBE OF DISSIPATION AND DEEXCITATION MECHANISMS IN HEAVY-ION REACTIONS"
International Symposium on Continuum Spectra of Heavy Ion Reactions, San Antonio, Texas,
December 3-5, 1979 (by W.U. Schröder).

"EXPERIMENTAL SUMMARY OF THE INTERNATIONAL SYMPOSIUM ON CONTINUUM SPECTRA OF HEAVY ION REACTIONS"
International Symposium on Continuum Spectra of Heavy Ion Reactions, San Antonio, Texas,
December 3-5, 1979 (by J.R. Huizenga).

"DISSIPATION AND DEEXCITATION MECHANISMS IN HEAVY ION REACTIONS"
Physics Colloquium, Brookhaven National Laboratory,
January 11, 1980 (by J.R. Huizenga).

"A COMPARISON OF EXPERIMENTAL DATA WITH CLASSICAL TRAJECTORY MODELS FOR HEAVY ION FUSION"
Physical Chemistry Seminar, University of Rochester,
January 14, 1980 (by L.E. Tubbs).

"MANIFESTATION OF THE QUANTUM-STATISTICAL NATURE OF EXCHANGE AND DISSIPATION MECHANISMS OPERATING IN DAMPED NUCLEAR REACTIONS"
International Workshop on Gross Properties of Nuclei and Nuclear Excitations VIII, Hirschegg, Austria,
January 17, 1980 (by W.U. Schröder).

"THE STRUCTURE OF THE STABLE ISOTOPES AT HIGH ANGULAR MOMENTA"
Nuclear Structure Seminar, University of Rochester,
January 31, 1980 (by H.J. Wollersheim).

"DEEP-INELASTIC HEAVY ION COLLISIONS"
Physics Colloquium, University of Wisconsin, Madison,
February 15, 1980 (by J.R. Huizenga).

"EXPERIMENTAL AND THEORETICAL FUSION CROSS SECTIONS: PROBLEMS AND UNCERTAINTIES"
International Symposium on Heavy Ion Fusion Reactions, Bad Honnef, Germany,
March 10, 1980 (by J.R. Huizenga).

"STATISTICAL AND QUANTUM ASPECTS OF HEAVY ION COLLISIONS"
Physics Colloquium, University of Pennsylvania, Philadelphia,
March 26, 1980 (by J.R. Huizenga).

"COLLECTIVE PROPERTIES OF THE STABLE DYSPROSIUM ISOTOPES"
Physics Colloquium, University of Pittsburgh, Pittsburgh,
April 17, 1980 (by H.J. Wollersheim).

"DISSIPATION AND EQUILIBRATION PROCESSES IN DAMPED NUCLEAR REACTIONS"
Physics Seminar, Michigan State University, East Lansing,
May 7, 1980 (by W.U. Schröder).

"WHAT HAPPENS WHEN TWO HEAVY IONS COLLIDE"?
Colloquium, Los Alamos Scientific Laboratory,
Los Alamos, New Mexico,
May 22, 1980 (by J.R. Huizenga).

"CLASSICAL TRAJECTORY MODELS IN HEAVY-ION FUSION"
Nuclear Structure Gordon Conference,
Tilton, New Hampshire,
July 8, 1980 (by J.R. Huizenga).

E. Professional Activities

Member of Faculty Recruiting Committee,
Department of Chemistry

Member of Research Grants and Contracts Committee,
Department of Chemistry

Member of Faculty Bridging Committee

Member of Los Alamos Meson Physics Facility
Program Advisory Committee

Member of Nuclear Chemistry Division Review Committee,
Lawrence Livermore Laboratory

Member of ACS Division of Nuclear Chemistry and
Technology Committee on Funding

Member of Program Committee of the Division of
Nuclear Physics, APS

Member of Visiting Committee of Chemistry Division of
Argonne National Laboratory

Member of Nuclear Science Advisory Committee to
DOE and NSF

Member of International Advisory Committee for
Conference on the Theory and Applications of Moment
Methods in Many Fermion Systems
(September 10-14, 1979, Ames, Iowa)

Member of International Advisory Committee for
Symposium on Continuum Spectra of Heavy Ion Reactions
(December 3-5, 1979, San Antonio, Texas)

V. PERSONNEL

Dr. J.R. Huizenga, Tracy H. Harris Professor of Chemistry and Physics

Dr. J.R. Birkelund, Research Associate

Dr. W.U. Schröder, Senior Research Associate

Dr. W.W. Wilcke, Research Associate

Dr. H.J. Wollersheim,* Research Associate

Mr. R.A. Atcher,** graduate student, Department of Chemistry

Ms. A.D. Hoover, graduate student, Department of Chemistry

Ms. L.E. Tubbs, graduate student, Department of Chemistry

Mr. J.P. Kosky, graduate student, Department of Chemistry

* On leave from GSI, Darmstadt, W. Germany

** Completed Ph.D. degree and presently a postdoctoral fellow in Nuclear Medicine at Harvard Medical School